

**ЛЕСНЫЕ ЭКОСИСТЕМЫ
В УСЛОВИЯХ ИЗМЕНЕНИЯ КЛИМАТА:
БИОЛОГИЧЕСКАЯ ПРОДУКТИВНОСТЬ И ДИСТАНЦИОННЫЙ МОНИТОРИНГ**

Международный сборник научных статей

**FOREST ECOSYSTEMS UNDER CLIMATE CHANGE:
BIOLOGICAL PRODUCTIVITY AND REMOTE MONITORING**

International Compendium of research papers

ISSN 2500-4263

МИНИСТЕРСТВО НАУКИ И ВЫСШЕГО ОБРАЗОВАНИЯ РОССИЙСКОЙ ФЕДЕРАЦИИ
ФГБОУ ВО «ПОВОЛЖСКИЙ ГОСУДАРСТВЕННЫЙ
ТЕХНОЛОГИЧЕСКИЙ УНИВЕРСИТЕТ»
ЦЕНТР УСТОЙЧИВОГО УПРАВЛЕНИЯ И ДИСТАНЦИОННОГО
МОНИТОРИНГА ЛЕСОВ

ЛЕСНЫЕ ЭКОСИСТЕМЫ
В УСЛОВИЯХ ИЗМЕНЕНИЯ КЛИМАТА:
БИОЛОГИЧЕСКАЯ ПРОДУКТИВНОСТЬ И ДИСТАНЦИОННЫЙ МОНИТОРИНГ

Международный сборник научных статей

FOREST ECOSYSTEMS UNDER CLIMATE CHANGE:
BIOLOGICAL PRODUCTIVITY AND REMOTE MONITORING

International Compendium of research papers

Йошкар-Ола
2020

Редакционная коллегия:

Э. А. Курбанов, д-р. с.-х. наук, профессор, Поволжский государственный технологический университет (отв. редактор)

С. А. Барталев, д-р техн. наук, профессор, Институт космических исследований РАН

С. И. Чумаченко, д-р биол. наук, профессор, Мытищинский филиал Московского государственного технического университета им. Н. Э. Баумана

В. К. Хлюстов, д-р с.-х. наук, профессор, Российский государственный аграрный университет - МСХА имени К.А. Тимирязева

О. Н. Воробьев, канд. с.-х. наук, доцент, Поволжский государственный технологический университет

Э.А. Терехин, канд. геогр. наук, доцент . Белгородский государственный университет

Д-р Иоаннис Гитас, профессор, лаборатория лесоуправления и дистанционного зондирования, Университет Аристотеля (г. Салоники, Греция)

Д-р Ша Цзиньмин, профессор, директор Китайско-Европейского центра управления окружающей средой и ландшафтом

Д-р Абрахам Томас, менеджер в области дистанционного зондирования, Совет по науке о Земле

Д-р Цзиньян Ванг, профессор, колледж туризма и географических наук, Юньнаньский педагогический университет

Лесные экосистемы в условиях изменения климата: биологическая продуктивность Л 50 и дистанционный мониторинг: международный сборник научных статей / отв. ред. проф. Э.А. Курбанов. – Текст: электронный.– Йошкар-Ола: Поволжский государственный технологический университет, 2020. – 174 с. – URL: <https://inter.volgatech.net/centre-for-sustainable-management-and-remote-monitoring-of-forests/forest-ecosystems-in-a-changing-climate/>

Основу сборника составили материалы международной научной конференции «Лесные экосистемы в условиях изменения климата: региональные и международные аспекты», цель которой – обмен научным и практическим опытом между учеными, преподавателями, научными сотрудниками вузов и научных организаций и объединение усилий для развития перспективных направлений науки в области лесного хозяйства и экологии.

УДК 630
ББК 43:20.18

Editorial board:

E.A. Kurbanov, Doctor of Agricultural Sciences, Professor, Volga State University of Technology

S.A. Bartalyov, Doctor of Engineering Science, Professor, Space Research Institute of Russian Academy of Sciences

S.I. Chumachenko, Doctor of Biological Sciences, Professor, Mytishchi Branch, Bauman Moscow State Technical University

V.K. Khlyustov, Doctor of Agricultural Sciences, Professor, Russian State Agrarian University - Moscow Timiryazev Agricultural Academy

O.N. Vorobiev, Ph.D., Associate Professor, Volga State University of Technology

E.A. Terekhin, Ph. D, Associate Professor, Belgorod State University

Dr. Ioannis Gitas, Professor, Laboratory of Forest Management and Remote Sensing of the Aristotle University of Thessaloniki

Dr. Sha Jinming, Director China-Europe Center for Environment and Landscape Management, College of Geography, Fujian Normal University

Dr. Abraham Thomas, Competency Manager of Remote Sensing, Council for Geoscience

Dr. Jinliang Wang, Professor, College of Tourism & Geographic Sciences, Yunnan Normal University

Forest ecosystems under climate change: biological productivity and remote monitoring :

F 75 compendium of research papers / Executive editor Prof. E.A. Kurbanov. – Text: electronic. – Yoshkar-Ola: Volga State University of Technology, 2020. – 174 p. – URL: <https://inter.volgatech.net/centre-for-sustainable-management-and-remote-monitoring-of-forests/forest-ecosystems-in-a-changing-climate/>

The purpose of the International Compendium of Research Papers "**Forest ecosystems under climate change: biological productivity and remote monitoring**" is the exchange of expertise between research staff of universities and R&D organizations .

UDC 630
BBK 43:20.18

ISSN 2500-4263

© Volga State University
of Technology, 2020
© Center of Sustainable forest management
and Remote sensing , 2020

ACKNOWLEDGEMENT

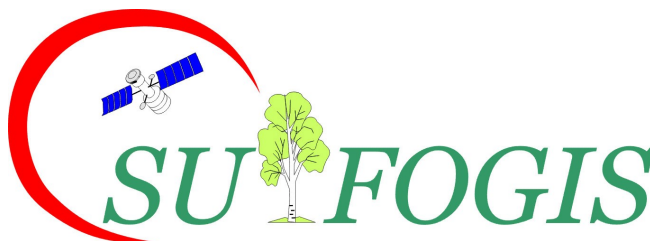
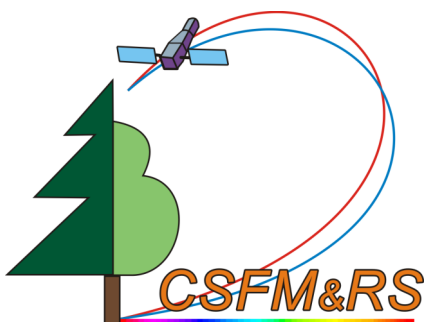
The Jean Monnet Center of Excellence “European Expertise and Technology for Environmental Protection and Sustainable Forestry (SUFEX)” and project «GIS and Remote Sensing for Sustainable Forestry and Ecology (SUFOGIS)» at Volga State University of Technology has been funded with support from the EU ERASMUS+ program.

The European Commission support for the production of this publication does not constitute an endorsement of the contents which reflects the views only of the authors, and the Commission cannot be held responsible for any use which may be made of the information contained therein.

Центр совершенства Жана Монне «Европейская экспертиза и технологии в области защиты окружающей среды и устойчивого лесоводства (SUFEX)» и проект «Геоинформационные системы и дистанционное зондирование Земли для устойчивого лесопользования и экологии (SUFOGIS)» в Поволжском государственном технологическом университете получили финансовую поддержку Европейского Союза.

Содержание сборника отражает точку зрения только ее авторов. Исполнительное агентство по вопросам образования, аудиовизуальной деятельности и культуры и Европейская Комиссия не несут ответственности за любое использование информации, содержащейся в этой публикации.

Co-funded by the
Erasmus+ Programme
of the European Union



MAPPING OF LAND USE / LAND COVER OF KLERKSDORP–ORKNEY–STILFONTEIN–HARTEBEESTFONTEIN (KOSH) REGION FOR THE YEARS 2020 AND 2019 USING SENTINEL-2 DATA

Abraham Thomas

Council for Geoscience, Pretoria 0184, South Africa.

The article presents mapping of current land use / land cover and of year 2019 of Klerksdorp–Orkney–Stilfontein–Hartebeestfontein (KOSH) region using Sentinel-2 data. This study made use of VNIR bands of Sentinel-2 acquired on 10 March 2020, 16 March 2019 and National Land Cover (NLC) dataset of year 2018 to investigate how land use change and vegetation alteration has occurred during 2018 to 2020. The Level 1 Sentinel-2 data were pre-processed to obtain ground reflectance using Sen2Cor algorithm. The classification system of NLC 2018 was used for identifying the training sites for 56 classes present. Further processing to produce intended classes and post processing of classification products were performed using Geomatica Object Analyst. The analysis involved image segmentation, attribute calculation for geometrical parameters, mean, standard deviation and 10 vegetation indices of pixels covered in segments of VNIR bands, training site selection, classification and post classification analysis. Though attempts were made to classify the images with training sites and different attributes, the best classification result was obtained with standard deviation of 4 VNIR bands and 10 vegetation indices. For classifying March 2019 image, the batch classification algorithm was applied using training model file generated for classification of March 2020 data. The percentage of total area covered by five major classes for the years 2020 and 2019 respectively are: grasslands - 49.32% & 42.14%; temporary crops (rainfed) - 32.90% & 32.92%; open woodland - 4.00% & 3.03%; mine waste (tailings) and resource dumps - 1.96% & 2.46%; residential formal (grass) - 1.53% & 1.46%.

Keywords: remote sensing, Sentinel-2, KOSH, land use / land cover dynamics, Object Analyst, classification.

Introduction

Knowledge of land cover and land use change is necessary in order to model the earth system and its environments (for example by studying aspects such as hydrological processes and climate change) and for many purposes related to land and natural resource management. The study of land cover change is quite important because of its impacts on local climate, hydrology, radiation balance, and the diversity and abundance of terrestrial species (Boriah et al., 2008). Most (80%) of the land cover in South Africa is natural or semi-natural, and monitoring and projecting changes in land cover is vital for proper management and development of its geographical areas and sustainable utilisation of the natural resources. Mining and agricultural practices are major human activities on the land in South Africa. The change of land cover due to mining and associated development in the area (changes in land use / land cover due to human activities that are linked to mining) has resulted in significant changes in climate and the environment (for example changes in the catchment hydrology resulting in increased surface runoff in certain areas and associated pollution and also depletion of surface water resources due to reduction of natural infiltration and ground water recharge).

South Africa has a mining history of more than 100 years. Today the South African mining industry still is a key sector to the economy with a contribution of 8% to the national GDP, even with the substantial decline of the gold mining in the Witwatersrand basin, as new mineral deposit types are being developed and exploited. However, the remnants of mining still exist today in the form of large tailings sites and underground shafts throughout the major mining areas in Gauteng, the North West and Free-State provinces, near the densely populated cities of the Gauteng Metropolitan Region. Even this post-mining landscape is very dynamic. Old tailings dam sites are being reprocessed, as new technologies become available, or rising commodity prices favour the extraction of leftover value. The problems that may be attributed to such a dynamic mining and post-mining landscape are for example the generation of acid mine drainage, metal transport in surface

water and groundwater, e.g., iron precipitation in water bodies, major subsidence and migration of tailings material to the neighbouring settlements. These may dramatically affect the existing natural cover, land use practices and the lives of the people in such a mining area, where the former settlements of the mineworkers have grown into these large economically thriving urban centres, which attracts people from rural parts of South Africa. The land-use in these population centres, e.g. for recreation, farming, and housing, conflicts with the future, current and former usage of the land by the mineral resource industry. The above listed problems and conflict faced in the country due to changes in land use practices / land cover severely affects the environment in complex ways, leading to complex situations that impact the ecological security for sustainable development/generation.

Freely available remote sensing datasets made available through optical satellites such as Advanced Space-borne Thermal Emission and Reflection (ASTER) radiometer, Landsat and Sentinel-2 are being widely used in land cover studies and monitoring as they aid in discriminating various land covers and land uses. This study aimed to conduct environmental monitoring and assessment of the current (year 2020) land use / land cover and one year ago (year 2019) of Klerksdorp–Orkney–Stilfontein–Hartebeestfontein or KOSH using geospatial technologies and remote sensing, using optical data from Sentinel-2 satellite. This research intended to make use of existing satellite-based land-cover products, recent satellite data to investigate how land use change and vegetation disturbances has altered during 2018 to 2020.

Presented here are the results obtained from different remote sensing data processing & analyses conducted on Sentinel-2 data covering the Klerksdorp–Orkney–Stilfontein–Hartebeestfontein (KOSH) region acquired in March 2020 and March 2019 using different tools available in SNAP and Geomatica software (using Object Analyst module) and their usefulness to aid in understanding the current land use / land cover classes and their dynamics.

Area of research and its characteristics

The area chosen initially for the environmental monitoring is the Klerksdorp–Orkney–Stilfontein–Hartebeestfontein (KOSH) region in the Northwest Province of South Africa, covering an area of 2755 km² and falling within the Vaal River catchment (fig. 1). The KOSH area is located approximately 160 km southwest of Johannesburg. The Vaal River flows through the south-eastern part of the KOSH region. The majority of the KOSH area has a sandy loam soil texture with an undulating relief, whereas the relief of the region south of Orkney is flat (Midgley, Pitman and Middleton, 1994). The KOSH region forms part of the Witwatersrand gold mining region, including the Far East, Central Rand, Western and Far West basins and the Free State gold mines, and which is at serious risk from acid mine drainage (Mail&Guardian, 2014).

Gold mining operations by a number of different gold mining companies have been undertaken in the KOSH area since 1950s (SAFLII, 2013). Gold mining entails the construction of shafts, underground tunnels and the excavation of rocks to access gold-bearing ore. Many years of gold mining have resulted in the underground interconnection of all the mines in the KOSH area. The labyrinth of interconnecting tunnels, shafts, mined-out areas and natural fissures have created a pathway through which the underground water flows from the aquifers into the shallower mines and shafts and from there into the deeper areas. It is an undisputed fact that mining of gold in the KOSH area over the years has contributed to the drainage of underground water into the mines. Thus, mining companies are spending huge amounts of money to pump water out of their mines. The area has a number of sinkholes in the vicinity of Buffelsfontein's Eastern Shaft that have developed as a result of the lowering of the water table following dewatering (Pulles et al., 2005).

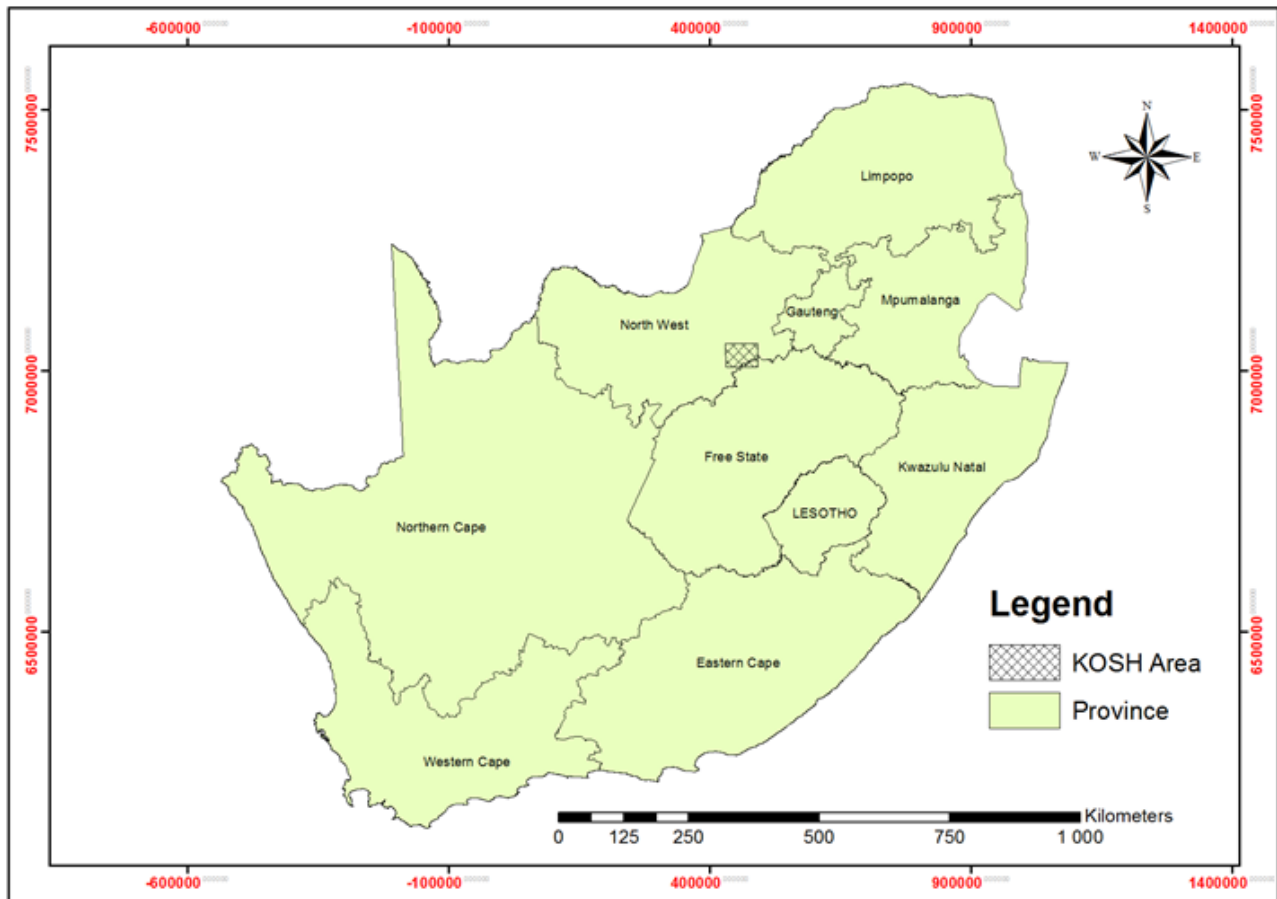


Fig. 1. Locality map of the KOSH area

Geological background of study area

The KOSH area is underlain mainly by an intercalated assemblage of sedimentary and extrusive rocks, porous unconsolidated and consolidated sedimentary strata, acid and intermediate intrusive rocks and basic/mafic lavas (such as dolomite, gold-bearing conglomerates, Black Reef quartzite, Ventersdorp lavas and dykes) and has shallow aquifers containing uncontaminated water relatively close to the surface (Midgley et al., 1994).

Materials and methods of research

Data and software used for remote sensing analyses

The satellite data used in this study comprised the Sentinel-2 satellite image having 13 optical image bands spanning from the Visible and Near Infra-Red (VNIR) and Short Wave Infrared (SWIR) spectral range having resolutions of 10m, 20 and 60 respectively. Multi Spectral Instrument (MSI) of Sentinel-2 measures the Earth's reflected radiance in 13 spectral bands from VNIR to SWIR. Sentinel-2 data acquired on 13 spectral bands in the VNIR and SWIR regions has the following resolutions for its different bands:

- four bands at 10 m: Band 2, Band 3, Band 4, and Band 8.
- six bands at 20 m: Band 5, Band 6, Band 7, Band 8a, Band 11, and Band 12
- three bands at 60 m: Band 1, Band 9, and Band 10.

Recent scenes of Sentinel-2 data covering the study area of KOSH region were searched in the Copernicus Scientific Data Hub (<https://scihub.copernicus.eu/dhus/#/home>) and two suitable cloud free images for the end of summer period (acquired on 10 March 2020 and 16 March 2019) were identified and downloaded them.

Software used for the analyses

The software used in this study are the following: the Sentinel Application Platform, known as SNAP Toolbox, developed by the European Space Agency (ESA), PCI Geomatica with its add on module Object Analyst, ArcGIS and Google Earth Pro. SNAP stands for “SeNtinels Application Platform” and it is a fully free and open-source toolbox platform that supports processing of raster imagery from ESA, Copernicus Sentinel 1/2/3, and many third party satellite missions (ESA-STEP, 2018). Object Analyst is an add-on package for PCI Geomatica software that provides tools for segmentation, classification, and feature extraction.

Product type of downloaded Sentinel-2 data

The downloaded Sentinel-2 data is a Level-1C product composed of 100 x 100 km² tiles comprising 13 bands (ortho-images) in a UTM projection. Per-pixel radiometric measurements of this data are provided in Top Of Atmosphere (TOA) reflectance along with the parameters to transform them into radiances. Level-1C products are resampled with a constant Ground Sampling Distance (GSD) or resolutions of 10, 20 and 60 m depending on the native resolution of the different spectral bands. As the Level-1C Sentinel -2 has already undergone radiometric and geometric correction, the main pre-processing required for this data is atmospheric correction to produce ground surface reflectance.

Initial data processing using SNAP software

The downloaded Sentinel-2 data was imported in SNAP software and processed for atmospheric correction using Sen2Cor software plugin installed in it. Sen2Cor is a processor for Sentinel-2 Level 2A product generation and formatting; it performs the atmospheric-, terrain and cirrus correction of TOA Level 1C input data. This step converted the Level-1C product type (having top of the atmosphere reflectance) to Level-2A data having surface reflectance. The Level 2 VNIR bands were saved in tiff file format. The extent of coverage of the pre-processed VNIR scene acquired on 10 March 2020 is shown in Figure 2. Later, this data set was subsetted for the area of interest covering the KOSH region using its geo-coordinate bounds (Figure 3). Similarly, the Sentinel-2 scene acquired on 16 March 2019 was processed to Level 2 and subsetted for the area of KOSH region (Figure 4). Figure 3 shows the satellite view of the KOSH region as seen through Sentinel-2 on 10 March in RGB: Band 4-Band 3-Band 2. Figure 4 shows the same area as seen through VNIR bands in RGB: Band 4- Band 3-Band 2 of the same satellite acquired on 16th March 2019.

Other dataset used

Other datasets used in this study are the National Land Cover (NLC) 2018 dataset covering KOSH having 20 m resolution derived from Sentinel-2 data of year 2017-2018 and Google Earth Pro Images of different years (mainly years 2018, 2019 and 2020). Figure 5 shows National Land Cover (NLC) 2018 data extracted for the KOSH region and the legend for this map is shown in Figure 6. There are 56 land cover types present in the subset of NLC 2018 covering the KOSH region. The original legend of the dataset has 73 land cover classes. The description of these land cover classes is given in Thompson (2019).

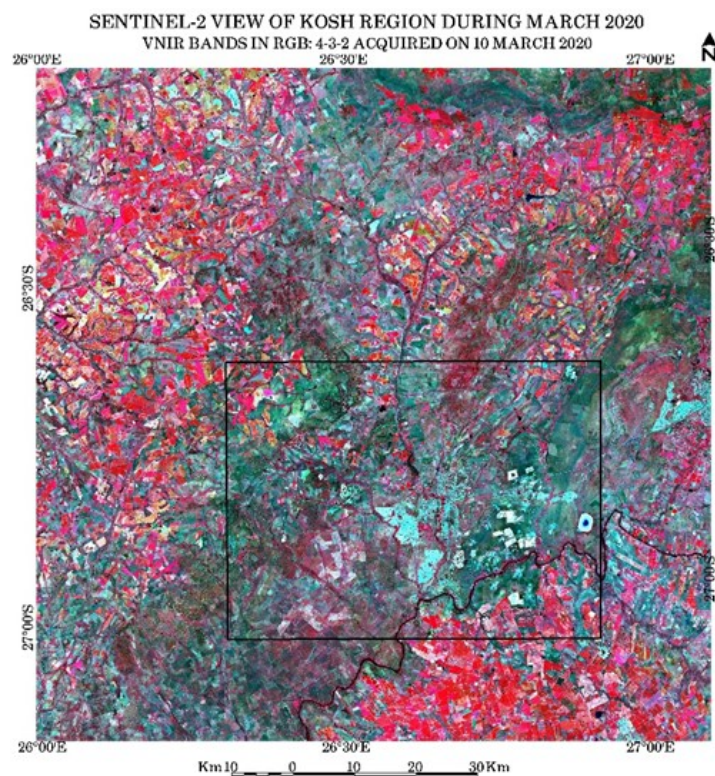


Fig. 2. The extent of full scene of Sentinel-2 imagery (VNIR bands in RGB: B4-B3-B2) acquired on 10 March 2020 overlaid with a polygon covering the extent of KOSH region

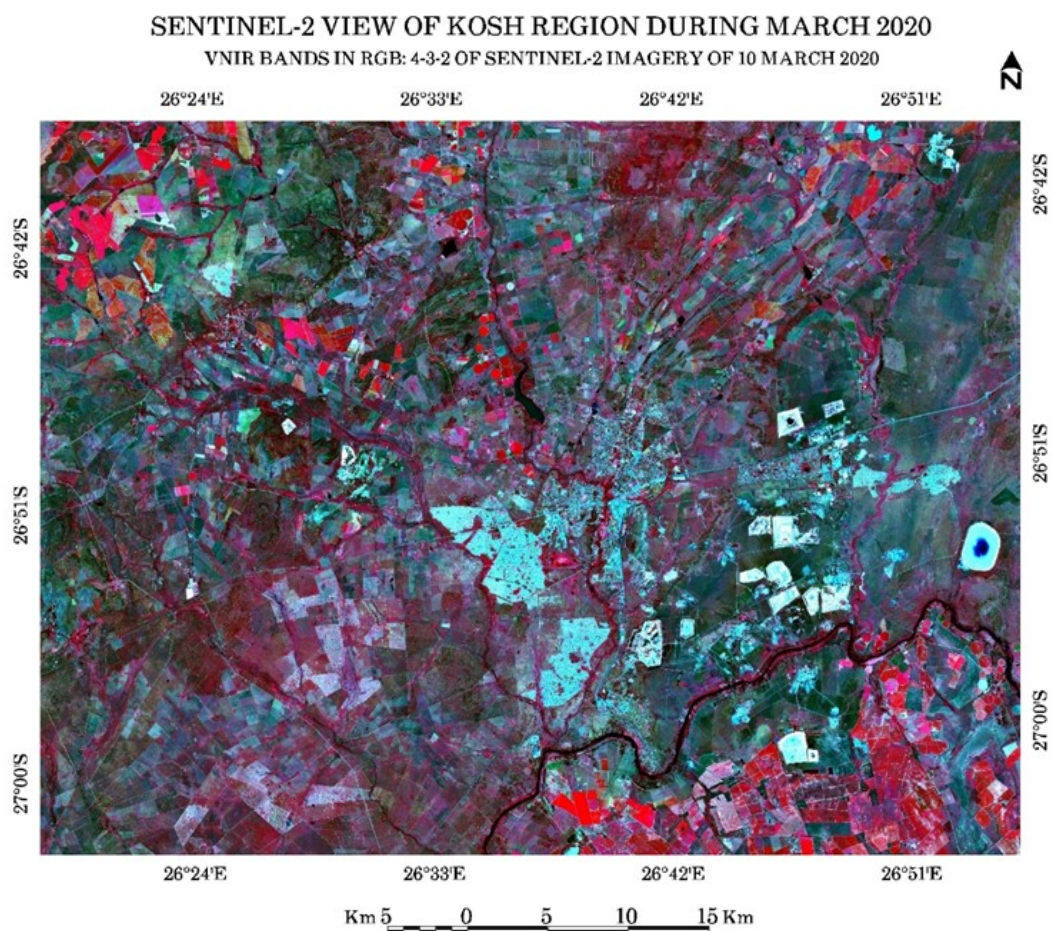


Fig. 3. Subset of Sentinel-2 imagery (VNIR bands in RGB: B4-B3-B2) acquired on 10 March 2020 covering the extent of KOSH region.

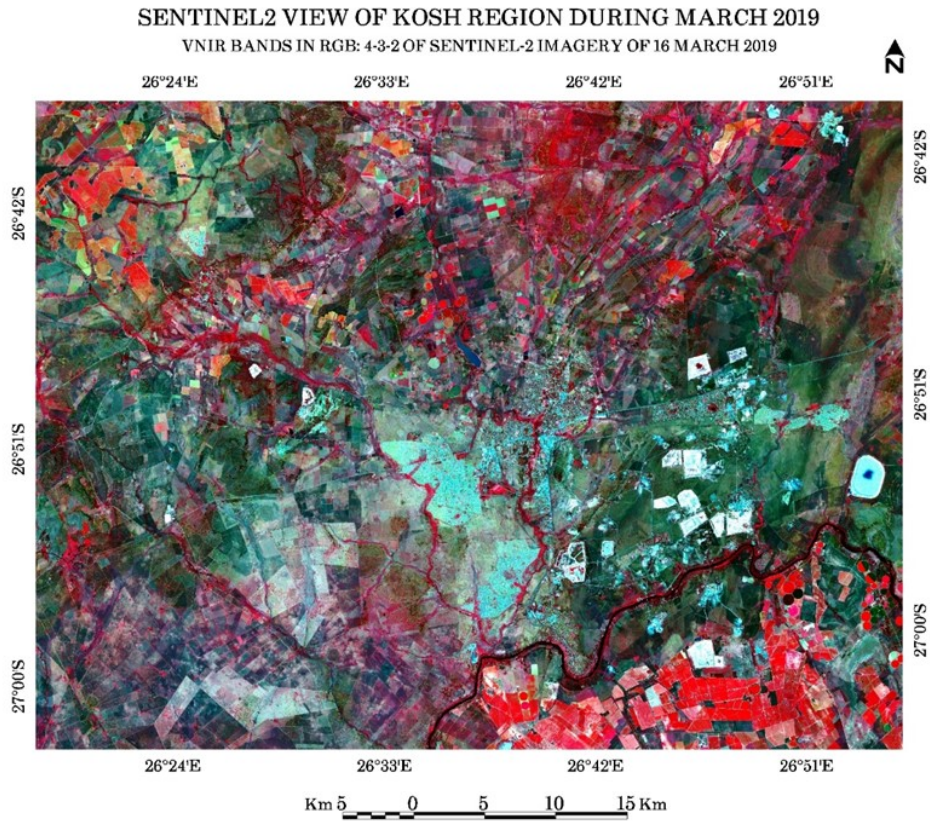


Fig. 4. Subset of Sentinel-2 imagery (VNIR bands in RGB: B4-B3-B2) acquired on 16 March 2019 covering the extent of KOSH region

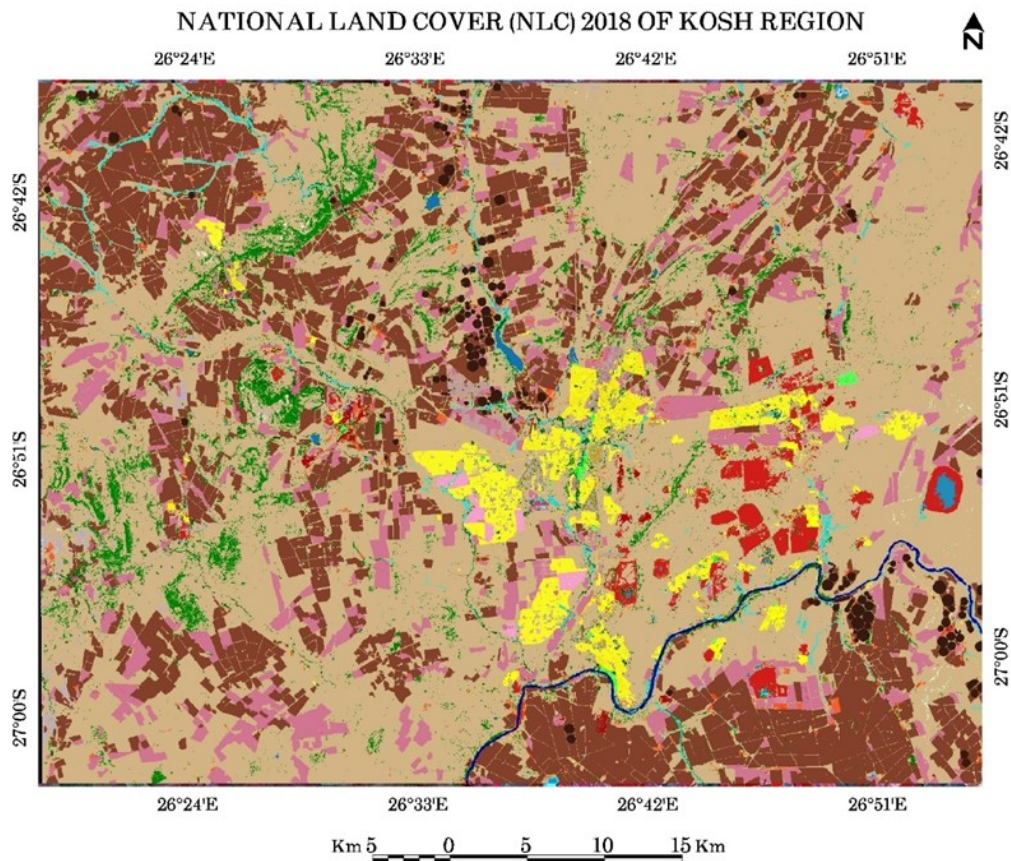


Fig. 5. The National Land Cover (NLC) 2018 dataset covering the extent of KOSH region

Class Name	Color	Class Name	Color
19 Artificial Dams / Waterbodies (19)		59 Smallholdings (low veg / grass) (59)	
14 Natural Waterbodies (14)		60 Smallholdings (Bare) (60)	
38 Cultivated Commercial Annuals Pivot Irrigated (38)		50 Residential Formal (Bare) (50)	
40 Temporary Crops-rainfed (40)		7 Temporary Unplanted Forest (7)	
13 Natural Grassland (13)		8 Low Shrubland (other regions) (8)	
4 Open Woodland (4)		12 Sparsely Wooded Grassland (12)	
44 Fallow Lands _Old Fields_Grass (44)		18 Natural Pans (flooded) (18)	
22 Herbaceous Wetlands (currently mapped) (22)		20 Artificial Sewage Ponds (20)	
49 Residential Formal (low veg / grass) (49)		21 Artificial Flooded Mine Pits (21)	
6 Open _Sparse Planted Forest (6)		23 Herbaceous Wetlands (previous mapped extent) (23)	
5 Contiguous _Dense Planted Forest (5)		25 Natural Rock Surfaces (25)	
68 Mines: Surface Infrastructure (68)		26 Dry Pans (26)	
69 Mines: Extraction Sites: Open Cast _Quarries combined (69)		27 Eroded Lands (27)	
71 Mines: Waste (Tailings) _Resource Dumps (71)		30 Bare Riverbed Material (30)	
67 Roads _Rail (Major Linear) (67)		31 Other Bare (31)	
47 Residential Formal (Tree) (47)		32 Cultivated Commercial Permanent Orchards (32)	
48 Residential Formal (Bush) (48)		39 Cultivated Commercial Annuals Non-Pivot Irrigated (39)	
3 Dense Forest _Woodland (3)		42 Fallow Land _Old Fields (Trees) (42)	
2 Contiguous Low Forest _Thicket (2)		43 Fallow Land _Old Fields (Bush) (43)	
57 Smallholdings (Tree) (57)		45 Fallow Land _Old Fields (Bare) (45)	
58 Smallholdings (Bush) (58)		46 Fallow Land _Old Fields (Low Shrub) (46)	

51 Residential Informal (Tree) (51)	
53 Residential Informal (low veg / grass) (53)	
54 Residential Informal (Bare) (54)	
52 Residential Informal (Bush) (52)	
55 Village Scattered (55)	
56 Village Dense (56)	
61 Urban Recreational Fields (Tree) (61)	
62 Urban Recreational Fields (Bush) (62)	
63 Urban Recreational Fields (Grass) (63)	
64 Urban Recreational Fields (Bare) (64)	
65 Commercial (65)	
66 Industrial (66)	
72 Landfills (72)	
73 Fallow Land _Old Fields (wetlands) (73)	

Fig. 6. Legend of the National Land Cover (NLC) 2018 dataset covering the KOSH region

A visual examination of the VNIR bands of Sentinel-2 data acquired on 10 March 2020 (Figure 3) with 2018 NLC data (Figure 5) reveals that there is some change in the extent of some land covers (e.g. change of grassland to agricultural use) during the last two years.

Image analysis for land use / land cover classification using Geomatica Object Analyst

A simple process flow for object-based image analysis (OBIA) is using Geomatica Object Analyst involves pre-processing of image, image segmentation, classification and post classification analysis. As the pre-processing and subsetting were already made using SNAP, the remaining steps of image segmentation classification and post classification analysis were carried out in Geomatica software using Object Analyst add on module. The first attempt made was to map land covers for the KOSH region using Sentinel-2 data acquired on 10 March 2020 based on the classification system followed in the National Land Cover (NLC) dataset of 2018 (after identifying 56 classes present in the subset of NLC 2018 for KOSH) using the Trial License of Geomatica Object Analyst module and Sentinel-2 data. The main steps to be followed in the workflow of image classification using Geomatica Object Analyst are the following: loading and examining input data, segmentation of the input data into a vector layer for training site generation and image classification, attribute calculation for image classification, training site editing, selection of classification method: whether supervised or unsupervised (supervised classification involves selection of the identified training sites) and post classification editing.

Segmentation is the process of extracting discrete regions of image objects from an image. The segmentation involves creating a vector layer showing boundaries of various objects present in the area of interest with specified bands of the imagery. The parameter values to be entered for the segmentation are scale, shape and compactness. The attribute calculation involves calculation of geometrical parameters (compactness, elongation, circularity and rectangularity), calculation of mean and standard deviation of the pixels beneath an object from the selected bands and calculation of vegetation indices attributes (e.g. NDVI, Leaf Area Index etc.). The vegetation indices that can be calculated using Object Analyst are shown in table 5.

Table 1

Descriptions of each Vegetation Index that can be calculated using Geomatica Object Analyst.

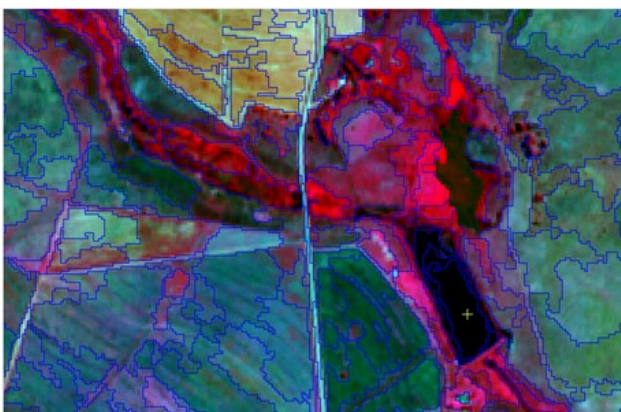
Attribute	Short name	Description
Green/Red Vegetation Index	GRVI	$GRVI = (Green - Red) \div (Green + Red)$
Greenness Index	GI	$GI = ((2.0 \times Green) - (Red + Blue)) \div ((2.0 \times Green) + Red + Blue)$
Vegetation Difference Index	VDI	$VDI = NIR - Red$
Ratio Vegetation Index	RVI	$RVI = NIR \div Red$
Normalized Difference Vegetation	NDVI	$NDVI = (NIR - Red) \div (NIR + Red)$
Transformed Difference Vegetation Index	TDVI	$TDVI = (NIR - Red) \div (NIR + Red) + .5$
Soil Adjusted Vegetation Index	SAVI	$SAVI = ((NIR - Red) \div (NIR + Red + L)) \times (1 + L)$ The L-value is based on the amount of green vegetative cover. L is a default of 0.5, which means, generally, areas of moderate green vegetative cover.
Modified Soil Adjusted Vegetation Index	MSAVI2	$MSAVI2 = (0.5) \times (2(NIR + 1) - \sqrt{(2 \times NIR + 1) - 8(NIR - Red)})$
Global Environmental Monitoring Index	GEMI	$GEMI = eta \times (1 - 0.25 \times eta) - ((Red - 0.125) \div (1 - Red))$ Where $eta = (2 \times (NIR - Red) + 1.5 \times NIR + 0.5 \times Red) \div (NIR + Red + 0.5)$
Leaf Area Index	LAI	$LAI = (3.618 \times EVI) - 0.118$ Where EVI (Enhanced Vegetation Index) $= 2.5 \times (NIR - Red) \div (1 + NIR + (6 \times Red) - (7.5 \times Blue))$

Source: PCI-Geomatics (2017).

The task of identifying training sites involves viewing of the image and interpreting the features present in it and giving proper names for the intended classes from the segmented vector layer.

The existing NLC 2018 data of KOSH region has 56 land cover classes. While generating training sites, the description of each such present land cover class was read to identify the corresponding classes from the image. Other useful data like existing Google Earth Pro imagery of different dates (since year 2014 and until May 2020) and NLC 2018 were also viewed while identifying the land cover types and assigning class names to the training site polygons. An example view of training site identification from zoomed segmented vector layer and zoomed view of Google Earth image for certain land cover classes are shown in Figure 7. Efforts were made to zoom into the image for different distant locations and identify at least 20 to 30 training sites for each class for an accurate classification of the image. Some land cover classes like landfill, bare river bed material and informal settlement (having trees or bush) have only limited numbers in the area of study for training site; the only available such sites (sometimes only single site is present) were marked as training sites. While examining the NLC 2018 data covering the KOSH region for training site identification, numerous errors were observed in this classified product. A few example errors observed are the following types:

- Class 61 Urban Recreational Fields (Grass) is classified as Class 3: Dense woodland (Fig. 8 and Fig. 9).
- Agricultural crop land classified as Class 3: Dense woodland (Fig. 10 and Fig. 11).



(a). Zoomed view of segmented polygons.



(b). Google Earth Pro view (27 June 2019).

Figure 7. Zoomed view of segmented polygons from Object Analyst overlaid with Sentinel-2 image of 10 March 2020 (a); Google Earth image of 27 June 2019 for marking training sites (b)

The study area was thoroughly examined in Google Earth Pro along with side by side displaying of the satellite image and the existing NLC 2018 dataset. In order to improve the classification accuracy, more typical patches classes were identified from the segmented vector as training sites. Any errors seen in the identification of land cover classes of the previously identified training sites were also edited in this step. The corresponding display colours of the classes of NLC 2018 in RGB were identified and assigned those colours to each class identified as training site. The assigned colours for different land use / land cover classes and the total number of training sites identified for the supervised classification using Geomatica Object Analyst for the 56 land cover classes present in the KOSH region based on the classes seen in the NLC 2018 dataset is shown in figure 12 to figure 14.

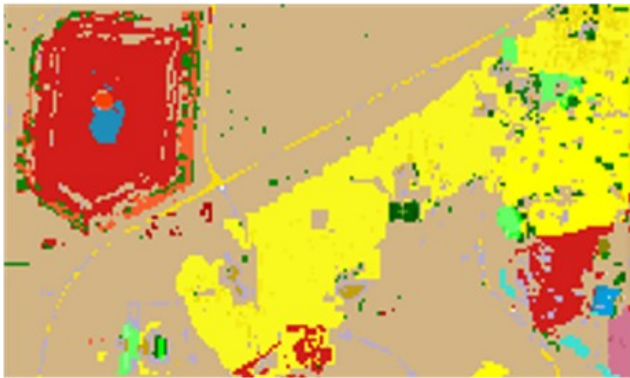


Fig. 8. Class 61: Urban Recreational Fields with grass (green patch) classified as Class 3: Dense forest & woodland in NLC 2018



Fig. 9. View of 10 March 2020 Sentinel-2 image confirming errors seen in NLC 2018 (grassy recreation area classified as woodland)



Fig. 10. Error of agricultural crop land classified as Class 3: Dense woodland in NLC 2018 data covering KOSH region



Fig. 11. Google Earth Pro image confirming errors observed in the classes of NLC 2018 (agricultural field area classified as woodland)

Class Name	Color	Training Count
19 Artificial Dams / Waterbodies (19)		66
14 Natural Waterbodies (14)		90
38 Cultivated Commercial Annuals Pivot Irrigated (38)		588
40 Temporary Crops-rainfed (40)		2717
13 Natural Grassland (13)		1905
4 Open Woodland (4)		319
44 Fallow Lands _Old Fields _Grass (44)		773
22 Herbaceous Wetlands (currently mapped) (22)		64
49 Residential Formal (low veg / grass) (49)		372
6 Open _Sparse Planted Forest (6)		50
5 Contiguous _Dense Planted Forest (5)		56
68 Mines: Surface Infrastructure (68)		76
69 Mines: Extraction Sites: Open Cast _Quarries combined (69)		136
71 Mines: Waste (Tailings) _Resource Dumps (71)		1639
67 Roads _Rail (Major Linear) (67)		166
47 Residential Formal (Tree) (47)		183
48 Residential Formal (Bush) (48)		60
3 Dense Forest _Woodland (3)		160
2 Contiguous Low Forest _Thicket (2)		46
57 Smallholdings (Tree) (57)		57
58 Smallholdings (Bush) (58)		45

Fig. 12. Part one of total training sites identified for the KOSH region using Object Analyst for the classification of 3 March 2020 Sentinel-2 image

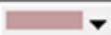
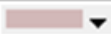

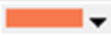
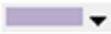




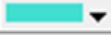











Class Name	Color	Training Count
59 Smallholdings (low veg / grass) (59)		48
60 Smallholdings (Bare) (60)		18
50 Residential Formal (Bare) (50)		559
7 Temporary Unplanted Forest (7)		10
8 Low Shrubland (other regions) (8)		180
12 Sparsely Wooded Grassland (12)		148
18 Natural Pans (flooded) (18)		9
20 Artificial Sewage Ponds (20)		11
21 Artificial Flooded Mine Pits (21)		7
23 Herbaceous Wetlands (previous mapped extent) (23)		95
25 Natural Rock Surfaces (25)		52
26 Dry Pans (26)		10
27 Eroded Lands (27)		10
30 Bare Riverbed Material (30)		5
31 Other Bare (31)		58
32 Cultivated Commercial Permanent Orchards (32)		8
39 Cultivated Commercial Annuals Non-Pivot Irrigated (39)		306
42 Fallow Land _Old Fields (Trees) (42)		61
43 Fallow Land _Old Fields (Bush) (43)		83
45 Fallow Land _Old Fields (Bare) (45)		47
46 Fallow Land _Old Fields (Low Shrub) (46)		66

Fig. 13. Part two of total training sites identified for the KOSH region using Object Analyst for the classification of 3 March 2020 Sentinel-2 image



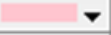


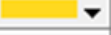








Class Name	Color	Training Count
51 Residential Informal (Tree) (51)		8
53 Residential Informal (low veg / grass) (53)		54
54 Residential Informal (Bare) (54)		46
52 Residential Informal (Bush) (52)		1
55 Village Scattered (55)		6
56 Village Dense (56)		15
61 Urban Recreational Fields (Tree) (61)		44
62 Urban Recreational Fields (Bush) (62)		23
63 Urban Recreational Fields (Grass) (63)		165
64 Urban Recreational Fields (Bare) (64)		18
65 Commercial (65)		331
66 Industrial (66)		409
72 Land-fills (72)		1
73 Fallow Land _Old Fields (wetlands) (73)		24

Fig. 14. Part three of total training sites identified for the KOSH region using Object Analyst for the classification of 3 March 2020 Sentinel-2 image

Figure 15 shows the spatial distribution and the extent of identified training sites for the 56 classes present in the KOSH region.

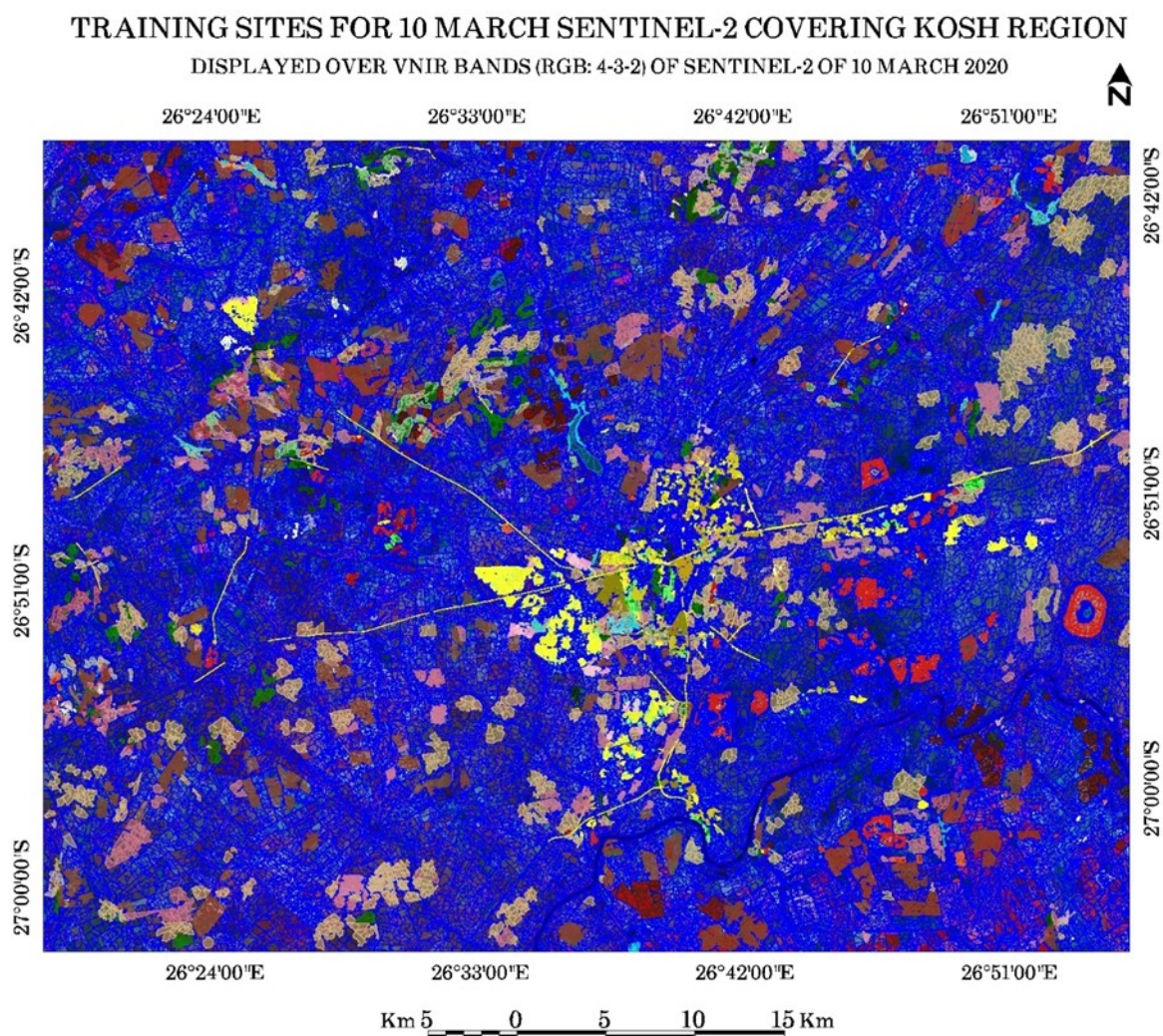


Fig. 15. Spatial distribution of training sites identified from the segmentation vector for the 3 March 2020 Sentinel-2 image covering KOSH region (overlaid with Sentinel-2 imagery)

Results and discussion

Many attempts of making supervised classification results were made in Object Analyst with different input options such as mean of four bands and NDVI, standard deviation and mean of four bands with all 10 available vegetation indices, standard deviation of 4 bands and all 10 vegetation indices, standard deviation of 4 bands, 10 vegetation indices and three geometric parameters (circularity, elongation and rectangularity) and standard deviation of 4 bands, 10 vegetation indices, elongation and circularity and finally with the inputs of standard deviation of 4 bands and 10 vegetation indices and elongation. The classification result obtained for the inputs of mean of four bands and NDVI from 10 March 2020 is shown in figure 16. Though this result showed better results for most of the areas including the urban part, some areas in the east and north-east were misclassified as residential patches with grassland cover wherein the real land use / land cover is cover is natural only grassland. Hence this result is not good to consider for a comparison with 2018 data. A better result of classification obtained for the year 2020 was with the attribute combination of standard deviation of 4 bands, and 10 vegetation indices (fig. 17).

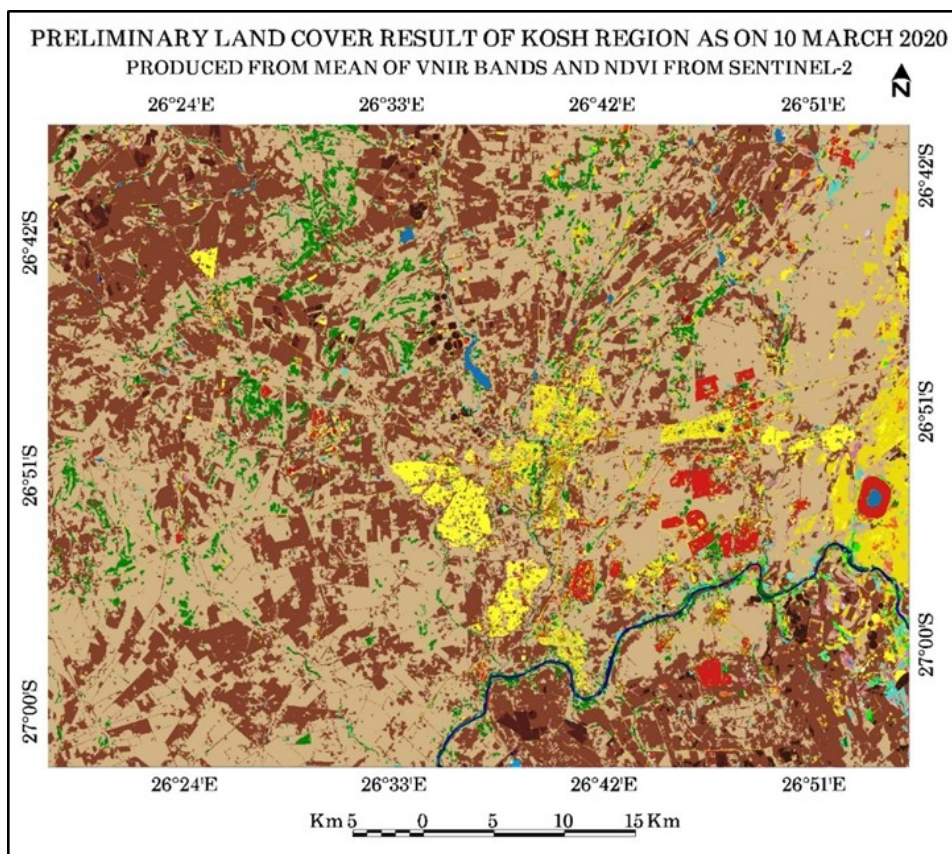


Fig. 16. Preliminary classification result obtained for 10 March 2020 with inputs of mean of 4 bands and NDVI values

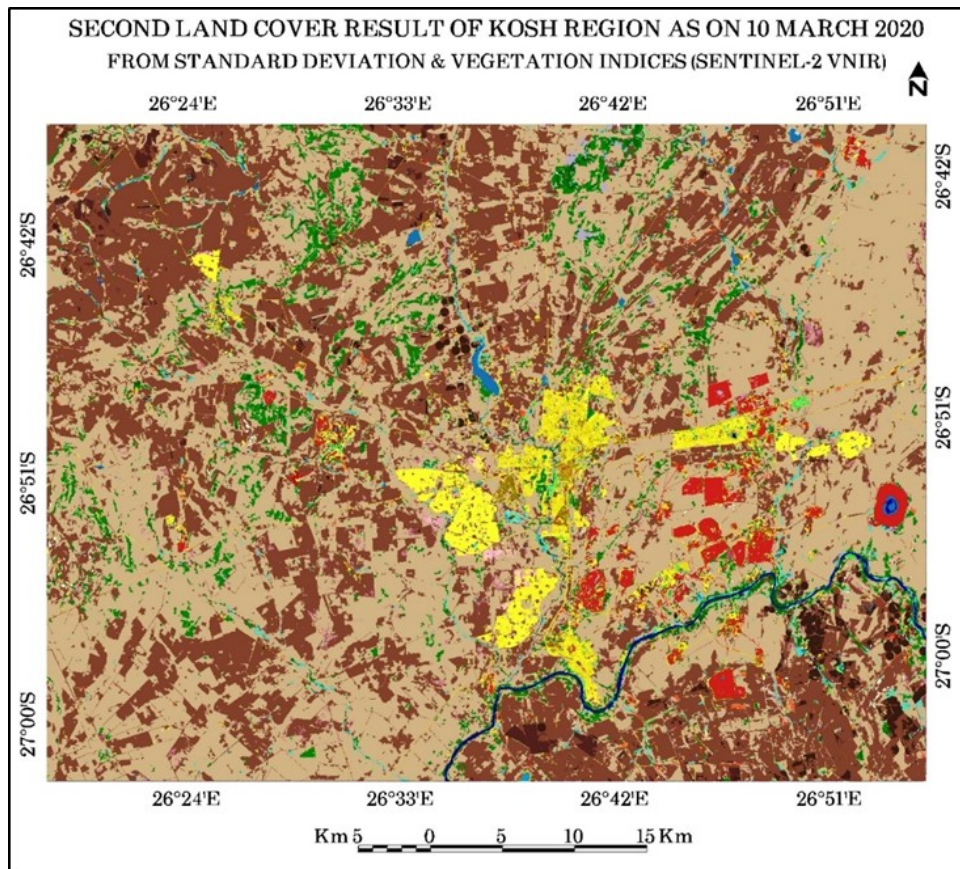


Fig. 17. Second classification result obtained for 10 March 2020 with inputs of standard deviation of 4 bands and ten vegetation indices values

On further examining this classification result by zooming into it some wrong classes or errors were noticed in the urban areas and surrounding areas of Klerksdorp. Many patches of urban residential, industrial and commercial sites were misclassified as mining dumps, some commercial areas were classified as industrial areas, and similarly some commercial and residential areas were classified as industrial areas. Due to similarities in pixel values of industrial & commercial and mining dumps, some sites in urban area were classified as these areas. More training sites were needed to distinguish such areas in the urban areas and surrounding areas of Klerksdorp. A zoomed view of urban area and surrounding areas of Klerksdorp showing such errors is shown in Figure 18. A comparison of the same area portion with the NLC 2018 data (fig. 19) reveals that the classification result is having similarity in many sites while certain areas were showing with more details than the NLC 2018 (especially in the residential, commercial and industrial areas). The major road network in this classified product is also much clearer as compared to the one seen in the NLC 2018 data. The extent of class 44 (fallow fields currently having grassland) is much less in the land use / land cover obtained for the year 2020 when compared with the 2018 NLC data.

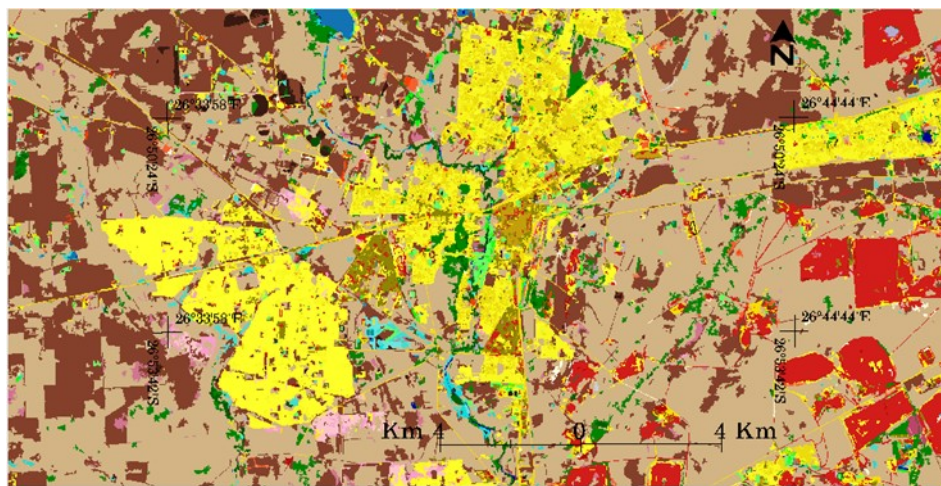


Fig. 18. Classification result of 10 March 2020 using standard deviation of 4 bands and 10 vegetation indices values showing some wrong classes in the urban areas and surrounding areas of Klerksdorp

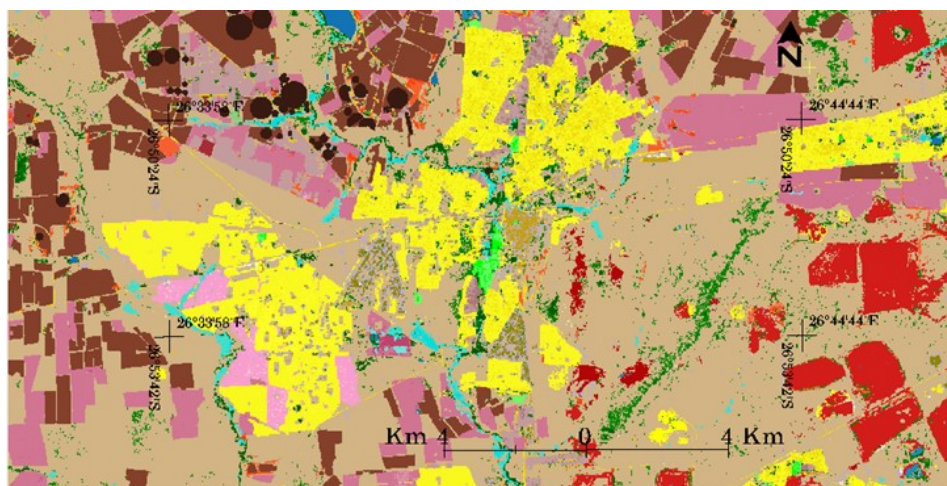


Fig. 19. Portion of NLC 2018 dataset covering urban and surrounding areas of Klerksdorp

A zoomed Sentinel-2 view of the urban and surrounding of the Klerksdorp was examined to identify and locate the misclassified segments. The misclassified patches were further selected and edited (re-assigned correct classes) after viewing those areas in the satellite image and Google Earth Pro image of the same year. A view of zoomed portion of Klerksdorp area as seen through the March 2020 satellite image, and the re-assigned (corrections made) portion of the same area

are shown in Figure 20. Some areas seen around the sites of mine dumps and mine surface infrastructure and exaction sites were also misclassified as other classes mainly Class 66 Industrial, Class 50 Residential Formal (Bare) and Class 49 Residential Formal (low veg / grass) due to similarities of the attribute values. There were many such misclassified small segments and all such sites were edited. It was a very time consuming task to distinguish such areas belonging to Class 68 Mines Surface Infrastructure (having yellow colour shades) with residential areas having similar yellow colour shades. On examining the total number of classes identified from the classification product, it was noticed that only 54 classes were mapped and two land cover classes viz. Class 32 Cultivated Commercial Permanent Orchards and Class 52 Residential Informal (Bush) were not classified or missing. The patches of these classes were identified by examining the NLC 2018 data, the Google Earth Pro images and the Sentinel-2 image and such areas were located and the corresponding polygon segments were reassigned with correct class names.

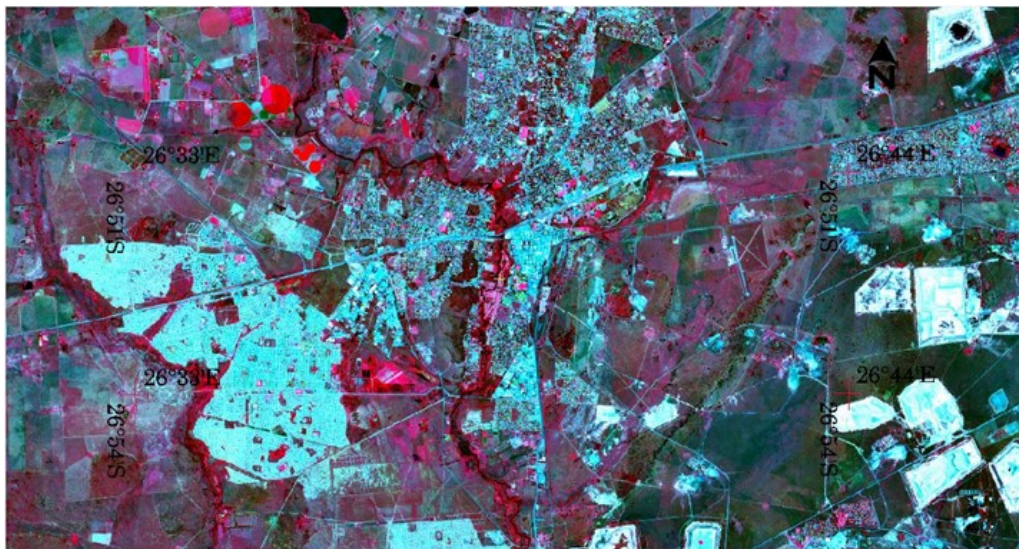


Fig. 20. A view of Klerksdorp and surrounding areas as seen through the Sentinel-2 on 10 March 2020

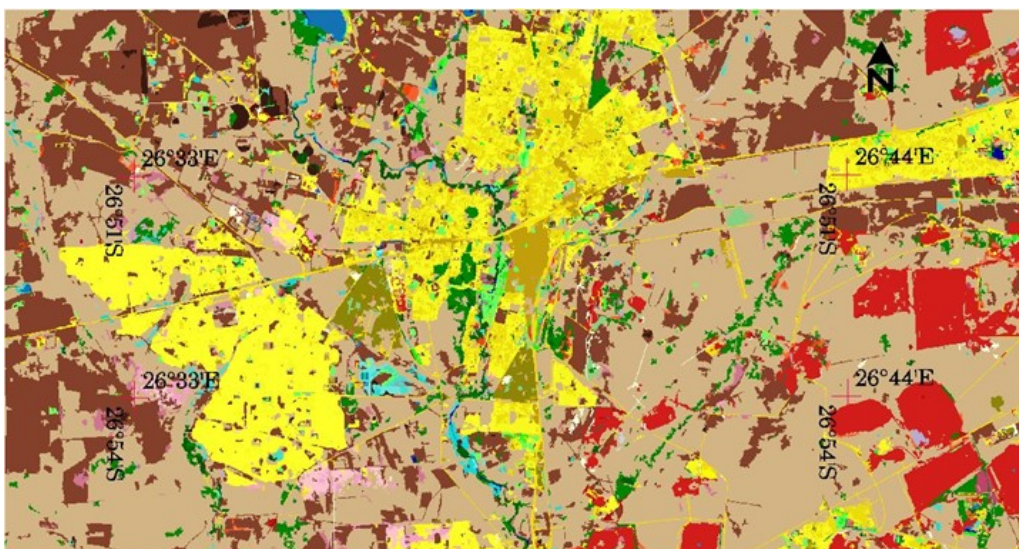


Fig. 21. A view of Klerksdorp and surrounding areas showing re-assigned (corrected) patches of land cover classification result

After doing re-assigning or editing of misclassified patches of the urban and peripheral area areas, mine dump areas, and the missing two classes, the final result of land use / land cover mapping obtained is shown in figure 22. The legend with 56 classes are shown in figure 23.

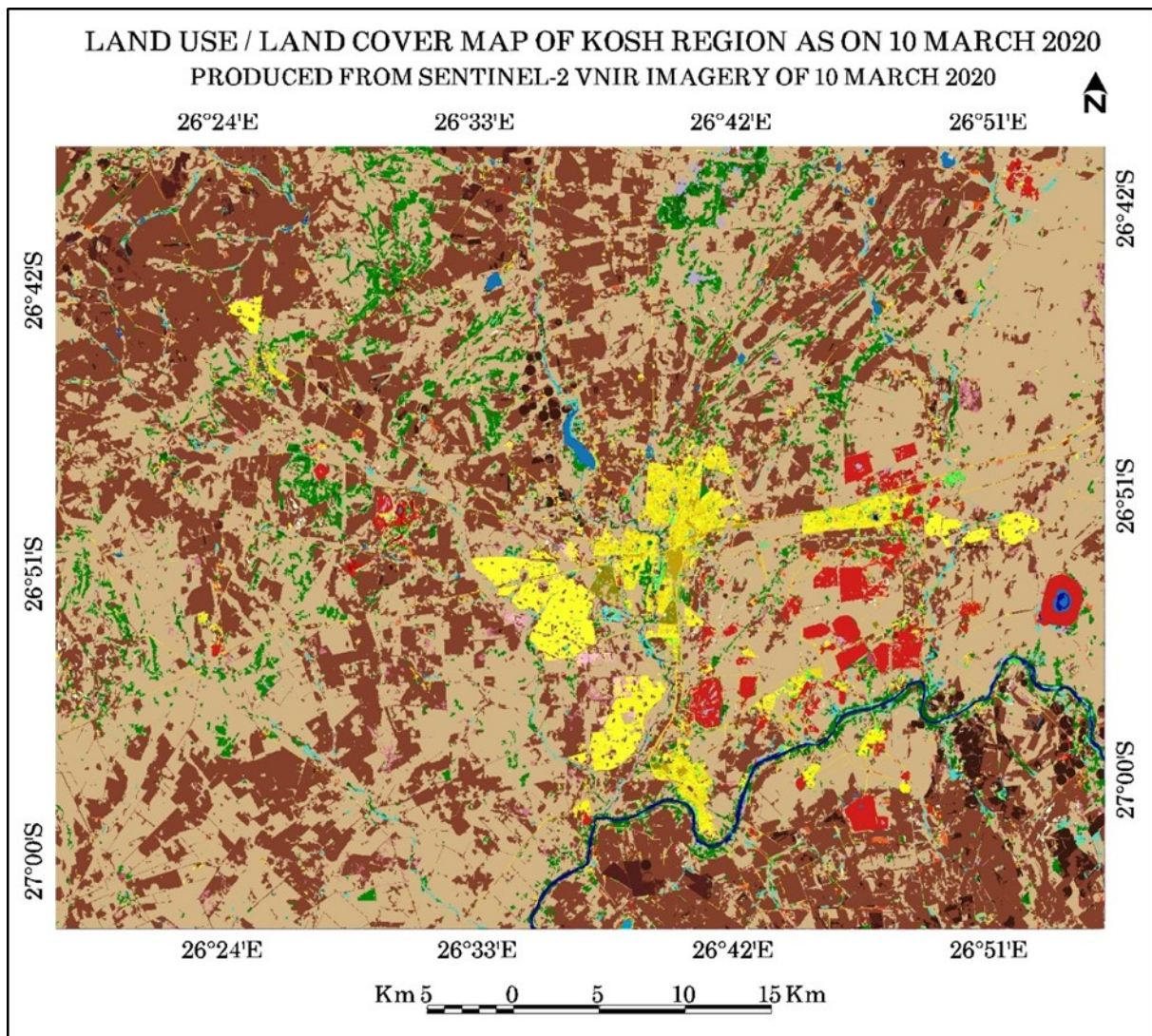


Fig. 22. Final land use / land cover map of KOSH region (after re-assigning of classes) obtained from Sentinel-2 data of 10 March 2020 with inputs of standard deviation of 4 bands and 10 vegetation indices

Comparison of land use / land cover classes for year 2020 with NLC 2018

A comparison of the final result of land use / land cover mapping for the year 2020 (fig. 22) with the NLC 2018 of KOSH region (fig. 4) reveals that land use / land cover map of year 2020 has more forest patches (open woodland patches) in the north, mining dumps and rain-fed agricultural fields whereas NLC 2018 of KOSH region has more patches of Class 44 Fallow Land & Old Fields _Grass (shown in light pink shade). The NLC 2018 is a smoothed 20 m resolution product whereas this map of 10 m is not smoothed. The number of patches of class 44 (Fallow Land & Old Fields currently with Grassland) is significantly reduced in this classification result for the year 2020. This is evident in the area figures of the major classes from the NLC 2018 showing a percentage of 7.95% for Class 44 (table 2) and area figure of 0.52% for Class 44 calculated for the land use / land cover map for the year 2020 (table 3).

Legend

2 Contiguous Low Forest & Thicket (2)		44 Fallow Lands & Old Fields_Grass (44)	
3 Dense Forest & Woodland (3)		45 Fallow Land & Old Fields (Bare) (45)	
4 Open Woodland (4)		46 Fallow Land & Old Fields (Low Shrub) (46)	
5 Contiguous & Dense Planted Forest (5)		47 Residential Formal (Tree) (47)	
6 Open & Sparse Planted Forest (6)		48 Residential Formal (Bush) (48)	
7 Temporary Unplanted Forest (7)		49 Residential Formal (low veg / grass) (49)	
8 Low Shrubland (other regions) (8)		50 Residential Formal (Bare) (50)	
12 Sparsely Wooded Grassland (12)		51 Residential Informal (Tree) (51)	
13 Natural Grassland (13)		52 Residential Informal (Bush) (52)	
14 Natural Waterbodies (14)		53 Residential Informal (low veg / grass) (53)	
18 Natural Pans (flooded) (18)		54 Residential Informal (Bare) (54)	
19 Artificial Dams / Waterbodies (19)		55 Village Scattered (55)	
20 Artificial Sewage Ponds (20)		56 Village Dense (56)	
21 Artificial Flooded Mine Pits (21)		57 Smallholdings (Tree) (57)	
22 Herbaceous Wetlands (currently mapped) (22)		58 Smallholdings (Bush) (58)	
23 Herbaceous Wetlands (previous mapped extent) (23)		59 Smallholdings (low veg / grass) (59)	
25 Natural Rock Surfaces (25)		60 Smallholdings (Bare) (60)	
26 Dry Pans (26)		61 Urban Recreational Fields (Tree) (61)	
27 Eroded Lands (27)		62 Urban Recreational Fields (Bush) (62)	
30 Bare Riverbed Material (30)		63 Urban Recreational Fields (Grass) (63)	
31 Other Bare (31)		64 Urban Recreational Fields (Bare) (64)	
32 Cultivated Commercial Permanent Orchards (32)		65 Commercial (65)	
38 Cultivated Commercial Annuals Pivot Irrigated (38)		66 Industrial (66)	
39 Cultivated Commercial Annuals Non-Pivot Irrigated (39)		67 Roads & Rail (Major Linear) (67)	
40 Temporary Crops-rainfed (40)		68 Mines: Surface Infrastructure (68)	
43 Fallow Land & Old Fields (Bush) (43)		69 Mines: Extraction Sites: Open Cast & Quarries combined (69)	
		71 Mines: Waste (Tailings) & Resource Dumps (71)	
		72 Land-fills (72)	
		73 Fallow Land & Old Fields (wetlands) (73)	

Fig. 23. Legend for the land use / land cover map of KOSH region prepared from Sentinel-2 data

Table 2

Area figures of the major classes from the NLC 2018 covering KOSH region

NLC 2018 Class	NLC2018 Code	Area (square m)	% Area
Natural grassland	13	1477709246	53,84%
Commercial annual crops rain-fed / dryland	40	621965313	22,66%
Fallow land & old fields (grass)	44	218126602	7,95%
Open woodland	4	99682011	3,63%
Residential formal (low veg / grass)	49	59050767	2,15%
Mine: tailings and resource dumps	71	42172445	1,54%
Commercial annual crops pivot irrigated	38	32203283	1,17%
Dense forest & woodland	3	27512798	1,00%
Low shrubland (other)	8	20322662	0,74%
Herbaceous wetlands (previously mapped)	23	18071345	0,66%
Open & sparse plantation forest	6	13731598	0,50%

Table 3

Area calculated for the different land use / land cover classes for the year 2020

1	13 Natural Grassland (13)	1 368 617 300	49,32%
2	40 Temporary Crops-rainfed (40)	913 123 000	32,90%
3	4 Open Woodland (4)	110 938 100	4,00%
4	71 Mines: Waste (Tailings) & Resource Dumps (71)	54 450 200	1,96%
5	49 Residential Formal (low veg / grass) (49)	42 396 900	1,53%
6	38 Cultivated Commercial Annuals Pivot Irrigated (38)	36 283 200	1,31%
7	50 Residential Formal (Bare) (50)	35 013 800	1,26%
8	3 Dense Forest & Woodland (3)	21 340 000	0,77%
9	47 Residential Formal (Tree) (47)	20 616 400	0,74%
10	67 Roads & Rail (Major Linear) (67)	18 490 300	0,67%
11	39 Cultivated Commercial Annuals Non-Pivot Irrigated (39)	16 359 500	0,59%
12	44 Fallow Lands & Old Fields Grass (44)	14 376 500	0,52%
13	23 Herbaceous Wetlands (previous mapped extent) (23)	11 774 000	0,42%
14	63 Urban Recreational Fields (Grass) (63)	9 129 300	0,33%
15	14 Natural Waterbodies (14)	8 430 900	0,30%
16	19 Artificial Dams / Waterbodies (19)	8 106 500	0,29%
17	22 Herbaceous Wetlands (currently mapped) (22)	7 313 600	0,26%
18	6 Open & Sparse Planted Forest (6)	7 072 100	0,25%
19	8 Low Shrubland (other regions) (8)	7 027 900	0,25%
20	66 Industrial (66)	6 700 200	0,24%
21	65 Commercial (65)	5 197 000	0,19%
22	12 Sparsely Wooded Grassland (12)	4 952 800	0,18%
23	31 Other Bare (31)	4 687 100	0,17%
24	5 Contiguous & Dense Planted Forest (5)	4 422 100	0,16%
25	61 Urban Recreational Fields (Tree) (61)	4 218 700	0,15%
26	69 Mines: Extraction Sites: Open Cast & Quarries combined (69)	3 811 000	0,14%
27	57 Smallholdings (Tree) (57)	3 489 500	0,13%
28	68 Mines: Surface Infrastructure (68)	3 261 200	0,12%
29	53 Residential Informal (low veg / grass) (53)	3 035 500	0,11%
30	25 Natural Rock Surfaces (25)	2 887 600	0,10%
31	54 Residential Informal (Bare) (54)	2 483 800	0,09%
32	58 Smallholdings (Bush) (58)	1 632 900	0,06%
33	48 Residential Formal (Bush) (48)	1 547 300	0,06%
34	2 Contiguous Low Forest & Thicket (2)	1 517 600	0,05%
35	42 Fallow Land & Old Fields (Trees) (42)	1 453 900	0,05%
36	73 Fallow Land & Old Fields (wetlands) (73)	1 329 300	0,05%
37	20 Artificial Sewage Ponds (20)	842 300	0,03%
38	62 Urban Recreational Fields (Bush) (62)	827 000	0,03%
39	18 Natural Pans (flooded) (18)	666 300	0,02%
40	46 Fallow Land & Old Fields (Low Shrub) (46)	658 000	0,02%
41	45 Fallow Land & Old Fields (Bare) (45)	621 300	0,02%
42	26 Dry Pans (26)	462 200	0,02%
43	7 Temporary Unplanted Forest (7)	455 400	0,02%
44	30 Bare Riverbed Material (30)	451 800	0,02%
45	59 Smallholdings (low veg / grass) (59)	411 200	0,01%
46	21 Artificial Flooded Mine Pits (21)	393 900	0,01%
47	27 Eroded Lands (27)	340 700	0,01%
48	32 Cultivated Commercial Permanent Orchards (32)	291 800	0,01%
49	43 Fallow Land & Old Fields (Bush) (43)	279 600	0,01%
50	64 Urban Recreational Fields (Bare) (64)	237 900	0,01%
51	56 Village Dense (56)	233 300	0,01%
52	60 Smallholdings (Bare) (60)	186 700	0,01%
53	55 Village Scattered (55)	153 500	0,01%
54	51 Residential Informal (Tree) (51)	87 900	0,003%
55	72 Land-fills (72)	65 100	0,002%
56	52 Residential Informal (Bush) (52)	36 700	0,001%
	Sum total	2 775 189 600	100,00%

Land cover mapping of KOSH region for year 2019 using batch classification

By using the batch classification algorithm of Object Analyst, one can run classification simultaneously on a group or collection of images with similar qualities of acquisition. The classification run on an individual image (e.g. satellite image of March 2020) can be used as reference for the batch (e.g. the image of March 2019) to be processed. The batch classification applies a segmentation step, an attribute-calculation step, a Support Vector Machine (SVM)-classification step (based on the training-model file created from the first individual image classified). The training model file created with the option of having input attributes of standard deviation of VNIR bands and 10 vegetation indices was used in the batch classification. The batch classification using a previous training model file helps to reduce the analysis time by avoiding the step of identifying training sites for a similar image of a different date of acquisition. The final result of land use / land cover obtained from the batch classification step run using the Sentinel-2 image acquired on 16 March 2019 is shown in figure 24. A visual examination of the result of land use / land cover classification result (fig. 24) using the Sentinel-2 data of 16 March 2019 reveals that most of the areas of Class 13 Natural Grassland is mapped correctly.

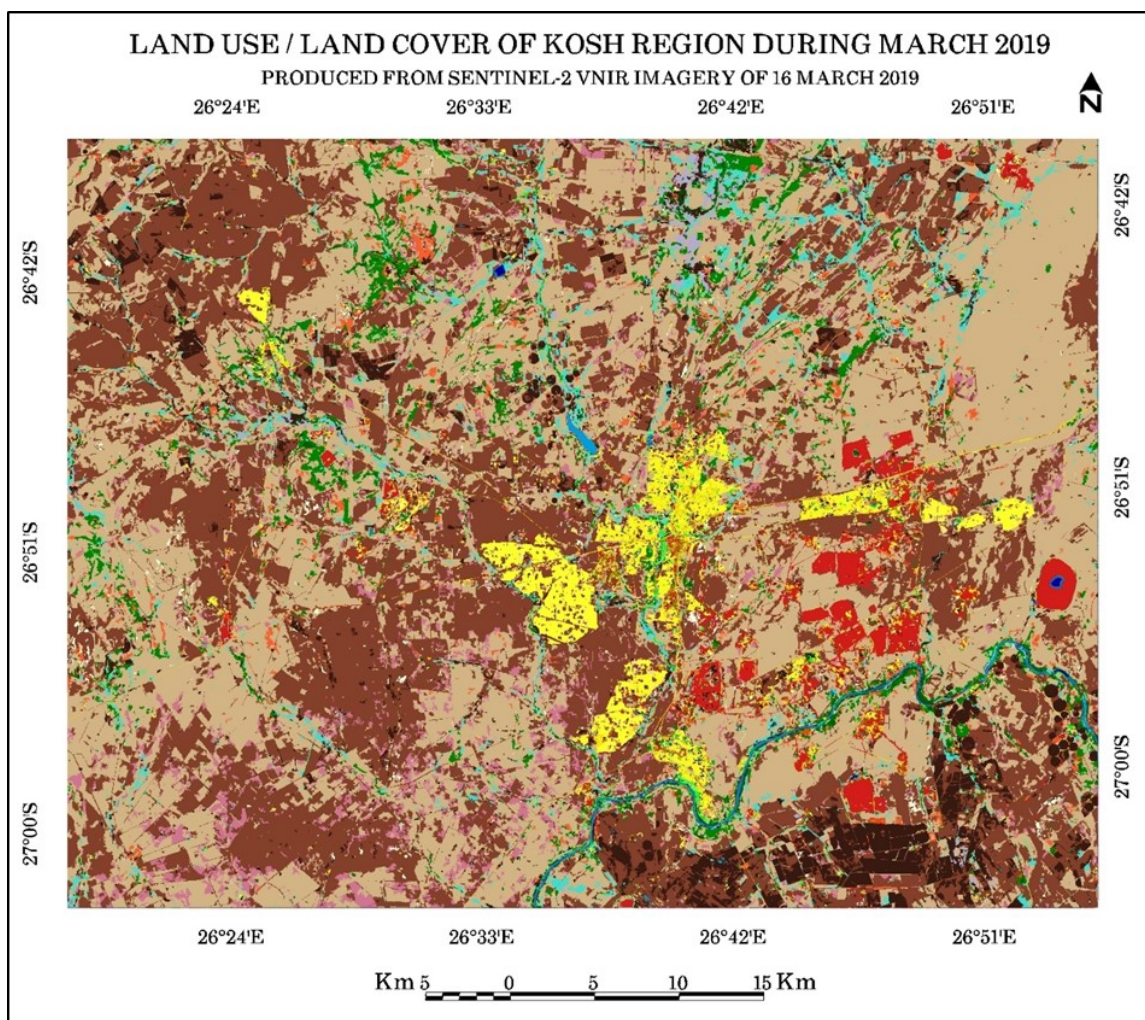


Fig. 24. Land cover classification result obtained from the Sentinel-2 image of 16 March 2019 using Batch Classification option of Object Analyst

Comparison of land covers of year 2019, year 2020 and NLC 2018

The north-eastern part of the land use / land cover map for the year (Figure 24) shows many patches of Class 23 Herbaceous Wetlands (previous mapped extent) that are actually Class 13 Natural Grassland in the land use / land cover of year 2020 and NLC 2018. The eastern part of year

2019 result shows more patches of Class 40 Temporary Crops-rainfed when compared with the result for year 2020. The south-eastern part of the result for the year 2019 shows more patches of Class 38 Cultivated Commercial Annuals Pivot Irrigated. Similarly, more patches of Class 23 Herbaceous Wetlands (previous mapped extent) are seen in the south-western region of the land use / land cover map for the year 2019. It is also found that most of the area of the Vaal River (Class 14 Natural waterbodies) seen in the south-eastern part of figure 24 is mapped as Class 20 Artificial Sewage Ponds, which is noticed as an error in the classification using batch classification. A portion of the results of land use / land cover classification for the years 2020 and 2019 showing the south-west part of KOSH region along with corresponding satellite images of years 2020 and 2019 showing the same extent is shown in figure 25.

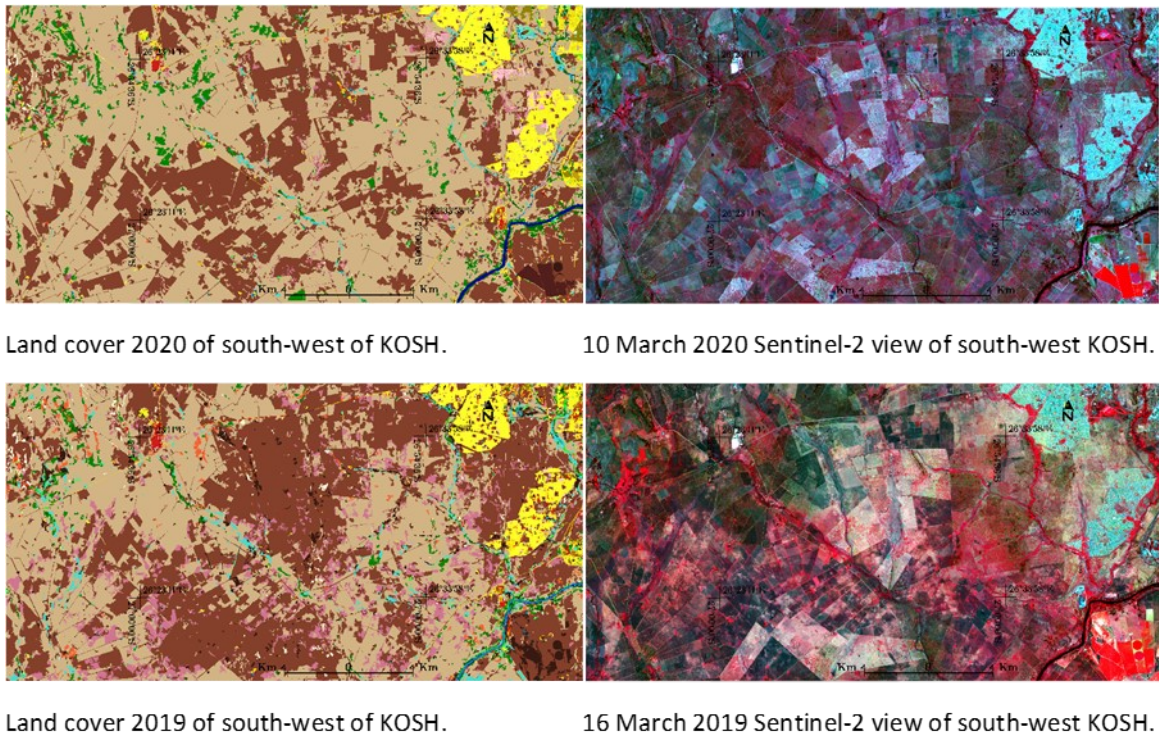


Fig. 25. A portion of the results of land use / land cover classification for years 2020 and 2019 showing the south-west part of KOSH region along with corresponding satellite images of years 2020 and 2019

A close look of these figures reveals that the result for the year 2019 is distinct with more small patches of class 44 Fallow Land & Old Fields _Grass (shown in light pink shade) that are seen towards the south-west part. On comparing the satellite images of March 2019 and 2020, it can be observed that some natural grassland (Class 13) seen in the year 2019 has become agricultural fields (in south-west) and such land use dynamics changes are evident through comparison of satellite images or land cover dataset. More vegetation cover is seen in the north of 2019 image. There is some slight dissimilarities in the appearance of these two satellite images due to some difference in pixel values. Such dissimilarities observed in the satellite images of two different years (year 2019 and year 2020) will give a different result when batch classification is applied on the other image with the training sites of year 2020.

A further examination of the classification result for the year 2019 revealed that three land use / land cover classes viz. Class 2 Contiguous Low Forest & Thicket, Class 32 Cultivated Commercial Permanent Orchards and Class 52 Residential Informal (Bush) were not mapped or missing in the attribute table. The number and areal extent of the training sites for these two classes were very less (not sufficient enough) and their attributes or characteristics were not so distinct, hence they were not mapped in the batch classification. Locations of such classes have to be identified in the

image and the corresponding polygon segments have to be manually re-assigned in order to show these classes in the final map. The land use / land cover map for the year 2019 requires further examination at many locations for accuracy check and subsequent editing or re-assigning of the wrong polygon segments.

The summarised area figures for the present 53 land cover classes for the year 2019 is shown in Table 4. Comparison of percentage area figures for the major land cover classes of year 2020 and 2019 show that Class 13 Natural Grassland constitutes 49.32% of the total area in the year 2020 whereas in the year 2019 the extent of this class is less (42.14% of the total area). The areal extent of the same class in NLC 2018 dataset is higher (53.84% of the total area). Class 40 Temporary crops rainfed constitutes 32.90% of total area during year 2020 whereas in year 2019 it covers nearly same extent (32.97% of total area). The same class seen in NLC 2018 covers much lesser areal extent (22.66% of total area).

Class 4 Open woodland covered 4% of the total area in the year 2020 whereas in the year 2019 it covered 3% of the total area. This class covered 3.6% of the total area in NLC 2018. The area figures of Class 4 Open woodland do not vary much in these years. Class 71 Mines: Waste (Tailings) & Resource Dumps constitute 1.96% of the total area in the year 2020. The extent of this class in the year 2019 is found to be 2.5% of the total area whereas in NLC 2018, this class is having an area of 1.5% of the total area. The higher resolution of VNIR bands at 10 m has contributed to more accurate mapping of this class. Class 44 Fallow Lands & Old Fields_Grass covered about 8% of the total area in NLC 2018 whereas in the year 2019 this class covered less area (3.3% of total area) whereas in year 2020 it decreased significantly to 0.5% of the total area. Class 49 Residential Formal (low veg / grass) had constituted 2.15% of the total area in NLC 2018 whereas in the land use / land cover map of year 2020 it covered only 1.53% of the total area. For this class during the year 2019 the calculated percentage area is 1.5% of the total area. Class 38 Cultivated Commercial Annuals Pivot Irrigated had covered 1.2% of the total area in NLC 2018 while this class has constituted 1.3% of the total area in the land use / land cover map of year 2020. For the year 2019, this class covered significantly higher percentage area of 5%. Class 3 Dense Forest & Woodland had covered 1% of the total percentage area in NLC 2018 whereas in the year 2020 the percentage of this class reduced to 0.8% of the total area. In the year 2019, the coverage of this class is still much lower (0.4% of the total area).

Conclusions

Recent Sentinel-2 satellite images acquired in March 2020 and 2019 covering the KOSH region could be classified using Geomatica Object Analyst and produced some useful land cover products to aid in land cover change detection and land use dynamics studies. The Sentinel-2 VNIR bands (10 m) are suitable for land cover mapping (for discriminating different land use / land covers including informal settlements, road network, mine dumps, urban recreation fields, different vegetation covers and agricultural practices etc.). Vegetation indices alone are not enough to differentiate urban areas (commercial/roads) and mining dumps. Use of lower resolution SWIR bands along with VNIR bands might improve the classification accuracy for urban area if a 20 m resolution output with lesser details is opted. The land cover datasets shown in this study would help in understanding the land use / land cover dynamics and also studies of environmental monitoring. This study could illustrate the usefulness of remote sensing analysis to aid in land cover mapping using freely available high resolution Sentinel-2 data. Editing of the identified training sites of year 2020 along with viewing of the features of 2019 satellite data will enhance the classification accuracy for year 2019.

Table 4

Area calculated for the different land use / land cover classes for the year 2019

Sr No.	Land use / land cover during March 2019	Area (m ²)	% Area
1	13 Natural Grassland (13)	1 169 347 200	42,14%
2	40 Temporary Crops-rainfed (40)	915 042 200	32,97%
3	38 Cultivated Commercial Annuals Pivot Irrigated (38)	139 129 500	5,01%
4	44 Fallow Lands & Old Fields Grass (44)	90 974 100	3,28%
5	4 Open Woodland (4)	84 056 900	3,03%
6	71 Mines: Waste (Tailings) & Resource Dumps (71)	68 146 800	2,46%
7	23 Herbaceous Wetlands (previous mapped extent) (23)	58 082 300	2,09%
8	49 Residential Formal (low veg / grass) (49)	40 510 100	1,46%
9	6 Open & Sparse Planted Forest (6)	40 115 400	1,45%
10	50 Residential Formal (Bare) (50)	38 608 000	1,39%
11	12 Sparsely Wooded Grassland (12)	16 352 700	0,59%
12	67 Roads & Rail (Major Linear) (67)	15 578 600	0,56%
13	8 Low Shrubland (other regions) (8)	12 300 300	0,44%
14	3 Dense Forest & Woodland (3)	11 509 900	0,41%
15	25 Natural Rock Surfaces (25)	9 014 200	0,32%
16	31 Other Bare (31)	6 396 200	0,23%
17	61 Urban Recreational Fields (Tree) (61)	6 377 500	0,23%
18	47 Residential Formal (Tree) (47)	5 411 100	0,19%
19	5 Contiguous & Dense Planted Forest (5)	5 107 100	0,18%
20	66 Industrial (66)	4 439 100	0,16%
21	20 Artificial Sewage Ponds (20)	4 031 500	0,15%
22	19 Artificial Dams / Waterbodies (19)	3 718 600	0,13%
23	63 Urban Recreational Fields (Grass) (63)	3 521 000	0,13%
24	69 Mines: Extraction Sites: Open Cast & Quarries combined (69)	3 309 900	0,12%
25	30 Bare Riverbed Material (30)	2 786 500	0,10%
26	22 Herbaceous Wetlands (currently mapped) (22)	2 193 600	0,08%
27	65 Commercial (65)	2 105 400	0,08%
28	73 Fallow Land & Old Fields (wetlands) (73)	1 778 600	0,06%
29	14 Natural Waterbodies (14)	1 707 000	0,06%
30	18 Natural Pans (flooded) (18)	1 665 800	0,06%
31	7 Temporary Unplanted Forest (7)	1 619 100	0,06%
32	58 Smallholdings (Bush) (58)	1 573 100	0,06%
33	48 Residential Formal (Bush) (48)	1 409 300	0,05%
34	54 Residential Informal (Bare) (54)	1 290 600	0,05%
35	39 Cultivated Commercial Annuals Non-Pivot Irrigated (39)	848 600	0,03%
36	53 Residential Informal (low veg / grass) (53)	610 900	0,02%
37	59 Smallholdings (low veg / grass) (59)	558 000	0,02%
38	26 Dry Pans (26)	508 200	0,02%
39	2 Contiguous Low Forest & Thicket (2)	504 200	0,02%
40	57 Smallholdings (Tree) (57)	457 900	0,02%
41	27 Eroded Lands (27)	441 100	0,02%
42	68 Mines: Surface Infrastructure (68)	404 100	0,01%
43	21 Artificial Flooded Mine Pits (21)	339 200	0,01%
44	51 Residential Informal (Tree) (51)	256 600	0,01%
45	55 Village Scattered (55)	211 400	0,01%
46	62 Urban Recreational Fields (Bush) (62)	178 300	0,01%
47	64 Urban Recreational Fields (Bare) (64)	141 400	0,01%
48	45 Fallow Land & Old Fields (Bare) (45)	133 400	0,005%
49	46 Fallow Land & Old Fields (Low Shrub) (46)	132 100	0,005%
50	56 Village Dense (56)	121 900	0,004%
51	72 Land-fills (72)	91 000	0,003%
52	60 Smallholdings (Bare) (60)	30 100	0,001%
53	52 Residential Informal (Bush) (52)	12 000	0,0004%
	Sum total	2 775 189 600	100,00%

The author would like to register his sincere thanks to the Council for Geoscience for providing an opportunity and various resources provided to undertake this study. The author would like to thank the National Research Foundation of South Africa for the grant provided through BRICS multilateral research collaboration project which enabled this study. The author likes to thank the European Space Agency (ESA) for providing Sentinel-2 data and the Department of Environment, Forestry and Fisheries (DEFF) for providing the 2018 South African NLC dataset used in this study. Finally the author would like to thank Mr Kevin Melhuish of MapAfrika and the PCI Geomatics team for providing evaluation license of Object Analyst and their assistance with tutorial documents for testing the software.

References

1. Boriah, S. et al. Land cover change detection: A case study, in *Proceedings of the ACM SIGKDD International Conference on Knowledge Discovery and Data Mining*, **2008**, pp. 857–865.
2. ESA-STEP, *ESA SNAP Toolbox surpasses 300000 downloads*, **2018**, Available at: <http://step.esa.int/main/esa-snap-toolbox-surpasses-300000-downloads/> (Accessed: 10 September 2019).
3. Mail&Guardian, Former mine owners to cough up, *Mail & Guardian*, **2014**, Available at: <http://mg.co.za/article/2014-01-17-00-former-mine-owners-to-cough-up>.
4. Midgley, D. C., Pitman, W. V. and Middleton, B. J., *Surface water resources of South Africa 1990: Book of Maps, Volume II. Drainage Region C Vaal - Report 298/2.2/94*, **1994**.
5. PCI-Geomatics, Object Analyst: Technical Specifications, *PCI Geomatics*, **2017**, p. 11. Available at: <https://www.pcigeomatics.com/pdf/geomatica/techspecs/2017/Object-Analyst.pdf>.
6. Pulles, W., Banister, S. and Van Biljon, M., *Development of appropriate procedures toward sand after closure of underground gold mines from a water management perspective: Report No.1215/1/05*, **2005**, Available at: [http://www.wrc.org.za/Lists/Knowledge Hub Items/Attachments/7697/1215-1-05_EXECUTIVE SUMMARY.pdf](http://www.wrc.org.za/Lists/Knowledge%20Hub%20Items/Attachments/7697/1215-1-05_EXECUTIVE%20SUMMARY.pdf).
7. SAFLII, Judgment of Case No: 971/12 from the Supreme Court of Appeal of South Africa, *SOUTHERN AFRICAN LEGAL INFORMATION INSTITUTE (SAFLII)*, **2013**, Available at: <http://www.saflii.org/za/cases/ZASCA/2013/206.pdf>.
8. Thompson, M., *South African National Land-Cover 2018 Report & Accuracy Assessment*, **2019**.

EXTRACTION AND MODELING OF INDIVIDUAL SIKANG PINE STEM BASED ON POINT CLOUD DATA

Jianpeng Zhang^{1,2,3}, Guangjie Liu⁴, Jinliang Wang^{1,2,3*}

¹Faculty of Geography, Yunnan Normal University

²Key Laboratory of Resources and Environmental Remote Sensing for Universities in Yunnan

³Center for Geospatial Information Engineering and Technology of Yunnan Province

⁴College of Resources and Environment, Yunnan Agricultural University

*Forest structure parameters are important parameters in tree volume and biomass estimation. Sikang pine (*Pinus densata*) is one of the main coniferous species and the pioneering tree species for barren mountain afforestation in western China. Its stem has the characteristics of tall and straight and has important timber value. In order to promote the ecological study of Sikang pine forest, with the point cloud of Sikang pine natural forest obtained by terrestrial laser scanning as the data source, the point cloud clustering algorithm based on Euclidean distance, the comparative shortest-path algorithm and the point cloud cylinder detection and extraction algorithm were used to extract and model of Sikang pine stem. The results show: (1) point cloud data can be used to extract stem from natural forest, and good extraction results can be obtained in natural forest with complex growth environment; (2) the higher extraction accuracy of the lower part of stem can be achieved, and it can be used to build a stem model. Research shows that the stem can be extracted well based on the point cloud data and can be modeled. But due to severe canopy occlusion in the upper stem, the high-precision extraction of upper stem point clouds needs further study.*

Key words: *Pinus densata*, terrestrial laser scanning, point cloud data, stem extraction, modeling

Introduction

Sikang pine (*Pinus densata*) is typical for western China. It has the characteristics of high growth, straight stem, and wide use of timber (Lu, Pan, 2008). It is an important tree species for forest greening and afforestation, and has important ecological and economic values. In recent years, many scholars have conducted various research of Sikang pine, including growth environment, forest fire prevention, biomass, forest parameters and carbon storage, etc. (Zhang et al., 2012; Li et al., 2016; Wang et al., 2019; Xiong et al., 2017). The growth morphology of the tree stem is one of important indicators for forest evaluation. Extracting the stem in the natural forest can provide the data basis and reference for research on the utilization and protection of this species.

The traditional forestry stem survey method requires investigators to go deep into the forest area for measurement and statistics. Even though this method can ensure the accuracy of the stem measurement, it is time-consuming, labor-intensive, and inefficient. The emergence and development of Light Detection and Ranging (LiDAR) remote sensing technology provides a new method for forest inventory and research. It can efficiently and accurately produce the three-dimensional spatial structure of the forest-point cloud data, and further explore forest data to make up for the shortcomings of traditional methods. Airborne Laser Scanning (ALS) and Terrestrial Laser Scanning (TLS) are currently the two main platforms for the application of Lidar technology in forests (Zhao et al., 2019). At present, forest ecology studies using ALS technology mostly focus on forest biomass and parameter inversion (Naesset, Gobakken, 2008; Wang et al., 2015; Geng et al., 2015). Due to difficulty of obtaining data about the structure of trees below the forest canopy, such as stems, it is difficult to conduct research on the extraction and modeling of stems using ALS technology. TLS point cloud data can clearly and accurately characterize the three-dimensional spatial structure information below the forest canopy, and has great potential for extracting information such as tree stems. At present, most researchers are keen on the extraction of parameters such as tree height and diameter at breast height (Beland et al., 2011; Li et al., 2012; Liu et al., 2014; Liu et al., 2018). And there are few studies on extraction and modeling of individual tree stem in natural forests (Liang et al., 2013; Xia et al., 2015).

Our research aims to extract stem and model the Sikang pine by using point cloud data to provide reference for research on this or other tree species.

Materials and Methods

Data acquisition and preprocessing

Shangri-La City is located in the northwestern part of Yunnan Province ($99^{\circ}33'E - 100^{\circ}58'E$, $27^{\circ}20'N - 28^{\circ}09'N$), with abundant forest resources and high vegetation coverage. In the study, Leica P40 3D laser scanner was used as the data acquisition equipment, and a natural Sikang pine forest sample plot was selected as the experimental object in Xiaozhongdian County, Shangri-La City, Yunnan Province of China to acquire point cloud data. In order to obtain the complete point cloud data from the research sample plot, 5 sites (1 in the center and 4 nearby) were selected in the sample plot for scanning, as shown in figure 1. After obtaining the cloud data of each site in the sample plot, stitch them to obtain the original point cloud data. Then, the four steps of thinning, denoising, filtering and normalization were preprocessed. Finally, we obtained the complete point cloud experimental data of the Sikang pine by cutting in a circle with a radius of 15 meters, as shown in figure 2.

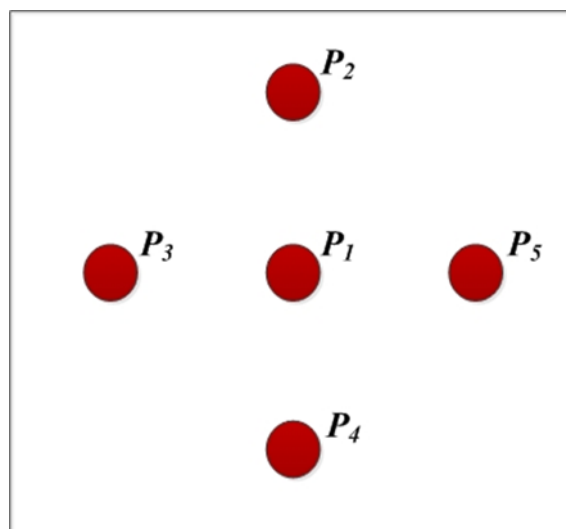


Fig. 1. Scanning station diagram

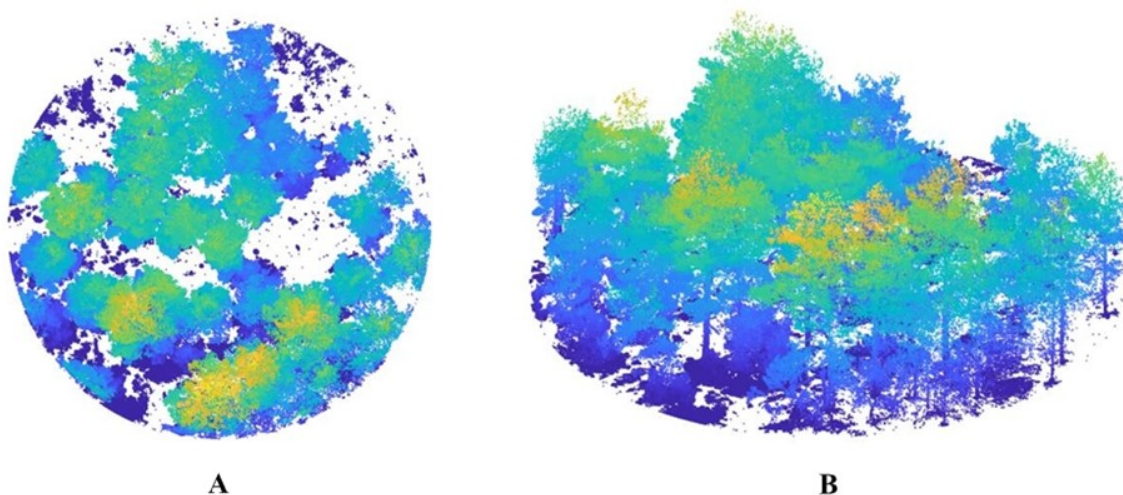


Fig. 2. Experimental data of the Sikang pine A) Top view; B) Front view

Research process

After preprocessing the data, the research firstly clustered the experimental data based on the point cloud clustering algorithm of Euclidean distance in order to filter and remove the point cloud

of shrub and grass, and extract the Sikang pine. Secondly, the comparative shortest-path algorithm (CSP) was used to segment the point cloud and extract individual trees. Finally, cylinder recognition was performed on the point cloud of an individual tree, the stem point cloud is extracted, and the cylinder is fitted to obtain the stem model. The research technical route is shown in figure 3.

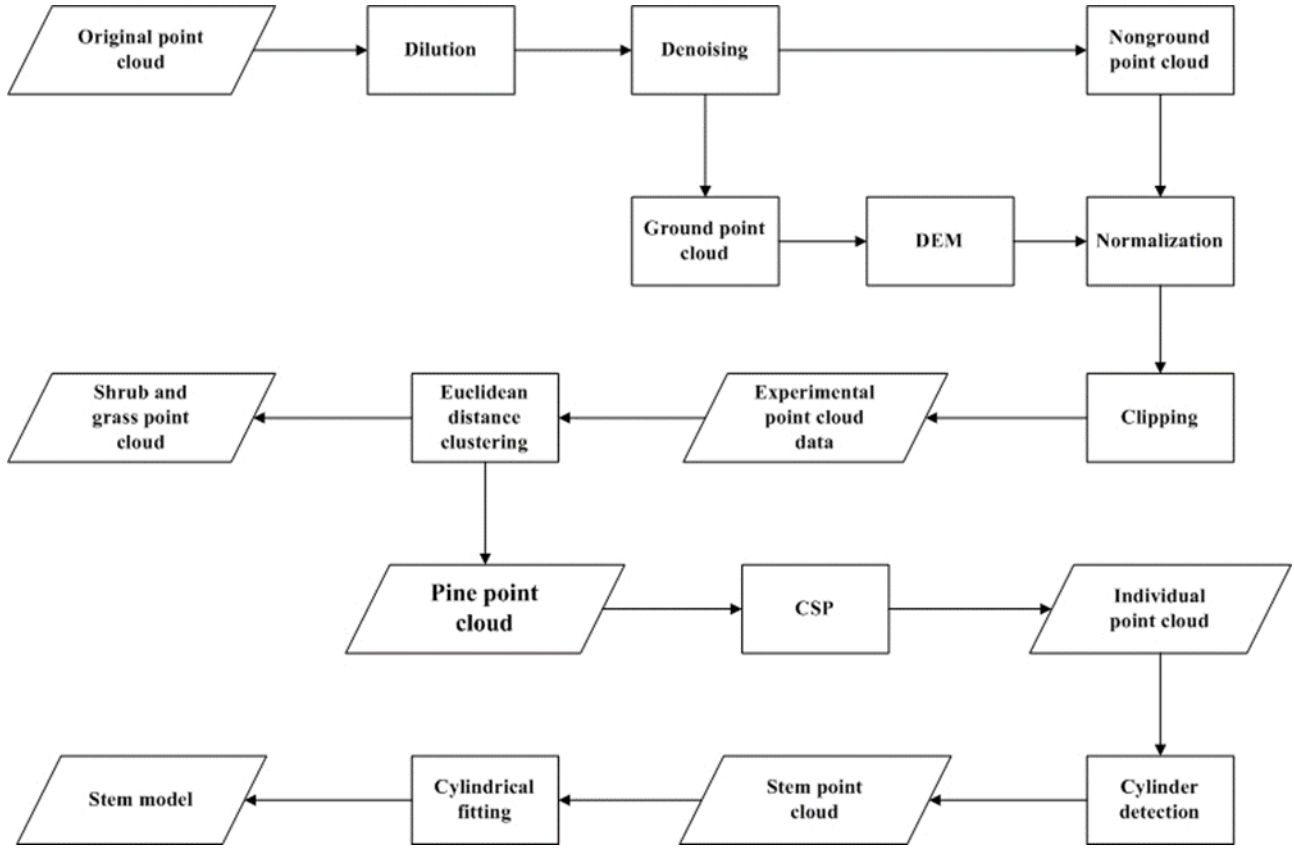


Fig. 3. Technology Roadmap

Euclidean distance clustering

The research uses the point cloud clustering algorithm of Euclidean distance to cluster the Sikang pine point cloud. The Euclidean distance between two points in three-dimensional space refers to the straight-line distance between the two points. The Euclidean distance d of two points in three-dimensional space $a(x_1, y_1, z_1)$, $b(x_2, y_2, z_2)$ is calculated by the formula (1).

$$d = \sqrt{(x_1 - x_2)^2 + (y_1 - y_2)^2 + (z_1 - z_2)^2} . \quad (1)$$

The point cloud is clustered through a given initial distance threshold. If the distance between the two points is less than the given threshold, the two points belong to the same category. According to this principle, the Sikang pine point cloud is extracted. The steps of the algorithm are as follows: (1) load point cloud data and find the ground plane to store it; (2) specify the minimum distance between two different types of clusters, cluster the point clouds that do not include the ground plane, and then assign the same label to the points belonging to the same cluster; (3) give an additional label to the ground plane point cloud; (4) extract point clouds of different categories based on labels. The research explored the minimum distance between two different types of clusters and revealed that when the minimum distance is 0.5m, the Sikang pine clustering result is the best, as shown in figure 4.

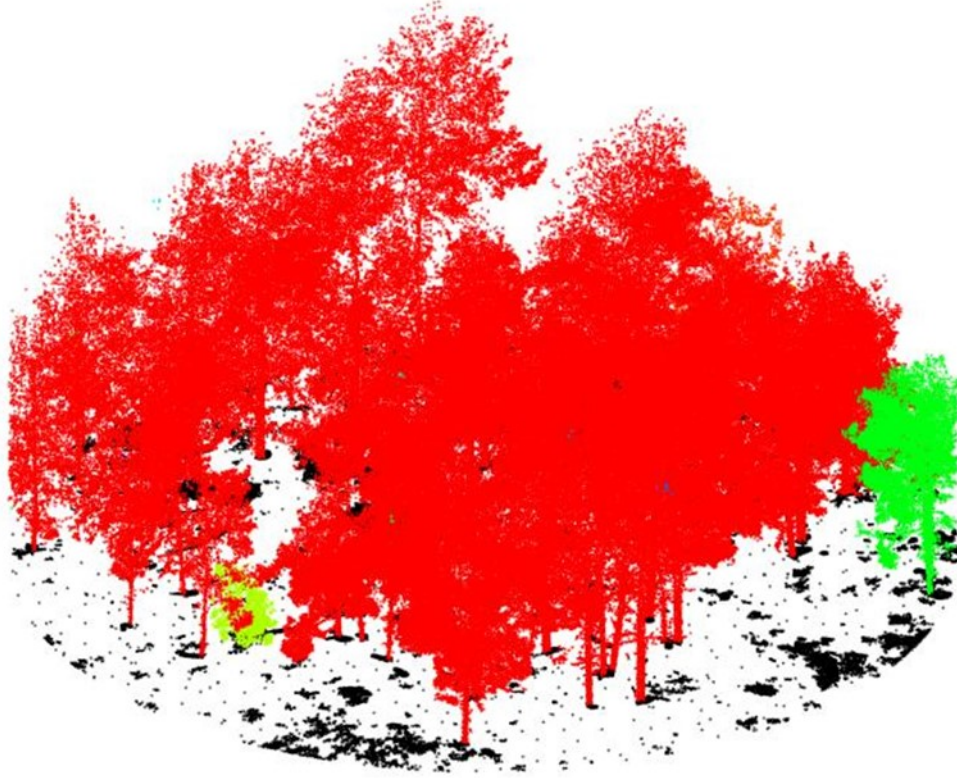


Fig. 4. Clustering results

It can be seen from figure 4 that the Sikang pine is basically clustered, but there are also some independent pines that are divided into different categories (green point cloud). Then we used filter and removed the shrub and grass point clouds in order to extract the Sikang pine, and perform the Sikang pine point cloud fusion using the CloudCompare point cloud processing software to obtain a complete point cloud in the experimental sample plot, as shown in figure 5.

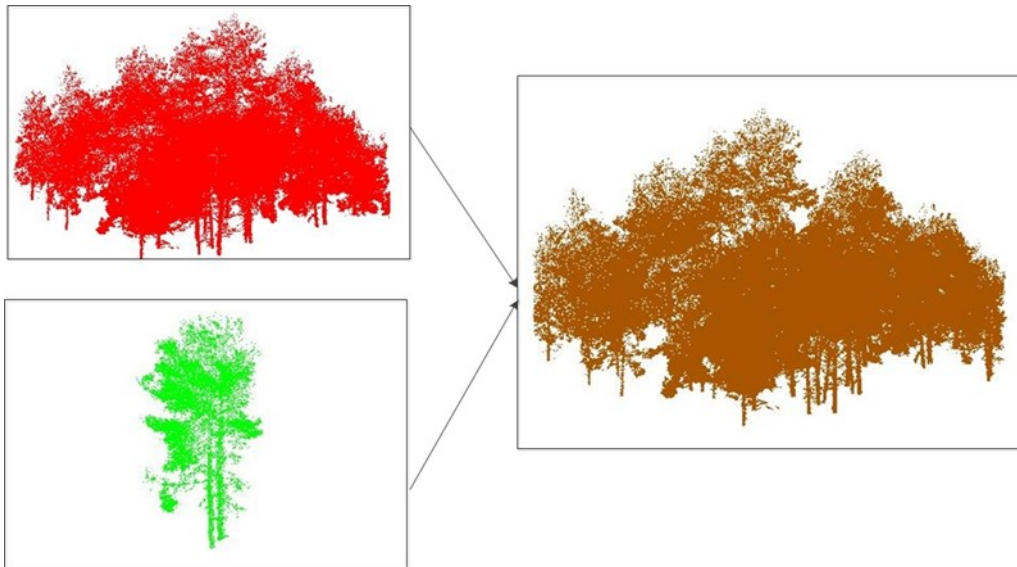


Fig. 5. The merger results of Sikang pine

CSP point cloud segmentation

CSP is a point cloud segmentation algorithm based on ecological theory proposed by Tao et al. (2015). The principle of the algorithm is as follows: according to the ecological theory "there are many conduits for nutrient transport in a tree". Let us assume the conduit from the leaves to the

roots of the tree to be the path, and the metabolic distance to be calculated based on the path distance from a leaf to the root, by comparing this metabolic distance. By applying the point cloud individual tree segmentation, we will get that the metabolic distance from a certain point to the root of the A tree is shorter than the metabolic distance to the root of the B tree, then the point belongs to the A tree. The metabolic distance of this path is calculated according to the formula (2):

$$D_{v \rightarrow Trunk}^N = D_{v \rightarrow Trunk} / DBH^{2/3}, \quad (2)$$

where, $D_{v \rightarrow Trunk}^N$ represents the metabolic distance from point v to the stem of the tree, $D_{v \rightarrow Trunk}$ represents the actual distance from point v to the stem of the tree, and DBH represents the diameter at breast height of the tree. The result of individual tree segmentation of Sikang pine point cloud by CSP algorithm is shown in figure 6.

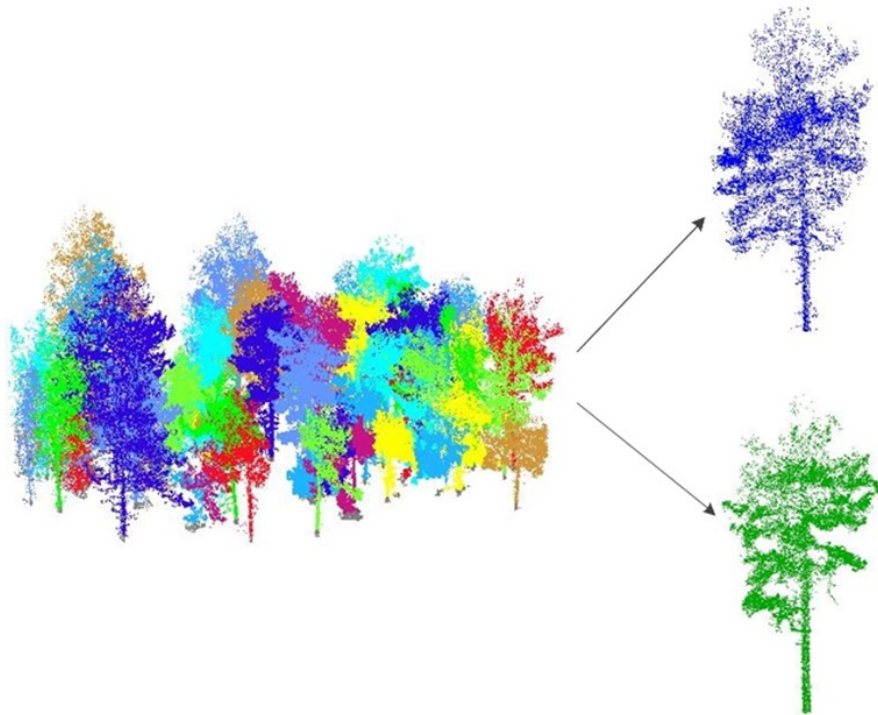


Fig. 6. The individual tree segmentation result of Sikang pine

Point cloud cylinder detection and recognition

The growth morphology of the Sikang pine stem is mainly cylindrical. According to this feature, the point cloud can be identified and extracted, and then the stem cylindrical model can be established. The research uses point cloud cylinder extraction and detection to extract Sikang pine stems. The principle is as follows: given the maximum distance from point to the cylindrical surface, if the shortest distance from point p to the cylindrical surface is less than the given distance, then point p belongs to the point on the tree stem. The steps of the algorithm are as follows: (1) load the point cloud data; (2) set the maximum distance from point to the cylindrical surface; (3) set a coordinate area for cylinder identification; (4) set a normal vector; (5) perform point cloud cylindrical detection and extraction.

Results and discussion

The research combines the point cloud clustering algorithm based on the Euclidean distance and the CSP point cloud segmentation algorithm to extract the individual Sikang pine, then recognizes and detects the cylinder to extract the Sikang pine stem. Sikang pine stem extraction and its stem model results are shown in the figure 7.

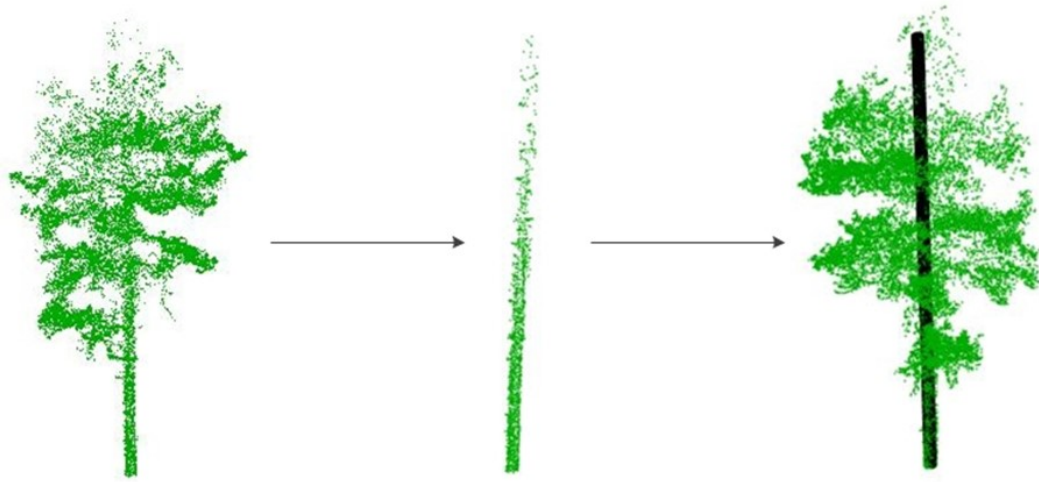


Fig. 7. Stem extraction and modeling results

It can be seen from figure 7 that the results of the stem extraction of Sikang pine are generally good, which was the purpose of the research. However, because the upper stem of the Sikang pine canopy is severely occluded, it is difficult to obtain a complete extraction of the stem point cloud, especially in the upper part of the stem, thus the accuracy of the extraction results is relatively low. The lower part of the stem is not obstructed, and the extraction results are better. This fits the growth results of the stem model and can basically reflect the growth of the stem. However, from the results of the model established by the stem, the thickness of the upper part of the stem model is the same as that of the lower part, which does not meet the actual growth of the stem. Through research and analysis, the upper canopy occlusion is still the main cause of this problem. The experiment was carried out on another Sikang pine natural forest sample plot with a more complicated growth environment. This sample plot contains other tree species and the growth density is also high. In order to improve the accurate identification and extraction of Sikang pine, when collecting point cloud data in this sample plot, the Sikang pine was numbered, and finally the Sikang pine was identified and stem extracted according to this number, in order to eliminate the interference of other tree species in the study. The stem extraction and model results of the Sikang pine in this sample plot are shown in figure 8.

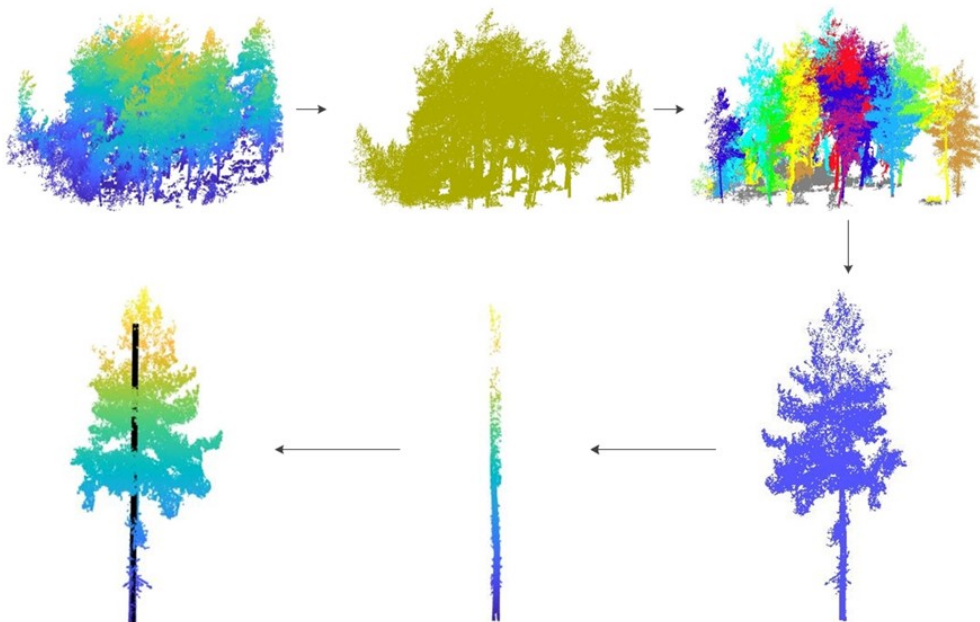


Fig. 8. Extraction and modeling results of Sikang pine stem in complex plots

It can be seen from figure 8 that for the research sample plot with complex growth environment, the stem extraction of Sikang pine based on TLS point cloud data can still be achieved. In particular, the accuracy of the extraction results from the lower part of the stem is good, and can serve as the basis for stem growth model development. However, there are also problems caused by canopy occlusion, and the extraction results of the upper part of the stem are relatively poor. We found there are two main aspects that affect the accuracy of the results, which are point cloud density and canopy occlusion. The influence of point cloud density and canopy occlusion on stem extraction and modeling is discussed below.

1) The effect of point cloud density on stem extraction and modeling.

The point cloud density is usually characterized by the distance between the two points of the point cloud. The smaller the distance between the two points, the greater the number of point clouds and the greater the point cloud density. Through research, the point cloud density has a certain influence on the main extraction and modeling of the Sikang pine. The greater the density of the point cloud, the greater the number of point clouds that make up the stem, and the extracted stem can more accurately reflect the growth of the stem, so that the stem can be modeled more accurately, but calculations increase with the increase of the point cloud density.

2) The influence of canopy occlusion on stem extraction and modeling.

The canopy around the upper part of the stem grows densely, which has an impact on the point cloud acquisition in the upper part of the stem, and it is difficult to obtain a complete point cloud compared to the lower part of the stem. For Sikang pine that the upper canopy of the stem grows sparsely and does not cover severely, the stem extraction results are more accurate and the model is more accurate. For Sikang pine with dense canopy growth, minimizing its influence on stem extraction and modeling will be the next focus of our research.

Conclusion

The research involved stem extraction and modeling of the individual Sikang pine in the natural forest based on TLS point cloud data. The results revealed that: (1) the stem of Sikang pine in natural forests can be extracted well, and good extraction results can still be obtained in natural forests with complex growth environments based on point cloud data. (2) the extraction results of the lower part of the Sikang pine stem are more accurate, and the stem model can be established, which can provide a reference for the forest ecology research of Sikang pine or other tree species. However, due to the complexity of the point cloud data and the occlusion of the upper part of the stem by the canopy, it is difficult to obtain a complete point cloud of the upper part of the stem. Therefore, in future research, it is still necessary to improve the accuracy of point cloud extraction on the upper part of the stem, in order to develop a more accurate model of stem.

We wish to thank Zhiyuan Liu and Huan Deng for their help in data collecting, we also wish to thank Yicheng Liu and Qianwei Liu for their help in the whole experiment. This work was supported by National Natural Science Foundation of P. R. China (Nos.41961060 and 41271230). This work was supported by Young and Middle-aged Academic and Technical Leaders Reserve Talents Training Program of Yunnan Province (No. 2008PY056). This work was supported by the Program for Innovative Research Team (in Science and Technology) in the University of Yunnan Province, IRTSTYN.

References

1. Beland M., Widlowski J.L., Fournier R.A., Cote J.F., Verstraete M.M. Estimating leaf area distribution in savanna trees from terrestrial LiDAR measurements. *Agricultural and Forest Meteorology*, **2011**, 9, pp. 1252-1266. <https://doi.org/10.1016/j.agrformet.2011.05.004>
2. Geng L., Li M., Fang W., Wang, B. Individual Tree Structure Parameters and Effective Crown of the Stand Extraction Base on Airborn LiDAR Data. *Scientia Silvae Sinicae*, **2018**, 07, pp. 62-72 (In Chinese) <https://doi.org/10.11707/j.1001-7488.20180707>

3. Li B., Cheng X.H., Lu L.X. Responses of radial growth to fire disturbance in alpine pine (*Pinus densata*) of different age classes in Nang County, Xizang, China. *Chinese Journal of Plant Ecology*, **2016**, 05, pp. 436-446. <https://doi.org/10.17521/cjpe.2015.0440>
4. Li, D., Pang, Y., Yue, C.R. A Review of TLS Application in Forest Parameters Retrieving. *World Forestry Research*, **2012**, 25, pp. 34-39 (in Chinese) <https://doi.org/10.13348/j.cnki.sjlyyj.2012.06.010>
5. Liang X., Kankare V., Yu X., Hyypä J., Holopainen M. Automated Stem Curve Measurement Using Terrestrial Laser Scanning. *IEEE Transactions on Geoscience and Remote Sensing*, **2013**, 52, pp. 1739–1748. <https://doi.org/10.1109/TGRS.2013.2253783>
6. Liu, G., Wang, J., Dong, P., Chen, Y., Liu, Z. Estimating Individual Tree Height and Diameter at Breast Height (DBH) from Terrestrial Laser Scanning (TLS) Data at Plot Level. *Forests*, **2018**, 9, pp. 1-18. <https://doi.org/10.3390/f9070398>
7. Liu L., Pang Y., Li Z., Xu G., Li D., Zheng G. Retrieving structural parameters of individual tree through terrestrial laser scanning data. *Journal of Remote Sensing*, **2014**, 02, pp. 365-377 (In Chinese) <https://doi.org/10.11834/jrs.20143091>
8. <https://doi.org/10.11834/jrs.20143091>
9. Lu S., Pan C. Distribution Pattern of *Pinus densata* Population in the Southeast Tibet. *Journal of northeast forestry university*, **2008**, 11, pp. 22-24 (In Chinese) <https://doi.org/10.3969/j.issn.1000-5382.2008.11.010>
10. Naesset E., Gobakken T. Estimation of above- and below-ground biomass across regions of the boreal forest zone using airborne laser. *Remote Sensing of Environment*, **2008**, 6, pp. 3079-3090. <https://doi.org/10.1016/j.rse.2008.03.004>
11. Tao S., Wu F., Guo Q., Wang Y., Li W., Xue B., et al. Segmenting tree crowns from terrestrial and mobile LiDAR data by exploring ecological theories. *ISPRS Journal of Photogrammetry & Remote Sensing*, **2015**, 110, pp. 66-76. <https://doi.org/10.1016/j.isprsjprs.2015.10.007>
12. Wang R., Xing Y., Sun X., You H. Research Progress on Airborne Large Footprint LiDAR Data in Estimation of Forest Structure Research Progress on Airborne Large Footprint LiDAR Data in Estimation of Forest Structure Parameters. *Remote Sensing Information*, **2015**, 03, pp. 3-93 (in Chinese) <https://doi.org/10.3969/j.issn.1000-3177.2015.03.001>
13. Wang X., Chen J., Xing Z., Zhang C. Study on Relationship between DBH and Crown Diameter of *Pinus densata* and its Application in Southeastern Tibet. *Forest Resources Management*, **2019**, 01, pp. 63-69 (in Chinese) <https://doi.org/10.13466/j.cnki.lyzygl.2019.01.011>
14. Xia S., Wang C., Pan F., Xi X., Zeng H., Liu H. Detecting Stems in Dense and Homogeneous Forest Using Single-Scan TLS. *Forests*, **2015**, 6, pp. 3923–3945. <https://doi.org/10.3390/f6113923>
15. Xiong H., Wei A., Xu H., Li C., Lu Y., Li X., et al. Wood carbon density variation of *Pinus densata* and establishment of mixed effects models. *Journal of Northwest A & F University (Natural Science Edition)*, **2017**, 04, pp. 102-110 (in Chinese) <https://doi.org/10.13207/j.cnki.jnwafu.2017.04.015>
16. Zhang L., Dai J., Gao Q., Liu H., Zhang H., Zhao W., et al. Seedling adaptation of hybrid pine *Pinus densata* and its parental species in the high elevation habitat. *Journal of Beijing Forestry University*, **2012**, 05, pp. 15-24 (In Chinese) <https://doi.org/10.13332/j.1000-1522.2012.05.016>
17. Zhao F., Wang J., Gao H., Zhang F., Lu, C. Extraction of real leaf area index of individual tree based on terrestrial laser scanner. *Science of Surveying and Mapping*, **2019**, 04, pp. 81-86 (In Chinese) <https://doi.org/10.16251/j.cnki.1009-2307.2019.04.013>

ON-THE-FLY LAND COVER MAPPING USING MACHINE LEARNING WITH MULTISPECTRAL SATELLITE IMAGERY ON GOOGLE EARTH ENGINE

S. Papaiordanidis, C. Minakou, I.Z. Gitas

Laboratory of Forest Management and Remote Sensing, School of Forestry and Natural Environment, Aristotle University of Thessaloniki

Land cover is one of the most important environmental variables used to describe natural ecosystems. Constant changes on the Earth's surface create the need for new, up-to-date, and accurate land cover maps. During the last decades, remote sensing products have been used in conjunction with field measurements for the production of land cover maps in a cost-efficient manner. The aim of the present study was the development of a method for reliable on-the-fly land cover mapping using the Random Forest classifier and Sentinel-2 multispectral imagery on the Google Earth Engine cloud platform. The Random Forests algorithm was employed, and two classification schemes were adopted, one using the original 44 land cover classes used by the CORINE land cover product, and one using five general land cover classes (Artificial surfaces, Agricultural areas, Forest and semi-natural areas, Wetlands, and Water bodies), resulting in the generation of two land cover maps. The 2018 CORINE land cover product was used to identify training samples and validate the resulting land cover maps. The results showcased that the 44-class land cover map had an overall accuracy of 72.85% and the 5-class land cover map 88.32%. Overall, the results of this research indicate the capability of Random Forest algorithm in the reliable land cover classification.

Keywords: Land cover mapping, Sentinel-2, Google Earth Engine, Random Forest, Remote sensing, Pixel-based classification

Introduction

Land cover type is highly correlated with the biophysical properties of an area, and thus it is considered one of the most important environmental variables (Mason et al., 2003). Natural processes on the Earth's surface have a notable impact on climate, biodiversity, and the ecosystems ability to fulfill the needs of the modern human society (Mahmood et al., 2014). Land cover mapping is essential for planning and management of natural resources, as well as modeling environmental variables (Gómez et al., 2016). Traditionally, field measurements of land cover are considered as one of the most reliable land cover mapping techniques, however they are also costly, time-consuming, and present spatial limitations (Friedl et al., 2002). Additionally, constant changes in the Earth's surface, often render the existing land cover maps obsolete, creating the need for new updated maps. These obstacles lead to shortages of up-to-date and reliable land cover maps, which limit management bodies in the decision-making process.

In order to address this challenge, many scientists have investigated the potential of various classification algorithms to produce accurate land cover maps using satellite imagery (Anthony et al., 2007; Mahdianpari et al., 2018; Moser et al., 2012; Rodriguez-Galiano et al., 2012). One of the most commonly used algorithms in land cover mapping is the Random Forests ensemble. Random Forests have been shown to provide high overall accuracy in complex land cover classification problems (Maxwell et al., 2019; Na et al., 2010; Pelletier et al., 2016; Stefanski et al., 2013; Waske and Braun, 2009).

One of the challenges of using Random Forests is the preparation and set-up of the algorithm and the required software, as well as the input dataset preprocessing, and selecting and labeling the training samples. Currently, new cloud-based technologies offer easy access to data and large amounts of processing power to their users. Google Earth Engine (GEE) constitutes one of the most commonly used platforms which provides instant access to data and high processing power. Users can access GEE platform either from its online integrated development environment (IDE), or from the Application Program Interface (API) that is offered. Through GEE, users gain access to a large variety of datasets, including geospatial, satellite imagery, meteorological, census, etc. (Gorelick et al., 2017).

The aim of this study is to evaluate the effectiveness of Random Forest algorithm in land cover mapping, using Sentinel-2 multispectral data through the Google Earth Engine platform. The specific objectives are:

- The implementation of a method for calling and filtering the Sentinel-2 imagery archive and calculating spectral indices used for land cover mapping.
- The implementation of a method for training sample extraction from the Coordination of Information on the Environment (CORINE) land cover dataset.
- Land cover classification using the Random Forest algorithm.
- The quantitative and qualitative evaluation of the results in terms of land cover map overall accuracy and implementation effort.

Study area

The study area is located at the northern part of Greece, around the city of Thessaloniki, extending from 41°54'54.81" to 40°53'62.74" North, and from 22°19'91" to 23°47'71.06" East (fig. 1). The altitude ranges from sea level to 2,029 meters, and the surface area is 10,000 km². The climate is typical Mediterranean, with warm and dry summers, and cool and wet winters. This particular area was chosen because of its wide variety of land cover classes. Agricultural, forested, and artificial surfaces can be found in different variations, making the study area a suitable location to test the land cover mapping capabilities of the Random Forests algorithm.

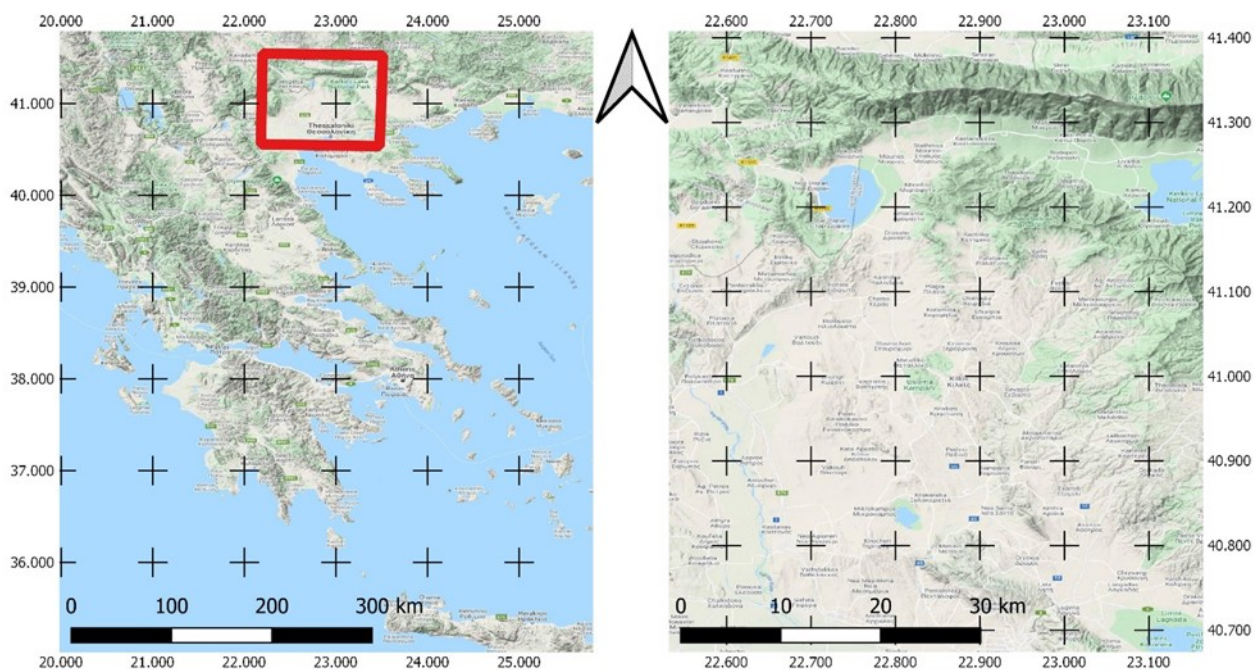


Fig. 1. Study area: Thessaloniki, Greece

Materials and methods

Sentinel-2 data

The satellite data that were used in this study included two images from Sentinel-2 MultiSpectral Instrument (MSI). The first image was acquired on October 26th, 2018 and the second on August 31st, 2020. Sentinel-2 imagery has a spatial resolution of 10, 20, and 60 meters (depending on the band), and a temporal resolution of 3-5 days depending on the location. The MSI instrument records spectral data in 13 bands ranging from the blue part of the electromagnetic spectrum (443 nm) to the short-wave infrared (2,190 nm).

The acquired images were already preprocessed to level 2A, which means that the images had been geometrically, radiometrically, and atmospherically corrected using the Sen2Cor algorithm by the Sentinel team (Main-Knorn et al., 2017).

CORINE data

The CORINE Land Cover (CLC) inventory provided by the Copernicus Land Monitoring Service was also used in this study (Büttner et al., 2004). The product is a thematic map with 44 land cover classes and a spatial resolution of 100 meters (fig. 2).

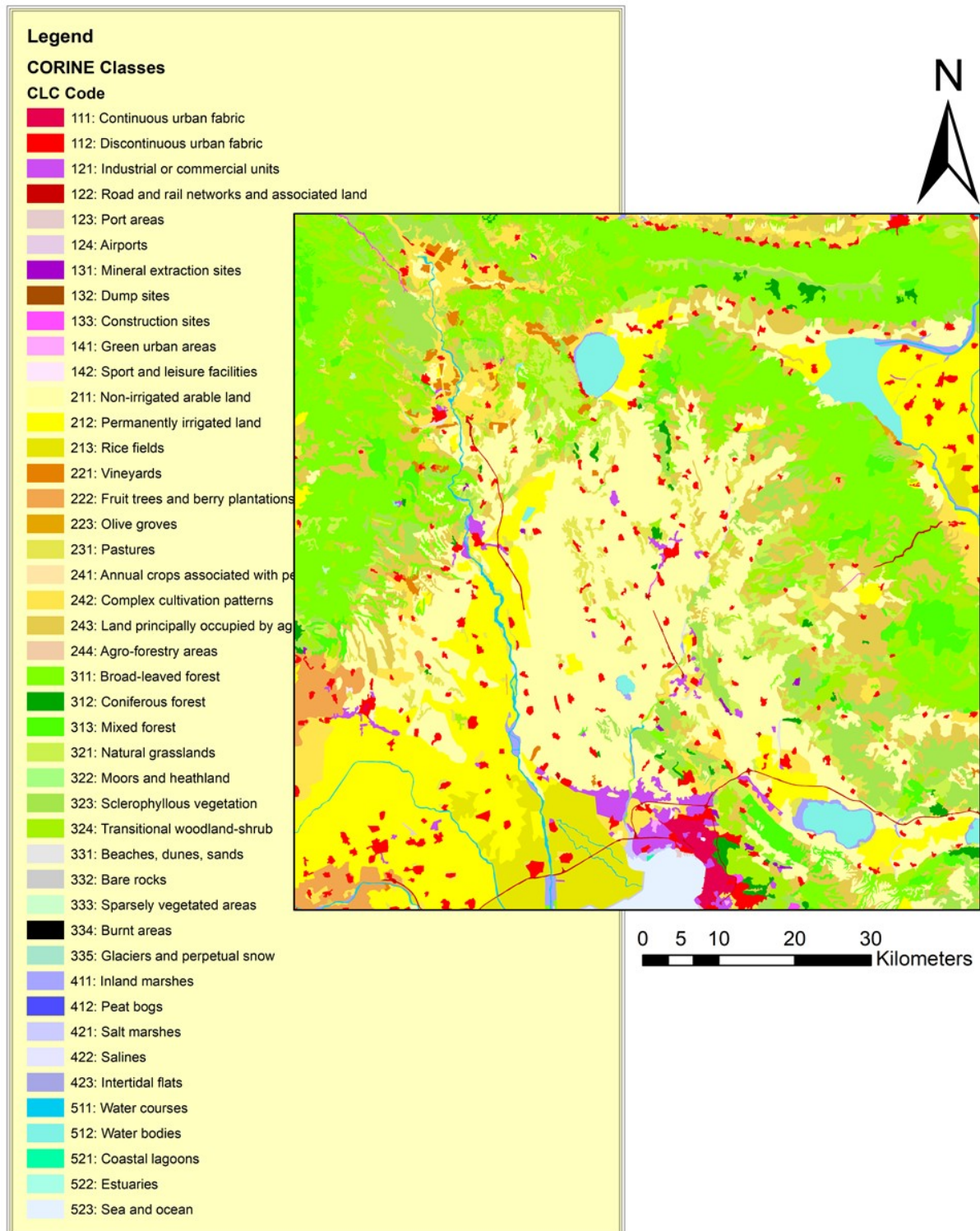


Fig. 2. CORINE land cover map of the study area with 44 classes

Additionally, a second map based on the CORINE product was constructed with the initial land cover classes summarized into five, namely Artificial surfaces, Agricultural area, Forest and semi-natural areas, Wetlands, and Water bodies (fig. 3).

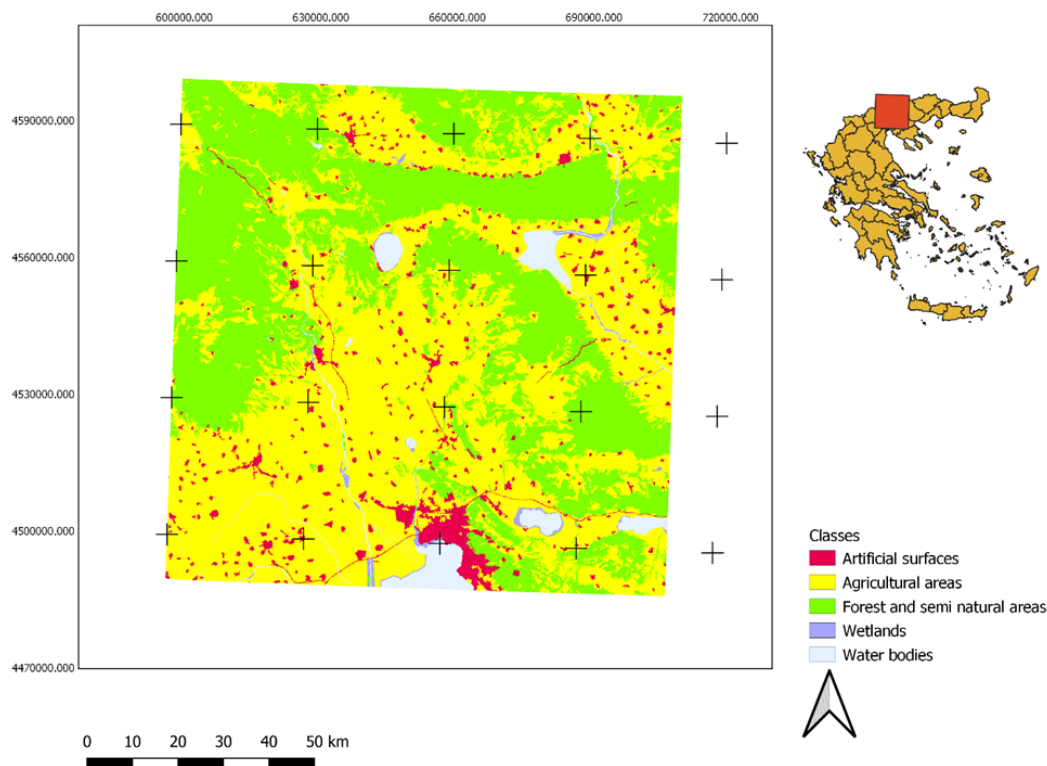


Fig. 3. CORINE land cover map of the study area with five classes

This was performed in order to investigate the potential effect of the employed classification scheme on the classifier's performance.

Methodology

The complete procedure of the methodology took part in GEE's online code editor (<https://code.earthengine.google.com/>). The steps followed are presented in the flowchart below (fig. 4).

The Sentinel-2 images were initially filtered by location and date. More specifically, the location filtering was carried out by setting a point in the study area and only keeping the Sentinel-2 images that their extent intersected with this point. The date filtering was done by limiting the images to ones that were acquired during 2018 and images that were acquired during 2020. The reason for that was to extract training

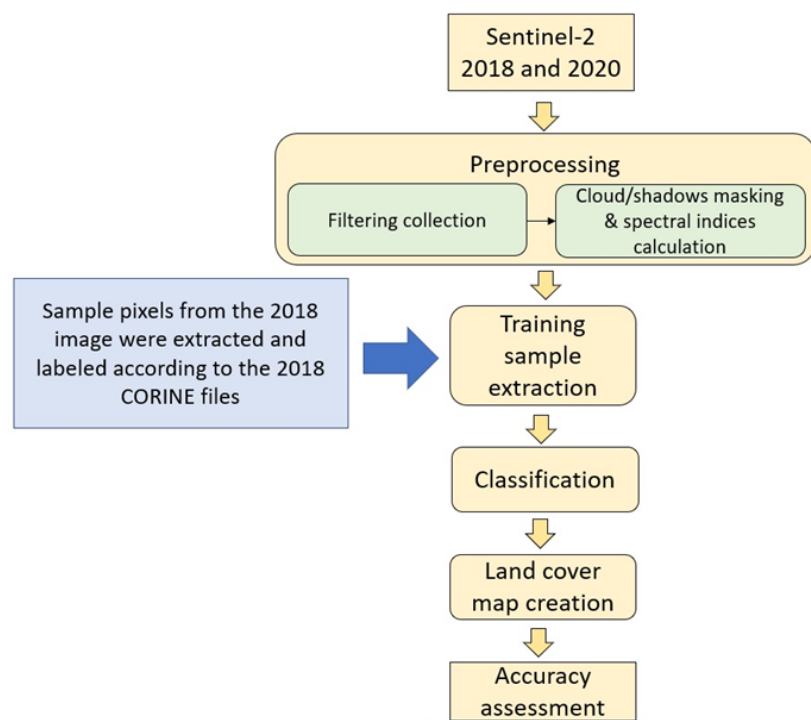


Fig. 4. Flowchart of the methodology

samples from the 2018 image, label them accordingly using the CORINE land cover map using random points, and then validate the trained algorithm using again random points (different from the ones used for training) labeled by the CORINE land cover product. The 2020 image was used to employ the trained algorithm and provide a land cover map for 2020.

The filtered images were then sorted in order of cloud cover using the Sentinel-2 metadata variable “CLOUDY_PIXEL_PERCENTAGE” and the least cloudy images for 2018 and 2020 were eventually selected. Next, a cloud and shadow mask was applied to the selected images by using the cirrus band and the cloud mask provided with Sentinel-2 2A level products.

After the examination of several spectral indices, BSI (Bare Soil Index), NDVI (Normalized Difference Vegetation Index), NDWI (Normalized Difference Water Index), and MCARI (Modified Chlorophyll Absorption in Reflectance Index) were selected to participate in the classification process (table 1).

Table 1

Spectral indices calculated

Index name	Formula	Citation
BSI	$((B6+B4)-(B5+B2))/((B6+B4)+(B5+B2))$	(Li and Chen, 2014)
NDVI	$((B8-B4))/(B8+B4)$	(Rouse Jr et al., 1974)
NDWI	$((B8-B11))/(B8+B11)$	(Gao, 1996)
MCARI	$[(B5-B4)-0.2*(B5-B3)]*(B5/B4)$	(Wu et al., 2008)

After the index calculation, 1000 random pixel samples were extracted from the 2018 Sentinel-2 image, labeled using the CORINE land cover map, and then the Random Forests algorithm was trained using 650 trees. Afterwards, 2000 random pixels (different from the ones used for training) were then selected in order to validate the classification accuracy using the CORINE land cover map. The validation was performed by GEE’s native error matrix construction functions and the overall accuracy was calculated.

Finally, a land cover map was produced using as input the 2020 Sentinel-2 image to the trained algorithm. This methodology process was repeated two times, using the 44-class and the 5-class CORINE land cover map, respectively.

Results & discussion

The produced land cover maps are presented below (fig. 5, fig. 6):

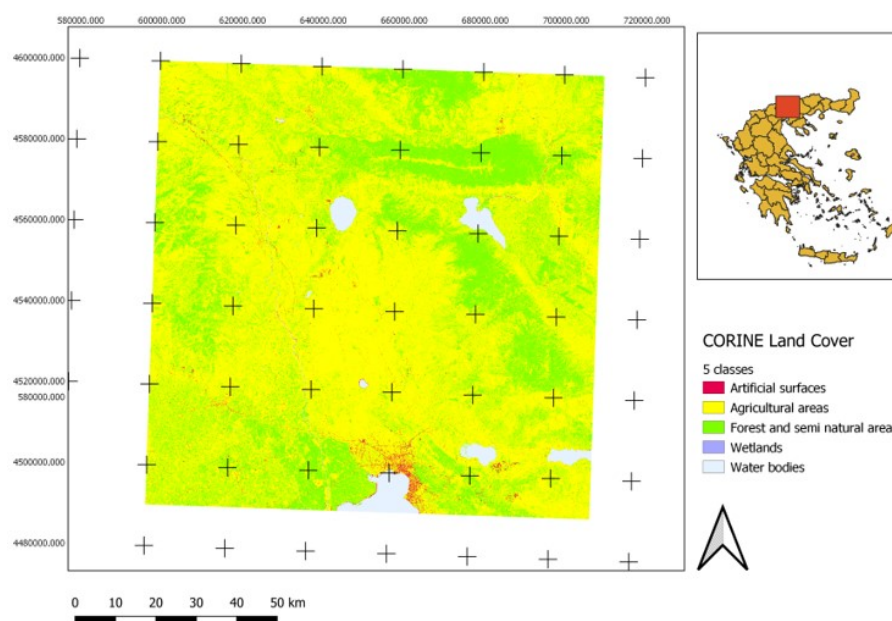


Fig. 5. Resulting 5-class land cover map produced by employing the Random Forests algorithm on the Sentinel-2 2020 image

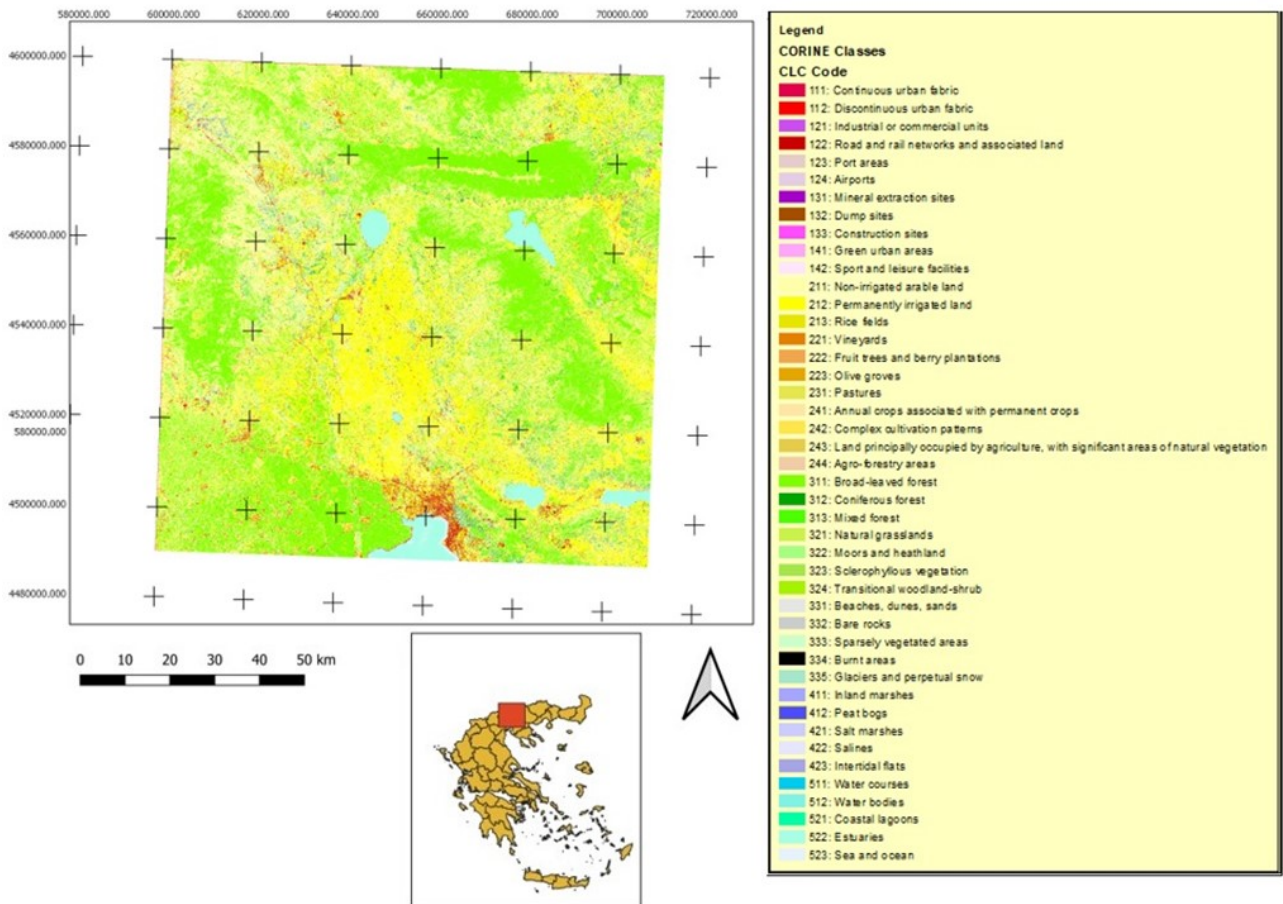


Fig. 6. Resulting 44-class land cover map produced by employing the Random Forests algorithm on the Sentinel-2 2020 image

The overall accuracies for the 5-class and the 44-class land cover maps were 88.32% and 72.85% respectively. Below, a comparison between each map and the corresponding original CORINE land cover map is presented (fig. 7, fig. 8).

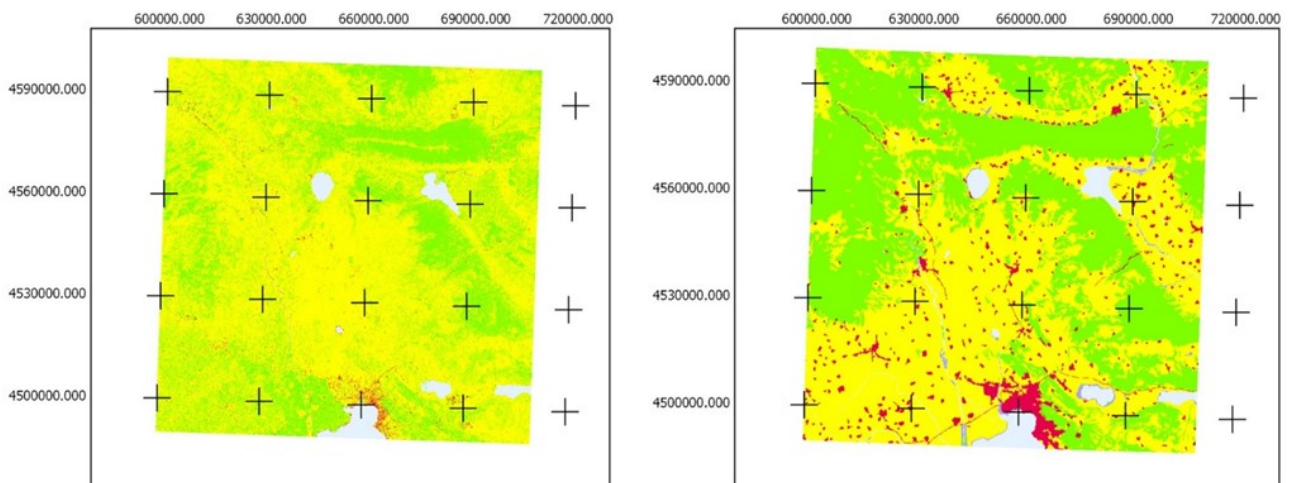


Fig. 7. The resulting 5-class land cover map (left) and the original 5-class CORINE land cover map (right)

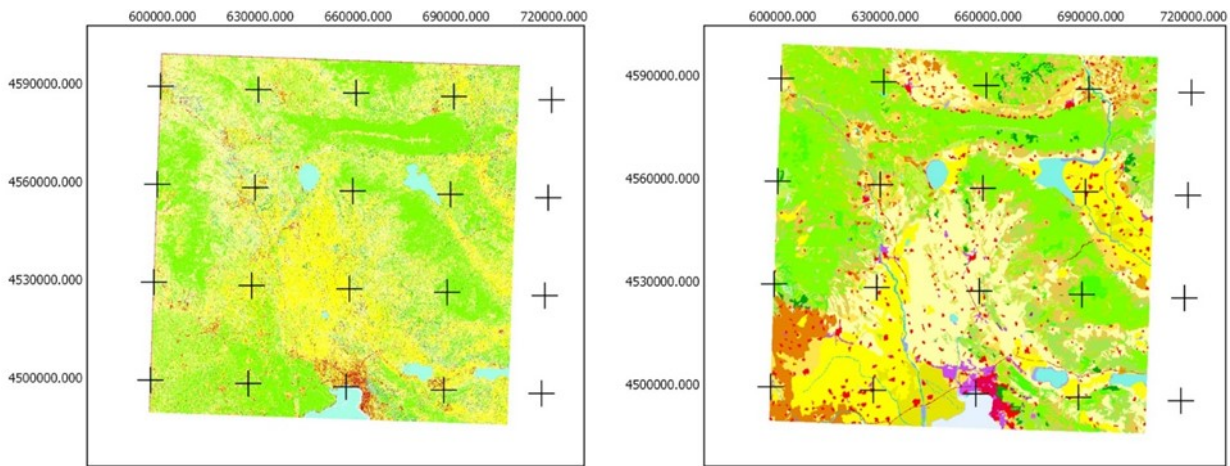


Fig. 8. The resulting 44-class land cover map (left) and the original 44-class CORINE land cover map (right)

It is obvious, that even though the overall accuracies of the resulting maps are quite high, and the general spatial distribution of the classes is correct, the fine details are lost. This classification error can be attributed to the fact that the spatial resolution of the CORINE land cover product is 100 meters, while Sentinel-2 spatial resolution is 10 meters. This could cause a problem in areas where a CORINE 100m pixel contains two different land cover classes. In these cases, only the value of the dominant class is given, while the spectral features recorded by Sentinel-2 are heterogeneous inside the confines of the CORINE pixel. Another issue with this classification is the fact that the distribution of classes was not taken into consideration. This means that since the training samples were selected randomly, minority classes (i.e. Wetlands) were not guaranteed to be part of the training samples.

One of the benefits of this methodology is that it can be used from any workstation with access to the internet and with no special preparation or special hardware requirements. Also, there is no need for downloading the required datasets since the whole procedure takes place in Google's remote servers. Another benefit of the methodology is its' time-efficiency since a Sentinel-2 tile can be classified in under a minute. This gives the ability to land managers to have a general idea of the spatial distribution of land covers in an area where no up-to-date land cover maps are available.

Conclusions

In this study, a method for calling the Sentinel-2 imagery archive and calculating spectral indices for land cover mapping was implemented. A method for training sample extraction from the CORINE land cover dataset was applied and a land cover classification using the Random Forest algorithm was performed. A method for confusion matrix construction and overall accuracy estimation was also employed for the validation of the classification results. Finally, a quantitative and qualitative evaluation of results in terms of land cover map accuracy and implementation effort was conducted.

The results showcased that produced maps had relatively high overall accuracy, but closer inspection of the maps revealed that there were some issues with the classification. For example, while the general class distribution was correct, the fine details of the land cover distribution were lost. This method provides the ability to land managers to trade between availability and accuracy. If an accurate and reliable land cover map is available there is no need to use this method, but when there is no such product, this method can rapidly generate a land cover map that represents the general spatial distribution of land cover in an area. More specifically:

- Using the Random Forest algorithm on Sentinel-2 imagery and CORINE land cover maps on Google Earth Engine cloud platform, greatly decreases the time needed for land cover mapping.
- Using the Random Forest algorithm on Sentinel-2 imagery and CORINE land cover maps on Google Earth Engine cloud platform, still produces comparable results to other land cover mapping products.

Future research could include the use of other machine learning classification techniques (i.e. Deep Learning) and Sentinel-2 imagery on Google Earth Engine. A different training set other than CORINE land cover map, or even different optical satellite datasets with higher resolution (i.e. WorldView). Finally, other types of remote sensing data like LiDAR or SAR could be investigated in combination with the above-mentioned methods.

This work was carried out in the Laboratory of Forest Management and Remote Sensing, in the School of Forestry and Natural Environment, in Aristotle University of Thessaloniki. The lead author (Stefanos Papaioordanidis) would like to thank Professor Ioannis Gitas for the helpful discussion and their insightful comments.

The European Commission support for the production of this publication does not constitute an endorsement of the contents which reflects the views only of the authors, and the Commission cannot be held responsible for any use which may be made of the information contained therein.

References

1. Anthony, G. Image classification using SVMs: one-against-one vs one-against-all, G. Anthony, H. Gregg, M. Tshilidzi, *arXiv preprint arXiv:0711.2914*, **2007**.
2. Büttner, G. The CORINE land cover 2000 project, Büttner, G., Feranec, J., Jaffrain, G., Mari, L., Maucha, G. and Soukup, T., *EARSeL eProceedings*, **2004**, Vol. 3, No. 3, pp 331-346.
3. Friedl, M. Global land cover mapping from MODIS: algorithms and early results M.A. Friedl, D.K. McIver, J.C.Hodges, X.Y. Zhang, D. Muchoney, A.H. Strahler, et al., *Remote sensing of Environment*, **2002**, Vol. 83, No. 1-2, pp. 287-302.
4. Gao, B.-C. NDWI—A normalized difference water index for remote sensing of vegetation liquid water from space, Gao, B.-C., *Remote sensing of Environment*, **1996**, Vol. 58, No. 3, pp 257-266.
5. Gómez, C. Optical remotely sensed time series data for land cover classification: A review, C. Gómez, J.C. White, and M.A.Wulder, *ISPRS Journal of Photogrammetry and Remote Sensing*, **2016**, Vol. 116, No., pp. 55-72.
6. Li, S. A new bare-soil index for rapid mapping developing areas using landsat 8 data, Li, S. and Chen, X., *The International Archives of Photogrammetry, Remote Sensing and Spatial Information Sciences*, **2014**, Vol. 40, No. 4, pp 139.
7. Mahdianpari, M. Very deep convolutional neural networks for complex land cover mapping using multispectral remote sensing imagery, Mahdianpari, M., Salehi, B., Rezaee, M., Mohammadimanesh, F. and Zhang, Y., *Remote Sensing*, **2018**, Vol. 10, No. 7, pp. 1119.
8. Mahmood, R. Land cover changes and their biogeophysical effects on climate, Mahmood, R., Pielke Sr, R. A., Hubbard, K. G., Niyogi, D., Dirmeyer, P. A., McAlpine, C. et al., *International journal of climatology*, **2014**, Vol. 34, No. 4, pp. 929-953.
9. Main-Knorn, M. Sen2Cor for sentinel-2, Main-Knorn, M., Pflug, B., Louis, J., Debaecker, V., Müller-Wilm, U. and Gascon, F., *Proc. Conf. Image and Signal Processing for Remote Sensing XXIII*, **2017**, International Society for Optics and Photonics.
10. Mason, P. The second report on the adequacy of the global observing systems for climate in support of the UN-FCCC, P. Mason, M. Manton, D. Harrison, A. Belward, A. Thomas, D. Dawson, et. al., *GCOS Rep*, **2003**, p. 82.
11. Maxwell, A. E. Large-Area, High Spatial Resolution Land Cover Mapping Using Random Forests, GEOBIA, and NAIP Orthophotography: Findings and Recommendations, Maxwell, A. E., Strager, M. P., Warner, T. A., Ramezan, C. A., Morgan, A. N. and Pauley, C. E., *Remote Sensing*, **2019**, Vol. 11, No. 12, pp 1409.
12. Moser, G. Land-cover mapping by Markov modeling of spatial-contextual information in very-high-resolution remote sensing images, Moser, G., Serpico, S. B. and Benediktsson, J. A., *Proceedings of the IEEE*, **2012**, Vol. 101, No. 3, pp 631-651.
13. Na, X. Improved land cover mapping using random forests combined with landsat thematic mapper imagery and ancillary geographic data, Na, X., Zhang, S., Li, X., Yu, H. and Liu, C., *Photogrammetric Engineering & Remote Sensing*, **2010**, Vol. 76, No. 7, pp 833-840.
14. Pelletier, C. Assessing the robustness of Random Forests to map land cover with high resolution satellite image time series over large areas, Pelletier, C., Valero, S., Inglada, J., Champion, N. and Dedieu, G., *Remote sensing of Environment*, **2016**, Vol. 187, No., pp 156-168.
15. Rodriguez-Galiano, V. F. An assessment of the effectiveness of a random forest classifier for land-cover classification, Rodriguez-Galiano, V. F., Ghimire, B., Rogan, J., Chica-Olmo, M. and Rigol-Sanchez, J. P., *ISPRS Journal of Photogrammetry and Remote Sensing*, **2012**, Vol. 67, No., pp 93-104.

16. Rouse Jr, J. Paper A 20, Rouse Jr, J., Haas, R., Schell, J. and Deering, D., Proc. Conf. *Third Earth Resources Technology Satellite-1 Symposium: The Proceedings of a Symposium Held by Goddard Space Flight Center at Washington, DC on December 10-14, 1973: Prepared at Goddard Space Flight Center*, **1974**, Scientific and Technical Information Office, National Aeronautics and Space
17. Stefanski, J. Optimization of object-based image analysis with random forests for land cover mapping, Stefanski, J., Mack, B. and Waske, B., *IEEE Journal of Selected Topics in Applied Earth Observations and Remote Sensing*, **2013**, Vol. 6, No. 6, pp 2492-2504.
18. Waske, B. Classifier ensembles for land cover mapping using multitemporal SAR imagery, Waske, B. and Braun, M., *ISPRS Journal of Photogrammetry and Remote Sensing*, **2009**, Vol. 64, No. 5, pp 450-457.
19. Wu, C. Estimating chlorophyll content from hyperspectral vegetation indices: Modeling and validation, Wu, C., Niu, Z., Tang, Q. and Huang, W., *Agricultural and forest meteorology*, **2008**, Vol. 148, No. 8-9, pp 1230-1241.

ASSESSMENT OF LAND SURFACE TEMPERATURE AND DROUGHT INDICES FOR THE KLERKSDORP-ORKNEY-STILFONTEIN-HARTEBEEFSFONTEIN (KOSH) REGION

Noluvuyo Dudumashe, Abraham Thomas
Council for Geoscience, Pretoria 0184, South Africa.

Land surface temperature (LST) is a key calculator of local climate, vegetation growth, and urban change. Spatial and temporal variation of LST over land use/land cover (LULC) features results in changes in environmental factors that influence the characteristics of the land surface. In this study, some remote sensing techniques have been applied to Landsat 8 data acquired during summer and spring seasons of years 2019, 2018, and 2013 to estimate normalized difference vegetation index (NDVI), LST, normalized difference built-up index (NDBI), three drought indices viz. vegetation supply water index (VWSI), crop water supply index (CWSI) and temperature condition index (TCI) and analysed the spatial-temporal trends in LST among major LULC of an arid part of North West Province of South Africa known as Klerksdorp-Orkney-Stilfontein-Hartebeesfontein (KOSH) region. The results shows that there is a direct negative relationship between LST and NDVI. The study compared three drought indices for monitoring the water scarcity of the area. The finding also indicates a positive relationship between LST and CWSI that is relevant to soil moisture and NDBI. The findings from the study prove the capability of optical remote sensing in monitoring LST and drought in the region. The study reveals the usefulness of the remotely sensed data of Landsat 8 satellite in estimating LST and drought changes in the KOSH area. This study also tried to assess the usefulness of Landsat 8 bands in deriving vegetation index and drought indices for monitoring drought in the KOSH region during three years (2013, 2018 and 2019).

Keywords: Landsat 8, land surface temperature, drought, remote sensing, vegetation and drought indices, climate change.

Introduction

Land surface temperature (LST) is the primary climatic parameter in calculating the surface radiation and the energy exchange (He et al., 2019). Climate change is one of the most critical challenges that the world faces. Many studies have reported that climate change has a significant effect on the land surface temperature and its other parameters (Brohan et al., 2006; Hansen et al., 2010). Simó et al. (2016) stated that LST is also important for controlling the dynamics of the earth's surface. Land use/land cover (LU/LC) and land surface temperature (LST) is the most important amid these parameters. Several researchers used LST for understanding changes in temperature fluctuations which are major aspects that change the land use/land cover (Owojori and Xie, 2005). LST is defined as the temperature felt when there is an exchange of long-wave radiation and turbulent heat fluxes within the surface-atmosphere interface. The LST is being increasingly used to evaluate climate change in urban zones. Several techniques previously have been applied for calculating land surface temperature through ground base data, but that is costly (Rehman et al., 2015). LST is needed for better environmental monitoring and climate change mitigation.

The time-series observations are frequently employed in monitoring approaches related to remote sensing (RS) and LST. The application of time series in the assessment of the climate variability over an extended period can be improved by the integration of spatial data from multiple satellite systems (Kothe et al., 2019). The Landsat imageries are the most valuable source of spatial information at 30-m resolution (Herrero-Huerta et al., 2019). It is also useful in continuous global coverage to provide an opportunity to characterize human-scale processes (Chen et al., 2017). Chastain et al. (2019) stated that operational Landsat 8 (OLI & TIRS) could supply a revisit frequency of 8 days at the equator. The Landsat sensors have a high spatial resolution helping in the monitoring of the urban thermal environment (XIAO et al., 2007a; Sobrino et al., 2012). Thermal infrared (TIR) bands are very important bands in estimating LST in an area and monitoring climate change. The USGS recommendation is not to use TIRS Band 11 due to its larger calibration uncertainty, only Band10 was used in the LST calculation. However, not every remote sensing

platform has the thermal-infrared bands on their sensor.

Ustin et al. (2004) stated that remote sensing must play a part in providing the data required to monitor the conditions and change of ecosystem at all spatial scales. This is an increasing field of environmental scientists. Therefore, acquiring LST from remotely sensed data becomes one of the important main factors for such studies. Torrion et al. (2014) outlined that LST is associated to surface energy fluxes, the latent heat flux, and evapotranspiration and water stress. According to Cammalleri and Vogt (2015), LST is connected to surface longwave emission and calculating soil moisture. Whereas Duan et al. (2014) stated that considering meteorological and hydrological processes in a changing climate is the best parameter in estimating LST. The presented study aimed to estimate the LST using Landsat 8 images acquired during the year 2013, 2018, and 2019, to map and monitor the area for changes in LST and drought through drought monitoring indices viz. vegetation supply water index (VWSI), crop water supply index (CWSI) and temperature condition index (TCI), and to compare the results for these three years.

Study area

The Klerksdorp-Orkney-Stilfontein-Hartebeesfontein (KOSH) region was selected as a study area. The geographic location of the KOSH area is in the North West province of South Africa (fig. 1). The region comprises four districts, namely Klerksdorp, Orkney, Stilfontein, Hartebeesfontein, covering an area of 2757 km². The climate of the region is warm to hot summers (November to February/March) and cool, dry winters (May to August) are typical. KOSH region is part of the Witwatersrand gold mining area, underlain by sedimentary, extrusive, and intrusive rocks of Transvaal Super Group (Thomas, 2020). Figure 2 depicts the land use/land cover of the area showing that the most area is covered by the grassland cover.

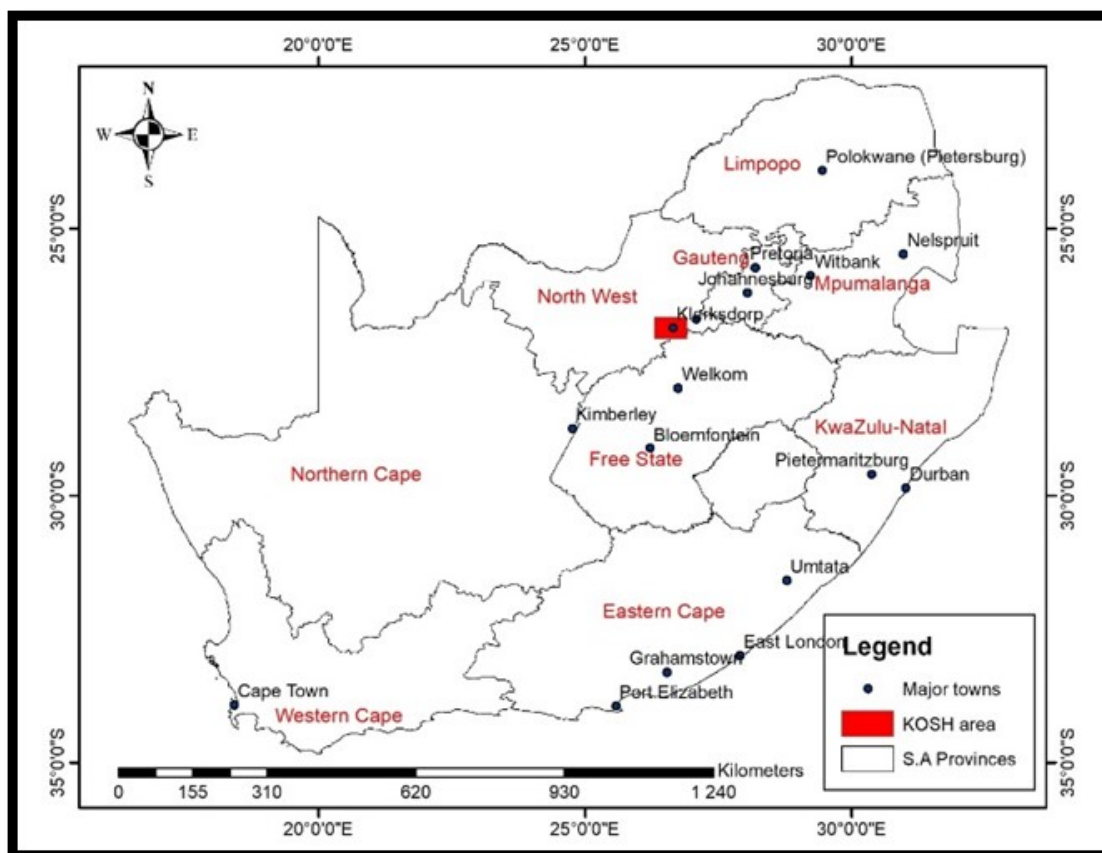


Fig. 1. Location map of Klerksdorp-Orkney-Stilfontein-Hartebeesfontein (KOSH) region

LAND USE / LAND COVER DISTRIBUTION OF KOSH AREA BASED ON NATIONAL LAND COVER DATASET 2013-2014

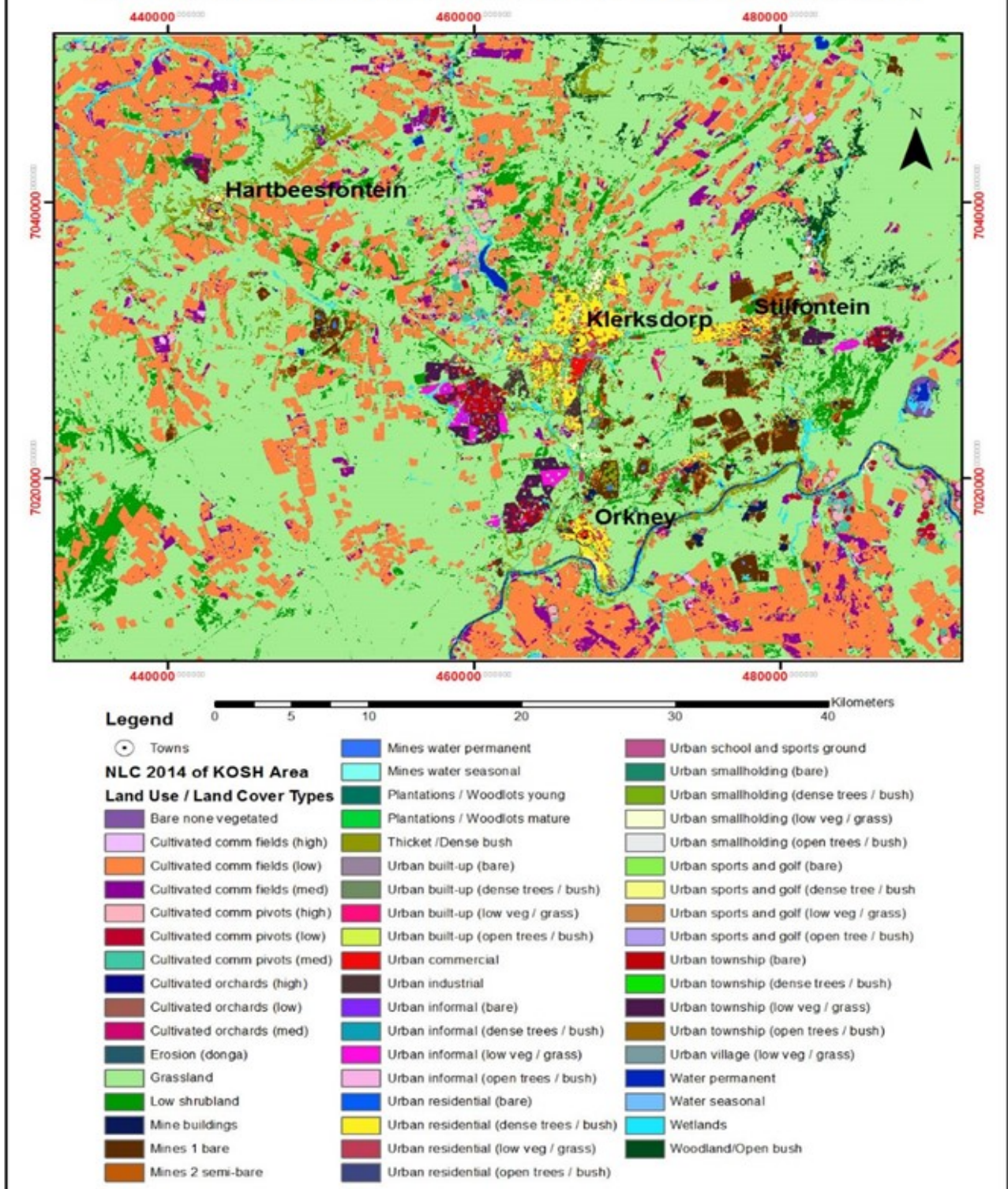


Fig. 2. Land use/ Land cover distribution of Klerksdorp-Orkney-Stilfontein-Hartebeesfontein (KOSH) area based on national land cover dataset 2013-2014

Data and software used for the research

Data used for remote sensing analysis

In this study, the first step was downloading Landsat 8 satellite data (cloud cover of 0%) of KOSH region from the USGS Earth Explorer website (<https://www.usgs.gov/>). The level-1 prod-

uct Landsat 8 data acquired during summer and spring seasons of three-years (2013, 2018, and 2019) were searched. The images were georeferenced using ArcGIS software to the Universal Transverse Mercator (UTM) Projection System. The images of Landsat 8 (footprint: 171/079) was used in this study. Satellite data were acquired over two different seasons (end of summer and the beginning of spring) for three different years to assess and monitor the study over time. Fig 3 shows the extent of the spatial coverage with the study area and Table 1 shows the band details of the data used. Thermal bands (TIR) were used for the calculation of the land surface temperature (LST) without being pre-processed. The band 10 was used from Landsat 8 OLI due to larger calibration uncertainty of band 11 found to have.

Table 1

Landsat image characteristics used in this research (Source: NASA 2003, USGS 2015)

Characteristics	Landsat 8 OLI/TIRS
Band number	30 m: Band 1- Coastal aerosol Band 2 – Blue Band 3 – Red Band 4 – Green Band 5 – NIR Band 6 – SWIR -1 Band 7 – SWIR -2 Band 9 – Cirrus 15m: Band 8 – Pan 100m: Band 10 - TIR -1 Band 11 – TIR - 2
Thermal band spectral range	Band 10 (10,60 – 11,19 nm) Band 11 (11,50 – 12,51 nm)
Acquisition dates	Summer 26/03/2013 03/02/2018 22/02/2019 Spring 02/09/2013 15/09/2018 02/09/2019

The software used for this study were ArcGIS 10.4 version and ENVI 5.5 version. LST and Normalized satellite indices were calculated using the raster calculator tool of ArcGIS 10.4. The shapefile of respective areas were created and area of interest (AOI) was extracted using ArcGIS.

Methodology

Land surface temperature (LST) calculation is one of the steps to determine the drought on the Earth's surface. The remotely sensed images can be used to derive this information using algorithms that are specifically developed to provide information using 'RT' – Real-time Terrain Corrected dataset containing both OLI & TIRS bands. The three bands used in this study are band 4, band 5 and thermal band 10. The thermal band 10 of this dataset was not processed for atmospheric correction and surface reflectance retrieval for land surface temperature; however, the red and near-infrared bands (bands 4 and 5) were pre-processed using ENVI software for atmospheric correction. Later NDVI values were calculated in ENVI software using the red and near-infrared bands.

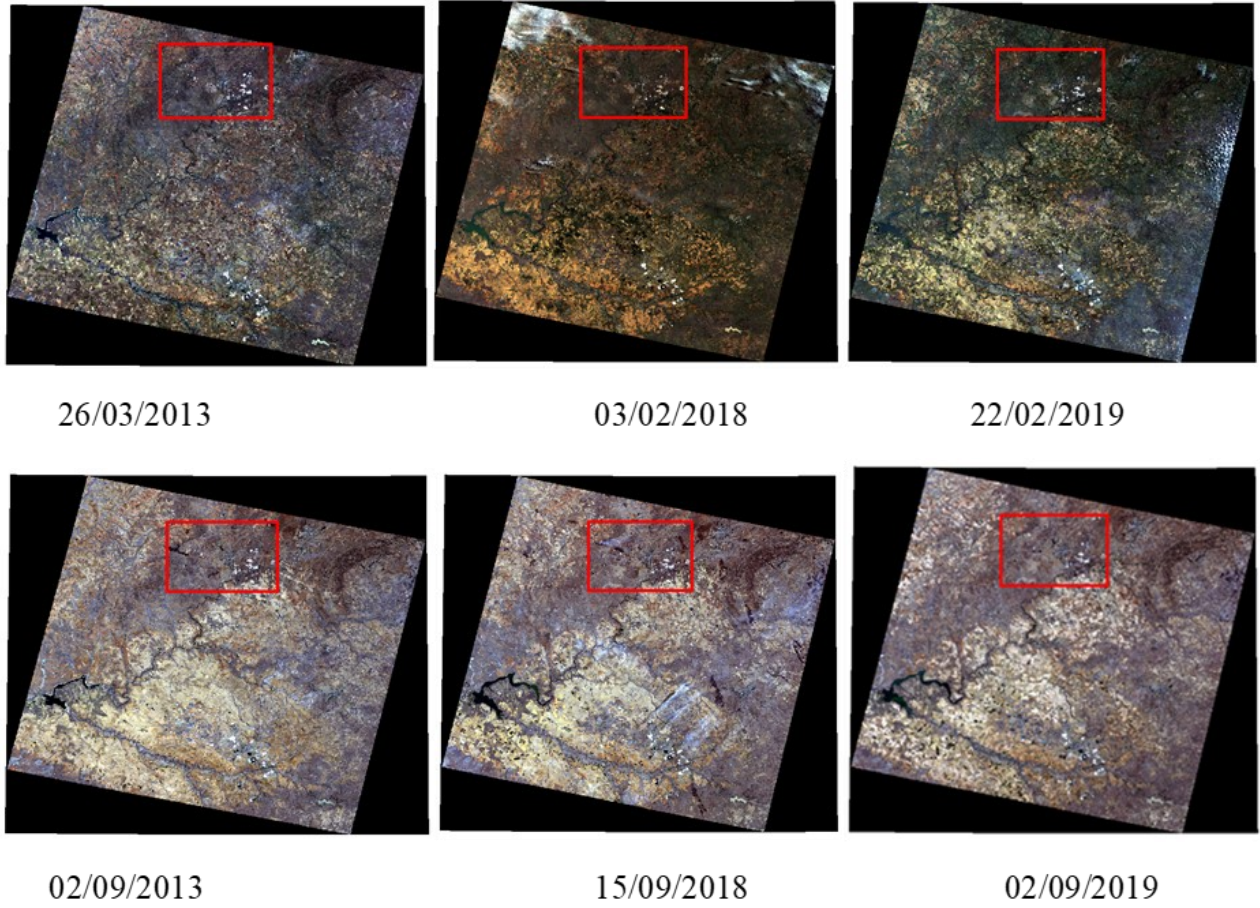


Fig. 3. Preview images of the used data of 2019, 2018, and 2013 to see the extent of spatial coverage with the extent of the study area

*Equations used to calculate Land Surface Temperature with Landsat 8 satellite images
TOA ($L\lambda$) spectral transmittance*

The first step in computing LST is to transform the DN of the thermal infrared band into spectral radiance ($L\lambda$) by using the following equation obtained from the Landsat user's handbook. The reason for transforming the DN was to calibrate for the produced noise from the sensors, which measure the reflectance from the Earth's surface in the form of Digital Numbers (DN) representing each pixel.

$$L\lambda = ML * Q_{cal} + AL, \quad (1)$$

where ML is the band specific multiplicative rescaling factor from the metadata, AL is the band specific additive scaling factor and Q_{cal} represents the symbolized values of quantized and calibrated standard product pixels (D). The DN of Landsat 8 of band 10 images were converted to spectral radiance, using the above equation which is given by Rosas et al. (2017).

Brightness Temperature

The second step is to convert the band radiance into brightness temperatures (TB) in Celsius using a conversion formula given below (equation 2). The TIR data values of band 10 were converted to brightness temperatures (TB), which is the microwave radiance travelling upward from the top of Earth's atmosphere, using the thermal constants provided in the metadata file (Yang et al., 2014). To achieve accuracy for the TB conversion, equation 2 was implemented through the ATCOR module of ArcGIS. The result in Kelvin was converted to Celsius by adding the absolute zero.

$$TB = (K2 / (\ln (K1 / L) + 1)) - 273.15 , \quad (2)$$

where TB is the satellite brightness temperature in Celsius, and K1 and K2 represent thermal conversion from the metadata (Suresh et al., 2016). Table 2 shows the constants K1 and K2 used for the Landsat satellites.

Table 2

Constants K1 and K2 for the Landsat satellites

Constant	Landsat 8 (Band 10)	Landsat 8 (Band 11)
K1 (watt/meter squared *ster*)	774.89	480.89
K2(Kelvin)	1321.08	1201.14
Rescaling	ML 0.0003342 AL 0.10	

Table 3

Center wavelength for Landsat satellites.

Satellite	Band	Center Wavelength
Landsat (OLI) 8	10	10.8
Landsat (OLI) 8	11	12

Normalized Difference Vegetation Index (NDVI)

NDVI is an indicator used to analyse the greenness of the observed area. As Weng et al. (2004) stated, estimating NDVI is essential since the amount of vegetation present is a factor for LST retrieval. NDVI is calculated using the following equation/formula:

$$NDVI = NIR \text{ (band 5)} - Red \text{ (band 4)} / NIR \text{ (band 5)} + Red \text{ (band 4)} , \quad (3)$$

where NDVI values range between -1 and 1.

Proportion of Vegetation Cover

Following the NDVI calculation, the vegetation index (Pv) was calculated according to the equation as described by XIAO et al. (2007b). According to Jin et al. (2015) and Quintano et al. (2015), the proportion of vegetation (Pv) is computed by using soil and vegetation NDVI values calculated by Equation 4:

$$Pv = \text{Square} ((NDVI - NDVI_{min}) / (NDVI_{max} - NDVI_{min})), \quad (4)$$

where NDVI is the normalized difference vegetation index. $NDVI_{min}$ and $NDVI_{max}$ are the minima and maximum values of the NDVI (Sobrino and Romaguera, 2004).

Estimation of emissivity

The land surface emissivity was derived from the NDVI as proposed by Ngie et al. (2017). According to Pal and Ziaul (2017), the Ground Emissivity (ϵ) values are calculated using equation 5:

$$\epsilon = m * Pv + 0.986 , \quad (5)$$

where $m=0,004$ and $n=0,986$. PV is the proportion of vegetation extracted from equation (4).

Land Surface Temperature

The Land surface temperature (LST) is estimated from the brightness temperature (TB). For estimating brightness temperatures (TB), it is assumed that the Earth is a blackbody, which is not, and this assumption can lead to some errors in surface temperature (Ogunode and Akombelwa, 2017). To minimize these errors, emissivity correction is important and this correction applied to equation 2 to retrieve the LST from TB:

$$LST = (TB / (1 + (0.00115 * TB / 1.4388) * \ln(\epsilon))) . \quad (6)$$

The main data processing steps (workflow) to be followed for data analysis using a GIS or a remote sensing software for retrieving LST from the Landsat 8 data is shown in figure 4.

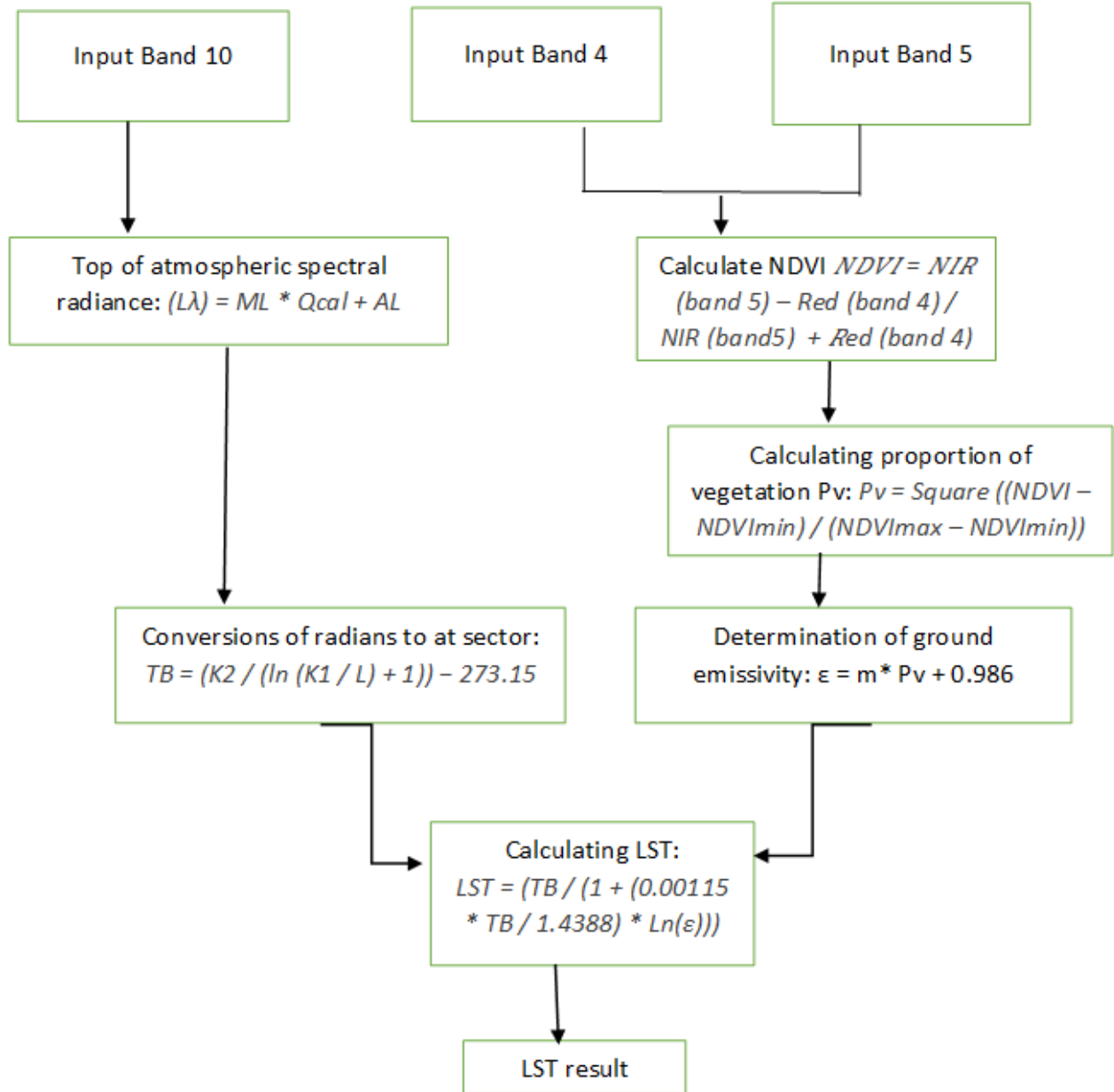


Fig. 4. LST retrieval flowchart

Normalized Difference Built-up Index

The NDBI is an index which is used to detect built-up area from other LULC types. The value of the NDBI is between -1 and 1, where the negative values indicate water body and positive value represent areas that have higher built up and other paved surface areas; whereas zero NDBI values represent areas covered with vegetation (Balew and Korme, 2020). This index can be computed as:

$$NDBI = B_{SWIR} - B_{NIR} / B_{SWIR} + B_{NIR} , \quad (7)$$

where B_{SWIR} is shortwave infrared band reflectance (band 6 of Landsat 8).

Drought indices: temperature condition index (TCI), crop water stress index (CWSI) and vegetation water supply index (VSWI)

Three drought indices were computed in this study to compare the drought in three different years. The first drought indices were calculated using the Temperature Condition Index (TCI) algorithm. Temperature Condition Index (TCI) is an algorithm developed by Kogan (1998) for detecting drought by viewing the difference from the surface temperatures level resulting in water-saturated soil, which affects vegetation stress level (Equation 8).

Secondly, we calculated the drought using the crop water stress index (CWSI) to identify areas where the crops are under water stress. Crop Water Stress Index (CWSI) is a technique for detecting drought due to water lost through evapotranspiration (Equation 9). Lastly, the vegetation supply water index (VSWI) calculated by dividing NDVI values with LST values (equation 10) was also used in identifying areas with drought. The three drought indices have an opposite index value explanation; zero in TCI indicates drought condition, but the wet condition in CWSI. The last index vegetation water supply index was used. Vegetation supply water index is the water supply in the vegetation. The reason for using the three indices was to compare the drought results and see if the algorithm can identify the same area with drought.

$$TCI = (LST_{max} - LST / LST_{max} - LST_{min}) * 100, \quad (8)$$

$$CWSI = LST - LST_{min} / LST_{max} - LST_{min}, \quad (9)$$

$$VSWI = NDVI / LST. \quad (10)$$

Statistical analysis is very important to analyse different variables. In this study, descriptive statistical analysis was applied for analysing LST, NDVI and NDBI for each study period. The results from this statistical analysis mainly show the mean, minimum, maximum and standard deviation of the calculated indices for different periods of study.

Results and discussion

The spatial-temporal pattern of Normalised difference vegetation index

Figure 5 and figure 6 show the spatial distribution/variation of NDVI values for the summer/spring periods of the year 2013, 2018 and 2019. The most affected areas are in the northern, middle, western and central parts of KOSH. Particularly the middle region of the KOSH shows an extreme drought condition. Results presented in figure 5 (summer 2013, 2018 and 2019), indicate that NDVI values observed were ranged from -0.27 to 0.64. Most areas of the KOSH had low NDVI because of low vegetation cover and high vegetation in areas with vegetation. However, places seen to the east of KOSH had lower NDVI values because the area's lack of vegetation cover and bare surfaces dominate the area 2018. In 2013, the maximum NDVI value was 0.57 and a minimum of -0.33 and with a mean of 0.17. However, the minimum, maximum and mean NDVI values in 2018 were increased to -0.27, 0.64, and 0.25. Furthermore, in the year 2019, the maximum NDVI was 0.63 but in the spring of 2019, it was declined to 0.59 (fig 6), while the mean decreased from 0.08 to 0.04 (table 4).

Table 4

Statistical summary of NDVI values in KOSH (2013, 2018 and 2019).

Year	Mean	Max	Min	STD
2013 Summer	0.17	0.57	-0.33	0.04
2013 Spring	0.11	0.56	-0.41	0.03
2018 Summer	0.25	0.64	-0.27	0.07
2018 Spring	0.13	0.60	-0.30	0.03
2019 Summer	0.29	0.63	-0.29	0.08
2019 Spring	0.14	0.59	-0.32	0.04

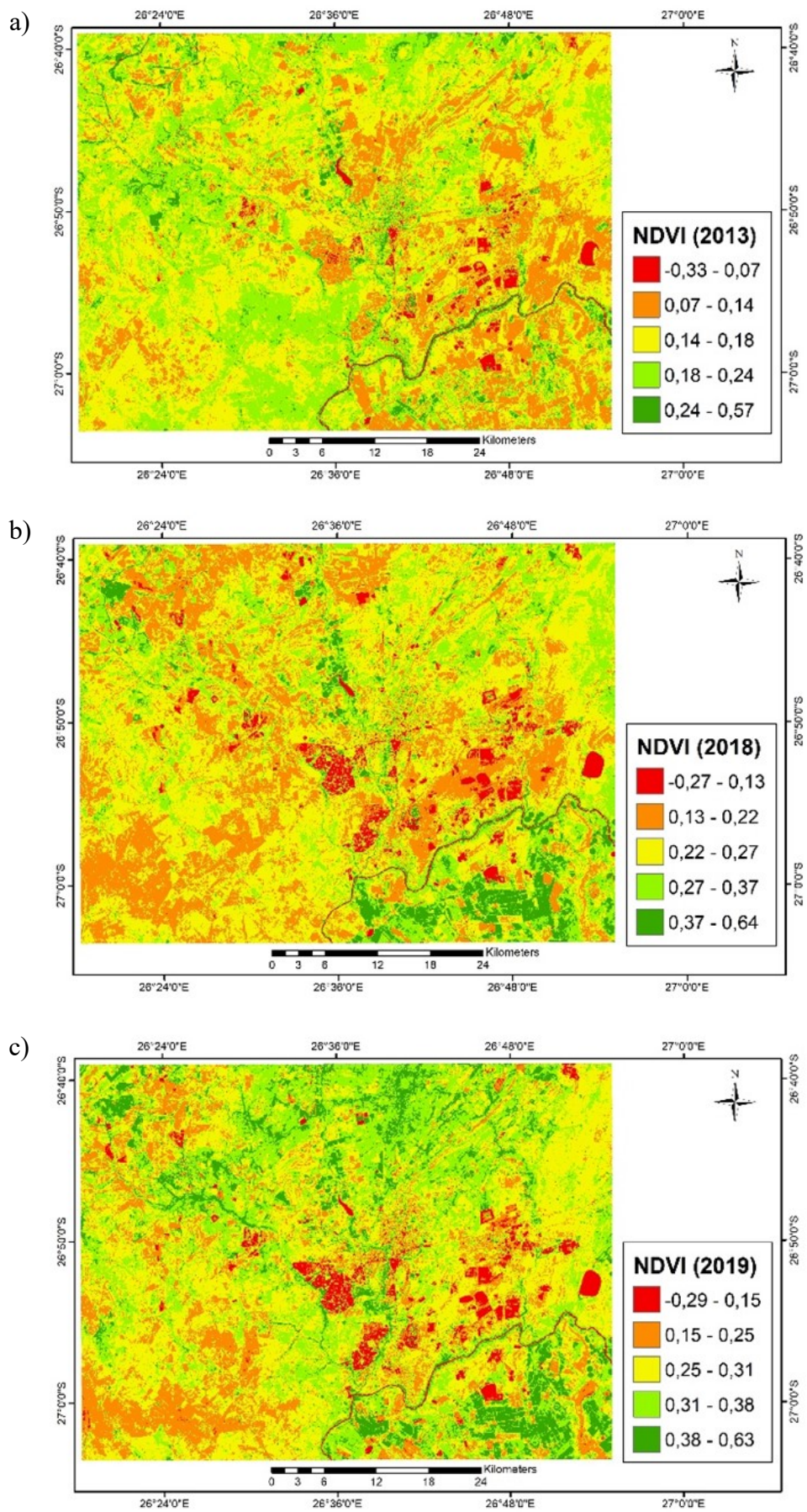


Fig. 5. Spatial-temporal pattern of NDVI dynamics of KOSH during the summer seasons of the year (a) 2013, (b) 2018, and (c) 2019

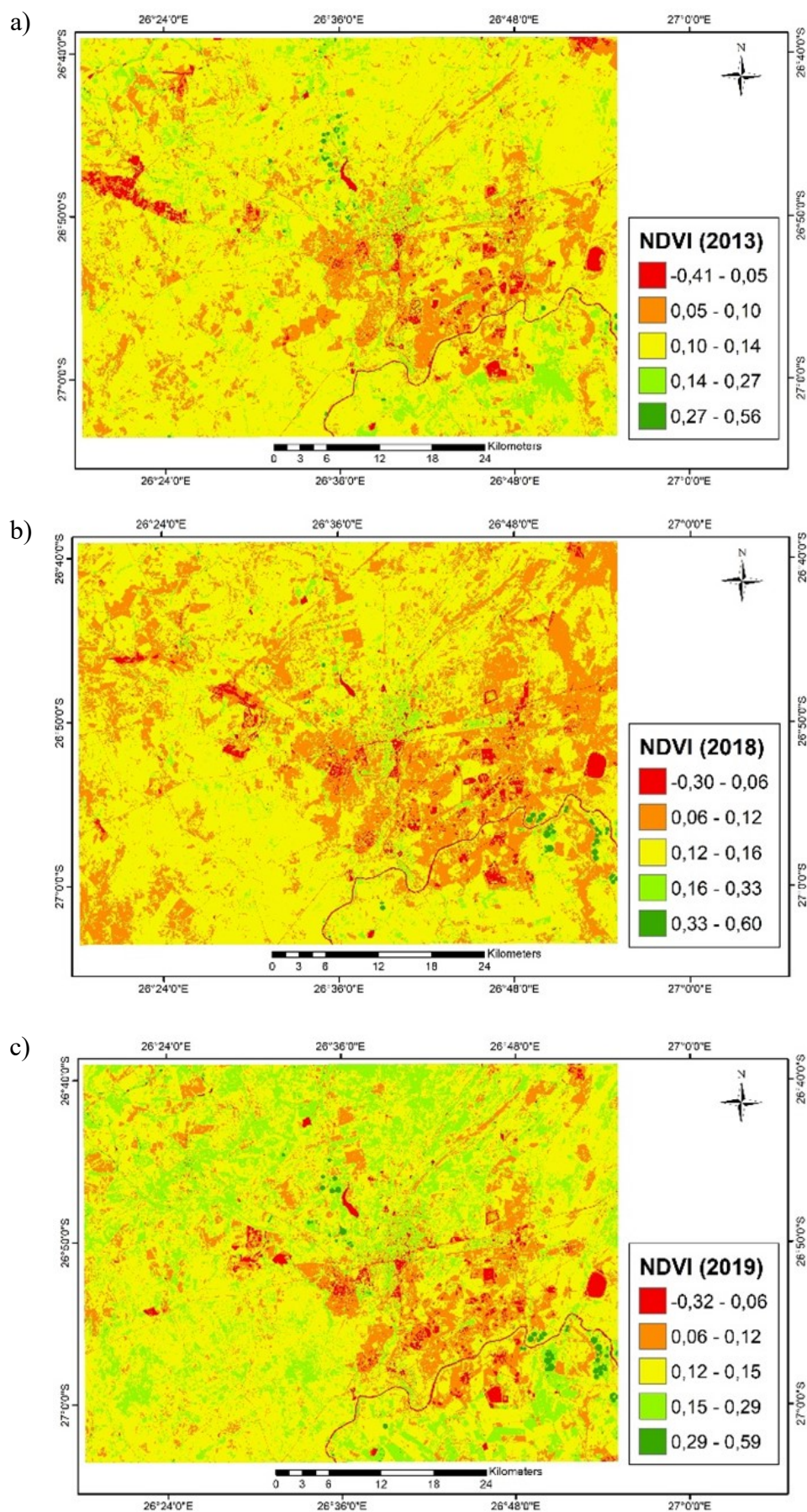


Fig. 6. Spatial-temporal pattern of NDVI dynamics of KOSH during the spring season of the year (a) 2013, (b) 2018 and (c) 2019

The spatial-temporal pattern of Land Surface Temperature

Figure 7 and figure 8 shows the spatial pattern results of LST and Table 5 shows statistical information. The green colour indicates that the areas have very low temperatures with certain land cover such as; the body of water, woodlands and area of shadows, or clouds (fig. 7 and fig. 8). On the three images selected in summer the north-west, south-west, northeast and east-south parts experienced higher LST ranging from 25.09 – 36.83 and in the areas with lower LST it ranges from 15.44 – 26.25. However, in some grassland areas, the LST ranges from 22.54 to 29.56. In spring results, 2013 and 2019 the maps show close similarity results than the results of 2018. LST value is high in most of the area because the area is mostly covered by short grass. In the spring season, high values are seen because the grass is very short and dry. The south-east part of the area is covered with water (river) and vegetation (crops/woodlands) so those areas have low LST and high NDVI values. The western and southwest part with grassland show high values of LST. NDVI has a negative correlation with LST meaning that the higher the NDVI the lower the LST. Similarly. In areas of the higher LST values, one can find lower NDVI values. There is a decrease in the values of statistical parameters between the season in all three years because of the difference in the climate of these seasons. The finding proves that where the region has high vegetation cover, the land surface temperature is less in such regions and where there is lesser vegetation cover, then the land surface temperature is higher.

Table 5

Statistical summary of LST (°C) values in KOSH and its surrounding (2013, 2018 and 2019)

Year	Mean	Max	Min	STD
2013 Summer	23.35	34.23	15.44	1.32
2013 Spring	22.44	34.07	9.14	1.97
2018 Summer	37.61	48.39	18.80	1.22
2018 Spring	34.72	94.97	18.37	2.53
2019 Summer	28.90	35.91	21.06	1.49
2019 Spring	27.73	41.35	15.44	1.95

The spatial-temporal pattern of Normalised Difference Built Index (NDBI)

Results indicate that during the year 2013 summer, the Normalised Difference Built Index (NDBI) values ranged from – 0.45 to 0.27 with the lowest temperature and highest temperature of 0 and 100 °C (fig. 9). In the year 2018, summer the NDBI values ranged from – 0.54 to 0.33 with the lowest temperature and highest temperature being 0 and 100 °C respectively (fig. 9). Whereas in the year 2019 the NDBI values ranged from -0.49 to 0.26. However, for the spring season in 2013, the range of NDBI is from -0.46 to 0.30, in the year 2018 it is between -0.46 to 0.73, and in the year 2019, it ranged between -0.48 to 0.27 (fig. 10). NDBI has a positive correction with LST that is the lower the NDBI the lower the LST and the higher the NDBI indicate higher the LST. In the study, there was a positive relationship between NDBI and LST. According to Faris and Reddy (2010), Built-up land plays the biggest role in increasing the temperature because of the hard concrete surface which contains almost nil water storage which leads to less humidity also.

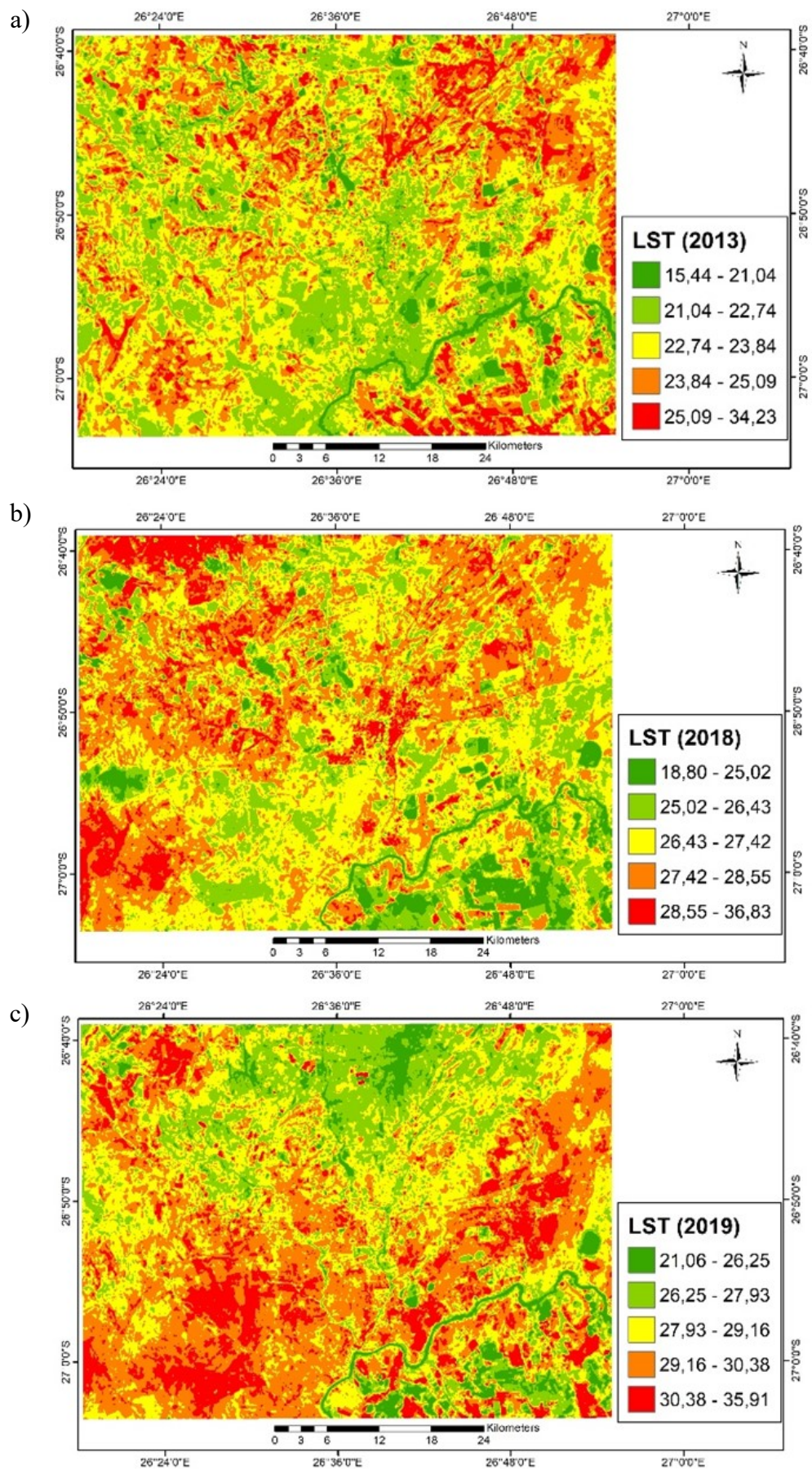


Fig. 7. Spatial-temporal pattern of LST dynamics of KOSH during the summer season of the year (a) 2013, (b) 2018 and (c) 2019

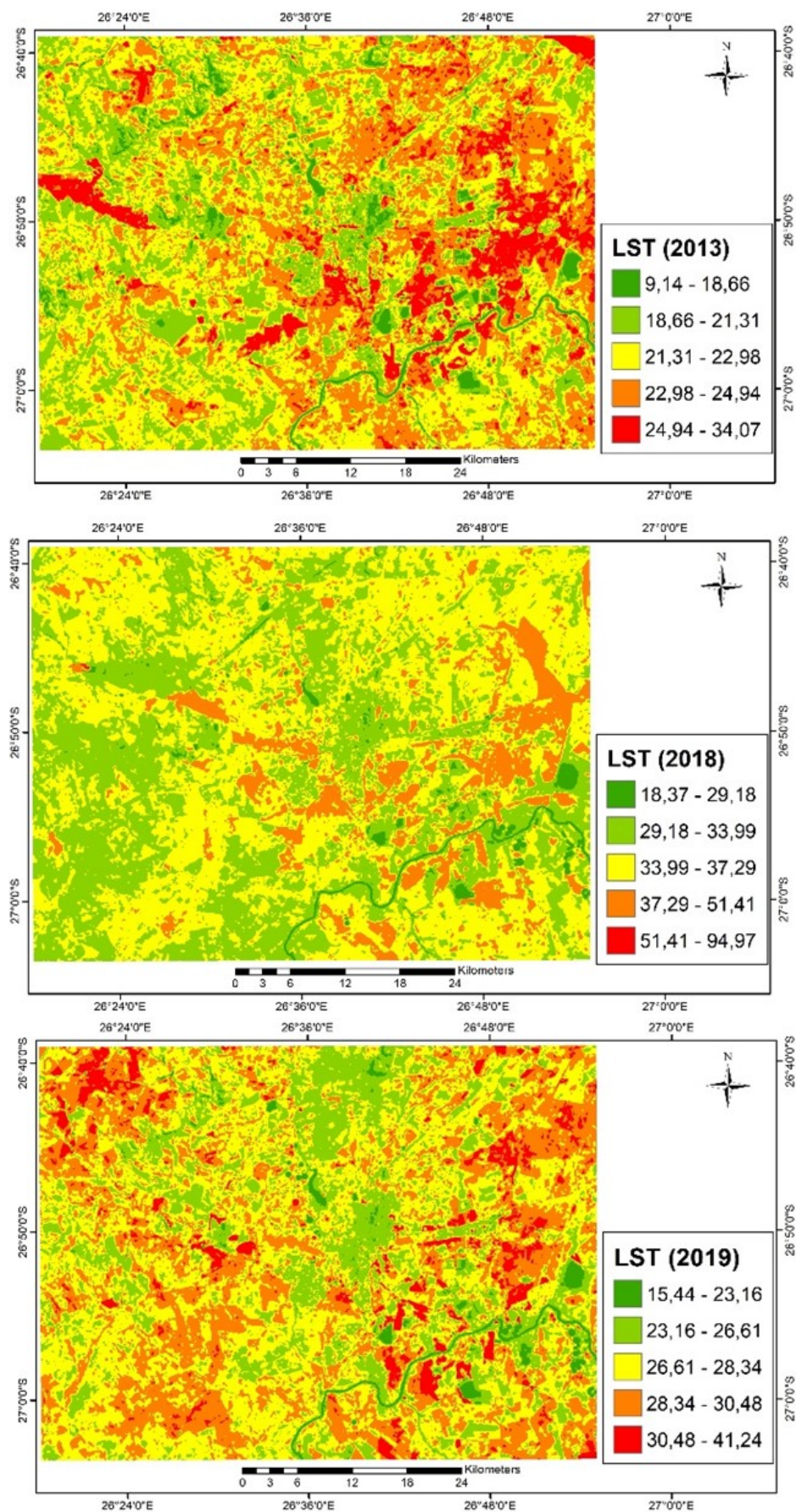


Fig. 8. Spatial-temporal pattern of LST dynamics of KOSH during the spring season of the year (a) 2013, (b) 2018 and (c) 2019

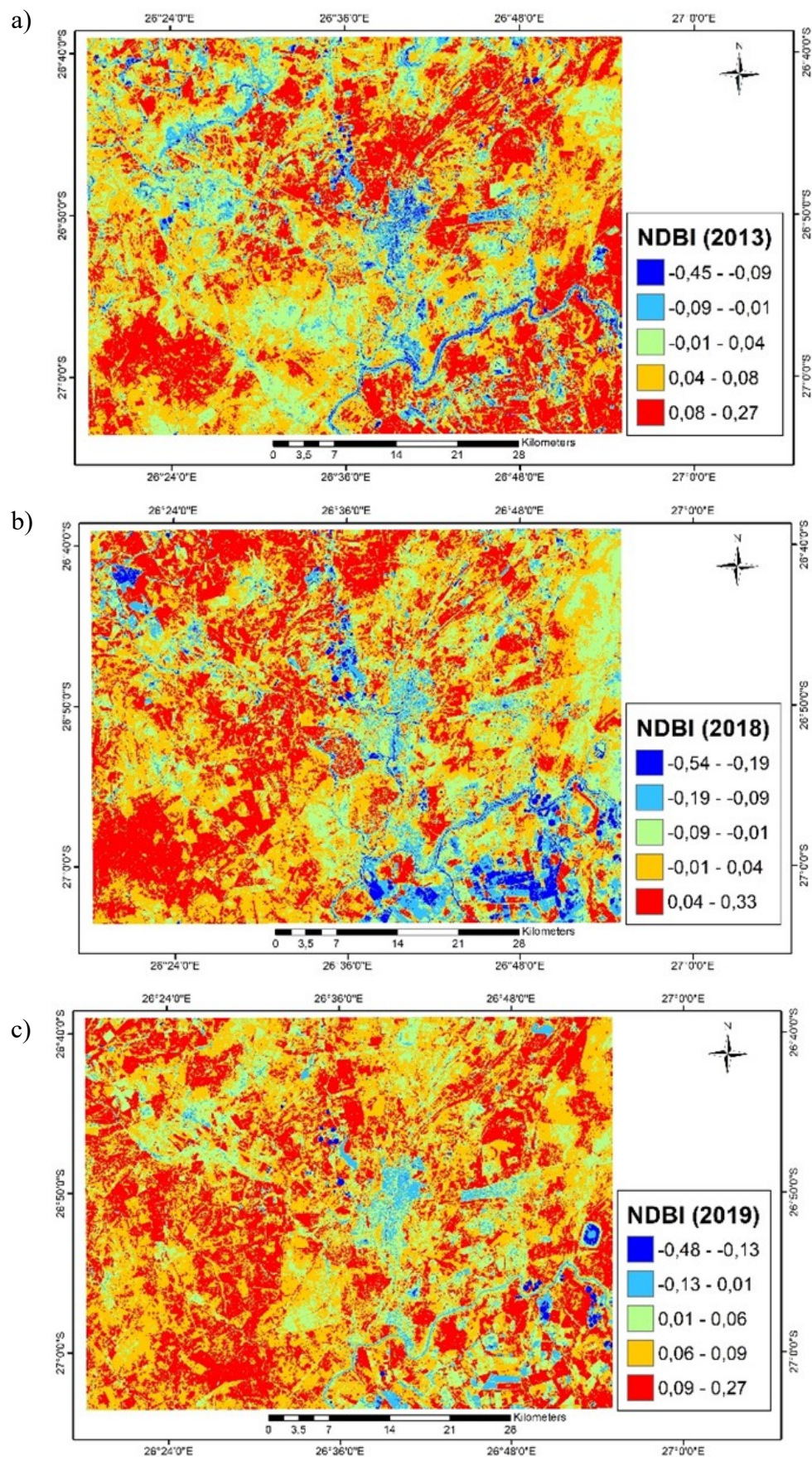


Fig. 9. Spatial-temporal pattern of NDBI dynamics of KOSH during the summer season of the year (a) 2013, (b) 2018, (c) 2019

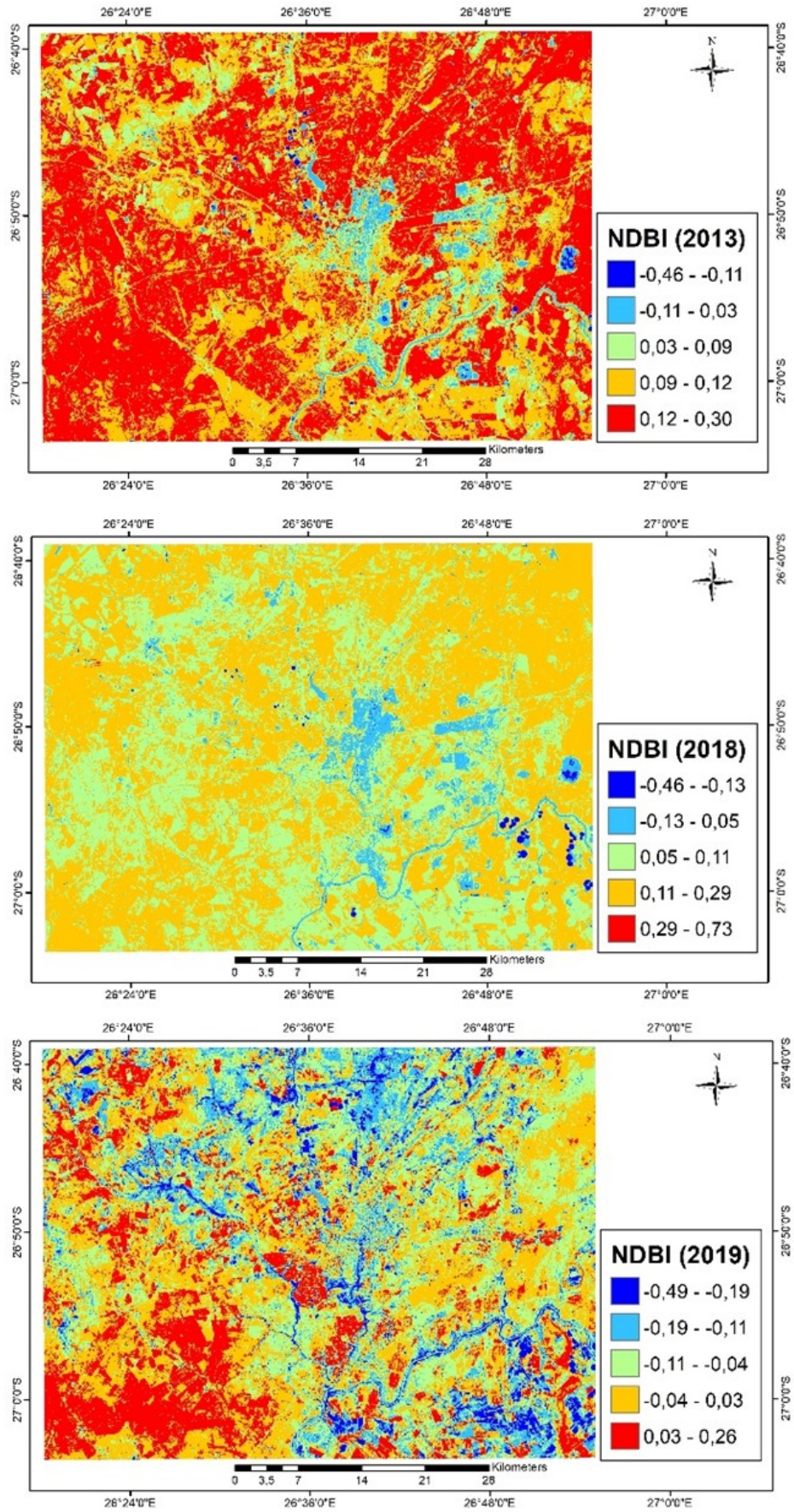


Fig. 10. Spatial-temporal pattern of NDBI dynamics of KOSH during the spring season of the year (a) 2013, (b) 2018 and (c) 2019

Table 6

Statistical summary of NDBI values in KOSH and its surrounding (2013, 2018 and 2020)

Year	Mean	Max	Min	STD
2013 Summer	0.05	0.27	-0.45	0.05
2013 Spring	0.11	0.30	-0.46	0.04
2018 Summer	-0.00	0.33	-0.54	0.08
2018 Spring	0.11	0.73	-0.46	0.04
2019 Summer	-0.04	0.26	-0.49	0.08
2019 Spring	0.08	0.27	-0.48	0.04

Drought indices monitoring

The spatial-temporal pattern of vegetation supply water index (VWSI)

VWSI can reflect the state of water supply for vegetation; but due to the great difference in the value ranges of NDVI and LST, very small values of VWSI were generated. VWSI values of the years 2013, 2018, and 2019 show most areas have experienced moderate to severe drought during the summer season. Whereas in spring seasons of these years, there is a less extreme severe drought in the area. Figure 11 shows more areas experience severe to moderate drought in all three years in a similar pattern in the summer season. The areas with extreme drought in the area are mostly the bare soil area, for example in mine tailing dumps in the area. The grassland regions are the major or mainland cover with severe drought impact. Figure 12 shows most of the areas experienced moderate drought with some parts having a severe drought. Most of KOSH shows a dominant mild to no drought condition in figure 12 and figure 11 shows areas with severe drought with moderate and no drought areas.

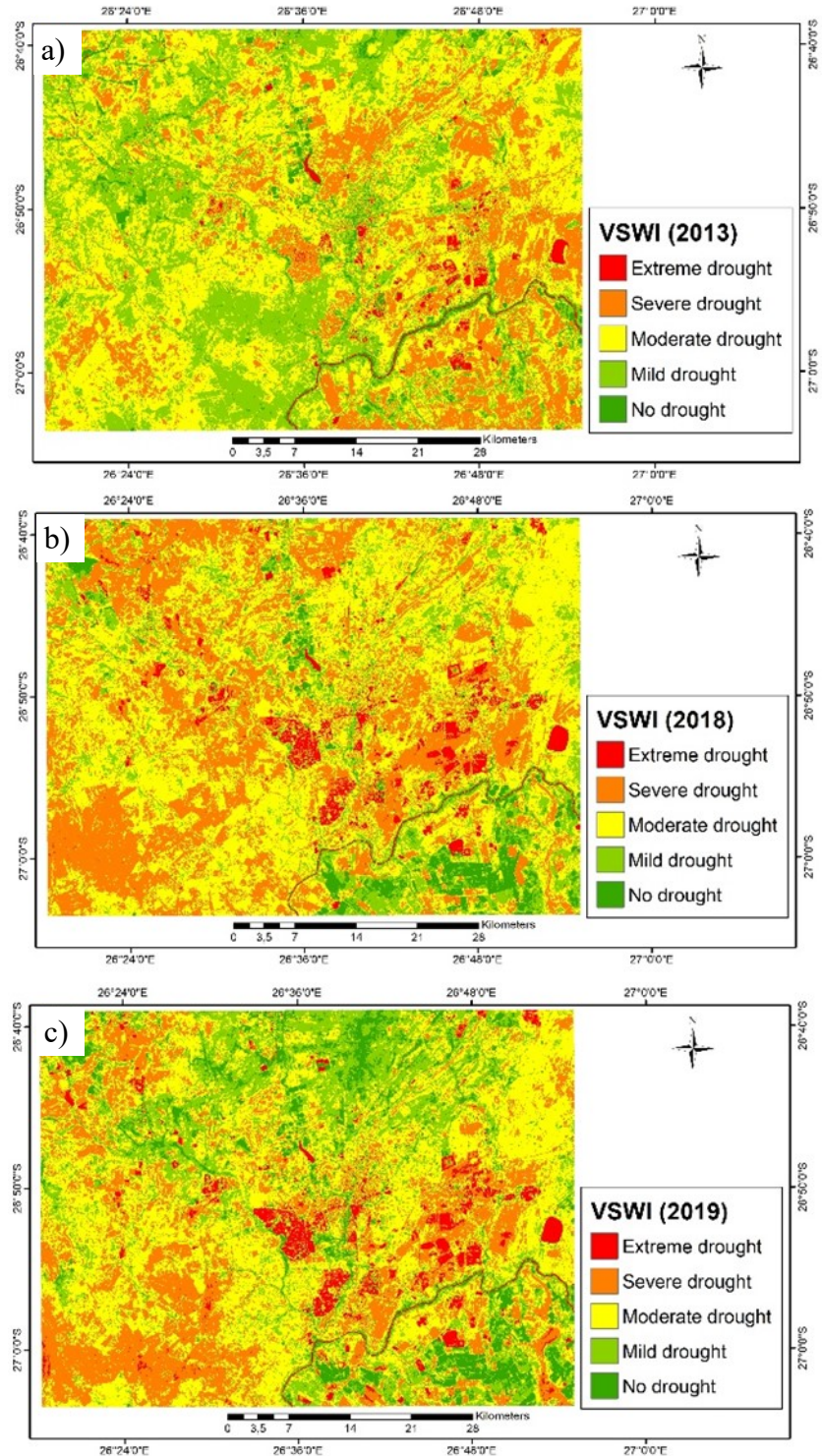


Fig. 11. Spatial-temporal pattern of VWSI dynamics of KOSH during the summer season of the year (a) 2013, (b) 2018 and (c) 2019

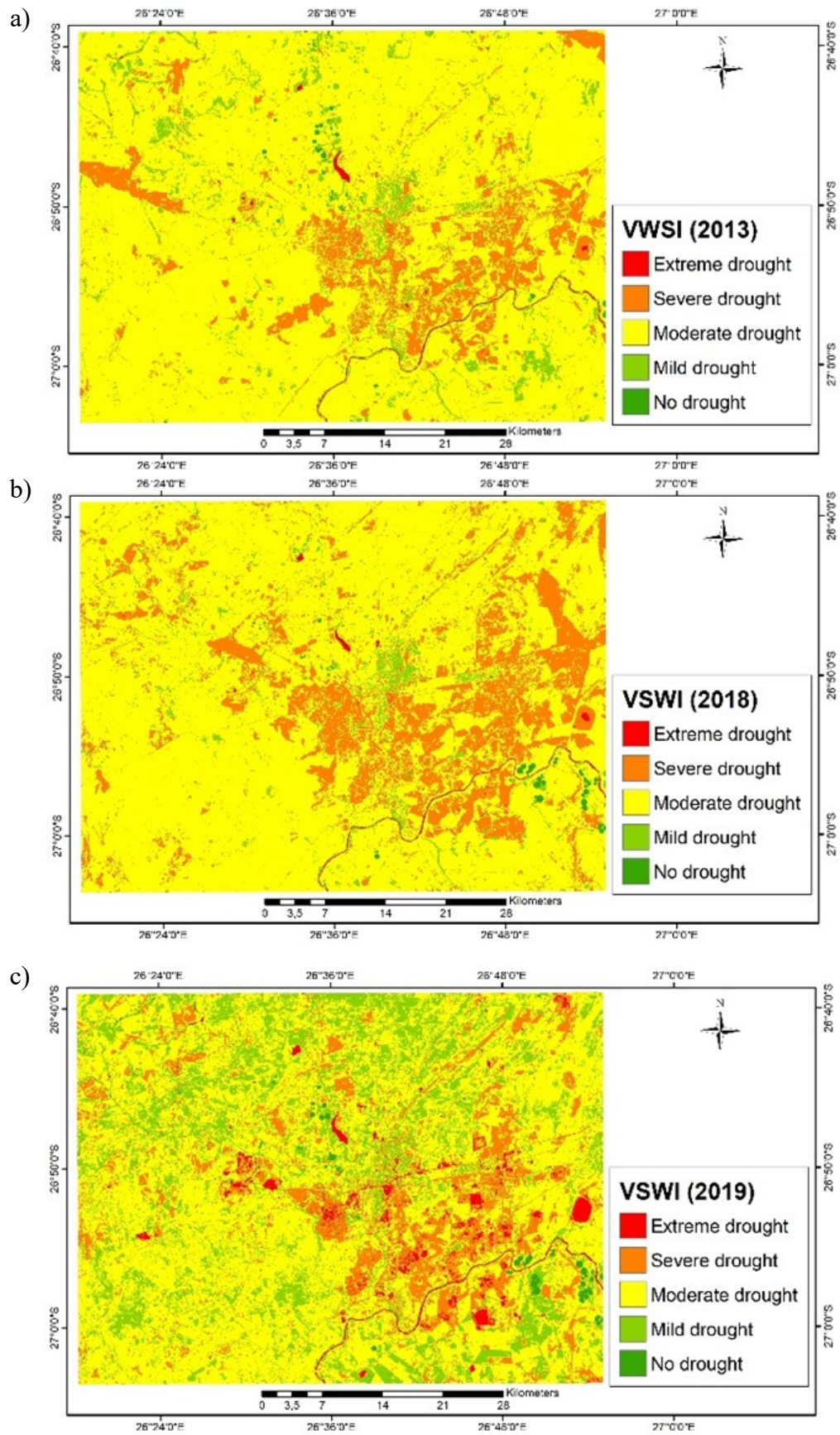


Fig. 12. Spatial-temporal pattern of VSWI dynamics of KOSH during the spring season of the year (a) 2013, (b) 2018 and (c) 2019

The spatial-temporal pattern of crop water supply index (CWSI)

Crop water supply algorithm show results of the spread of drought-affected land cover-open class land. CWSI method for all three years showed locations with water stress (fig. 13). CWSI is very different due to the appearance of undeveloped land which has a dominant value of high surface temperatures. CWSI is more relevant to the condition of having low soil moisture which proved that in many areas there is not much water on the surface. Figure 14 shows spring season results were in the year 2018 the results shows differs than the year 2013 and 2019.

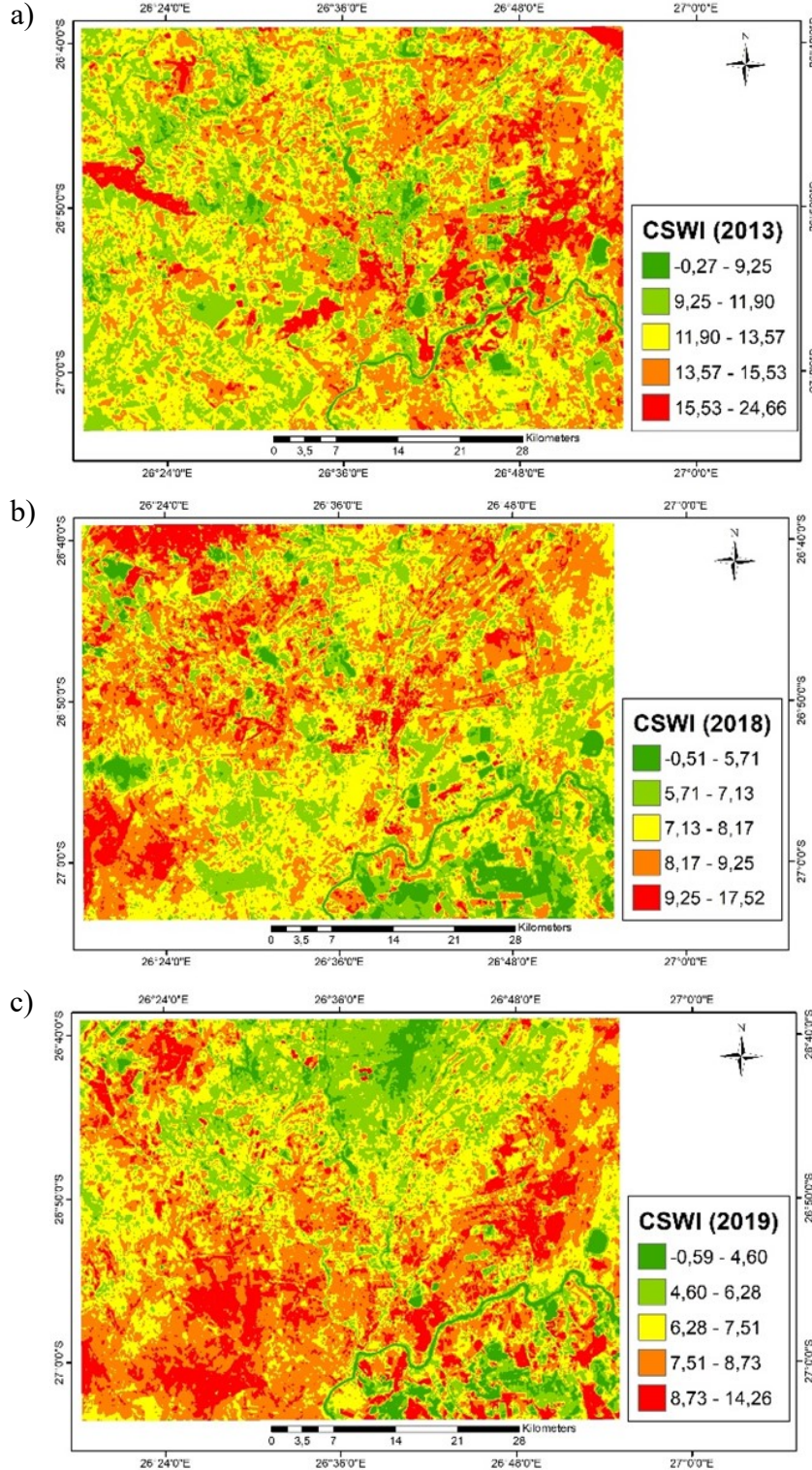


Fig. 13. Spatial-temporal pattern of CWSI dynamics of KOSH in the summer season of the year (a) 2013, (b) 2018 and (c) 2019

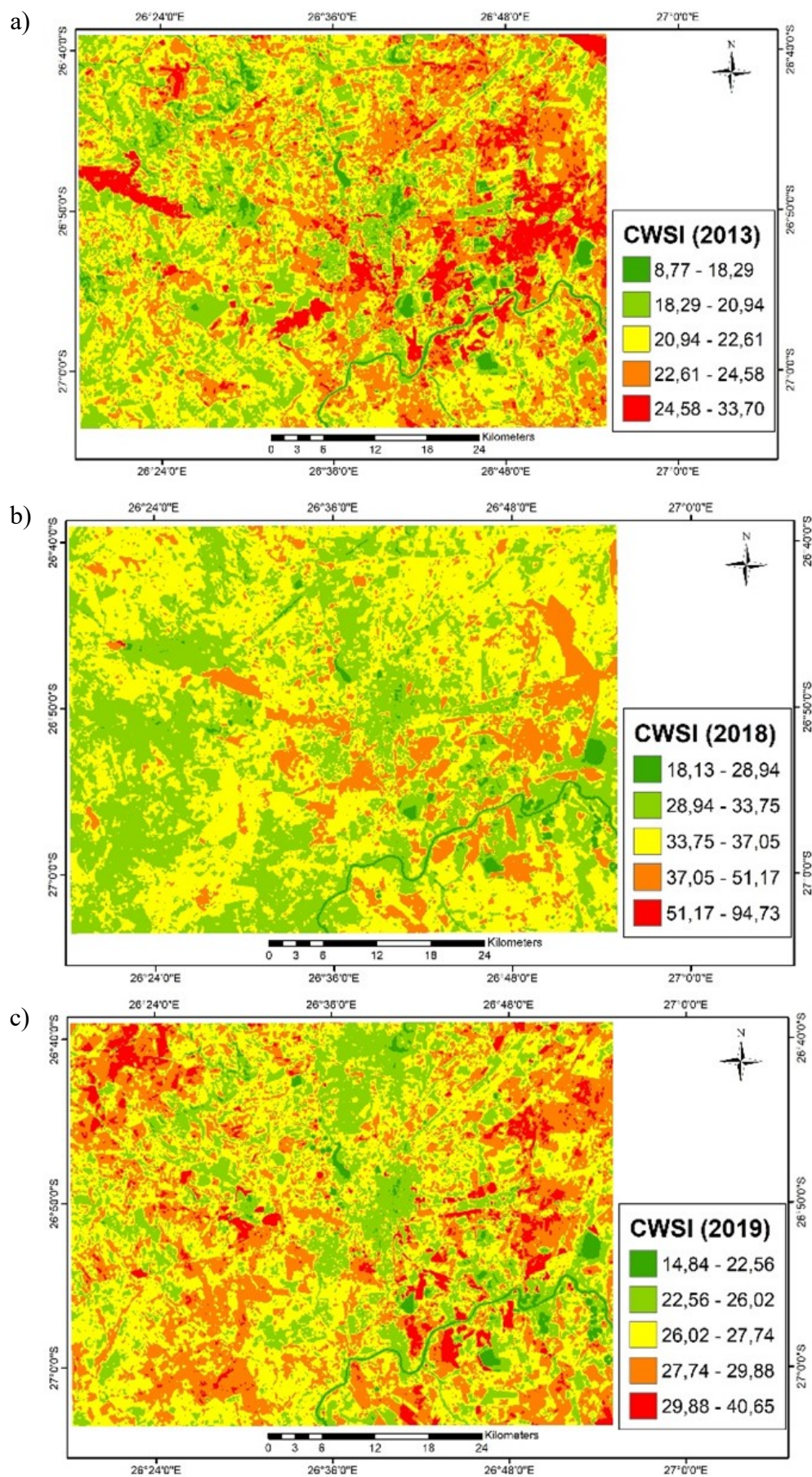


Fig. 14. Spatial-temporal pattern of CWSI dynamics of KOSH during the spring season of the year (a) 2013, (b) 2018 and (c) 2019

The spatial-temporal pattern of temperature condition index (TCI)

The results of TCI and CWSI methods in the year 2013 help to detect similar areas where there is drought. Figure 15 and figure 16 show the result of TCI for the summer season of the year 2019 and spring season of the year 2018.

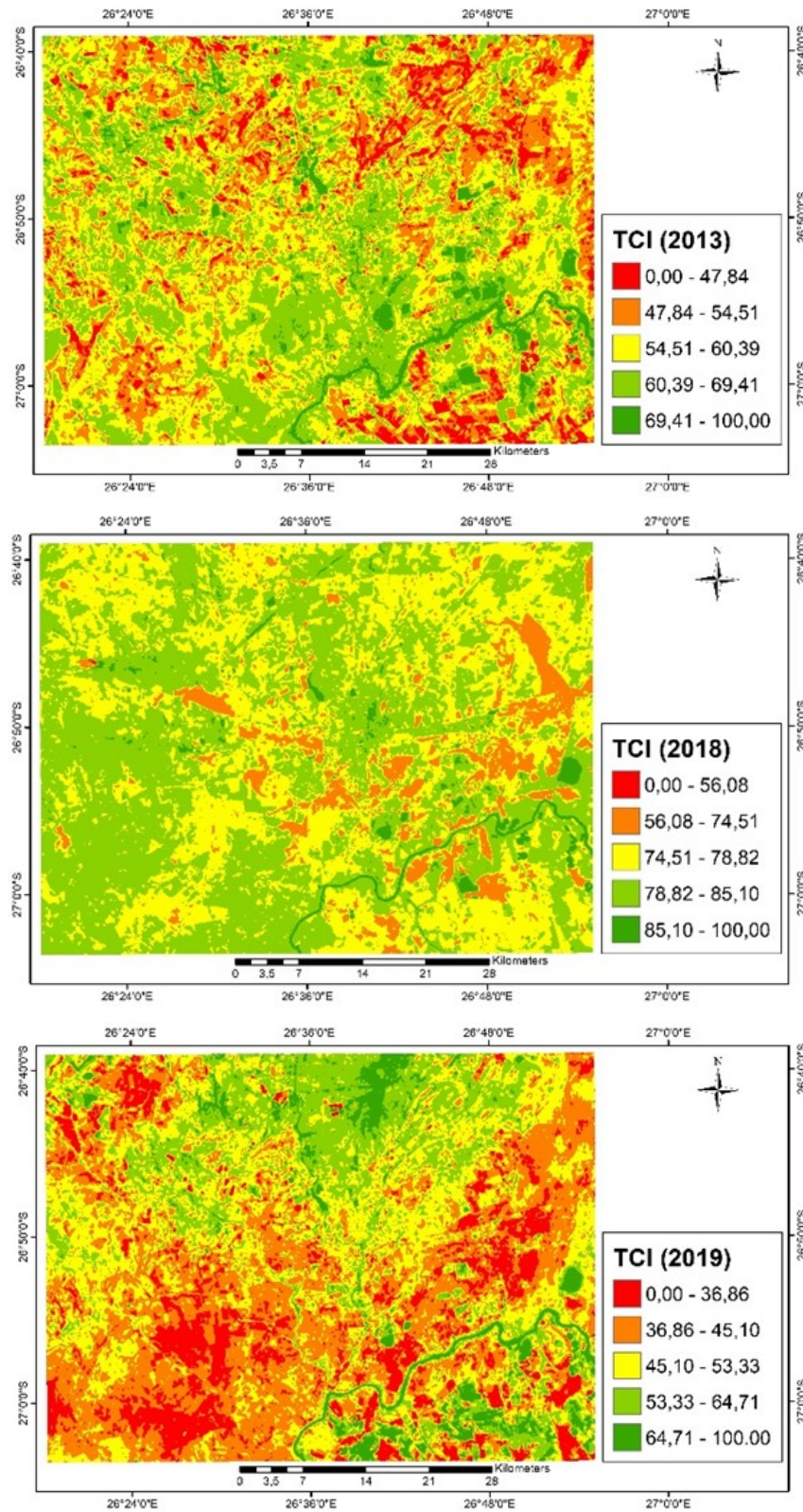


Fig. 15. Spatial-temporal pattern of TCI dynamics of KOSH during the summer season of the year (a) 2013, (b) year 2018 and (c) year 2019

From the TCI results, it can be seen that the dominant value of high surface temperatures seen in the years 2018 and 2019 matches with areas of high drought. In the year 2019, the appearance of TCI and CWSI is very different due to the appearance of undeveloped land which has a dominant value of high surface temperatures. TCI in 2019 is still able to distinguish the wet location. In all three images in the summer seasons of the study period, more areas that are experiencing drought can be detected (fig. 16).

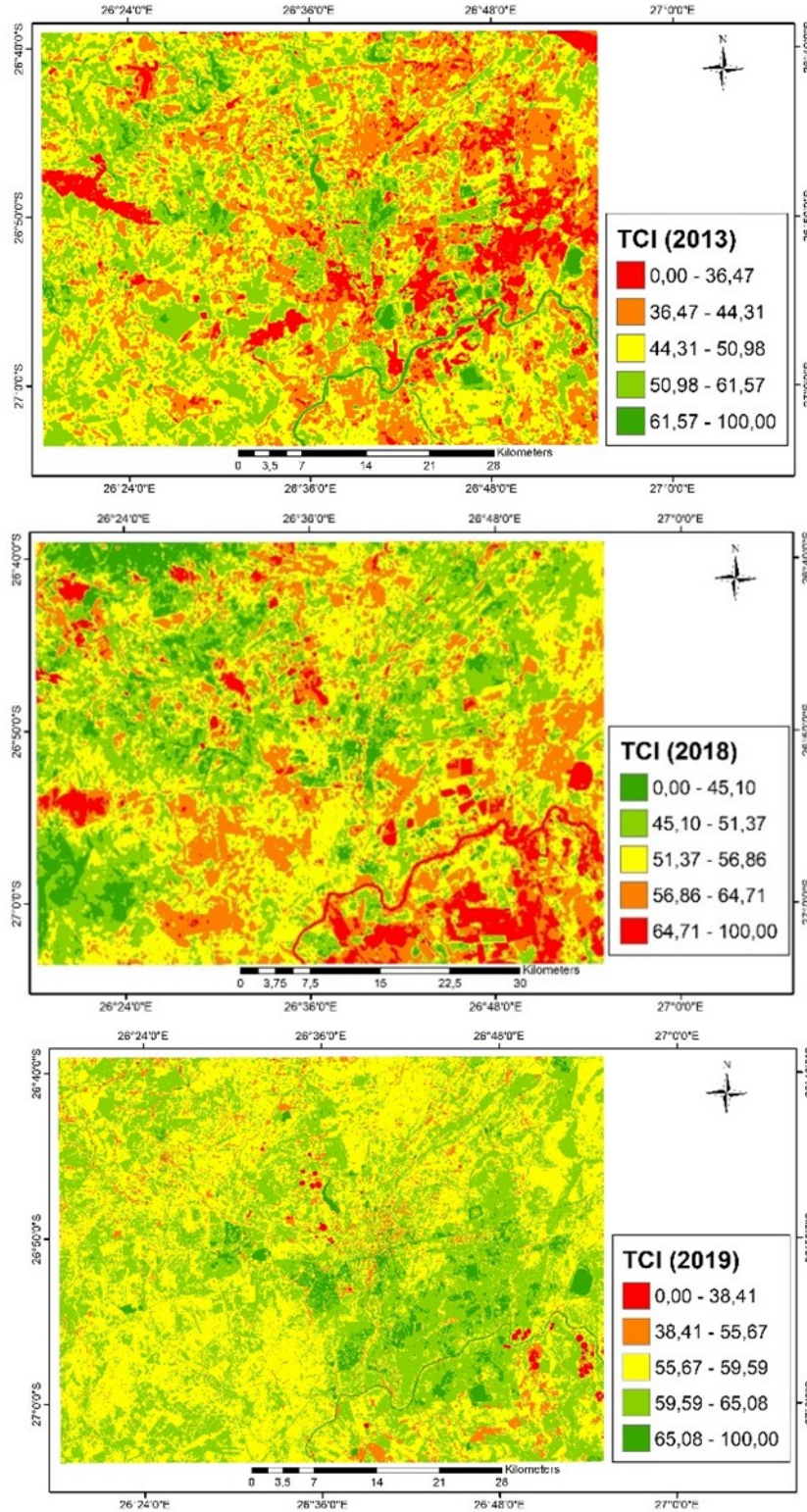


Fig. 16. Spatial-temporal pattern of TCI dynamics of KOSH during the spring season of the year (a) 2013, (b) 2018 and (c) 2019

Conclusion

The presented study could successfully estimate land surface temperature (LST) and drought indices and analyse the changing pattern of the LST and other indices. The results show that high surface temperature values have a positive correlation with drought events in an area; the higher the surface temperature the higher the drought and a negative correlation with wet conditions. The drought indices VSIW, TCI and CWSI methods were tested for drought monitoring. The results also show that the LST helps to determine areas with drought without making use of drought indices. Grassland that covers most of the area in the study area experience more drought than other land covers. The finding shows areas where there is grassland cover, the LST values are high; whereas the cultivated area shows low values of LST. The findings show that LST has a negative relationship with NDVI and positive relationship with NDBI. The study also indicates mean variation between NDBI, NDVI and LST. The mean of the LST increases from 2013 – 2019 on both seasons. The results also verified that some areas have experienced drought mostly in areas with grassland cover. Most areas of the KOSH had low NDVI because of low vegetation cover. The VSWI, TCI and CSWI show results of the spread of drought across the area where some areas experience severe drought. The results indicate that LST in certain parts of the area especially to the southwest, northwest and northeast regions experience high LST values. It is recommended that LULC mapping should also be conducted for particular periods of study to understand the dynamics of land surface temperature fluctuation concerning a specified period.

The study has shown the importance of land use/land cover in estimating the land surface temperature. An inverse (negative) relationship between LST and water bodies and vegetation cover was found while a direct positive relationship between LST and built up, and barren land area was observed. It was concluded that the increase in vegetation and water bodies can greatly decrease the land surface temperature of any region. The relationship between the LST and VI are negative which implies that the lower the LST the higher the NDVI and the higher the LST the lower the NDVI. Vegetation plays the biggest role in reducing the land surface temperature from increasing whereas on the other hand built-up area plays a major role in increasing land surface temperature. Therefore, a better option to have lower LST is to reduce the built-up land when the population is growing; rather increase in vegetation cover in the built-up area can reduce the LST.

The authors would like to register their sincere thanks to the Council for Geoscience for various resources provided for this study and the National Research Foundation of South Africa for the grant provided to undertake this study. The USGS is also hereby thanked for providing free access to the Landsat 8 data used in this study.

References

1. Balew, A.; Korme, T. Monitoring land surface temperature in Bahir Dar city and its surrounding using Landsat images. *Egyptian Journal of Remote Sensing and Space Science*. 2020. <https://doi.org/10.1016/j.ejrs.2020.02.001>
2. Brohan, P.; Kennedy, J.J.; Harris, I.; Tett, S.F.; Jones, P.D. Uncertainty estimates in regional and global observed temperature changes: a new data set from 1850. *Journal of Geophysical Research: Atmospheres*, **2006**, *111*, D12106. <http://dx.doi.org/10.1029/2005JD006548>
3. Cammalleri, C.; Vogt, J. On the Role of Land Surface Temperature as Proxy of Soil Moisture Status for Drought Monitoring in Europe. *Remote Sensing*, **2015**, *7*, 16849–16864.
4. Chastain, R., Housman, I., Goldstein, J.; Finco, M. Empirical cross sensor comparison of Sentinel-2A and 2B MSI, Landsat-8 OLI, and Landsat-7 ETM+ top of atmosphere spectral characteristics over the conterminous United States. *Remote Sensing of Environment*, **2019**, *221*, 274–285.
5. Chen, F.; Yang, S.; Yin, K.; Chan, P. Challenges to quantitative applications of Landsat observations for the urban thermal environment. *Journal of Environmental Sciences*, **2017**, *59*, 80–88.
6. Duan, S.B.; Li, Z.L.; Tang, B.H.; Wu, H.; Tang, R.. Generation of a time-consistent land surface temperature product from MODIS data. *Remote Sensing of Environment*, **2014**, *140*, 339–349.
7. Faris, A.A.; Reddy, Y.S. Estimation of urban heat island using Landsat ETM+ imagery at Chennai city—a case study. *International Journal of Earth Sciences and Engineering*, 2010, *3*, 332–340.

8. He, J.; Zhao, W.; Li, A.; Wen, F.; Yu, D. The impact of the terrain effect on land surface temperature variation based on Landsat-8 observations in mountainous areas. *International Journal of Remote Sensing*, **2019**, *40*, 1808–1827.
9. Herrero-Huerta, M.; Lagüela, S.; Alfieri, S.M.; Menenti, M. Generating high-temporal and spatial resolution TIR image data. *International Journal of Applied Earth Observation and Geoinformation*, **2019**, *78*, 149–162.
10. Hansen, J.; Ruedy, R.; Sato, M.; Lo, K. Global surface temperature change. *Reviews of Geophysics*, **2010**, *48*, RG4004. <https://doi.org/10.1029/2010RG000345>
11. Jin, M., Li, J., Wang, C. and Shang, R. 2015. A practical split-window algorithm for retrieving land surface temperature from Landsat-8 data and a case study of an urban area in China. *Remote Sensing*, *7*, 4371–4390.
12. Kogan, F.N. 1998. Global drought and flood-watch from NOAA polar-orbiting satellites. *Advances in Space Research*, *21*, 477–480.
13. Kothe, E.J., Ling, M., North, M., Klas, A., Mullan, B.A. and Novoradovskaya, L. 2019. Protection motivation theory and pro-environmental behaviour: A systematic mapping review. In: *Australian Journal of Psychology*. Wiley-Blackwell Publishing Ltd, 411–432.
14. Landsat 8 Data Users Handbook. Available at <https://www.usgs.gov/core-science-systems/nli/landsat/landsat-8-data-users-handbook> (accessed 11 September 2020).
15. Ngie, A., Abutaleb, K., Ahmed, F., Taiwo, O.J., Darwish, A.A. and Ahmed, M. 2017. Estimation of land surface temperatures from landsat ETM+ images for Durban, South Africa. *Rwanda Journal*, *1*.
16. Owojori, A. and Xie, H. 2005. Landsta image-based LULC changes of San Antonio, Texas using advance atmospheric correction and object-orientated image analysis approaches. *Remote sensing image processing and analysis* (ES 6973).
17. Pal, S. and Ziaul, S. 2017. Detection of land use and land cover change and land surface temperature in English Bazar urban centre. *Egyptian Journal of Remote Sensing and Space Science*, *20*, 125–145.
18. Quintano, C., Fernández-Manso, A., Calvo, L., Marcos, E. and Valbuena, L. 2015. Land surface temperature as a potential indicator of burn severity in forest Mediterranean ecosystems. *International Journal of Applied Earth Observation and Geoinformation*, *36*, 1–12.
19. Rehman, Z., Kazmi, S., Khanum, F. and Samoon, Z. 2015. Analysis of Land Surface Temperature and NDVI Using Geo-Spatial Technique: A Case Study of Ketu Bunder, Sindh, Pakistan. *Journal of Basic & Applied Sciences*, *11*, 514–527.
20. Rosas J, Houborg R, McCabe M.F. 2017. Sensitivity of Landsat 8 surface temperature estimates to atmospheric profile data: a study using MODTRAN in dryland irrigated systems. *Remote Sens* *9*:1–27. <https://doi.org/10.3390/rs9100988>
21. Simó, G., García-Santos, V., Jiménez, M., Martínez-Villagrasa, D., Picos, R., Caselles, V. and Cuxart, J. 2016. Landsat and Local Land Surface Temperatures in a Heterogeneous Terrain Compared to MODIS Values. *Remote Sensing*, *8*, 849.
22. Sobrino, J.A., Oltra-Carrió, R., Soria, G., Bianchi, R. and Paganini, M. 2012. Impact of spatial resolution and satellite overpass time on evaluation of the surface urban heat island effects. *Remote Sensing of Environment*, *117*, 50–56.
23. Sobrino, J.A. and Romaguera, M. 2004. Land surface temperature retrieval from MSG1-SEVIRI data. *Remote Sensing of Environment*, *92*, 247–254.
24. Suresh S, Ajay SV, Mani K (2016) Mountain landscape of Devikulam Taluk using Landsat 8 data. *Int J Res Eng Technol* *5*:92–96.
25. Thomas, A. Mapping of surface deformation associated with the 5.2 magnitude Stilfontein earthquake of 3 April 2017 using radar interferometry. *Egyptian Journal of Remote Sensing and Space Science*. **2020** <https://doi.org/10.1016/j.ejrs.2020.01.005>
26. Torrión, J.A., Maas, S.J., Guo, W., Bordovsky, J.P. and Cranmer, A.M. 2014. A three-dimensional index for characterizing crop water stress. *Remote Sensing*, *6*, 4025–4042.
27. Ustin, S.L., Roberts, D.A., Gamon, J.A., Asner, G.P. and Green, R.O. 2004. Using imaging spectroscopy to study ecosystem processes and properties. *BioScience*, *54*, 523–534.
28. Weng, Q., Lu, D. and Schubring, J. 2004. Estimation of land surface temperature-vegetation abundance relationship for urban heat island studies. *Remote Sensing of Environment*, *89*, 467–483.
29. Xiao, R. bo, Ouyang, Z. yun, Zheng, H., LI, W. feng, Schienke, E.W. and Wang, X. ke 2007a. Spatial pattern of impervious surfaces and their impacts on land surface temperature in Beijing, China. *Journal of Environmental Sciences*, *19*, 250–256.
30. Xiao, R. bo, OUYANG, Z. yun, zheng, H., LI, W. feng, Schienke, E.W. and Wang, X. ke 2007b. Spatial pattern of impervious surfaces and their impacts on land surface temperature in Beijing, China. *Journal of Environmental Sciences*, *19*, 250–256.
31. Yang, L., Cao, Y.G., Zhu, X.H., Zeng, S.H., Yang, G.J., He, J.Y. and Yang, X.C. 2014. Land surface temperature retrieval for arid regions based on Landsat-8 TIRS data: A case study in Shihezi, Northwest China. *Journal of Arid Land*, *6*, 704–716.

COMPREHENSIVE EVALUATION OF ECOLOGICAL ENVIRONMENT IN DAZHANGXI BASIN BASED ON MULTI-SOURCE REMOTE SENSING DATA

Junjun Fang¹, Jinming Sha^{1,2}, Xuerui Guo³, Gaopeng Sun⁴, Qixin Lin¹

¹College of Geographical Sciences, Fujian Normal University, China

²China-Europe Environment Center, Fujian Normal University, China

³Wageningen University & Research, Netherland

⁴College of geography and tourism, Shaanxi Normal University, China

Ecosystem assessment plays an important role in ensuring regional ecological security and promoting the coordinated development of social economy and ecological environment protection. Remote sensing technology can objectively and quantitatively evaluate the spatial-temporal change of ecological environmental quality. This paper uses multi-source data to comprehensively analyze land surface temperature, land use and land cover, net primary productivity (NPP) and remote sensing ecological index in 2013 and 2017. The comprehensive evaluation system of the ecological environment in Dazhangxi basin is established by qualitative analysis of the ecological environment from multi perspectives and multi spatial and temporal scales. The results showed that: 1) The urban construction land at the intersection of Dazhongxi River and Minjiang River have expanded rapidly from 2013 to 2017, and the thermal environment effect is enhanced, forming local heat island effect. 2) The vegetation coverage in the study area is high, reaching more than 60%. Compared with 2013, the types of forest land and agricultural land decreased significantly in 2017, while the construction land and unused land increased significantly. 3) NPP showed a downward trend, and the reduction area was mainly forest. 4) Compared with 2013, the higher ecological and lower ecological zone decreased, while the medium ecological zone increased in 2017, which means the better ecological environment has been damaged and the areas with serious ecological environment problems have been partially improved. 5) During 2013-2017, the ecological environment of the study area showed a trend of slight deterioration, but it was alleviated by human intervention.

Keywords: ecological environment, comprehensive assessment, dynamic monitoring, remote sensing technology, Landsat, Dazhangxi basin.

Introduction

With the rapid development of economy and society, the ecological environment is inevitably suffering huge damages, such as losses of natural resources, reduction in biodiversity, environmental pollution and global climate change (Almeida et al., 2017; Chai, Lha, 2018; Ostrom, 2009). In order to achieve the goal of sustainable development, ecological environment has attracted more and more attention (Jing et al., 2020; Liu et al., 2018). Monitoring and comprehensive assessment of ecological environment, proposing protection measures and enhancing ecosystem services have become a hotspots in the field of environmental research. However, it is difficult to comprehensively evaluate the ecological environment due to its complexity and inherent interdisciplinary characteristics (Miao et al., 2016; Vorobyev et al., 2015).

Most of the previous studies evaluated the ecological environment from one or just a few aspects, which limits the accuracy of the assessment. Wang et al (2019) and Zhang et al (2020) reported the relationship between ecological environment and land use simulation, without considering other factors. Zheng et al (2020) reported the impact of urbanization on ecological environment. Li et al (2020) and Wang et al (2019) discussed the relationship between economy development and ecological environment. However, the reasonable integration of the above evaluation indicators into a comprehensive evaluation model requires more in-depth research.

Modern remote sensing earth observation system is widely used recently for the environmental evaluation study (Kurbanov, 2016; Jing et al., 2020). It provides multi-source data for extracting and synthesizing ecological evaluation indicators. Besides, remote sensing technology has great potential in large-scale monitoring and quality assessment of ecological environment (Kurbanov et al, 2014; Zhang et al., 2017; Niu, Wang, 2017). In 2006, the State Environmental Protection Ad-

ministration (2006) regulated the ecological environmental status index (EI) based on biological abundance index, vegetation cover index, water network density index, land degradation index, and environmental quality index. All of these indices have been widely applied in many research works. However, many scholars have tried different adjustments to the indices and weights due to the heterogeneity of different research regions (Zhu et al., 2017; Meng, Zhao, 2009). Therefore, EI cannot be used universally in different research areas.

Remote sensing ecological index (RSEI) is a new type of remote sensing based index for comprehensively ecological evaluation, the evaluation factors include greenness, heat, dryness and humidity, which are mainly obtained from satellite images (Gupta et al., 2012). These four indicators can be easily obtained and integrated into RSEI, thus easier to monitor regional ecological environment variation (Xu, 2013).

In China, different indicators reflect the ecological and environmental problems in different regions. One reason for this is the complexity and particularity of natural environmental conditions, the other is the long history of human activities and their profound impact on the ecological environment (Chai, Lha, 2018; Chi et al., 2018). Dazhangxi is the largest tributary of the lower Minjiang River in central Fujian Province, China. It plays an important role in regulating climate and maintaining ecological balance of the area. In addition, there have been limited studies on multi-temporal and comprehensive ecological environment evaluation of this basin. Combined with the Comprehensive Planning of Fujian Dazhangxi Basin Report (Fujian Water Resources and Hydro-power Institute, 2014), this study could give more detailed evaluation of the ecological environment in [Dazhangxi](#).

The main purpose of this study is to provide scientific basis for ecological environment protection, comprehensive management, and sustainable development of Dazhangxi. Therefore, the following processes will be conducted in this study.

(1) Calculate the land surface temperature (LST), land use and land cover (LULC), net primary productivity (NPP) and RSEI in 2013 and 2017, respectively. (2) Analyze the ecological environmental indicators and their relationship between the two periods of the study area comprehensively and quantitatively. (3) Explore the spatial difference of ecological environment quality and discuss the results.

Material and Methods

Study area

Dazhangxi (at 118°59'14" to 119°16'29"N latitude and 25°49'06" to 25°59'32"E longitude) is the largest tributary of Minjiang River downstream, which is located in the central part of Fujian Province, China (fig.1). The drainage area of Dazhangxi is 4,843 km². The total length of the river is 234 km, and the average river slope is 2.1%. Dazhangxi has been the main waterway connecting the three coastal counties with the surrounding areas. The basin is rich in water resources and has many water diversion projects. Since the founding of the People's Republic of China, a large number of reservoirs and power stations have been built. This provides important conditions for local economic and social development. Meanwhile, due to human activities and hydropower development, the environment has been greatly affected.

Therefore, it is very important to quantitatively retrieve and monitor the LULC, LST, NPP and RSEI by remote sensing technology, which is beneficial to the protection of natural environment, human economy and ecology. It is not only real-time, rapid and accurate, but also significantly cost-effective in terms of manpower field investigation.

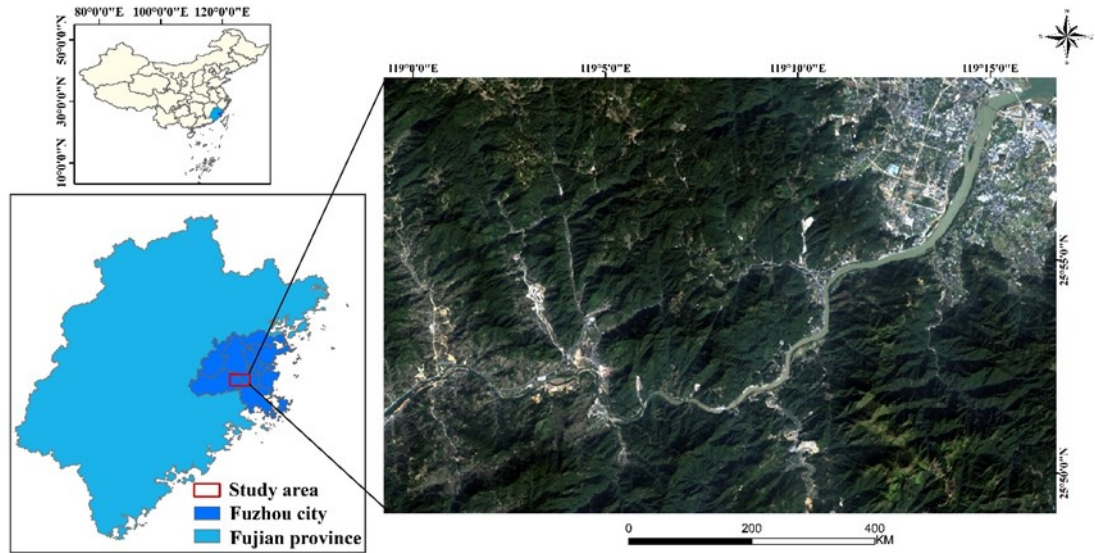


Fig.1. Location of study area and true color image

Methodology

The overall research process is shown in Fig. 2. It illustrates the framework for evaluating ecological environment using Landsat and ancillary data. The main steps include collection and pre-processing of remote sensing and other ancillary data, extraction of variables from remote sensing and ancillary data, evaluation of ecological environment from four aspects, and analysis of overall ecological environment of study area.

Data collection and preprocessing

Table 1 summarizes the data sets used in research, including two Landsat 8 images dated on October 23 of 2013 and December 21 of 2017, the ASTER Global Digital Elevation Model (GDEM), MODIS product data MOD11A1, weather station data, and the Comprehensive Planning of Fujian Dazhangxi Basin Report of this research area. Both Landsat images were calibrated by radiometric calibration, atmospheric correction and topographic correction in ENVI 5.5. GDEM with 30-m cell size were used for the topographic correction. Both images and GDEM data have the same Universal Transverse Mercator (UTM) coordinate system with World Geodetic. The pan sharpening method was used to fuse Landsat images to improve the spatial resolution for subse-

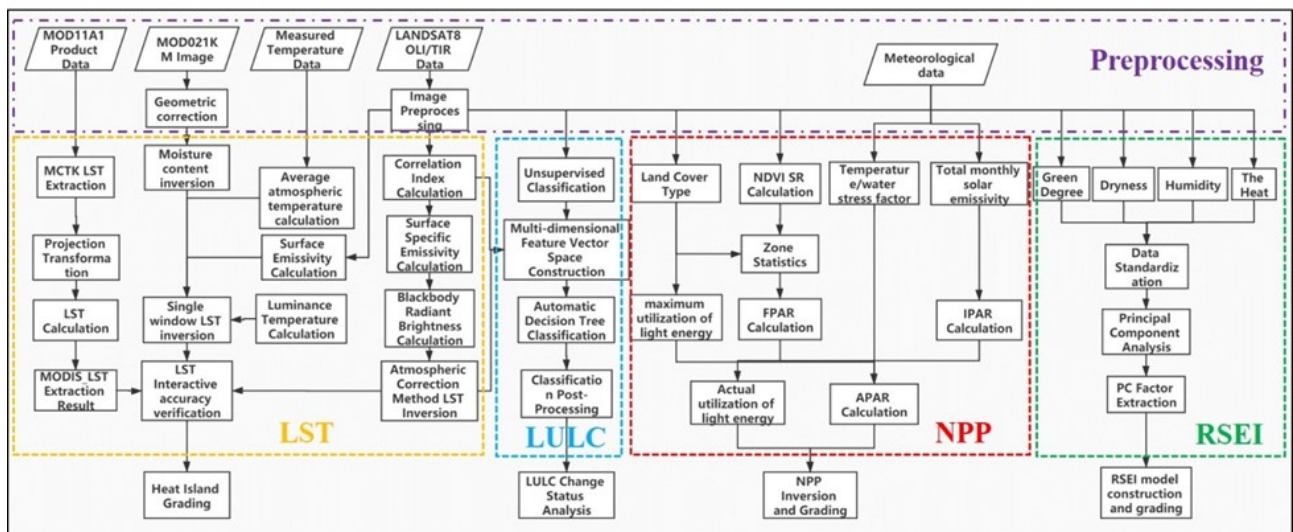


Fig. 2. The framework for ecological environment assessment

Table 1

Data sets used in research

Data sets	Description
Landsat 8 OLI images	Landsat 8 OLI images on October 23, 2013 (LC81190422013296LGN01) and December 21, 2017 (LC81190422017355LGN00)
30m GDEM	Aster Global Digital Elevation Model (GDEM) data with 30 m cell size
MOD11A1	Daily temperature product data
Weather station data	Daily rainfall and temperature data of Fujian in 2013 and 2017
Comprehensive Planning of Fujian Dazhangxi Basin Report	Environmental impact report on comprehensive planning of Dazhangxi Basin

Extraction of variables from remote sensing

Normalized difference vegetation index (NDVI), normalized difference building index (NDBI) and modified normalized difference water index (MNDWI) are used in this study. The principle of NDVI is that vegetation has different absorption in near-infrared band and red band. Vegetation information can be highlighted by calculation, so it is often used to characterize the coverage of surface vegetation. NDBI is a remote sensing index, which is used to distinguish urban and other building information. Xu (2005) proposed MNDWI on the basis of NDWI, which can better reveal the micro characteristics of water body. Their calculation is shown in Table 2.

Table 2

Calculation of indices

Indices	Calculation	Landsat 8 bands	Band math
NDVI	$(\rho_{NIR} - \rho_R)/(\rho_{NIR} + \rho_R)$	b5, b4	$(b5 - b4)/(b5 + b4)$
NDBI	$(\rho_{MIR} - \rho_{NIR})/(\rho_{MIR} + \rho_{NIR})$	b6, b5	$(b5 - b4)/(b5 + b4)$
MNDWI	$(\rho_{Green} - \rho_{MIR})/(\rho_{Green} + \rho_{MIR})$	b3, b6	$(b3 - b6)/(b3 + b6)$

Thermal environment model

(1) Impervious Surface Coverage (ISC)

The increase of ISC is a significant feature of urbanization and has a significant impact on regional ecological environment factors. In this study, normalized difference impervious surface index (NDISI) is used to extract impervious surface (Xu, 2008). Based on the spectral difference between impervious surface and other surface features, single band or multi band combination remote sensing is the most commonly used method to extract impervious surface. As a method that can automatically and quickly extract impervious surface in a large range, the principle of NDISI index is to construct strong reflection group and weak reflection group of impervious surface in spectral band of remote sensing image, and carry out band operation, so as to expand the contrast between impervious surface and sand soil, vegetation, water body and other surface features, so as to enhance the impervious surface information. The formula of the index is as follows:

$$NDISI = \frac{TIR - (MNDWI + NIR + MIR_1)/3}{TIR + (MNDWI + NIR + MIR_1)/3} \quad (1)$$

TIR, NIR and MIR_1 represent thermal infrared, near infrared and mid infrared bands of remote sensing image respectively, and MNDWI refers to modified normalized differential water index. Both MNDWI and TIR bands need linear stretching of 0-255 gray level to unify the quantization series of each band. The NDISI results were normalized and converted to ISC for further analysis.

The calculation formula is as follows:

$$ISC = \frac{NDISI_i - NDISI_{min}}{NDISI_{max} - NDISI_{min}} \times 100\% . \quad (2)$$

ISC is classified by mean-standard deviation method (table 3), which is also used in the following classification.

Table 3

Criteria for classification of impervious surface coverage

ISC levels	Division basis
First	$ISC_{mean} + s < ISC_{ni}$
Second	$ISC_{mean} + 0.5s < ISC_{ni} \leq ISC_{mean} + s$
Third	$ISC_{mean} - 0.5s \leq ISC_{ni} < ISC_{mean} + 0.5s$
Fourth	$ISC_{mean} - s \leq ISC_{ni} < ISC_{mean} - 0.5s$
Fifth	$ISC_{ni} < ISC_{mean} - s$

Note: ISC_{ni} is the normalized pixel value, ISC_{mean} is the average value of all pixels after normalization, s is the standard deviation.

(2) LST inversion

The atmospheric correction method and single window algorithm are used to retrieve the LST, and MOD11A1 are used to verify the accuracy. Finally, the LST retrieved by atmospheric correction method is selected to classify the heat island grade.

Atmospheric correction method: firstly, the influence of the atmosphere on the surface thermal radiation is estimated, and then this part of the atmospheric impact is subtracted from the total thermal radiation observed by satellite sensors to obtain the surface thermal radiation intensity, and then the thermal radiation intensity is converted into the corresponding surface temperature.

The brightness value L_λ of thermal infrared radiation received by the satellite sensor consists of three parts: the upward radiance of the atmosphere, the energy of the real radiance of the ground after passing through the atmosphere, and the reflected energy of the downward radiation from the atmosphere to the ground. The expression of thermal infrared radiance value L_λ received by satellite sensor (radiative transfer equation) can be written as:

$$L_\lambda = [\varepsilon_{B(T_s)} + (1 - \varepsilon)L \downarrow] \tau + L \uparrow , \quad (3)$$

where, ε is the surface emissivity, T_s is the real surface temperature (K), $B(T_s)$ is the blackbody thermal radiance brightness, and τ is the atmospheric transmittance in the thermal infrared band. Then the radiance $B(T_s)$ of the blackbody with temperature T in the thermal infrared band is:

$$B(T_s) = [L_\lambda - L \uparrow - \tau(1 - \varepsilon)L \downarrow] / \tau\varepsilon . \quad (4)$$

T_s can be obtained by the function of Planck's formula.

$$T_s = K_2 / \ln(K_1 / B(T_s) + 1) . \quad (5)$$

For TIRS band10, $K_1 = 774.89 \text{ w} / (\text{M}^2 * \mu\text{m} * \text{sr})$, $K_2 = 1321.08 \text{ K}$. LST is divided into five grades by means of mean-standard deviation method: high temperature zone, sub high temperature zone, medium temperature zone, sub low temperature zone and low temperature zone. Sub high temperature zone and high temperature zone are considered as heat island area.

(3) Vegetation fractional coverage (VFC)

The calculation of VFC was shown below:

$$FVC = (NDVI - NDVI_{soil}) / (NDVI_{veg} - NDVI_{soil}) . \quad (6)$$

According to the situation of remote sensing images, $NDVI_{soil}$ and $NDVI_{veg}$ are replaced by $NDVI_{min}$ and $NDVI_{max}$ respectively. Due to the inevitable noise, $NDVI_{min}$ and $NDVI_{max}$ generally take the maximum and minimum values within a certain confidence range, and the confidence values are mainly determined as 5% and 95% according to the actual situation of the image.

LULC classification

The automatic decision tree method is used to classify the images of Dazhangxi Basin in 2013 and 2017. The decision tree method obtains the classification rules through the experience of experts, simple mathematical statistics and induction methods, and carries out remote sensing classification. The classification rules are easy to understand, and the classification process is in line with human cognitive process, and the biggest feature is the use of multi-source data. NDVI, MNDWI, NDBI, ISC and LST are selected as auxiliary data for decision tree classification. According to the LULC classification standard in 1984, the land in the study area is divided into six categories: construction land, unused land, farmland, water body area, forest and grassland.

Two ROIs are drawn independently on Google Earth, which are used to model and verify the classification. According to the separability report of ROI, it is greater than 1.99, which proves that the selection of ROI is very reasonable. After classification, principal component analysis and cluster analysis are used to process the classification results.

NPP estimation

CASA model was used to retrieve NPP, considering the effects of solar radiation, temperature and precipitation. Based on Landsat 8 OLI and meteorological data, NPP estimation models for different land types in the Dazhangxi Basin were constructed. Compared with other NPP of vegetation at home and abroad, CASA model is more simple and convenient. The parameters can be determined respectively by using remote sensing information extraction and GIS, which avoids unnecessary errors caused by artificial simplification or estimation of parameters due to lack of parameters. The specific calculation process of CASA model is as follows:

$$NPP(x, t) = APAR(x, t) * \varepsilon(x, t) , \quad (7)$$

x is the spatial position and t is the time; $NPP(x, t)$ is the NPP ($gC \cdot m^{-2} \cdot month^{-1}$) of pixel x in t month; $APAR(x, t)$ is the photosynthetic effective radiation absorbed by pixel x in t month ($MJ \cdot m^{-2} \cdot month^{-1}$); $\varepsilon(x, t)$ is the actual light energy utilization rate of pixel x in month t ($gC \cdot MJ^{-1}$).

According to formula (7), $NPP(x, t)$ is determined by $APAR(x, t)$ and $\varepsilon(x, t)$, and $APAR(x, t)$ can be calculated as (8):

$$APAR(x, t) = Q(x, t) * FPAR(x, t) * 0.5 , \quad (8)$$

$Q(x, t)$ is the total solar radiation at pixel x in month t ; $FPAR(x, t)$ is the absorption ratio of incident photosynthetically active radiation by vegetation layer; the constant 0.5 represents the proportion of solar effective radiation (wavelength $0.38 \sim 0.71 \mu m$) available for vegetation in total solar radiation. $\varepsilon(x, t)$ can be calculated as (9):

$$\varepsilon(x, t) = \varepsilon_{max} * T_{\varepsilon 1(x, t)} * T_{\varepsilon 2(x, t)} * W_{\varepsilon(x, t)} , \quad (9)$$

$T_{\varepsilon 1(x, t)}$ and $T_{\varepsilon 2(x, t)}$ denote the stress effect of low temperature and high temperature on light energy utilization efficiency, $W_{\varepsilon(x, t)}$ is the influence coefficient of water stress, and ε_{max} is the maximum

light energy utilization rate of vegetation under ideal conditions, which is related to vegetation types. The maximum photosynthetic utilization rate of Chinese typical vegetation simulated by Zhu et al (2006) was used here. In particular, the farmland in the study area are mainly evergreen broad-leaved forest and evergreen coniferous forest. According to the research results, the average value of evergreen broad-leaved forest and evergreen coniferous forest (0.687) is taken as the maximum light energy utilization rate of forest land.

(1) Calculation of $Q(x,t)$

$$Q(x,t) = Q_0 * \left(a + b * \frac{n}{N} \right), \quad (10)$$

Q is the monthly total solar radiation received by the earth's surface; Q_0 is the monthly astronomical total radiation; n/N is the percentage of monthly sunshine. a and b are empirical coefficients, which are taken as 0.25 and 0.50 respectively. FAO suggests that this should be set when no measured solar radiation data can be used and the accuracy correction of a and b parameters is not improved (Wang et al., 2014). The monthly total astronomical radiation Q_0 is calculated by the method of daily summation of the total astronomical radiation Q_i , and the daily total astronomical radiation is calculated by formula (11)

$$Q_i = \frac{TG_{sc}}{\pi} * \rho^2 * (\omega_0 \sin \varphi \sin \delta + \cos \varphi \cos \delta \sin \omega), \quad (11)$$

Q_i is the total daily astronomical radiation ($\text{MJ} \cdot \text{m}^{-2} \cdot \text{D}^{-1}$); T is the period ($24 \times 60 \times 60\text{s}$); G_{sc} is the solar constant ($13.67 \times 10^{-4} \text{ MJ} \cdot \text{m}^{-2} \cdot \text{s}^{-1}$); ρ is the relative distance between the sun and the earth; ω_0 is the sunset angle (rad); φ is the geographical latitude (rad); δ is the solar declination (rad). The relative distance between the sun and the earth is calculated by equation (12).

$$\rho = \sqrt{\frac{1}{1 + 0.033 \cos \frac{2\pi J}{365}}}, \quad (12)$$

J is the day ordinal number of a day in the year, from 1 January 1 to 365 December 31. The sunset angle ω_0 is calculated by equation (13)

$$\omega_0 = \arccos(-\tan \varphi \tan \delta). \quad (13)$$

The declination of the sun is calculated by equation (14)

$$\delta = 0.409 \sin\left(\frac{2\pi J}{365} - 1.39\right). \quad (14)$$

(2) Calculation of $FPAR(x,t)$

Because the $FPAR$ estimated by $NDVI$ will be higher than the measured value, while the $FPAR$ estimated by SR will be lower than the measured value, it is necessary to obtain the actual photosynthetic effective radiation absorption ratio ($FPAR$) by adjusting coefficient α (0.5 in this study).

$$FPAR(x,t) = \alpha * FPAR_{NDVI(x,t)} + (1 - \alpha) * FPAR_{SR(x,t)}, \quad (15)$$

$FPAR_{NDVI(x,t)}$ and $FPAR_{SR(x,t)}$ are the proportion coefficients of photosynthetic effective radiation absorption of vegetation canopy calculated by $NDVI$ and SR , respectively, which are calculated by (16) and (17).

$$FPAR_{NDVI(x,t)} = \frac{NDVI(x,t) - NDVI_{i,min}}{NDVI_{i,max} - NDVI_{i,min}} * (FPAR_{max} - FPAR_{min}) + FPAR_{min}. \quad (16)$$

In equation (16), $NDVI(x, t)$ is the NDVI of pixel x in month t . $NDVI_{i, \max}$ is the value of NDVI with confidence level of 95% for the i -th land cover type, and $NDVI_{i, \min}$ is the value of NDVI confidence level of 5% for unused land; the values of $FPAR_{\min}$ and $FPAR_{\max}$ are 0.001 and 0.95, respectively.

$$FPAR_{SR(x,t)} = \frac{SR(x,t) - SR_{i,\min}}{SR_{i,\max} - SR_{i,\min}} * (FPAR_{\max} - FPAR_{\min}) + FPAR_{\min}, \quad (17)$$

$SR(x, t)$ is the ratio vegetation index of pixel x in month t (18); $SR_{i, \max}$ is the value of NDVI with confidence level of 95% for the i -th land cover type, and $SR_{i, \min}$ is the value of NDVI confidence level of 5% for unused land; the values of $FPAR_{\min}$ and $FPAR_{\max}$ are 0.001 and 0.95, respectively.

$$SR(x,t) = \frac{1 + NDVI(x,t)}{1 - NDVI(x,t)}. \quad (18)$$

(3) Calculation of $T_{\varepsilon 1(x,t)}$

$$T_{\varepsilon 1(x,t)} = 0.8 + 0.02 * T_{opt}(x) - 0.0005 * [T_{opt}(x)]^2, \quad (19)$$

$T_{opt}(x)$ is the optimum temperature for plant growth, which is defined as the average temperature of the month when the NDVI value reaches the highest in a certain region in a year. For the study area, the average temperature in July is taken as the optimum; when the average temperature in a certain month is less than or equal to -10°C , $T_{\varepsilon 1(x,t)}$ is taken as 0.

(4) Calculation of $T_{\varepsilon 2(x,t)}$

$$T_{\varepsilon 2(x,t)} = 1.184 / \{1 + \exp[0.2 * (T_{opt}(x) - 10 - T(x,t))]\} * 1 / \{1 + \exp[0.3 * (-T_{opt}(x) - 10 + T(x,t))]\} \quad (20)$$

When the average temperature of a month $T(x, t)$ is 10°C higher or lower than the optimum temperature $T_{opt}(x)$, the value of $T_{\varepsilon 2(x,t)}$ in the month is equal to half of the value of $T_{\varepsilon 2(x,t)}$ when the monthly average temperature $T(x, t)$ is the optimal temperature $T_{opt}(x)$.

(5) Calculation of $W_{\varepsilon(x,t)}$

$$W_{\varepsilon}(x,t) = 0.5 + 0.5 * C(x,t) / C_p(x,t), \quad (21)$$

$C(x,t)$ is the actual regional transpiration (mm), which is calculated according to the regional actual evapotranspiration model established by Zhou and Zhang (1995) (Eq. 22); $C_p(x,t)$ is the regional potential evapotranspiration (mm), which is calculated according to the complementary relationship between EET and PET (Luo, 2010) (Eq. 23). The required parameter data are provided by monthly average temperature $T(x, t)$ and monthly total precipitation $W(x, t)$.

$$EET = \frac{r \bullet Rn(r^2 + Rn^2 + r \bullet Rn)}{(r + Rn) \bullet (r^2 + Rn^2)}, \quad (22)$$

$$2PET = Ep + EET, \quad (23)$$

r is the monthly accumulated precipitation (mm); R_n is the regional accumulated surface net radiation. Since many parameters for calculating the net surface radiation are difficult to obtain, they can be estimated by using the empirical model (Eq. (24)) established by Zhou and Zhang (1996).

$$Rn = (Ep \bullet r)^2 \times [0.369 + 0.598(\frac{Ep}{r})^{0.5}], \quad (24)$$

Ep in equations (24) and (25) is local potential evapotranspiration (mm), which is calculated by using the vegetation climate relationship model (Thornthwaite, 1948) as formula (25).

$$Ep = 2037.98 - 18.8308LAT - 4.5801LONG - 0.157861ALT, \quad (25)$$

LAT is the latitude of the research site, LONG is the longitude of the research site, and ALT is the altitude of the research site.

NPP was divided into five grades by mean-standard deviation method: high biomass area, secondary high biomass area, medium biomass area, secondary low biomass area and low biomass area. The high biomass area and the secondary high biomass area were regarded as the areas with rich biomass.

RSEI ecological index

RSEI includes four important indicators of natural ecological environment: greenness, humidity, heat and dryness. Among the many natural factors reflecting ecological quality, these four factors are closely related to human survival, and are also the most important indicators for human beings to intuitively feel the quality of ecological conditions. Remote sensing technology can obtain the information of these four indicators from remote sensing images, such as vegetation index, humidity component, surface temperature and soil index to represent greenness, humidity, heat and dryness respectively

$$RSEI = f(NDVI, WET, LST, NDSI), \quad (26)$$

NDVI is vegetation index; Wet is humidity component; LST is surface temperature; NDSI is soil index. NDVI is undoubtedly the most widely used vegetation index, which is closely related to plant biomass, leaf area index and vegetation coverage. Therefore, NDVI is selected to represent the greenness index. The brightness, greenness and wetness obtained by tassell cap transformation have been widely used in ecological environment monitoring. The humidity component reflects the humidity of water, soil and vegetation, which is closely related to ecology. Therefore, the humidity index of this study is represented by wetness:

$$WET = 0.0315\rho_1 + 0.2021\rho_2 + 0.3102\rho_3 + 0.1594\rho_4 - 0.6806\rho_5 - 0.6109\rho_7, \quad (27)$$

where: $\rho_i (i = 1, \dots, 5, 7)$ is the reflectivity of each band. LST uses the best atmospheric correction inversion results after the interactive accuracy verification of MOD11A1 data to obtain the index. The NDSI is selected as the dryness index. However, in the regional environment, there is a considerable number of construction lands, which also cause the drying of the surface. Therefore, the dryness index can be synthesized by the soil index (SI) and the building index (NDBI).

$$NDSI = (SI + IBI) / 2, \quad (28)$$

where

$$SI = [(\rho_5 + \rho_3) - (\rho_4 + \rho_1)] / [(\rho_5 + \rho_3) + (\rho_4 + \rho_1)], \quad (29)$$

$$NDBI = (\rho_5 - \rho_4) / (\rho_5 + \rho_4), \quad (30)$$

Principal component analysis (PCA) is a multi-dimensional data compression technology which selects a few important variables by orthogonal linear transformation. In this study, PCA is used to integrate indicators. Before this transformation, we must normalize these indices and map their values to [0,1]. Finally, the RSEI based on PC1 is between [0,1]. The closer to 1, the better the ecology. The comprehensive representativeness of RSEI can also be analyzed from the correlation between RSEI and each index. The stronger the correlation between RSEI and each index is, the more comprehensively it can represent each index.

RSEI is divided into five grades by means of a mean-standard deviation method: excellent ecological area, sub optimal ecological area, medium ecological area, sub poor ecological area and poor ecological area.

Results and discussion

Remote sensing indices

(1) NDVI

Figure 3 is the overall trend of NDVI distribution in 2013 and 2017, the high values are mainly concentrated in the upper, middle and lower right parts of the basin, and the low values are distributed in the west and northeast of the basin. According to the distribution of power stations reported in the Report, it can be seen that the low value of NDVI in the study area is mainly spread around the power station location. The low value in the northeast is mainly caused by the underlying surface being residential area. The NDVI value in 2017 was generally lower than that in 2013. It is obvious that taking the power station as the center, the relevant building land has been built or expanded around it, and the road facilities connecting the main stream of Dazhangxi and the power station have been built, which has affected the NDVI value of the whole research basin to a certain extent, and has an impact on the ecological environment.

(2) MNDWI

There is no significant difference in the distribution of MNDWI values between the two years (fig. 4). However, due to the fact that the image of 2013 is October and the image of 17 years is December, it is obvious that the discharge of 2017 is less than that of 2013 in the main part of Dazhangxi, especially in the west of the trunk part.

(3) NDBI

Compared with 2013, the building area increased in 2017 (fig. 5), and the fragmentation of building patches increased. In the western part of the basin, the increase is obvious in the western part of the basin, while the increase in other parts is not obvious, but the patch becomes more fragmented. This may be due to the construction of power stations in the basin and the intervention of human activities.

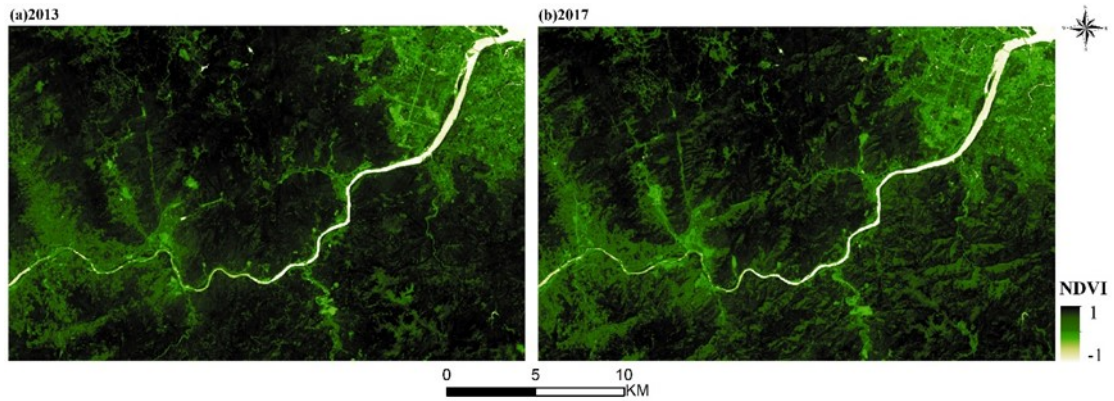


Fig. 3. NDVI of 2013 and 2017

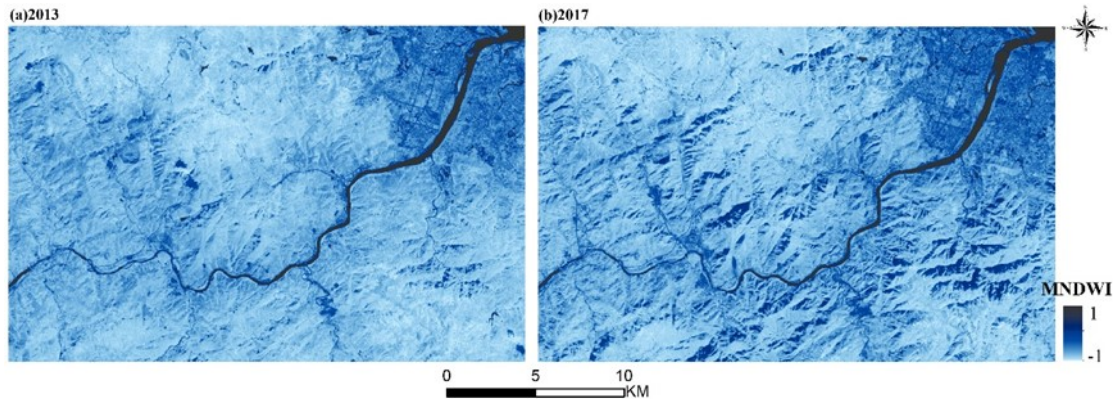


Fig. 4. MNDWI of 2013 and 2017

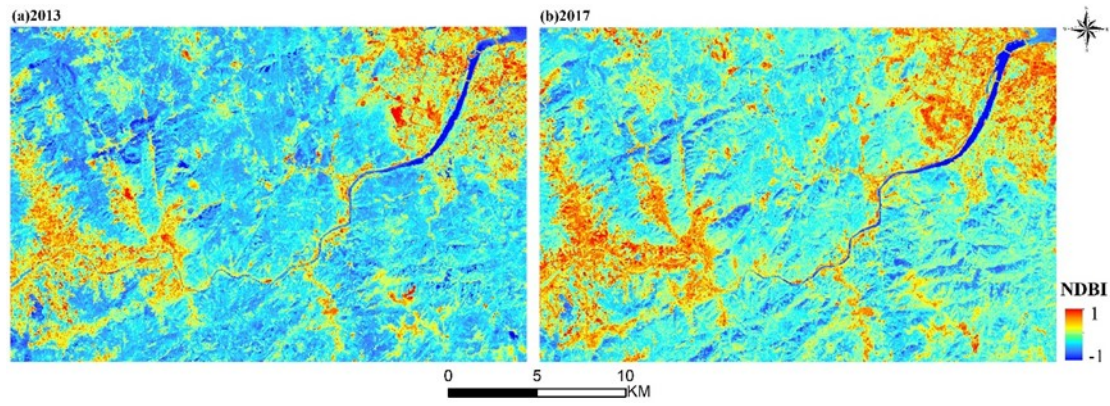


Fig. 5. NDBI of 2013 and 2017

Thermal environment

ISC

As can be seen from figure 6, compared with 2013, the first-class area in 2017 decreased, the second-class area increased slightly, the third-class area increased more significantly, and the area of fourth and fifth class areas decreased significantly. Combined with the situation of the study area, from 2013 to 2017, the buildings developed from contiguous to scattered, the road area increased, the forest area decreased, and the forest land gradually developed to sparse forest land.

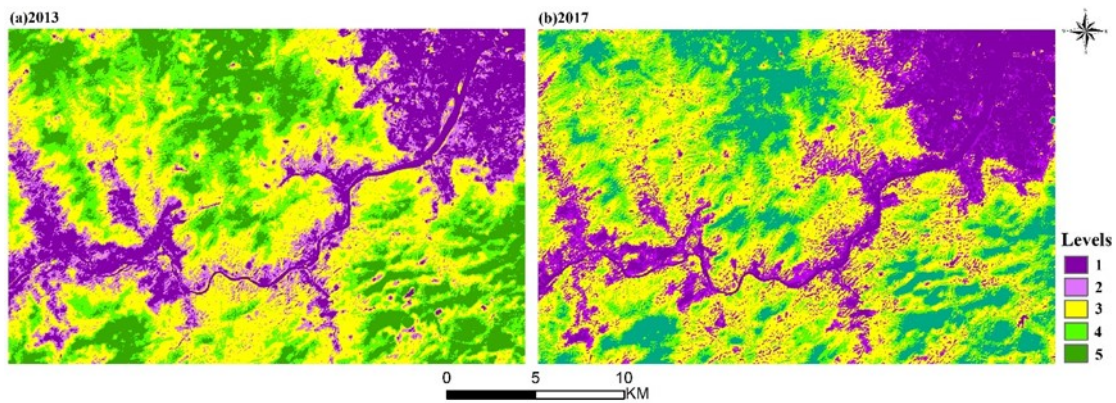


Fig. 6. ISC of 2013 and 2017

LST

Using the MOD11A1 data, the real LST of the study area was extracted. 200 random points are created in the research area. After resampling the atmospheric correction and single window algorithm inversion results, the temperature values of corresponding points are extracted. After the relevant data processing and regression model establishment, the correlation coefficient and R^2 were obtained. The specific results are shown in figure 7. In the two years, the atmospheric correction method is better in 2017, and the single window algorithm is better in 2013. However, the temperature of single window algorithm in 2017 is compressed in a narrow range, overall the atmospheric correction method is better. The following analysis is based on the results of atmospheric correction.

The LST results after grading are shown in figure 8. According to the final LST distribution map, combined with the ISC index classification results, the construction land in the downstream and along the banks of the Dazhangxi Basin has a significant heat island effect in 2013-2017. It can be concluded that LST and ISC results are significantly related to the degree of urbanization, but may also be restricted by vegetation, water and other factors. For example, the greening and environmental improvement in the central urban area may reduce its thermal environment effect to a certain extent.

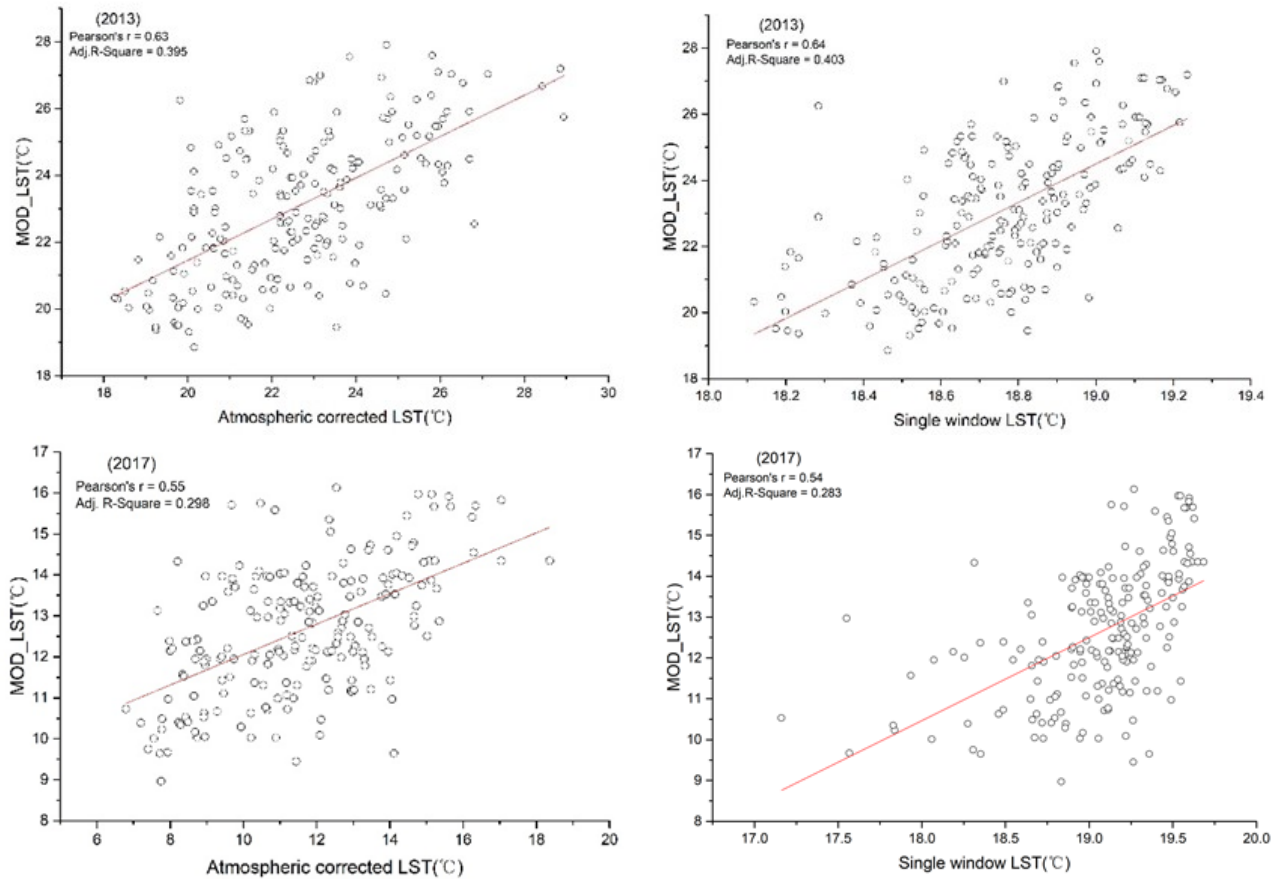


Fig. 7. LST regression model in 2013 and 2017

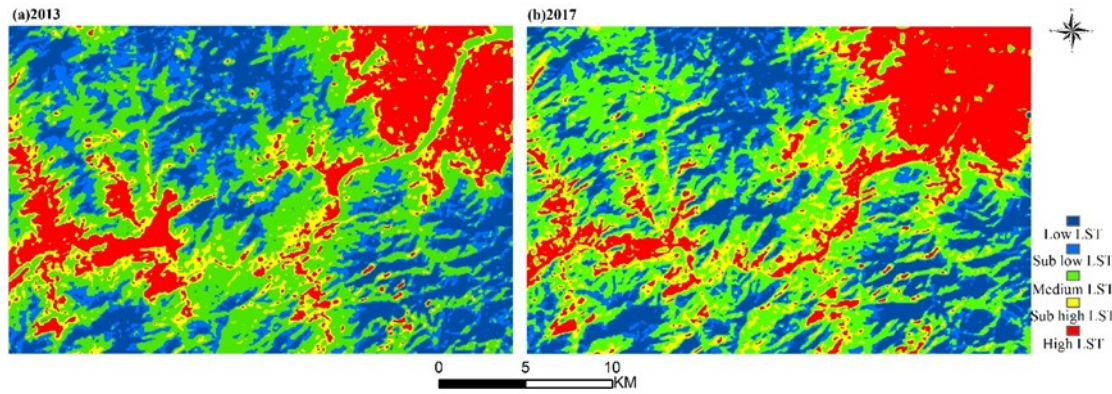


Fig. 8. LST levels distribution map in 2013 and 2017

VFC

Through comparative analysis, it can be found that the vegetation coverage in 2017 has an obvious trend of reduction, especially in the northeast and west of the basin, the vegetation area decreased significantly. In the southeast of the basin, there are also some areas where the vegetation coverage decreases. The main reason is that the operation of the power station needs some human intervention, which leads to the destruction of the ecological environment.

LULC monitoring and change detection

The classification accuracy based on the automatic decision tree method was 94.14% in 2013 and 90.69% in 2017, and the kappa coefficient was 0.92 and 0.88, respectively. The images of Dazhangxi watershed in 2013 and 2017 are classified, and the classification results are shown in figure 10.

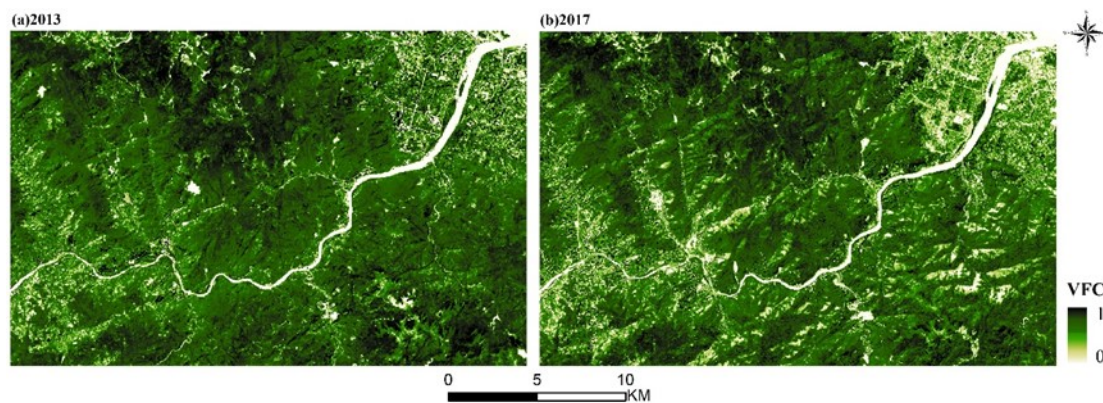


Fig. 9. VFC in 2013 and 2017

The construction land is mainly distributed along the river and mainly distributed in the north-east of Dazhangxi Basin, while the farmland is mainly distributed near the construction land. Compared with the land use map of 2013 and 2017, it can be found that the changes of construction land, farmland and unused land are more obvious. In 2017, the area of construction land increased, the area of agricultural land decreased, and the area of unused land increased.

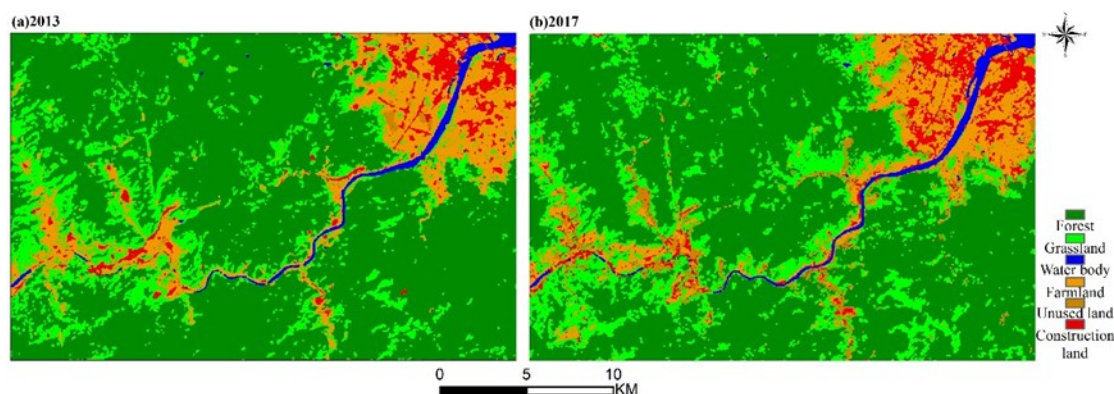


Fig. 10. LULC in 2013 and 2017

The classification results were statistically analyzed and a pie chart was drawn (fig. 11). The vegetation coverage rate of Dazhangxi basin is higher, reaching more than 60%. However, the vegetation coverage rate in 2017 was lower than that in 2013, the proportion of forest land and farmland decreased significantly, and the proportion of construction land and unused land increased significantly. This shows that with the advancement of urbanization, the land use in the Dazhangxi Basin has changed. The land use inclines to the construction land, and part of the farmland is used for urban construction. To a certain extent, this has affected the vegetation coverage rate and ecological environment of Dazhangxi Basin.

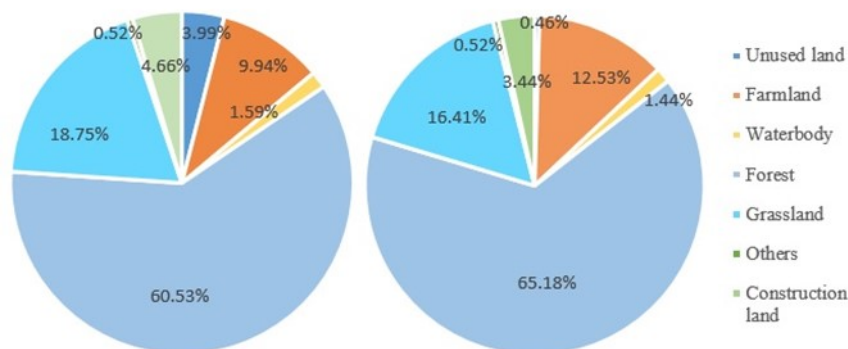


Fig. 11. Proportion of land use types in 2013 and 2017

In order to further reflect the land use change of Dazhangxi River Basin from 2013 to 2017, the concept of land transfer matrix (Liu, Zhu, 2010) was introduced and calculated the detailed land use type area transfer change from 2013 to 2017, as shown in table 4.

From the perspective of land transfer, the land with large transfer-out area was forest land, grassland and farmland in order from 2013 to 2017, with the transfer-in area of 33952.59 ha, 210725.66 ha and 7175.61 ha respectively. The largest transfer-in area was forest land, grassland and farmland, and the transfer area was 30559.86 ha, 11795.31 ha and 5665.23 ha respectively. The overall situation of the transfer in and out shows a decreasing trend in forest land, and it is mainly converted into grassland, and the construction land shows an increasing trend, and the main source of increase is the conversion of farmland to construction land.

From the area ranking, the vast majority of land types in Dazhangxi basin are forest land, grassland and farmland. Forest land is an important indicator of the natural and ecological environment in the region, which indicates that the ecological maintenance of Dazhangxi basin is relatively good. However, compared with 2013, the proportion of forest land decreased in 2017, and it was mainly transferred out to grassland, and the forest land and grassland were transformed from each other, mainly due to the impact of human activities. The proportion of construction land is increased, and it mainly comes from the conversion of farmland. Urban construction needs new expansion. But maintaining enough farmland area is also the key to ensure the economic and food sources of urban residents. While promoting the construction of urbanization, the Dazhangxi river basin should take into account the protection of ecological environment, so as to realize sustainable development.

Table 4

Land use change area transfer matrix from 2013 to 2017 (ha)

Land use	Grassland	Construc- tion land	Forest	Farmland	Water body	Unused land	Transfer- out
Grassland	4984.29	219.87	3612.24	1147.32	5.4	756.54	10725.66
Construc- tion land	29.25	904.68	5.22	675.18	71.55	263.43	1949.31
Forest	5778.63	39.87	26871.39	287.01	4.59	971.1	33952.59
Farmland	994.32	1310.58	70.65	3424.68	37.98	1337.4	7175.61
Water body	2.43	17.73	0.09	28.44	745.2	18.99	812.88
Unused land	6.39	155.43	0.27	102.6	12.6	131.58	408.87
Transfer-in	11795.31	2648.16	30559.86	5665.23	877.32	3479.04	55024.92

NPP monitoring and analysis

The NPP grading distribution in 2013 and 2017 was finally as shown in figure 12. Through comparative analysis, we can see that compared with 2013, the low biomass areas in 2017 increased significantly. Taking the main trunk of Dazhangxi as the center, the areas around it are almost all low biomass areas, and they are shown in a more contiguous form. However, the NPP inversion results in 2013 showed that there were a few high or sub high biomass areas in the form of broken patches near the main trunk of Dazhangxi. The main reason for this phenomenon is that the operation of the power station near the basin has destroyed the forest around it, thus affecting the biomass of the area. Another obvious change is that the high biomass area in 2017 has a certain reduction compared with 2013. Especially in the west, North and southeast of the basin, this situation is obvious.

The results of the changes of two years are detected as figure 13. On the whole, the NPP of the study area showed a decreasing phenomenon, and the decreasing area was mainly forest land type, which indicated that the forest land was affected in this process. There is a high spatial correlation between the unchangeable region and the low biomass area. The low biomass area is mainly water

land type. The biomass of water body is generally very low. It is impossible to develop into forest land type with high NPP in a short time. The NPP corresponding to all water body types will remain unchanged. The rising areas are mainly distributed in forest, especially in the East and West of the basin. In order to improve the ecological living conditions of local residents, some green belts were planted by human intervention. The NPP in Western China will increase sporadically, which is mainly due to the comprehensive utilization of Longxiang reservoir from power generation to water supply. This location has a certain ecological mitigation effect on this area.

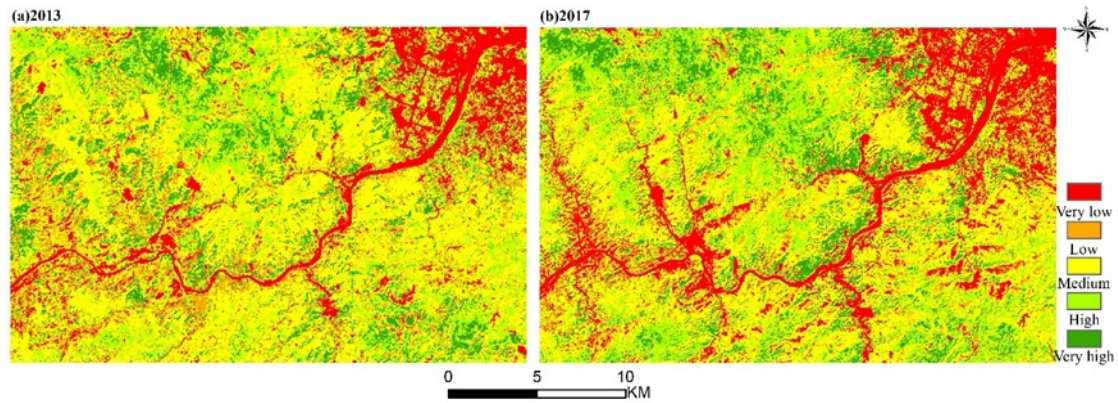


Fig. 12. NPP distribution map in 2013 and 2017

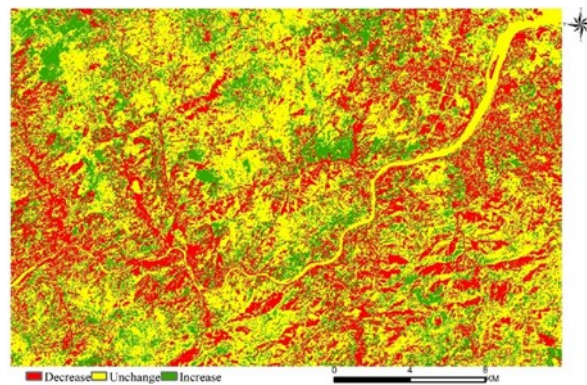


Fig. 13. NPP transform detection distribution

The NPP results, LST and VFC values of two periods was extracted by creating 200 random points in the study area. Statistical software was used to describe the spatial relationship among them. The results are shown in the figure 14.

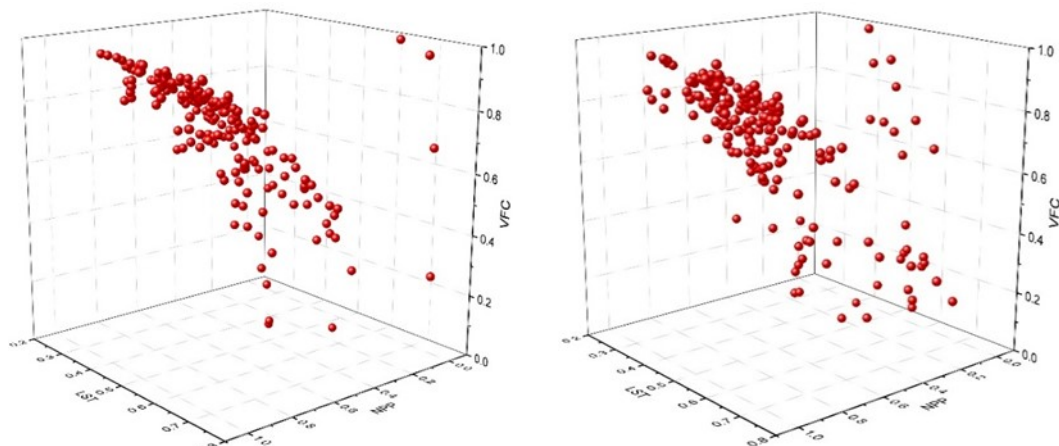


Fig. 14. Scatter map of 3D feature space (left 2013, right 2017)

According to the above analysis, NPP has a high correlation with VFC. With the increase of VFC, NPP increased except for a few sites. VFC, to a certain extent, represents the dense situation of ground vegetation. When the vegetation is lush, it can make full use of solar radiation and produce more NPP. Analysis of a small number of special points shows that NPP is always low no matter how the VFC changes, which may be caused by the model method. The calculation of the absorption of incident photosynthetically active radiation (PAR) by vegetation layer is based on different types of surface features. This study cannot guarantee that each type of ground feature can be identified completely and correctly. The corresponding pixel of this point may have vegetation surface feature spectral information and has high VFC, but its corresponding NPP value is underestimated because the ground feature type is not classified into vegetation.

In addition, there is no direct correlation between NPP and LST. In different temperature ranges, the corresponding NPP values are basically the same. In this study, we use the remote sensing image obtained at a certain time, and the temperature retrieved from it is also instantaneous, which will not have a direct impact on NPP. On the other hand, the study area is the Dazhangxi basin with a small scope. Even though different types of surface features have an impact on surface temperature, the overall impact is small, so the impact of temperature on net primary productivity is not obvious in this region.

RSEI monitoring and assessment

As can be seen from the table 5, The first principal component (PC1) of the four indicators in the study area has the following characteristics: 1) The contribution rate of PC1 is greater than 70%, indicating that it has concentrated most of the characteristics of the four indicators; 2) The four indicators have a certain degree of contribution to PC1, and are relatively stable, not like in other characteristic components (PC2 ~ PC4). 3) In PC1, NDVI and WET which represent the greenness and humidity are positive, indicating that they contribute positively to the ecology. LST and NDSI, which represent heat and dryness, are negative in PC1, indicating that they have negative effects on ecology, which is consistent with the actual situation. However, in PC2 ~ PC4, these indicators are sometimes positive and sometimes negative, which is difficult to explain the ecological phenomenon. Therefore, compared with other components, PC1 concentrates the characteristics of each index to the greatest extent, and can reasonably explain the ecological phenomenon, so it can be used to create comprehensive ecological index.

Table 5

Results of principal component analysis

Indices	2013				2017			
	PC1	PC2	PC3	PC4	PC1	PC2	PC3	PC4
dryness	-0.955	0.023	-0.249	0.157	-0.903	0.222	-0.327	0.169
greenness	0.841	0.526	0.084	0.096	0.713	0.654	0.239	0.085
heat	-0.891	0.024	0.452	0.040	-0.816	-0.171	0.547	0.071
humidity	0.875	-0.456	0.108	0.120	0.867	-0.468	-0.021	0.173

According to PC1, the comprehensive representativeness of RSEI can also be analyzed from its correlation with each index. The stronger the correlation between RSEI and each index is, the more comprehensively it can represent each index. Table 6 shows the correlation coefficient between each index and RSEI, as well as the correlation coefficient between each index itself. For a single indicator, the highest average correlation between indices is NDSI, reaching 0.849 in 2013, The two-year average is 0.792. However, the annual average correlation coefficient between RSEI and these four indicators is greater than 0.61, and the two-year average is 0.725, which is 6.4% higher than the average of the lowest NDVI. Obviously, the higher correlation between RSEI and

each index indicates that it is more representative than any single index and can comprehensively represent the information of each index.

Table 6

Correlation coefficient matrix of each index and RSEI index

Indices	2017					2013				
	NDSI	NDVI	LST	WET	RSEI	NDSI	NDVI	LST	WET	RSEI
NDSI	1	-0.562	0.532	-0.85	-0.678	1	-0.797	0.745	-0.855	-0.692
NDVI	-0.562	1	-0.557	0.322	0.819	-0.797	1	-0.694	0.516	0.812
LST	0.532	-0.557	1	-0.627	-0.701	0.745	-0.694	1	-0.737	-0.667
WET	-0.85	0.322	-0.627	1	0.729	-0.855	0.516	-0.737	1	0.698
Average correlation	0.736	0.610	0.679	0.700	0.732	0.849	0.752	0.794	0.777	0.717
Two year average	NDSI=0.792 NDVI=0.681 LST=0.737 WET=0.738 RSEI=0.725									

Note: the average correlation is calculated based on the absolute value of the correlation coefficient between itself and other indicators. Take NDSI in 2017 as an example: average correlation NDSI = $(|-0.562| + |0.532| + |-0.85| + |1|)/4 = 0.736$.

RSEI can also be used to establish ecological models to simulate and predict the trend of regional ecological change. Firstly, the thematic images of NDVI, WET, LST, NDSI and RSEI of each year are sampled, and then the relationship model is established by stepwise regression analysis with RSEI as dependent variable and NDVI, WET, LST and NDSI as independent variables, 28000 sample points were collected from each image. Enough sample points and sampling method throughout the whole image can ensure the representativeness and objectivity of regression analysis results, and avoid the uncertainty caused by small sample and local sampling. In 2013, the model is $RSEI = 0.277Wet + 0.266NDVI - 0.302NDSI - 0.282LST + 0.477$ ($R^2 = 0.992$); while in 2017, it is $RSEI = 0.313Wet + 0.258NDVI - 0.326NDSI - 0.295LST + 0.483$ ($R^2 = 0.989$). From the regression coefficient of each index, the coefficients of NDVI and WET are positive, indicating that they have positive effect on RSEI, while LST and NDSI are negative. Further study on the change of regression coefficient shows that the comprehensive influence of NDVI and WET on RSEI is more than that of NDSI and LST, because the sum of the two coefficients is greater than the absolute sum of NDSI and LST.

The RSEI grading results was shown in the figure 15. Compared with 2013, the low biomass areas in 2017 increased significantly. Taking the main trunk of Dazhangxi as the center, the areas around it are almost all low biomass areas, and they are shown in a more contiguous form. However, the NPP inversion results in 2013 showed that there were a few high or sub high biomass areas in the form of broken patches near the main trunk of Dazhangxi. The main reason for this phenomenon is that the operation of the power station near the basin has destroyed the forest around it, thus affecting the biomass of the area. Another obvious change is that the high biomass area in 2017 has a certain reduction compared with 2013. Especially in the west, North and south-east of the basin, this situation is obvious.

Figure 16 shows the results of changes between the two periods. Overall, the NPP of the study area showed a decrease, and the decrease area was mainly forest land type, which indicated that forest land was affected in this process. There is a high spatial correlation between the unchangeable region and the low biomass area. The low biomass area is mainly water body. The biomass of water body is generally very low. It is impossible to develop into forest with high NPP in a short time. The NPP corresponding to all water body types will remain unchanged. The rising areas are mainly distributed in forest, especially in the East and West of the basin. In order to improve the ecological living conditions of local residents, some green belts were planted by human intervention. The NPP in Western also increased sporadically, which is mainly due to the comprehensive

utilization of Longxiang reservoir from power generation to water supply. The development orientation has a certain ecological mitigation effect on the region.

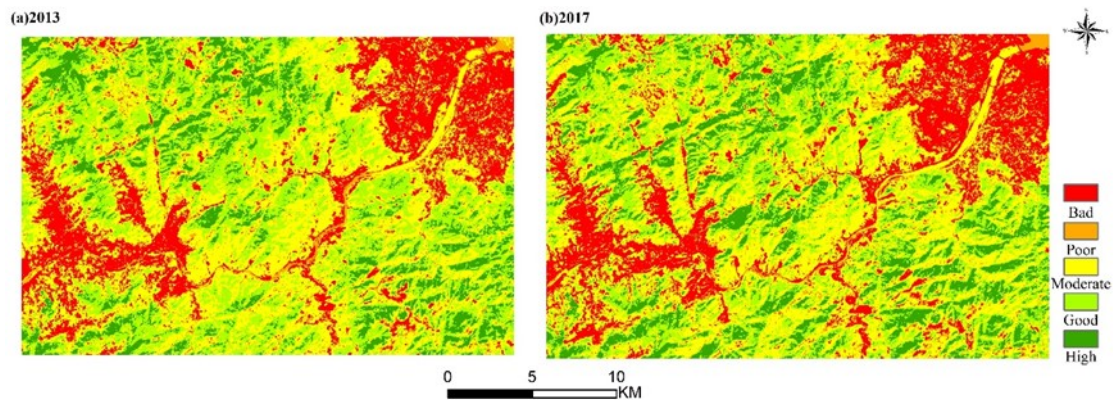


Fig. 15. RSEI grade distribution map

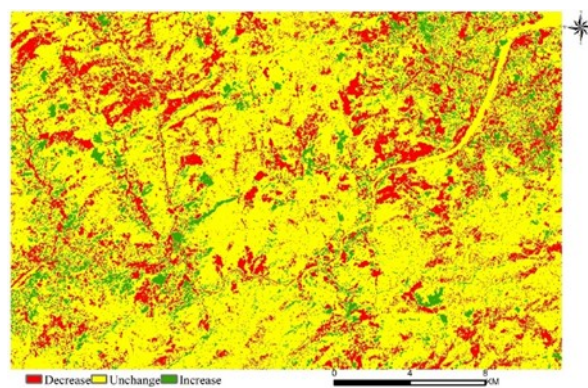


Fig. 16. RSEI transform detection distribution

The relationship between each index and the RSEI is investigated from the distribution of their scatter points in the 3-D characteristic space (fig. 17). The top of the scattered point group is the gathering area with good ecological conditions, mainly the high coverage vegetation area; the bottom end of the scattered point group is the gathering area with poor ecological conditions, representing the bare soil area. Generally speaking, both regression model and PCA show that the greenness represented by NDVI and the dryness represented by NDSI have the greatest impact on the ecological environment, and the impact of NDVI is greater than that of NDSI. The results of this data simulation also prove that the effect of controlling soil and water loss by increasing greenness in this area is greater. If the 2017 model is used for prediction, the NDVI will be increased by 0.253 for every 0.1 increase of RSEI.

Comprehensive evaluation of ecological environment

From the perspective of thermal environment, due to the rapid expansion of urban construction land along the banks of Dazhangxi, the intersection of tributaries and Minjiang River downstream, the thermal environment effect has been increasing, forming the local heat island effect. This has quite negative effect on ecological environment

As for land use change, the vegetation coverage rate of the study area is higher as a whole, reaching more than 60%. In 2017, compared with 2013, forest land and farmland declined obviously, while construction land and unused land have a large increase. This shows that with the advancement of urbanization, the land use in the Dazhangxi River Basin has changed significantly. The land use inclines to the construction land, and some forest land and farmland have changed into urban construction land. This phenomenon also damaged ecological environment to some extent.

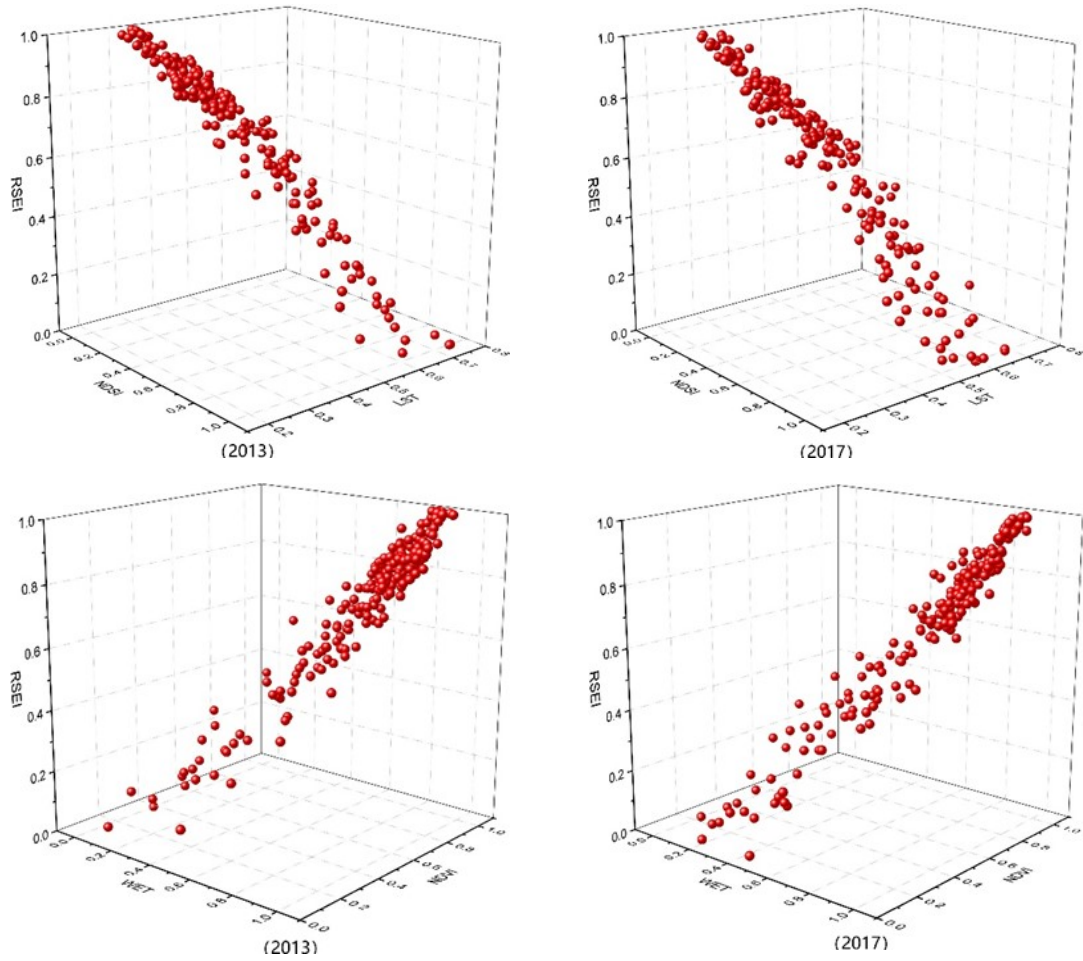


Fig. 17. Relationship between RSEI and variables

The NPP of the study area decreased in 2017, and the decreasing area was mainly forest land type. There is a high spatial correlation between the unchangeable area and the low biomass area, which is mainly caused by the water body in the low biomass area. The increasing areas are scattered in forest, especially in the East and West of the basin. This is mainly caused by the improvement of human intervention and the comprehensive utilization of Longxiang reservoir from power generation to water supply, taking into account power generation and other comprehensive utilization.

From the analysis of RSEI, compared with 2013, the area of excellent ecological area decreased significantly, the area of medium ecological area increased, and the area of poor ecological area decreased. This shows that in the process of these years, the areas with good ecological environment have been damaged to a certain extent, and the areas with serious ecological environment have been improved to a certain extent, making the ecological situation in 2017 mostly in the middle level.

Combined with the above analysis, from 2013 to 2017, the ecological environment of Dazhangxi Basin showed a slight deterioration trend, but due to human intervention, it has been improved to a certain extent in the later stage. Ecological environment plays an important role in people's quality of life. While planning urban construction, the local government should pay attention to the local conditions. At the same time, it should pay attention to the problems of urban expansion and forest land protection, avoid excessive concentration of heat island effect, so as to ensure the normal and balanced development of the region. In addition, the Dazhangxi basin is responsible for water supply, power generation, shipping and other important social functions in Fuzhou. Therefore, it is necessary to focus on measures such as increasing awareness of environmental protec-

tion, paying attention to ecological balance and reducing pollution emissions for urban construction land along the Bank of Dazhangxi. For the unreasonable and inefficient power station, we should make a comprehensive plan and change its main functions, so as to improve the ecological environment of the region and inject inexhaustible power into the sustainable development of the ecological environment in this area.

Conclusion and Recommendation

Through the combination of multi-source remote sensing data and a large number of field measured data, this work comprehensively evaluates the ecological environment of the study area from four aspects: thermal environment, LULC, NPP and RSEI, which provides certain reference and auxiliary decision-making basis for relevant government departments in planning and governance.

From four aspects, the ecological environment of Dazhangxi River Basin has been damaged in 2013-2017, but it has been improved in the later stage due to human intervention. Therefore, compared with 2013, the excellent ecological area and poor ecological area in 2017 have decreased, while the ecological area in the middle level has increased to a certain extent. In the reduced area, the land use mainly comes from forest land, and the ecological environment around the power station has been compensated and improved. According to the current ecological environment of the study area, the following suggestions are put forward: 1) When planning urban construction, the government should pay attention to local conditions and speed up appropriately, avoid excessive concentration of heat island effect, and ensure the balance of regional development trend. 2) The unreasonable and inefficient power stations in the basin should be comprehensively planned to change their main functions and improve the ecological environment.

Although this paper quantitatively evaluated the ecological environment of the study area from many aspects, there are still many factors that affect the ecological environment do not consider, such as soil terrain factors, biological resources, etc. (Chang et al., 2019). The evaluation of this study is to evaluate the ecological environment from every single aspect, but not form a comprehensive index. The future research can combine the local characteristics, comprehensively consider the factors affecting the ecological environment, and create an integrated framework, so as to make a more comprehensive and accurate evaluation of the study area. Because of its special function orientation of power supply and transportation, the ecological environment of Dazhangxi basin is inevitably disturbed by human beings. In the future, human factors can also be quantified as an indicator to evaluate the ecological environment more accurately.

The paper was supported by EU Erasmus+ project “GIS and Remote Sensing for Sustainable Forestry and Ecology (SUFOGIS)” (598838-EPP-1-2018-EL-EPPKA2-CBHE-JP), “Innovation on Remote Sensing Education and Learning (IRSEL)” (586037-EPP-1-2017-1-HU-EPPKA2-CBHE-JP”, and Chinese MOST international cooperation program “Using geospatial technology to monitor and assess the impact of land use / land cover change on Regional Ecological Security”(2018YFE0184300).

The European Commission support for the production of this publication does not constitute an endorsement of the contents which reflects the views only of the authors, and the Commission cannot be held responsible for any use which may be made of the information contained therein.

References

1. Almeida T.A. das N., Cruz L., Barata E., García-Sánchez I. M. Economic growth and environmental impacts: An analysis based on a composite index of environmental damage. *Ecological Indicators*, **2017**, 76, 119-130. <https://doi.org/10.1016/j.ecolind.2016.12.028>.
2. Chai L.H., Lha D. A new approach of deriving indicators and comprehensive measure for ecological environmental quality assessment. *Ecological Indicators*, **2018**, 85, 716-728. <https://doi.org/10.1016/j.ecolind.2017.11.039>.

3. Chang Y., Hou K., Wu Y., Li X., Zhang J. A conceptual framework for establishing the index system of ecological environment evaluation – A case study of the upper Hanjiang River, China. *Ecological Indicators*, **2019**, 107. <https://doi.org/10.1016/j.ecolind.2019.105568>
4. Chi Y., Zheng W., Shi H., Sun J., Fu Z. Spatial heterogeneity of estuarine wetland ecosystem health influenced by complex natural and anthropogenic factors. *Science of the Total Environment*, **2018**, 634, 1445-1462 <https://doi.org/10.1016/j.scitotenv.2018.04.085>
5. Fujian Water Resources and Hydropower Institute. Comprehensive Planning of Fujian D Zhangxi Basin Report, 2014, China.
6. Gupta K, Kumar P, Pathan S.K., Sharma K.P. Urban neighborhood green index - A measure of green spaces in urban areas. *Landscape and Urban Planning*, **2012**, 105, 325–335.
7. <https://doi.org/10.1007/s11434-006-0457-1> (in Chinese)
8. <https://doi.org/10.1016/j.landurbplan.2012.01.003>
9. Jing Y., Zhang F., He Y., Kung H. te., Johnson V. C., Arikena M. Assessment of spatial and temporal variation of ecological environment quality in Ebinur Lake Wetland National Nature Reserve, Xinjiang, China. *Ecological Indicators*, **2020**, 110. 105874 <https://doi.org/10.1016/j.ecolind.2019.105874>
10. Kurbanov E.A. Two decades of vegetation cover research with the use of MODIS. *Forest ecosystems under climate change: biological productivity and remote sensing*, **2016**, 2, 123-132 (in Russian).
11. Kurbanov E.A., Vorobyev O.N., Gubayev A.V., Lezhnin S.A., Polevshikova Y.A., Demisheva E.N. Four decades of forest research with the use of Landsat Images. *Vestnik of Volga State University of Technology. Ser. Forest Ecology. Nature Management*. **2014**, 21, 18-32 (in Russian).
12. Li W., Yi P., Zhang D., Zhou Y. Assessment of coordinated development between social economy and ecological environment: Case study of resource-based cities in Northeastern China. *Sustainable Cities and Society*, **2020**, 59. <https://doi.org/10.1016/j.scs.2020.102208>
13. Liu Q., Wu J., Li L., Yu L., Li J., Xin X., et al. Ecological environment monitoring for sustainable development goals in the Belt and Road region. *Journal of Remote Sensing (Chinese)*, **2018**, 22, <https://doi.org/10.11834/jrs.20187264>
14. Liu R, Zhu D.L. Discussion on land use change information mining method based on transfer matrix. *Resource science*, **2010**, 32, 1544-1550 (in Chinese).
15. Luo L. Simulation of net primary productivity (NPP) of Western Songnen grassland based on remote sensing mechanism model. Changchun: Northeast Institute of geography and agricultural ecology, Chinese Academy of Sciences, 2010. (in Chinese)
16. Meng Y., Zhao G.X. Ecological environment condition evaluation of estuarine area based on quantitative remote sensing - a case study in Kenli County. *China Environmental Science*, **2009**, 29, 163–167. (in Chinese)
17. Miao C.L., Sun L.Y., Yang L. The studies of ecological environmental quality assessment in Anhui Province based on ecological footprint. *Ecological Indicators*, **2016**, 60, 879-883 <https://doi.org/10.1016/j.ecolind.2015.08.040>
18. Niu Y.Q., Wang S.L. Research on coupling relationship between fragile ecological environment and poverty in Gansu province. *Acta Ecologica Sinica*, **2017**, 37, 6431–6439 (in Chinese).
19. Ostrom E. A general framework for analyzing sustainability of social-ecological systems. *Science*, **2009**, 325, 419-422. <https://doi.org/10.1126/science.1172133>
20. State Environmental Protection Administration. Environmental protection industry standard (Trial) HJT192-2006. (in Chinese)
21. Thornthwaite C.W. An approach toward a rational classification of climate. *Geographical Review*, **1948**, 38: 55-94. DOI:10.2307/210739
22. Vorobyev O.N., Kurbanov E.A., Gubayev A.V., Demisheva E.N. Method of stepwise classification of satellite images for the thematic mapping of forest cover. *Vestnik of Volga State University of Technology. Ser. Forest Ecology. Nature Management*. **2015**, 28, 57-72 (in Russian).
23. Wang C., Jiang Q., Shao Y., Sun S., Xiao L., Guo J. Ecological environment assessment based on land use simulation: A case study in the Heihe River Basin. *Science of the Total Environment*, **2019**, 697. <https://doi.org/10.1016/j.scitotenv.2019.133928>
24. Wang C., Yue T., Fan Z. Solar Radiation Climatology Calculation in China. *Journal of Resources and Ecology*, **2014**, 5, 132-138. DOI:10.5814/j.issn.1674-764x.2014.02.005
25. Wang J., Sui L., Yang X., Wang Z., Ge D., Kang J., et al. Economic globalization impacts on the ecological environment of inland developing countries: A case study of Laos from the perspective of the land use/cover change. *Sustainability (Switzerland)*, **2019**, 11, 3940 <https://doi.org/10.3390/su11143940>
26. Xu H.Q. A new remote sensing index for fast extraction of impervious surface. *Journal of Wuhan University: Information Science Edition*, **2008**, 33, 1150-1153 (in Chinese)
27. Xu H.Q. Extraction of water information by improved normalized difference water index (MNDWI). *Acta remote sensing*, **2005**, 5, 589-595 (in Chinese)
28. Xu H.Q. A remote sensing urban ecological index and its application. *Acta Ecologica Sinica*, **2013**, 33, 7853-7862. (in Chinese)
29. Zhang T.Y., Wang L., Wang H., Peng L., Luo C. Remote sensing monitoring of ecological environment in salinized irrigation areas of Manas river basin. *Acta Ecologica Sinica*, **2017**, 37, 3009–3018 (in Chinese)
30. Zhang Y., Song W., Fu S., Yang D. Decoupling of land use intensity and ecological environment in Gansu province, China. *Sustainability (Switzerland)*, **2020**, 12, 2779 <https://doi.org/10.3390/su12072779>

31. Zheng J., Hu Y., Boldanov T., Bazarzhapov T., Meng D., Li Y., et al. Comprehensive assessment of the coupling coordination degree between urbanization and ecological environment in the Siberian and Far East Federal Districts, Russia from 2005 to 2017. *PeerJ-Life and Environment*, **2020**, 6. <https://doi.org/10.7717/peerj.9125>
32. Zhou G.S, Zhang X.S. Net primary productivity of natural vegetation in China under global climate change. *Acta phytoecology*, **1996**, 1, 11-19 (in Chinese)
33. Zhou G.S, Zhang X.S. Preliminary study on net primary productivity model of natural vegetation. *Acta phytoecology*, **1995**, 3, 193-200 (in Chinese)
34. Zhu J.W., Xie X.T., Xin H.L. Research on evaluation of ecological environment carrying capacity - taking HeNan province as an example. *Acta Ecologica Sinica*, **2017**, 37, 1-9 (in Chinese)
35. Zhu W.Q., Pan Y.Z., He H, Yu D.Y., Hu H-B. Simulation of maximum light use efficiency for some typical vegetation types in China. *Chinese Science Bulletin*, **2006**, 51, 457-463.

АНАЛИТИЧЕСКИЙ ОБЗОР ПУБЛИКАЦИЙ В ОБЛАСТИ ПРИМЕНЕНИЯ ДЗЗ И ГИС ДЛЯ ОЦЕНКИ ДИНАМИКИ РАСТИТЕЛЬНОГО ПОКРОВА

Э.А. Курбанов, С.А. Лежнин, О.Н. Воробьёв, С.А. Меньшиков, Д.М. Дергунов,
И. Ван, Л.В. Тарасова, Л.Н. Смирнова
Поволжский государственный технологический университет

В ближайшие годы прогнозируется усиление роли геопространственных данных и ДЗЗ в решении вопросов мониторинга окружающей среды, оценке растительного (лесного) покрова и предотвращения экологических бедствий. Понимание тенденций развития этих направлений в условиях меняющегося климата позволит совершенствовать подходы к устойчивому управлению лесами. Авторами проведён аналитический обзор научных статей, посвященных использованию ДЗЗ и ГИС для оценки изменений наземного покрова на международном уровне в период между 2000 и 2020 гг. Рассмотренные исследования были сгруппированы по пяти направлениям: 1) проблема изменения климата и нарушения лесных экосистем; 2) мониторинг и оценка фрагментированности растительного (лесного) покрова; 3) урбанизация и городские леса (зелёная инфраструктура); 4) оценка глобальных и региональных запасов углерода; 5) оценка влияния на изменения наземного покрова комплекса различных факторов. Выявлено, что дистанционный мониторинг растительного (лесного) покрова в мире проводится в рамках международных программ во многих странах. В последние годы такие исследования широко практикуются в быстро развивающихся странах юго-восточной Азии, имеющих свою специфику управления природными ресурсами, соответствующие экологические проблемы и возможности валидации тематических карт наземными данными. Результаты исследования также показывают устойчивый рост точности и детальности разрабатываемых тематических карт на основе повышения пространственного разрешения спутниковых изображений и ГИС технологий. Это в свою очередь увеличивает точность прогнозов и моделей динамики растительного (лесного) покрова с учётом воздействия на него комплекса природных и антропогенных факторов. В заключение подчёркивается важность совершенствования и дальнейшего использования данных ДЗЗ и ГИС для решения глобальных и региональных задач в области мониторинга растительного (лесного) покрова.

Ключевые слова: ГИС, ДЗЗ, спутниковые изображения, лес, LUCS, изменение климата, российские и зарубежные исследования.

APPLICATIONS OF REMOTE SENSING AND GIS FOR ESTIMATION OF LAND USE / COVER CHANGE: A REVIEW

E.A. Kurbanov, S.A. Lezhnin, O.N. Vorobev, S.A. Menshikov, D.M. Dergunov,
Y. Wang, L.V. Tarasova, L.N. Smirnova
Volga State University of Technology

In the coming years, it is expected that the role of geospatial data and remote sensing will increase in resolving problems of monitoring of environment, estimation of the vegetation (forest) cover and preventing ecological disasters. Understanding the development trends of these areas in the conditions of climate change will increase approaches to sustainable forest management. The study provides an analytical review of research articles related to the use of remote sensing and GIS in the field of Land Use / Cover Change (LUCS) worldwide between 2000 and 2020. The research overview was grouped in five areas: 1) the problem of climate change and disturbance of forest ecosystems; 2) monitoring and assessment of fragmentation of vegetation (forest) cover; 3) urbanization and urban forests (green infrastructure); 4) estimation of global and regional carbon stocks; 5) assessment of the impact of various factors on the LUCS. The review reveals that remote sensing of vegetation (forest) cover in the world is carried out in many countries of the world within the framework of international programs. In recent years, such studies have been widely practiced in the rapidly developing countries of Southeast Asia, having their own specifics of nature management, environmental problems and the possibility of validating thematic maps with ground data. The overview also shows a stable increase in the accuracy and detail of the developed thematic maps based on the increased spatial resolution of satellite images and the use of GIS technologies. This, in turn, leads to the accuracy of predictions and models of the vegetation (forest) cover dynamics, taking into account the

impact of a complex of natural and anthropogenic factors. In conclusion, the importance of improving and further use of remote sensing and GIS data for solving global and regional problems in the field of monitoring of vegetation (forest) cover is emphasized.

Key words: *GIS, remote sensing, satellite images, forest, LUCC, climate change.*

Введение

Исследование проблем изменения землепользования и наземного покрова (LUCC – *англ.* Land Use / Cover Change), которое неизбежно происходит в связи с природными явлениями и хозяйственной деятельностью человека, в последние десятилетия проводится учёными во всём мире. Проект LUCC был запущен в 1994 году в рамках международной программы геосферы-биосферы (IGBP – *англ.* International Geosphere-Biosphere Programme), посвящённой феномену глобальных изменений во взаимодействии с человеческими системами (IGBP). После завершения программы IGBP в 2015 г. исследования в области LUCC продолжились в 2016 году в рамках программы «Глобальная земельная программа» После завершения программы IGBP в 2015 году исследования в области LUCC продолжились в 2016 году в рамках программы «Глобальная земельная программа» (GLP – *англ.* Global Land Programme) (Global land...). Считается, что LUCC оказывает значительное влияние на различные экологические, экономические и социальные процессы в мировом масштабе (Chen et al., 2020; Lai et al., 2016). Эти процессы приводят к вырубке лесных насаждений, деградации растительного покрова, стихийным бедствиям, утрате биоразнообразия, потере уникальных экосистем и нарушению глобального баланса атмосферного углерода (Pan et al., 2011; Cohen et al., 2016; Knott et al., 2019).

В российской научной литературе при оценках растительного покрова и динамики ландшафтов обычно используют такие понятия, как «наземный покров», «подстилающая поверхность», «ландшафтный покров» и т.п. (Черных и др., 2018). Для понимания (прогнозирования) тенденций и принятия решений по управлению LUCC требуются крупномасштабные периодические наблюдения за экономической деятельностью человека и состоянием растительного покрова на региональном и глобальном уровнях (Yang, Lo, 2002; Барталев и др., 2005; Li, Qu, 2018). Традиционные методы сбора данных (картографирование и наземная съёмка) для подобных задач являются трудозатратными, занимают много времени и требуют значительных средств. Поэтому для анализа геопространственных данных в области LUCC находят широкое применение изображения дистанционного зондирования Земли (ДЗЗ) и технологии ГИС (геоинформационные системы), которые обеспечивают актуальное, своевременное и реалистичное представление наземного покрова (Лупян и др., 2011; Курбанов и др., 2014; Moulds et al., 2018). Эти технологии на сегодняшний день являются наиболее эффективными инструментами наблюдения за изменениями наземного покрова благодаря возможности быстрого и оперативного получения изображений в широком диапазоне электромагнитного спектра (Елсаков, 2012; Taubert et al., 2018; Im, 2020).

Исследования и разработки в области LUCC с применением данных ДЗЗ и ГИС выполняются во всём мире по различным тематическим направлениям. Значительная часть таких работ приходится на оценку и мониторинг растительного (лесного) покрова.

Целью работы является обзор научных исследований LUCC в области оценки растительного покрова с помощью ДЗЗ и ГИС технологий и выявление основных научно-практических направлений их применения при мониторинге лесов на региональном и национальном уровнях.

Материалы и методика исследований

В работе анализировались зарубежные и отечественные научные публикации по теме исследования за период с 2000 по 2020 год. Для поиска литературных источников на английском языке была использована международная наукометрическая база данных Scopus. Публикации на русском языке по тематике исследования были найдены в российской научной электронной библиотеке elibrary.ru. Для подборки публикаций использованы следующие ключевые слова: LUCC, forest (лес), GIS (ГИС) и remote sensing (дистанционное зондирование). Литературные источники, рассматриваемые в этом исследовании, включали опубликованные статьи, материалы конференций и главы книг.

Первоначально в базе данных Scopus было найдено 1127, а в российском сегменте 348 публикаций, имеющих отношение к рассматриваемой проблеме. Статьи, в названии, ключевых словах и аннотации которых не было условий поиска, в дальнейшем были удалены из списка. После уточнения подобранных статей, включённых в аналитический обзор и затрагивающих непосредственно тему LUCC и растительного (лесного) покрова, для анализа было оставлено 209 публикаций, из которых 32 были выявлены в российской базе данных elibrary. Ссылки на используемые источники включают 106 публикаций.

Результаты

Анализ литературных источников по теме использования ГИС и ДЗЗ для оценки LUCC позволил систематизировать существующие работы в несколько тематических направлений, которые за последние два десятилетия были актуальны для отечественных и зарубежных исследователей.

Исследование показало, что значительная часть работ в области LUCC связана с *проблемой изменения климата и нарушенности лесных экосистем*. Обобщение последних полученных результатов в этой области способствует развитию концепций устойчивого управления лесами и устойчивого развития (Cao et al., 2020). Характеристика взаимодействий ландшафта (растительного покрова) и изменения климата (например, влияния на местные и региональные климатические процессы, подходы к смягчению последствий изменения климата и адаптации) стала одной из главных задач ландшафтной экологии (Wu, 2013).

Влияние снижения площадей лесов на температуру атмосферы в значительной степени зависит от географической широты ландшафта (местности). В частности, было установлено, что вырубка лесов вызывает похолодание в высоких широтах из-за увеличения альбедо поверхности, в то время как прогнозируемое потепление в результате снижения суммарного испарения будет наблюдаться в регионах низких широт (Bonan, 2008; Tölle et al., 2017). Сведение лесов в средних широтах Европы не повлияло на летнюю температуру атмосферы, в то время как зимняя температура снизилась на 1,5 °C (Broucke et al., 2015). Геопространственные данные LUCC провинции Хэйлунцзян (КНР) за 1900-2010 гг. показали, что существует значительная корреляция между переводом лесных насаждений, общая площадь которых снизилась за исследуемый период на 28 %, под сельскохозяйственные угодья, и индексами экстремальных температур атмосферы (Zhang et al., 2017). Положительные корреляции также наблюдаются между уменьшением площади лесов этой провинции, более частым возникновением экстремально высоких температур и повышением максимального значения дневной минимальной температуры.

Результаты анализа LUCC в пойме долины Киломберо (Танзании) за период 1990-2016 гг. по снимкам Landsat и с использованием принятых глобальных коэффициентов стоимости и модифицированных локальных коэффициентов стоимости экосистемных услуг (ESV - ecosystem services values) показали снижение показателей ESV лесов, кустарников, водно-

болотных угодий и воды (Msofe et al., 2020). Это привело к общей потере 811,5 млн долларов США (26,6 %) в ESV за последние 26 лет при расчётах с модифицированным коэффициентом локального значения и до 3000,7 млн долларов США (42,3 %) при расчёте с использованием глобальных коэффициентов.

Для оценки мангровых лесов 10 стран юго-восточной Азии, которые уязвимы к процессам LUCC, был проведён корреляционный анализ между данными MODIS и динамикой площадей этих экосистем за 2000-2012 гг. Исследование показало, что 22,64 % общей вырубленной площади мангровых лесов было преобразовано под сельское хозяйство, 5,85 % – под аквакультуру, 0,69 % – под инфраструктуру, а 16,35% осталось под влиянием других сфер деятельности человека (Fauzi et al., 2019).

Исследование сукцессионной динамики бореальных лесов, режимов нарушений (пожары) и их реакции на изменение климата проведено на примере бассейна реки Юкон (США и Канада). Авторами была смоделирована настоящая (за 2000-2008 гг.) и прогнозируемая продуктивность (NDVI) в ненарушенных насаждениях на основе различных источников абиотических данных, а также созданы модели сплайновой регрессии и меняющегося климата. Результаты показали, что максимальная аномалия экосистемы наступает через 30-40 лет после пожара, а лиственные древостои обычно имеют более высокий этот показатель, чем хвойные (Wylie et al., 2014).

Считается, что изменение климата влияет на продуктивность и распространение лесных насаждений (Beck, Goetz, 2012). Тем не менее, степень и скорость этого воздействия на общую долгосрочную продуктивность бореальных лесов остаются неопределёнными. Прогнозируется, что лиственные породы бореального пояса более позитивно будут реагировать на изменение климата (Johnstone et al., 2010), чем бореальные хвойные породы, и, вероятно, их ареал станет распространяться в более теплом направлении (Wolken et al., 2011; Им и др., 2020; Зуев и др., 2019). В то же время отмечается, что уровень воздействия климатических изменений на растительный покров тундр Западной Сибири уже является критическим (Титкова, Виноградова, 2015). В лесостепной зоне Центрального Черноземья России доля нарушенных хвойных лесов выросла с 1985 по 2018 гг. в 9 раз, а в лиственных лесах доля нарушенных участков увеличилась незначительно (Терехин, 2020).

Непосредственное отношение к процессам LUCC имеют работы *по мониторингу и оценке фрагментированности растительного (лесного) покрова*. Фрагментация и деградация лесов, вызванные LUCC, могут иметь негативные влияния на экологические системы в пространственных масштабах (Sharma, Roy, 2007; Riutta et al., 2014). Группой учёных были идентифицированы примерно 130 миллионов фрагментов лесных насаждений в трёх тропических и субтропических регионах (Центральная Америка, Африка, Азия и Австралия), которые обладали приблизительно схожими размерами, периметрами и фрактальной структурой (Taubert et al., 2018) (рис. 1). Прогнозные модели данного исследования показывают, что в течение 50 лет дополнительная потеря леса приведёт к значительному увеличению общего количества фрагментированных участков леса, а также к уменьшению их размеров, и что эти последствия могут быть частично смягчены за счёт лесовозобновления и охраны лесов.

Индийскими учёными была получена динамика долгосрочных изменений лесного покрова и его пространственно-временной структуры на основе анализа набора топографических карт (1930-е гг.) и наборов спутниковых изображений Landsat MSS (1975 и 1985 гг.), IRS 1B LISS-I (1995 г.), IRS P6 AWiFS (2005 г.) и Resourcesat-2. Исследование показало, что за рассматриваемый период в горных восточных Гатах Индии наблюдается существенное снижение площади больших участков леса (Reddy et al., 2016). Общее количество участков леса в

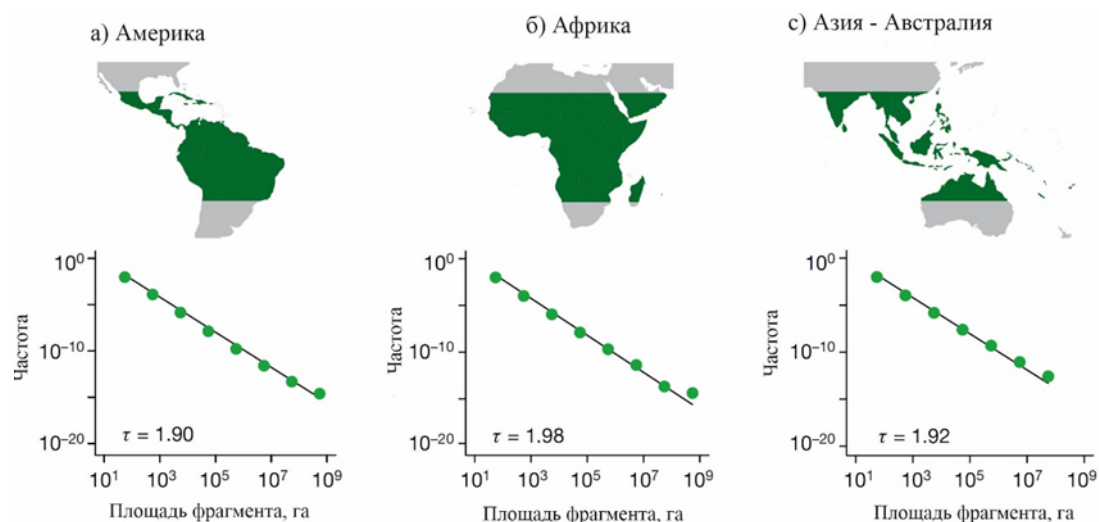


Рис. 1. Распределение фрагментов тропических и субтропических лесов в континентальном масштабе по площади: а) для Северной и Южной Америки ($n = 55,5$ млн фрагментов); б) Африки ($n = 44,8$ млн фрагментов); в) Азии и Австралии ($n = 30,5$ млн фрагментов). Сплошными линиями показаны аппроксимации степенных распределений с показателем τ . На картах приведена вся территория тропического пояса, а выбранные тропические регионы отмечены зелёным цветом (Taubert et al., 2018).

этом регионе увеличилось с 2688 (1930 г.) до 13009 (2013 г.). Самый большой участок леса в 1930 году имел площадь 41669 км², которая к 2013 году сократилась до 27800 км². Согласно пространственному анализу, наряду с вырубкой лесов свой вклад в фрагментированность лесов вносят сельское хозяйство, деградация кустарников и фруктовые плантации.

Подобные же результаты получены для гималайских лесов Индии, которые были подвержены антропогенной деятельности в связи с экономическим развитием (Lele et al., 2008; Chakraborty et al., 2017; Sahana et al., 2018). Исследователи при оценке фрагментации обычно используют статистические модели, описывающие пространственную взаимосвязь между вырубкой лесов и другими факторами в среде ГИС (Kumar et al., 2007; Wang et al., 2013). Для этого применяются различные модели: множественной линейной регрессии (Culas, 2007; Freitas et al., 2010), логистической регрессии (Echeverria et al., 2008) или географически взвешенной регрессии (Pineda et al., 2010).

Для характеристики процессов фрагментации растительного покрова исследователи также применяют модель фрагментации Рииттерса (Riitters et al., 2000), которая широко адаптирована для оценки лесов с использованием различных спутниковых карт лесного покрова на глобальном (Riitters et al., 2016; Wade et al., 2003), национальном (Li et al., 2011; Wickham et al., 2010; Yemshanov et al., 2015) и региональном уровнях (Dong et al., 2014). Модель основана на классификации лесного покрова на фрагментированные участки в зависимости от количества лесных пикселей (доля пикселей с лесом, окружённых пикселями, не относящимися к лесу) и лесных пикселей, расположенных внутри лесного массива. Эти типы фрагментированных участков классифицируются в соответствии со значениями P_f и P_{ff} ландшафте, окружающем этот пиксель. В результате классификации соответствующего участка

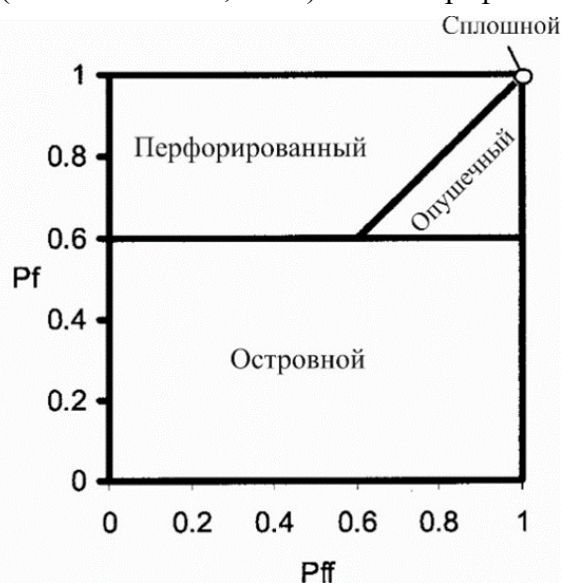


Рис. 2. Модель, используемая для характеристики компонентов фрагментации леса. P_f и P_{ff} характеризуют густоту и соседство (смежность, связанность) лесов для соответствующей площади ландшафта (Riitters et al., 2002)

спутникового снимка пикселям присваиваются четыре типа фрагментации: «сплошной» (англ. core), «перфорированный» или «лес с полянами» (perforated), «опушечный» (edge), «островной» (patch) (рис. 2).

Следующим направлением, которому посвящено много публикаций, является *оценка LUCC в связи с урбанизацией и городскими лесами (зелёная инфраструктура)*. Стремительная урбанизация в мире вызывает серьёзную тревогу, особенно в развивающихся странах, что вызвано в основном несанкционированной и незапланированной застройкой окраин городов (Farooq, Ahmad, 2008; Ghosh, 2019). Это также приводит к резкому изменению ландшафта и экологическим проблемам.

Для дешифрирования городских земель и выделения их от других классов наземного покрова китайскими учёными предлагаются различные индексы, такие как нормализованный разностный индекс непроницаемой поверхности (MNDISI – Normalized Difference Impervious Surface Index) (Liu et al., 2013), биофизический композиционный индекс (Biophysical Composition Index) (Deng, Wu, 2012), нормализованный разностный городской индекс (NDUI – Normalized Difference Urban Index) (Zhang et al., 2015), нормализованный разностный индекс застроенности (NDBI - Normalized Difference Built-up Index) (Zha et al., 2003; Статакис и др., 2012) и нормализованный разностный индекс открытых участков (NDBaI – Normalized Difference Bareness Index (Li, Chen, 2014). В частности, индекс MNDISI используется для классификации на снимках городских территорий по комбинированным данным температуры наземной поверхности Landsat и изображений высокого пространственного разрешения ночного освещения городов, получаемых с Международной космической станции (Liu et al., 2013). Для исследований в области LUCC городских территорий также находят применение ландшафтные показатели, на основе которых определяется индекс изменения ландшафта (Landscape change index). Этот индекс обычно используется для оценки изменений за разные периоды времени (Liu, Yang, 2015).

Среди многих полезных индексов, интерпретирующих взаимосвязь между LUCC городов и глобальным изменением климата, наиболее используемым является индекс «тепловой остров города» (UHI – Urban Heat Island), который тесно связан с качеством воздуха (Civerolo et al., 2007; Han et al., 2009; Cho, Choi, 2014), потреблением энергии (Kolokotroni et al., 2006; Santamouris et al., 2001) и риском для здоровья населения (Johnson et al., 2012; Rinner et al., 2010). Для оценки UHI успешное применение находят сканерные данные теплового инфракрасного канала (TIR – Thermal Infrared) с различным пространственным разрешением, включая AVHRR (8 км), MODIS (1 км), HJ-1 B (300 м), Landsat TM (120 м), ASTER (90 м) и Landsat ETM+ (60 м) благодаря их низкой стоимости и временному разрешению (Jusuf et al., 2007; Hao et al., 2016; Kitsara et al., 2018).

Chen и др. (2006) предложили оценивать взаимосвязь между UHI и LUCC по зависимости температуры от нормализованного разностного водного индекса (NDWI), NDBaI (для включения показателя открытых участков), нормализованного разностного вегетационного индекса (NDVI) и нормализованного разностного индекса застроенности (NDBI). Было установлено, что при ограниченных значениях NDVI (<0) корреляции между индексами NDVI, NDWI, NDBaI и температурой отрицательны, в то время как между NDBI и температурой наблюдается положительная корреляция.

Китайскими учёными на основе временных рядов изображений спутников Landsat TM/ETM+ и демографических данных по городу Шанхай за 1997 и 2008 годы была проведена количественная оценка взаимосвязи между LUCC и миграцией населения и их влиянием на пространственно-временные модели UHI с использованием комплексного подхода ДЗЗ, ГИС и статистического анализа (Zhang et al. 2013). Результаты показали, что за исследуе-

мый период произошло расширение городской площади на 219,50 %, примерно 72,52 % из которых были в прошлом пахотными землями (24,79 %), залежами (21,21 %), лесными насаждениями и кустарниками (18,97 %), открытыми участками (6,62 %) и водоёмами (0,93 %). Такие изменения в LUCC и увеличение городского населения привели к значительным изменениям в пространственно-временных моделях UHI на территории Шанхая из-за потери водоёмов и покрытых растительностью земель (рис. 3).

Оценка LUCC с 1976 по 2003 годы была проведена в городской зоне Тирупати (Индия) с использованием топографической карты Survey of India 570/6 и ДЗЗ LISS III и PAN IRS ID 2003 г. (Mallupattu, Reddy, 2013). Сравнение LUCC за исследуемый период показывает, что наблюдается значительное увеличение площади городской застройки, городских лесов, плантаций и других земель.

Для другого индийского города Бхопал был проведён анализ LUCC за 1991-2016 годы по разновременным изображениям спутника Landsat (Ghosh, 2019). Результаты также свидетельствуют о том, что город пережил стремительное горизонтальное расширение. Площадь Бхопала увеличилась с 15,8 км² в 1991 году до 184,5 км² в 2016 году при средней скорости прироста 7 км² год⁻¹ с учётом пространственной диспропорции. Расширение застроенной площади в основном происходит за счёт сельскохозяйственных и лесных земель.

Для территории США была проведена оценка LUCC зелёной инфраструктуры на национальном уровне за период с 1992 по 2001 годы. Авторы предложили использовать морфологический пространственно-структурный анализ (morphological spatial pattern analysis) в качестве дополнительного способа составления тематической карты зелёной инфраструктуры по снимкам Landsat, расширения географического охвата и включения информации об LUCC (Wickham et al., 2010). В результате было идентифицировано более 100 хабов (большие площади растительности) и около 4000 крупных сетей (зелёные коридоры, соединяющие хабы) на территории США, из которых примерно 10 % пересекали границы штатов.

ДЗЗ и ГИС становятся основными инструментами *при оценках глобальных и региональных запасов углерода* в наземных экосистемах. Процессы LUCC, связанные с вырубкой и нарушениями в лесных насаждениях, вызывают эмиссию CO₂ и других парниковых газов, что вызывает широкое обсуждение в научном сообществе (Stocker et al., 2013; Nabuurs et al., 2013). В настоящее время имеются дан-

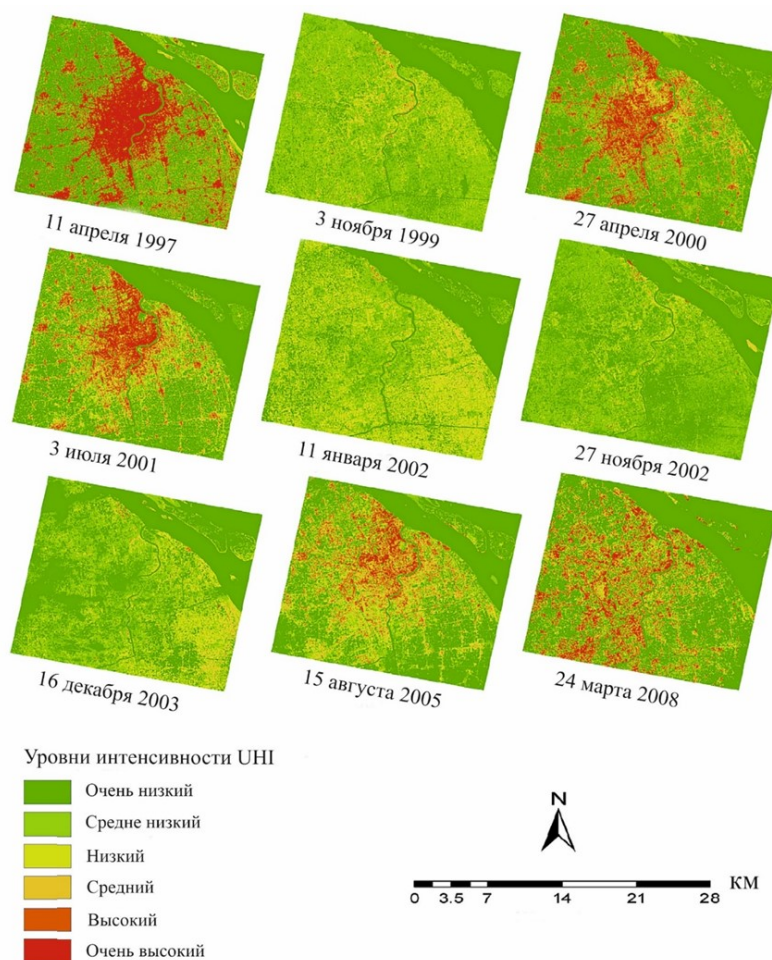


Рис. 3. Уровни интенсивности UHI (городской тепловой остров) г. Шанхай по разновременным спутниковым данным Landsat TM/ETM+ (H. Zhang et al., 2013)

ные о том, что в некоторых случаях фитомасса лесов в связи с изменением климата увеличивается, однако прямое или косвенное влияние экстремальных климатических явлений на этот процесс изучено недостаточно (Ruiz-Benito et al., 2014).

Парижское соглашение в рамках Рамочной конвенции ООН об изменении климата, принятое в 2015 году 195 странами, уделяет основное внимание ограничению повышения глобальной температуры до уровня менее 2 °C по сравнению с доиндустриальной эпохой (Парижские соглашения, 2015). Проблемы изменения климата заставили многие страны вернуться к вопросу инвентаризации национальных парниковых газов и запасов углерода в наземных экосистемах, в первую очередь в лесных насаждениях. Для этого страны участницы соглашения используют руководящие принципы Межправительственной группы экспертов по изменению климата (IPCC), которые строго придерживаются требований мониторинга пула углерода в результате процессов LUCC (IPCC, 2006).

При ретроспективных оценках пространственно-временной динамики запасов углерода в фитомассе лесов обычно используют разновременные спутниковые изображения Landsat (Galidaki et al., 2017; Барталев и др., 2009; Potter, 2013) и MODIS (Lunetta et al., 2006; Pouliot et al., 2014). В течение последних трёх десятилетий были разработаны различные методы обнаружения изменений в растительном (лесном) покрове с использованием спутниковых изображений, включая постклассификационное сравнение (post-classification comparison), дифференциацию изображений, анализ главных компонент (PCA – principal component analysis) и дифференцирование различных индексов растительности (Khatami et al., 2016; Lu et al., 2004; Nery et al., 2019). Общее повышение точности классификации карт LUCC представляет практический интерес с точки зрения их потенциального использования для моделирования изменений землепользования (Manandhar et al., 2009).

Для определения динамики фитомассы и связанных с LUCC потерь углерода лесными насаждениями в Национальном парке Маргаллах-Хиллз (Пакистан) были использованы мультиспектральные спутниковые изображения Landsat за 1990, 2000, 2010, 2017 годы и данные полевой инвентаризации, полученные путём случайной выборки данных по лесам за исследуемый период времени (Mannan et al., 2018). Исследование показало, что в результате LUCC за 27-летний период в атмосферу было эмитировано 154 ГгС (5,70 ГгС год⁻¹), что связано с антропогенными нарушениями древостоев в парке.

В последние десятилетия в Китае произошли существенные изменения в LUCC, которые во многом обусловлены его беспрецедентным экономическим развитием. Для анализа соответствующих изменений в депонировании С растительностью и почвой в период с 1990 по 2010 год были использованы разновременные данные Landsat (Lai et al., 2016). Результаты демонстрируют значительное сокращение площадей пастбищ (-6,85 %; $20,83 \times 10^6$ га) и увеличение площадей городов (+ 43,73 %; $6,87 \times 10^6$ га), сельхоз угодий (+ 0,84 %; $1,48 \times 10^6$ га) и лесов (+0,67 %; $1,52 \times 10^6$ га). Общий запас почвенного органического углерода сокращался примерно на 11,5 млн т С год⁻¹, тогда как в пуле биомассы депонировалось 13,2 млн т С год⁻¹. Большие потери углерода (примерно 101,8 млн т С год⁻¹) являются результатом неэффективного землепользования, включая лесные пожары и другие нарушения.

Для китайской провинции Чжэцзян проведён пространственно-временной анализ и выявлены закономерности выбросов углерода в период 1970-1990 и 1990-2010 гг., вызванных LUCC (Zhu et al., 2019). При исследовании были использованы цифровые карты землепользования провинции и спутниковые данные Landsat MSS/TM/ETM+. Результаты исследования показали последовательное сокращение площадей сельскохозяйственных угодий ($2,8 \times 10^5$ га или - 9,15 % и $5,9 \times 10^5$ га или - 20,49 %) и пастбищ ($3,4 \times 10^4$ га или -10,73 % и $1,5 \times 10^5$ га или - 54,1 %), а также устойчивое увеличение площади лесов ($2,0 \times 10^4$ га или 0,33 %

и $1,7 \times 10^5$ га или 2,81%) и городской застройки ($2,07 \times 10^5$ га или 78,41% и $6,49 \times 10^5$ га или 137,8%) (рис. 4). В провинции Чжэцзян с 1970 по 1990 год произошло сокращение примерно 8,3 млн т общего запаса углерода, включая в растительности на 0,4 млн т и органике почв на 7,9 млн. т. В то же время с 1990 по 2010 год произошло сокращение примерно 17,5 млн т накопленного С, что представляет собой баланс 2,8 млн т депонированного углерода растительностью и его снижение на 20,3 млн т С в почве.

Карта наземной биомассы (AGB - aboveground biomass) за 2008-2010 гг. была получена с разрешением 30 м для бореальных лесов в бассейне реки Юкон на Аляске с использованием данных Landsat и наземных измерений (Ji et al., 2015). Для этого авторами была разработана модель множественной регрессии, включающая полевые данные AGB, показатели спектральной яркости растительного покрова по изображениям Landsat и индексы растительности. При оценке региональной наземной плотности углерода (AGB) субальпийских лесов с умеренным климатом на северо-западе Китая были интегрированы данные лидарной съёмки и изображений Landsat (Du et al., 2015). Разработанная модель для крупномасштабных оценок объяснила 76 % дисперсии AGB лесов при систематической ошибке $27,9 \text{ т С га}^{-1}$. Для оценки и картирования запасов углерода в подзолах Амазонки также была применена комбинация изображений ДЗЗ (Shuttle Radar Topographic Mission (SRTM), Landsat 8 и полевые данные, что позволило точно выделить и классифицировать разные группы растительности с различным гидрологическим режимом почв (Pereira et al., 2015).

Испанские учёные использовали временные ряды изображений Landsat (1984-2009 гг.) для оценки изменений в биомассе лесов с преобладанием сосны центральной части Испании (Gómez et al., 2012). Для выявления изменений на уровне ландшафта и распределения лесов использовались методы объектно-ориентированного анализа. Результаты свидетельствуют, что общая площадь соснового леса за исследуемый 25-летний период увеличилась на 40 % – с 1211 км^2 до 1698 км^2 . Следуя логике процессов накопления углерода, наши результаты показывают, что это также ведёт к увеличению депонированных запасов углерода.

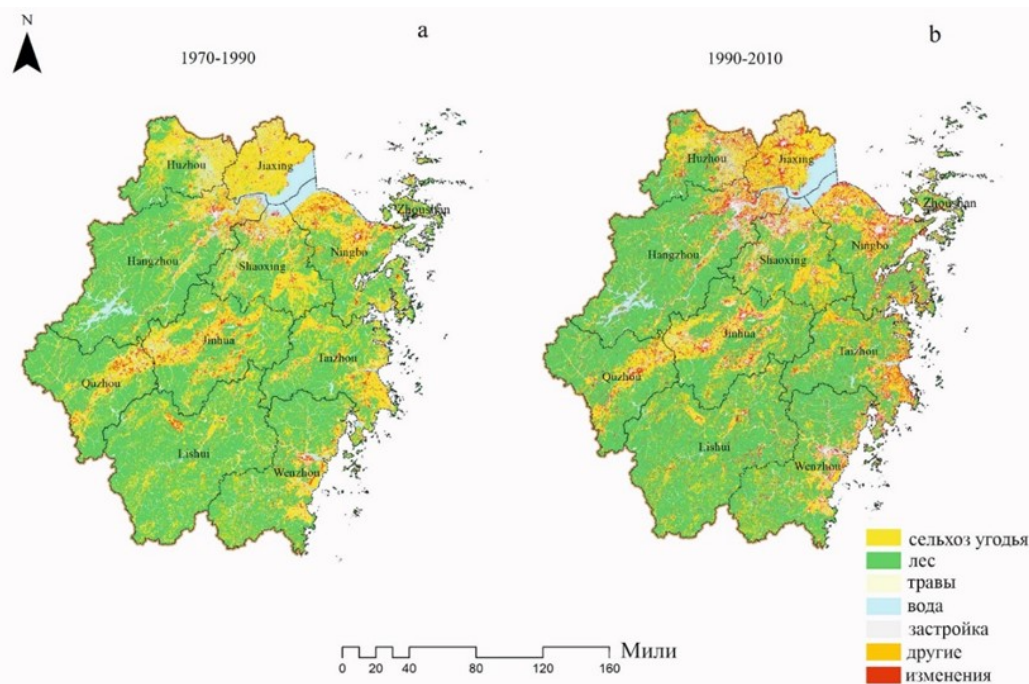


Рис. 4. Пространственное распределение LUCC в Чжэцзяне: а) с 1970 по 1990 г. и б) с 1990 по 2010 г. Красным цветом показаны площади, преобразованные в другой тип землепользования.

Ещё одним распространённым типом исследований является *оценка влияния на LUCC комплекса различных факторов*, имеющих внешние (востребованность на международ-

ных рынках, политика в области окружающей среды, международные соглашения и т.п.) или внутренние причины (рост населения, развитие инфраструктуры, рост экономики) (Bürgi et al., 2005). При использовании в этих исследованиях анализа «обнаружения изменений» ДЗЗ и ГИС способствуют включению таких важных факторов, как высота над уровнем моря, населённые пункты, удаленность от дорог и расстояние от рек (Nurda et al., 2020; Zhang et al., 2019). В большинстве таких случаев LUCC имеет отношение к вырубке лесов или переводу земель под другие виды пользования (Acheson, McCloskey, 2008).

На основании изображений Landsat (с 1979 по 2010 гг.) исследованы физические и социально-экономические факторы, влияющие на тенденции LUCC (лесные насаждения) в центральной Аргентине (Hoyos et al., 2018). Для этого была разработана ГИС с тематическими картами, показывающими различные движущие силы этих процессов, и проведён анализ РСА. Основной тенденцией сокращения площадей лесных насаждений в этом регионе явился перевод земель в сельское хозяйство.

Для национального уровня Индии разработана модель LUCC, основанная на данных инвентаризации всех её штатов и спутниковых изображений высокого разрешения за период с 1960 по 2010 год (Moulds et al., 2018). Пространственно-временная динамика LUCC с 1986 по 2014 год в бассейне верхнего течения реки Телис-Пирис (Бразильской Амазонии), проведённая на основе управляемой классификации изображений сенсоров ТМ (Thematic Mapper) Landsat 5 и TIRS (Thermal Infrared Sensor), показала наибольшие различия за период исследования для тематических классов «сельскохозяйственные угодья» и «тропический лес» (Zaiatz et al., 2018). На основе тематической классификации изображений Landsat за 1997, 2004 и 2011 годы методом «естественных границ» (natural breaks classification) были проанализированы LUCC и экологическая уязвимость региона Яньань (провинция Шэньси, КНР), придерживающегося политики возврата сельхозугодий в лесной фонд. В сочетании с данными о землепользовании, социально-экономическими показателями и состоянием природных ресурсов экологическая уязвимость территории Яньань оценивается с использованием модели пространственного анализа главных компонент (SPCA) (Hou et al., 2016).

Ретроспективный анализ динамики LUCC и её причин, проведённый с использованием спутниковых изображений Landsat 5 ТМ 1984, Landsat 5 ТМ 1999 и Landsat 8 ТМ 2015 для бассейна реки Бересса (Эфиопия), показал небольшое приращение площадей лесных насаждений с 1999 по 2015 год со скоростью $7,1 \text{ га год}^{-1}$, что в свою очередь связано с вовлечением местных сообществ в посадку деревьев вокруг усадеб и сельскохозяйственных ферм (Meshesha et al., 2016). Оценка динамики LUCC в Бенине с использованием карт CCI-LC (*англ.* Climate change initiative land cover) Европейского космического агентства (ESA) за 2001, 2008 и 2013 годы в программе QGIS позволили спрогнозировать на 2025 и 2037 годы темпы увеличения посевных площадей и лесов, а также значительное сокращение площади земель саванны (Guidigan et al., 2019). Классификация разновременных спутниковых изображений серии Landsat и метод «обнаружения изменений» (*англ.* change detection) использовались для картирования LUCC региона Замбези (Намибия) за период в двадцать шесть лет, разделённых на три этапа (1984-1991, 1991-2000 и 2000-2010). Исследование показало, что на процессы изменений лесного покрова в этом регионе влияют четыре пространственно-временных фактора: расстояние до ближайшей дороги, расстояние до населённых пунктов, плотность населения и сроки между пожарами (Kamwi et al., 2018).

Учёные из Иордании оценили пространственную динамику LUCC в бассейне реки Ярмук (Иордания) за 22 года (1987-2009) методами обнаружения изменений и по данным NDVI. Результаты анализа выявили радикальные изменения в снижении площадей лесов: на 14 % под сельскохозяйственные угодья и 2 % под городскую застройку (Obeidat et al., 2019). Исследование динамики LUCC с 1992 по 2018 год также показало уменьшение площадей

лесного покрова на территории северных Гималаев Кашмира (Индия) за счёт роста населения и экономического роста, расширения площадей под застройку поселений и садоводство (Fayaz et al., 2020).

По данным Landsat, Средиземноморские леса района Джабаль Ахдар (Ливия) потеряли за 32 года (1985-2017) в результате LUCC 39 % своей площади, при этом самый высокий процент сведения лесов наблюдался в период 2010-2017 гг (Alawamy et al., 2020). В Израиле на основе индекса NDVI, полученного по 14-летним временным рядам MODIS между 2000 и 2014 гг., установлено влияние на LUCC двух основных факторов - расширение сельскохозяйственных угодий и городов (Levin, 2016). Рост населения, урбанизация и расширение пахотных земель явились главными причинами сокращения лесных земель на 25 % в бассейне реки Аваш (Австралия) по данным спутниковых изображений Landsat с 1988 по 2018 гг. (Tadese et al., 2020). В Среднем Поволжье России за период 2001-2014 гг. по 5 основным классам наземного покрова тематических карт Landsat наблюдается снижение площади класса «лес» на 2,7 %, увеличение класса «кустарниково-древесной растительности» и класса «не покрытого растительностью» на 0,6 % (Курбанов и др., 2016). Существенное сокращение лесного покрова на 41 % с 1925 по 2012 год также наблюдалось в районе Идукки (округ в индийском штате Керала), что было вызвано затоплением земель в результате строительства гидроэлектростанции и вырубкой лесов (Ramachandran, Reddy, 2017).

Заключение и выводы

Анализ литературных источников показал высокий исследовательский интерес к проблеме LUCC и использованию технологий ДЗЗ и ГИС для решения задач по оценке динамики растительного покрова во всём мире. Основная часть научных публикаций по рассматриваемой тематике была найдена в англоязычных журналах, индексируемых в международной наукометрической базе данных Scopus.

Большинство российских научных коллективов проводят оценки динамики растительного (лесного) покрова в различных регионах страны методами ДЗЗ и ГИС без привязки к международным программам IGBP и GLP. Основанием для таких исследований в российских публикациях обычно служат федеральные целевые и государственные программы: «Исследования и разработки по приоритетным направлениям развития научно-технологического комплекса России на 2014-2020 годы», «Развитие науки и технологий на 2013-2020 годы», «Научно-технологическое развитие Российской Федерации».

При оценках LUCC учёными используется широкий спектр методических подходов, доступных спутниковых изображений и геопространственных моделей. Исследования также имеют разную направленность, в связи с этим мы выделили пять, на наш взгляд, имеющих непосредственное отношение к динамике растительного (лесного) покрова и экологическим проблемам современного мира. К таким направлениям исследований в области оценки LUCC нами были отнесены: 1) проблема изменения климата и нарушенности лесных экосистем; 2) мониторинг и оценка фрагментированности растительного (лесного) покрова; 3) урбанизация и городские леса (зелёная инфраструктура); 4) оценка глобальных и региональных запасов углерода; 5) оценка влияния на LUCC комплекса различных факторов.

Проведённый анализ литературных данных с начала 2000-х годов показывает устойчивый рост детальности исследований по тематике LUCC в связи с увеличением доступных для широкого круга пользователей геопространственных данных (спутники, БПЛА) и их разрешения.

В целом комплексное использование геопространственных данных с различным геопространственным и временным разрешением для мониторинга лесного покрова будет способ-

ствовать успешному решению вопросов устойчивого развития и снижению экологических рисков.

Исследование выполнено при финансовой поддержке РФФИ в рамках научного проекта № 19-55-80010\19

The European Commission support for the production of this publication does not constitute an endorsement of the contents which reflects the views only of the authors, and the Commission cannot be held responsible for any use which may be made of the information contained therein.

Библиографический список

1. Барталев С.А., Егоров В.А., Жарко В.О., Лупян Е.А., Плотников Д.Е., Хвостиков С.А. Состояние и перспективы развития методов спутникового картографирования растительного покрова России // Современные проблемы дистанционного зондирования Земли из космоса. 2015. Т. 12, № 5. С. 203-221.
2. Барталев С.А., Ховратович Т.С., Елсаков В.В. Использование спутниковых изображений для оценки потерь углерода лесными экосистемами в результате вырубок // Современные проблемы дистанционного зондирования Земли из космоса. 2009. Т. 2, № 6. С. 343-351.
3. Елсаков В.В. Спутниковая съёмка в оценке продуктивности экосистем Европейского Севера // Современные проблемы дистанционного зондирования Земли из космоса. 2012. Т. 9, № 1. С. 71-79.
4. Зуев В.В., Короткова Е.М., Павлинский А.В. Климатически обусловленные изменения растительного покрова тайги и тундры западной Сибири в 1982-2015 гг. по данным спутниковых наблюдений // Исследование Земли из космоса. 2019. № 6. С. 66-76. <https://doi.org/10.31857/S0205-96142019666-76>
5. Им С.Т., Харук В.И., Ли В.Г. Миграция северной границы вечнозелёных хвойных древостоев в Сибири в XXI столетии // Современные проблемы дистанционного зондирования Земли из космоса. 2020. Т. 17, № 1. С. 176-187. DOI: 10.21046/2070-7401-2020-17-1-176-187
6. Курбанов Э.А., Воробьев О.Н., Губаев А.В., Лежнин С.А., Полевщикова Ю.А., Демишева Е.Н. Четыре десятилетия исследований лесов по снимкам Landsat // Вестник Поволжского государственного технологического университета. Серия «Лес. Экология. Природопользование». 2014. № 1(21). С. 18-32.
7. Курбанов Э.А., Воробьев О.Н., Губаев А.В., Лежнин С.А., Полевщикова Ю.А. Оценка точности и сопоставимости тематических карт лесного покрова разного пространственного разрешения на примере Среднего Поволжья // Современные проблемы дистанционного зондирования Земли из космоса. 2016. Т. 13, № 1. С. 36-48.
8. Лупян Е.А., Савин И.Ю., Барталев С.А., Толпин В.А., Балашов И.В., Плотников Д.Е. Спутниковый сервис мониторинга состояния растительности («Вега») // Современные проблемы дистанционного зондирования Земли из космоса. 2011. Т. 8, № 1. С. 190-198.
9. Парижское соглашение. ООН, 2015, 30 с. URL: <https://unfccc.int/process-and-meetings/the-paris-agreement/the-paris-agreement>
10. Статакис Д., Перакис К., Савин И.Ю. Дешифрирование урбанизированных территорий по спутниковым данным Landsat // Исследование земли из космоса. 2012. № 5. С. 22-29.
11. Терехин Э.А. Изменение нарушенности лесных экосистем лесостепной зоны Центрального Черноземья в конце XX – начале XXI века // Исследование Земли из космоса. 2020. № 3. С. 26-37. DOI: 10.31857/S0205961420030069
12. Титкова Т.Б., Виноградова В.В. Отклик растительности на изменение климатических условий в бореальных и субарктических ландшафтах в начале XXI века // Современные проблемы дистанционного зондирования Земли из космоса. 2015. Т. 12, № 3. С. 75-86.
13. Черных Д.В., Бирюков Р.Ю., Золотов Д.В., Першин Д.К. Пространственно-временная динамика ландшафтов водосборных бассейнов Алтайского региона в последние 40 лет // География и природные ресурсы. 2018. № 3. С. 104-115 [https://doi.org/10.21782/GIPR0206-1619-2018-3\(104-115\)](https://doi.org/10.21782/GIPR0206-1619-2018-3(104-115))
14. Acheson J.M., McCloskey J. Causes of deforestation: The Maine case // Human Ecology. 2008. Vol. 36. P. 909-922. <https://doi.org/10.1007/s10745-008-9204-3>
15. Alawamy J.S., Balasundram S.K., Hanif A.H.M., Sung C.T.B. Detecting and Analyzing Land Use and Land Cover Changes in the Region of Al-Jabal Al-Akhdar, Libya Using Time-Series Landsat Data from 1985 to 2017 // Sustainability (Switzerland). 2020. Vol. 12(11). 4490 <https://doi.org/10.3390/su12114490>
16. Beck P.S.A., Goetz S. J. Satellite observations of high northern latitude vegetation productivity changes between 1982 and 2008: Ecological variability and regional differences // Environmental Research Letters. 2011. 6, 045501 <https://doi.org/10.1088/1748-9326/7/2/029501>
17. Broucke S.V., Luyssert S., Davin E.L., Janssens I., van Lipzig N. New insights in the capability of climate models to simulate the impact of LUC based on temperature decomposition of paired site observations // Journal of Geophysical Research: Atmospheres. 2015. Vol. 120, № 11. P. 5417-5436. <https://doi.org/10.1002/2015JD023095>
18. Bürgi M., Hersperger A.M., Schneeberger N. Driving forces of landscape change - Current and new directions// Landscape Ecology. 2005, Vol. 19, № 8. P. 857-868. <https://doi.org/10.1007/s10980-004-0245-8>
19. Cao Q., Liu Y., Georgescu M., Wu J. Impacts of landscape changes on local and regional climate: a systematic review // Landscape Ecology. 2020. Vol. 35, № 6. P. 1269-1290. <https://doi.org/10.1007/s10980-020-01015-7>

20. Chakraborty A., Ghosh A., Sachdeva K., Joshi, P.K. Characterizing fragmentation trends of the Himalayan forests in the Kumaon region of Uttarakhand, India // *Ecological Informatics*. 2017. 38. P. 95–109. <https://doi.org/10.1016/j.ecoinf.2016.12.006>
21. Chen C., He X., Liu Z., Sun W., Dong H., Chu Y. Analysis of regional economic development based on land use and land cover change information derived from Landsat imagery // *Scientific Reports*. 2020. Vol. 10 № 1, P. 1–16. <https://doi.org/10.1038/s41598-020-69716-2>
22. Cho H. S., Choi M. J. Effects of compact Urban development on air pollution: Empirical evidence from Korea // *Sustainability* (Switzerland). 2014. Vol. 6, № 9. P. 5968–5982. <https://doi.org/10.3390/su6095968>
23. Civerolo K., Hogrefe C., Lynn B., Rosenthal J., Ku J.Y., Solecki W., et al. Estimating the effects of increased urbanization on surface meteorology and ozone concentrations in the New York City metropolitan region // *Atmospheric Environment*. 2007. Vol. 41, № 9. P. 1803–1818. <https://doi.org/10.1016/j.atmosenv.2006.10.076>
24. Cohen W. B., Yang Z., Stehman S.V., Schroeder T.A., Bell D.M., Masek J.G. et al. Forest disturbance across the conterminous United States from 1985–2012: The emerging dominance of forest decline // *Forest Ecology and Management*. 2016. 360. P. 242–252. <https://doi.org/10.1016/j.foreco.2015.10.042>
25. Culas R.J. Deforestation and the environmental Kuznets curve: An institutional perspective // *Ecological Economics*. 2007. 61(2–3). P. 429–437. <https://doi.org/10.1016/j.ecolecon.2006.03.014>
26. Deng C., Wu C. BCI: A biophysical composition index for remote sensing of urban environments // *Remote Sensing of Environment*. 2012. 127. 247–259. <https://doi.org/10.1016/j.rse.2012.09.009>
27. Dong J., Xiao X., Sheldon S., Biradar C., Zhang G., Duong N.D., et al. A 50-m forest cover map in Southeast Asia from ALOS/PALSAR and its application on forest fragmentation assessment. *PLoS ONE*. 2014. Vol. 9, № 1. <https://doi.org/10.1371/journal.pone.0085801>
28. Du J., He Z., Chen L., Yang J., Zhu X., Zhao W. Integrating lidar with Landsat data for subalpine temperate forest aboveground carbon estimation // *International Journal of Remote Sensing*. 2015. Vol. 36, № 23. P. 5767–5789. <https://doi.org/10.1080/01431161.2015.1101651>
29. Echeverria C., Coomes D. A., Hall M., Newton, A.C. Spatially explicit models to analyze forest loss and fragmentation between 1976 and 2020 in southern Chile // *Ecological Modelling*. 2008. Vol. 212(3–4). P. 439–449. <https://doi.org/10.1016/j.ecolmodel.2007.10.045>
30. FAO. The State of the World's Forests 2018 – Forest pathways to sustainable development. Rome, 2018. 118 p.
31. Farooq S., Ahmad S. Urban sprawl development around Aligarh city: A study aided by satellite remote sensing and GIS // *Journal of the Indian Society of Remote Sensing*. 2008. Vol. 36, № 1. P. 77–88. <https://doi.org/10.1007/s12524-008-0008-0>
32. Fauzi A., Sakti A., Yayusman L., Harto A., Prasetyo L., Irawan B., Kamal M., Wikantika K. Contextualizing mangrove forest deforestation in southeast Asia using environmental and socio-economic data products // *Forests*. 2019. Vol. 10, № 11. P. 1–18. <https://doi.org/10.3390/f10110952>
33. Fayaz A., Shafiq M., Singh H., Ahmed P. Assessment of spatiotemporal changes in land use/land cover of North Kashmir Himalayas from 1992 to 2018 // *Modeling Earth Systems and Environment*. 2020. Vol. 6, № 2. P. 1189–1200. <https://doi.org/10.1007/s40808-020-00750-9>
34. Freitas S.R., Hawbaker T.J., Metzger J.P. Effects of roads, topography, and land use on forest cover dynamics in the Brazilian Atlantic Forest // *Forest Ecology and Management*. 2010. Vol. 259, № 3. P. 410–417. <https://doi.org/10.1016/j.foreco.2009.10.036>
35. Galidaki G., Zianis D., Gitas I., Radoglou K., Karathanassi V., Tsakiri-Strati M., et al. Vegetation biomass estimation with remote sensing: focus on forest and other wooded land over the Mediterranean ecosystem // *International Journal of Remote Sensing*. 2017. Vol. 38, № 7. P. 1940–1966. <https://doi.org/10.1080/01431161.2016.1266113>
36. Ghosh S. A city growth and land-use/land-cover change: a case study of Bhopal, India // *Modeling Earth Systems and Environment*. 2019. Vol. 5, № 4. P. 1569–1578. <https://doi.org/10.1007/s40808-019-00605-y>
37. Global Land Programme (accessed 16.11.2020) <https://glp.earth/>
38. Gómez C., Wulder M.A., White J.C., Montes F., Delgado J.A. Characterizing 25 years of change in the area, distribution, and carbon stock of Mediterranean pines in Central Spain // *International Journal of Remote Sensing*. 2012. Vol. 33, № 17. P. 5546–5573. <https://doi.org/10.1080/01431161.2012.663115>
39. Guidigan M.L.G., Sanou C.L., Ragatoa D.S., Fafa C.O., Mishra V.N. Assessing Land Use/Land Cover Dynamic and Its Impact in Benin Republic Using Land Change Model and CCI-LC Products // *Earth Systems and Environment*. 2019. 3(1). P. 127–137. <https://doi.org/10.1007/s41748-018-0083-5>
40. Han S., Bian H., Tie X., Xie Y., Sun M., Liu A. Impact of nocturnal planetary boundary layer on urban air pollutants: Measurements from a 250-m tower over Tianjin, China // *Journal of Hazardous Materials*. 2009. Vol. 162, № 1. P. 264–269. <https://doi.org/10.1016/j.jhazmat.2008.05.056>
41. Hao P., Niu Z., Zhan Y., Wu Y., Wang L., Liu, Y. Spatiotemporal changes of urban impervious surface area and land surface temperature in Beijing from 1990 to 2014 // *GIScience and Remote Sensing*. 2016. Vol. 53, № 1. P. 63–84. <https://doi.org/10.1080/15481603.2015.1095471>
42. Hou K., Li X., Wang J.J., Zhang J. An analysis of the impact on land use and ecological vulnerability of the policy of returning farmland to forest in Yan'an, China // *Environmental Science and Pollution Research*. 2016. 23. P. 4670–4680. <https://doi.org/10.1007/s11356-015-5679-9>
43. Hoyos L.E., Cabido M.R., Cingolani A.M. A multivariate approach to study drivers of land-cover changes through remote sensing in the dry Chaco of Argentina // *ISPRS International Journal of Geo-Information*. 2018. 7(5), P. 1–15. <https://doi.org/10.3390/ijgi7050170>
44. IGBP. Land use and Cover Change (accessed 16.11.2020) <http://www.igbp.net/researchprojects/igbpcoreprojectsphaseone/landuseandcoverchange.4.1b8ac20512db692f2a680009062.html>

45. Im J. Earth observations and geographic information science for sustainable development goals // *GIScience and Remote Sensing*. 2020. Vol. 57, № 5. P. 591–592. <https://doi.org/10.1080/15481603.2020.1763041>
46. Ji L., Wylie B.K., Brown D.R.N., Peterson B., Alexander H.D., Mack M.C., et al. Spatially explicit estimation of aboveground boreal forest biomass in the Yukon River Basin, Alaska // *International Journal of Remote Sensing*. 2015. Vol. 36, № 4. P. 939–953. <https://doi.org/10.1080/01431161.2015.1004764>
47. Johnson D.P., Stanforth A., Lulla V., Lubert G. Developing an applied extreme heat vulnerability index utilizing socioeconomic and environmental data // *Applied Geography*. 2012. Vol. 35 (1–2). P. 23–31. <https://doi.org/10.1016/j.apgeog.2012.04.006>
48. Jusuf S.K., Wong N.H., Hagen E., Anggoro R., Hong Y. The influence of land use on the urban heat island in Singapore // *Habitat International*. 2007. Vol. 31(2). P. 232–242. <https://doi.org/10.1016/j.habitatint.2007.02.006>
49. Kamwi J.M., Cho M.A., Kaetsch C., Manda S.O., Graz F.P., Chirwa P.W. Assessing the spatial drivers of land use and land cover change in the protected and communal areas of the Zambezi Region, Namibia // *Land*. 2018. 7(4). <https://doi.org/10.3390/land7040131>
50. Khatami R., Mountrakis G., Stehman S.V. A meta-analysis of remote sensing research on supervised pixel-based land-cover image classification processes: General guidelines for practitioners and future research // *Remote Sensing of Environment*. 2016. 177. P. 89–100. <https://doi.org/10.1016/j.rse.2016.02.028>
51. Kitsara G., Papaioannou G., Retalis A., Paronis D., Kerkides P. Estimation of air temperature and reference evapotranspiration using MODIS land surface temperature over Greece // *International Journal of Remote Sensing*. 2018. Vol. 39, № 3. P. 924–948. <https://doi.org/10.1080/01431161.2017.1395965>
52. Knott J.A., Desprez, J.M., Oswalt, C.M., Fei S. Shifts in forest composition in the eastern United States // *Forest Ecology and Management*. 2019. Vol. 433. P. 176–183. <https://doi.org/10.1016/j.foreco.2018.10.061>
53. Kolokotroni M., Giannitsaris I., Watkins R. The effect of the London urban heat island on building summer cooling demand and night ventilation strategies // *Solar Energy*. 2006. Vol. 80, № 4. P. 383–392. <https://doi.org/10.1016/j.solener.2005.03.010>
54. Kumar A., Uniyal S.K., Lal B. Stratification of forest density and its validation by NDVI analysis in a part of western Himalaya, India using Remote sensing and GIS techniques // *International Journal of Remote Sensing*, 2007. Vol. 28, № 11. P. 2485–2495. <https://doi.org/10.1080/01431160600693583>
55. Lai L., Huang X., Yang H., Chuai X., Zhang M., Zhong T., et al. Carbon emissions from land-use change and management in China between 1990 and 2010 // *Science Advances*. 2016. 2(11). P. 1–9. <https://doi.org/10.1126/sciadv.1601063>
56. Lele N., Joshi P.K., Agrawal S.P. Assessing forest fragmentation in northeastern region (NER) of India using landscape matrices // *Ecological Indicators*. 2008. Vol. 8, № 5. P. 657–663. <https://doi.org/10.1016/j.ecolind.2007.10.002>
57. Levin N. Human factors explain the majority of MODIS-derived trends in vegetation cover in Israel: a densely populated country in the eastern Mediterranean // *Regional Environmental Change*. 2016. Vol. 16, № 4. P. 1197–1211. <https://doi.org/10.1007/s10113-015-0848-4>
58. Li M., Zhu Z., Vogelmann J.E., Xu D., Wen W., Liu A. Characterizing fragmentation of the collective forests in southern China from multitemporal Landsat imagery: A case study from Kecheng district of Zhejiang province // *Applied Geography*. 2011. Vol. 31, № 3. P. 1026–1035. <https://doi.org/10.1016/j.apgeog.2011.02.004>
59. Li S., Chen X. A new bare-soil index for rapid mapping developing areas using landsat 8 data // *International Archives of the Photogrammetry, Remote Sensing and Spatial Information Sciences - ISPRS Archives*, 2014. Vol. 40, № 4. P. 139–144. <https://doi.org/10.5194/isprsarchives-XL-4-139-2014>
60. Li X., Qu Y. Evaluation of Vegetation Responses to Climatic Factors and Global Vegetation Trends using GLASS LAI from 1982 to 2010 // *Canadian Journal of Remote Sensing*. 2018. Vol. 44, № 4. P. 357–372. <https://doi.org/10.1080/07038992.2018.1526064>
61. Liu C., Shao Z., Chen M., Luo H. MNDISI: A multi-source composition index for impervious surface area estimation at the individual city scale // *Remote Sensing Letters*. 2013. Vol. 4, № 8. P. 803–812. <https://doi.org/10.1080/2150704X.2013.798710>
62. Lu D., Mausel P., Brondizio E., Moran E. Change detection techniques // *International Journal of Remote Sensing*. 2004. Vol. 25, № 12/ P. 2365–2401. <https://doi.org/10.1080/0143116031000139863>
63. Lunetta R.S., Knight J.F., Ediriwickrema J., Lyon J.G., Worthy L.D. Land-cover change detection using multi-temporal MODIS NDVI data // *Remote Sensing of Environment*. 2006. Vol. 105, № 2. P. 142–154. <https://doi.org/10.1016/j.rse.2006.06.018>
64. Manandhar R., Odeh I.O.A., Ancev T. Improving the accuracy of land use and land cover classification of Landsat data using post-classification enhancement // *Remote Sensing*. 2009, Vol. 1, № 3. P. 330–344. <https://doi.org/10.3390/rs1030330>
65. Mannan A., Feng Z., Ahmad A., Liu J., Saeed S., Mukete B. Carbon dynamic shifts with land use change in margallah hills national park, Islamabad (Pakistan) from 1990 to 2017 // *Applied Ecology and Environmental Research*. 2018. Vol. 16, № 3. P. 3197–3214. https://doi.org/10.15666/aecer/1603_31973214
66. Meshesha T.W., Tripathi S.K., Khare D. Analyses of land use and land cover change dynamics using GIS and remote sensing during 1984 and 2015 in the Beressa Watershed Northern Central Highland of Ethiopia. Modeling Earth Systems and Environment. 2016. 2(4). P. 1–12. <https://doi.org/10.1007/s40808-016-0233-4>
67. Moulds S., Buytaert W., Mijic A. Data Descriptor: A spatio-temporal land use and land cover reconstruction for India from 1960–2010 // *Scientific Data*. 2018. Vol. 5. P. 1–11. <https://doi.org/10.1038/sdata.2018.159>
68. Msofe N.K., Sheng L., Li Z., Lyimo J. Impact of land use/cover change on ecosystem service values in the Kilombero valley floodplain, southeastern Tanzania // *Forests*. 2020. Vol. 11, № 1. P. 1–17. <https://doi.org/10.3390/f11010109>

69. Nabuurs G.J., Lindner M., Verkerk P.J., Gunia K., Deda P., Michalak R., Grassi, G. First signs of carbon sink saturation in European forest biomass // *Nature Climate Change*. 2013. Vol. 3, № 9. P. 792–796. <https://doi.org/10.1038/nclimate1853>
70. Nery T., Sadler R., Solis A.M., White B., Polyakov M. Discriminating native and plantation forests in a Landsat time-series for land use policy design // *International Journal of Remote Sensing*. 2019. Vol. 40, № 11. P. 4059–4082. <https://doi.org/10.1080/01431161.2018.1558375>
71. Nurda N., Noguchi R., Ahamed T. Change detection and land suitability analysis for extension of potential forest areas in Indonesia using satellite remote sensing and GIS // *Forests*. 2020. Vol. 11, № 4. P. 1–22. <https://doi.org/10.3390/F11040398>
72. Obeidat M., Awawdeh M., Lababneh A. Assessment of land use/land cover change and its environmental impacts using remote sensing and GIS techniques, Yarmouk River Basin, north Jordan // *Arabian Journal of Geosciences*. 2019. Vol. 12, № 22. <https://doi.org/10.1007/s12517-019-4905-z>
73. Pan Y., Birdsall R.A., Fang J., Houghton R., Kauppi P.E., Kurz W.A., et al. A large and persistent carbon sink in the world's forests // *Science*. 2011. Vol. 333, № 6045. P. 988–993. <https://doi.org/10.1126/science.1201609>
74. Pereira O.J.R., Montes C.R., Lucas Y., Santin R.C., Melfi A.J. A multi-sensor approach for mapping plant-derived carbon storage in Amazonian podzols // *International Journal of Remote Sensing*. 2015. Vol. 36, № 8. P. 2076–2092. <https://doi.org/10.1080/01431161.2015.1034896>
75. Pineda J.N.B., Bosque S.J., Gómez D.M., Franco P.R. Exploring the driving forces behind deforestation in the state of Mexico (Mexico) using geographically weighted regression // *Applied Geography*. 2010. Vol. 30, № 4. P. 576–591. <https://doi.org/10.1016/j.apgeog.2010.05.004>
76. Potter C. Ten Years of Vegetation Change in Northern California Marshlands Detected Using Landsat Satellite Image Analysis // *Journal of Water Resource and Protection*. 2013. Vol. 5, № 5. P. 485–494. <https://doi.org/10.4236/jwarp.2013.55048>
77. Pouliot D., Latifovic R., Zabcic N., Guindon L., Olthof I. Development and assessment of a 250m spatial resolution MODIS annual land cover time series (2000–2011) for the forest region of Canada derived from change-based updating // *Remote Sensing of Environment*. 2014. Vol. 140. P. 731–743. <https://doi.org/10.1016/j.rse.2013.10.004>
78. Ramachandran R.M., Reddy C. S. Monitoring of deforestation and land use changes (1925–2012) in Idukki district, Kerala, India using remote sensing and GIS // *Journal of the Indian Society of Remote Sensing*. 2017. Vol. 45, № 1. P. 163–170. <https://doi.org/10.1007/s12524-015-0521-x>
79. Reddy C.S., Satish K.V., Pasha S.V., Jha C.S., Dadhwal V.K. Assessment and monitoring of deforestation and land-use changes (1976–2014) in Andaman and Nicobar Islands, India using remote sensing and GIS // *Current Science*. 2016. Vol. 111, № 9. P. 1492–1499. <https://doi.org/10.18520/cs/v111/i9/1492-1499>
80. Riitters K., Wickham J., Costanza J.K., Vogt P. A global evaluation of forest interior area dynamics using tree cover data from 2000 to 2012 // *Landscape Ecology*. 2016. Vol. 31. P. 137–148. <https://doi.org/10.1007/s10980-015-0270-9>
81. Riitters K., Wickham J., O'Neill R.O., Jones B., Smith E. Global-Scale Patterns of Forest Fragmentation // *Conservation Ecology*. 2000. Vol. 4, № 2. <https://www.jstor.org/stable/26271763>
82. Riitters K.H., Wickham J.D., O'Neill R.V., Jones, K.B., Smith E.R., Coulston J.W., et al. Fragmentation of Continental United Forests // *Ecosystems*. 2002. Vol. 5, № 8. P. 815–822.
83. Rinner C., Patychuk D., Bassil K., Nasr S., Gower S., Campbell M. The role of maps in neighborhood-level heat vulnerability assessment for the city of Toronto // *Cartography and Geographic Information Science*. 2010. Vol. 37, № 1. P. 31–44. <https://doi.org/10.1559/152304010790588089>
84. Riutta T., Slade E.M., Morecroft M.D., Bebbler D.P., Malhi Y. Living on the edge: Quantifying the structure of a fragmented forest landscape in England // *Landscape Ecology*. 2014. Vol. 29, № 6. P. 949–961. <https://doi.org/10.1007/s10980-014-0025-z>
85. Ruiz-Benito P., Gómez-Aparicio L., Paquette A., Messier C., Kattge J., Zavala M.A. Diversity increases carbon storage and tree productivity in Spanish forests // *Global Ecology and Biogeography*. 2014. Vol. 23, № 3. P. 311–322. <https://doi.org/10.1111/geb.12126>
86. Sahana M., Hong H., Sajjad H., Liu J., Zhu A.X. Assessing deforestation susceptibility to forest ecosystem in Rudrapur district, India using fragmentation approach and frequency ratio model // *Science of the Total Environment*. 2018. Vol. 627. P. 1264–1275. <https://doi.org/10.1016/j.scitotenv.2018.01.290>
87. Santamouris M., Papanikolaou N., Livada I., Koronakis I., Georgakis C., Argiriou A., Assimakopoulos D.N. On the impact of urban climate on the energy consumption of building // *Solar Energy*. 2001. Vol. 70, № 3. P. 201–216. [https://doi.org/10.1016/S0038-092X\(00\)00095-5](https://doi.org/10.1016/S0038-092X(00)00095-5)
88. Sharma S., Roy P.S. Forest fragmentation in the Himalaya: A Central Himalayan case study // *International Journal of Sustainable Development and World Ecology*. 2007. Vol. 14, № 2. P. 201–210. <https://doi.org/10.1080/13504500709469720>
89. Tadese M., Kumar L., Koech R., Kogo B.K. Mapping of land-use/land-cover changes and its dynamics in Awash River Basin using remote sensing and GIS // *Remote Sensing Applications: Society and Environment*. 2020. Vol. 19, № 100352 <https://doi.org/10.1016/j.rsase.2020.100352>
90. Taubert F., Fischer R., Groeneveld J., Lehmann S., Müller M. S., Rödig E., et al. Global patterns of tropical forest fragmentation // *Nature*. 2018. Vol. 554, № 7693. P. 519–522. <https://doi.org/10.1038/nature25508>
91. Tölle M.H., Engler S., Panitz H.J. Impact of abrupt land cover changes by tropical deforestation on Southeast Asian climate and agriculture // *Journal of Climate*. 2017. Vol. 30, № 7. P. 2587–2600. <https://doi.org/10.1175/JCLI-D-16-0131.1>
92. Wade T.G., Riitters K.H., Wickham J.D., Jones K.B. Distribution and causes of global forest fragmentation // *Ecology and Society*. 2003. Vol. 7, № 2. <https://doi.org/10.5751/es-00530-070207>

93. Wang N., Brown D.G., An L., Yang S., Ligmann-Zielinska A. Comparative performance of logistic regression and survival analysis for detecting spatial predictors of land-use change // *International Journal of Geographical Information Science*. 2013. Vol. 27, № 10. P. 1960–1982. <https://doi.org/10.1080/13658816.2013.779377>
94. Wickham J.D., Riitters K.H., Wade T.G., Vogt P. A national assessment of green infrastructure and change for the conterminous United States using morphological image processing // *Landscape and Urban Planning*. 2010. Vol. 94 (3–4). P. 186–195. <https://doi.org/10.1016/j.landurbplan.2009.10.003>
95. Wolken J.M., Hollingsworth T.N., Rupp T.S., Chapin F.S., Trainor S.F., Barrett T.M., et al. Evidence and implications of recent and projected climate change in Alaska's forest ecosystems // *Ecosphere*. 2011. Vol. 2, № 11. <https://doi.org/10.1890/ES11-00288.1>
96. Wu J. Key concepts and research topics in landscape ecology revisited: 30 years after the Allerton Park workshop // *Landscape Ecology*. 2013. Vol. 28, № 1. P. 1–11. <https://doi.org/10.1007/s10980-012-9836-y>
97. Wylie B., Rigge M., Brisco B., Murnaghan K., Rover J., Long J. Effects of disturbance and climate change on ecosystem performance in the Yukon River basin boreal forest // *Remote Sensing*. 2014. Vol. 6, № 10. P. 9145–9169. <https://doi.org/10.3390/rs6109145>
98. Yang X., Lo C.P. Using a time series of satellite imagery to detect land use and land cover changes in the Atlanta, Georgia metropolitan area // *International Journal of Remote Sensing*. 2002. Vol. 23, № 9. P. 1775–1798. <https://doi.org/10.1080/01431160110075802>
99. Yemshanov D., Koch F.H., Riitters K.H., Mcconkey B., Huffman T., Smith S. Assessing land clearing potential in the Canadian agriculture-forestry interface with a multi-attribute frontier approach // *Ecological Indicators*. 2015. Vol. 54. P. 71–81. <https://doi.org/10.1016/j.ecolind.2015.02.019>
100. Zaiatz A.P.S.R., Zolin C.A., Vendrusculo L.G., Lopes T.R., Paulino J. Agricultural land use and cover change in the Cerrado/Amazon ecotone: A case study of the upper Teles Pires river basin // *Acta Amazonica*. 2018. Vol. 48, № 2. P. 168–177. <https://doi.org/10.1590/1809-4392201701930>
101. Zha Y., Gao J., Ni S. Use of normalized difference built-up index in automatically mapping urban areas from TM imagery // *International Journal of Remote Sensing*. 2003. Vol. 24, № 3. P. 583–594. <https://doi.org/10.1080/01431160304987>
102. Zhang C., Wang X., Liu Y. Changes in quantity, quality, and pattern of farmland in a rapidly developing region of China: a case study of the Ningbo region // *Landscape and Ecological Engineering*. 2019. Vol. 15, № 3. P. 323–336. <https://doi.org/10.1007/s11355-019-00382-x>
103. Zhang H., Qi, Z. fang, Ye X. yue, Cai Y. bin, Ma W. chun, Chen M. nan. Analysis of land use/land cover change, population shift, and their effects on spatiotemporal patterns of urban heat islands in metropolitan Shanghai, China // *Applied Geography*. 2013. Vol. 44. P. 121–133. <https://doi.org/10.1016/j.apgeog.2013.07.021>
104. Zhang L., Pan T., Zhang H., Li X., Jiang L. The effects of forest area changes on extreme temperature indexes between the 1900s and 2010s in Heilongjiang Province, China // *Remote Sensing*. 2017. Vol. 9, № 12. <https://doi.org/10.3390/rs9121280>
105. Zhang Q., Li B., Thau D., Moore R. Building a better Urban picture: Combining day and night remote sensing imagery // *Remote Sensing*. 2015. Vol. 7, № 9. P. 11887–11913. <https://doi.org/10.3390/rs70911887>
106. Zhu E., Deng J., Zhou M., Gan M., Jiang R., Wang K., Shahtahmassebi A.R. Carbon emissions induced by land-use and land-cover change from 1970 to 2010 in Zhejiang, China // *Science of the Total Environment*, 2019. Vol. 646. P. 930–939. <https://doi.org/10.1016/j.scitotenv.2018.07.317>

References

1. Bartalev S.A., Egorov V.A., Zharko V.O., Lupyan E.A., Plotnikov D.E., Khvostikov S.A. Sostoyanie i perspektivy razvitiya metodov sputnikovogo kartografirovaniya rastitel'nogo pokrova Rossii [State and prospects for the development of methods of satellite mapping of vegetation cover in Russia], *Sovremennye problemy distantsionnogo zondirovaniya Zemli iz kosmosa*, **2015**, T. 12, № 5, P. 203–221.
2. Bartalev S.A., Khovratovich T.S., Elsakov V.V. Ispol'zovanie sputnikovykh izobrazhenii dlya otsenki poter' ugleroda lesnymi ekosistemami v rezul'tate vyrubok [Using satellite imagery to estimate carbon loss in forest ecosystems from deforestation], *Sovremennye problemy distantsionnogo zondirovaniya Zemli iz kosmosa*, **2009**, Vol. 2, № 6, P. 343–351.
3. Elsakov V.V. Sputnikovaya s'emka v otsenke produktivnosti ekosistem Evropeiskogo Severa [Satellite imagery in assessing the productivity of ecosystems in the European North], *Sovremennye problemy distantsionnogo zondirovaniya Zemli iz kosmosa*, **2012**, Vol. 9, № 1. P. 71–79.
4. Zuev V.V., Korotkova E.M., Pavlinskii A.V. Klimaticheski obuslovlennyye izmeneniya rastitel'nogo pokrova taigi i tundry zapadnoi Sibiri v 1982–2015 gg. po dannym sputnikovykh nablyudenii [Climatically caused changes in the vegetation cover of taiga and tundra in western Siberia in 1982–2015 according to satellite observations], *Issledovanie Zemli iz kosmosa*, **2019**, № 6, P. 66–76. <https://doi.org/10.31857/S0205-96142019666-76>
5. Im S.T., Kharuk V.I., Li V.G. Migratsiya severnoi granitsy vечнозеленых хвойных древостоев в Сибири в XXI столетии [Migration of the northern border of evergreen coniferous stands in Siberia in the XXI century], *Sovremennye problemy distantsionnogo zondirovaniya Zemli iz kosmosa*, **2020**, Vol. 17, № 1, P. 176–187. DOI: 10.21046/2070-7401-2020-17-1-176-187
6. Kurbanov E.A., Vorob'ev O.N., Gubaev A.V., Lezhnin S.A., Polevshchikova Yu.A., Demisheva E.N. Chetyre desyatiletiya issledovaniy lesov po snimkam Landsat [Four decades of forest research from Landsat imagery], *Vestnik Povolzhskogo gosudarstvennogo tekhnologicheskogo universiteta. Seriya «Les. Ekologiya. Prirodopol'zovanie»*, **2014**, № 1(21), P. 18–32.

7. Kurbanov E.A., Vorob'ev O.N., Gubaev A.V., Lezhnin S.A., Polevshchikova Yu.A. Otsenka tochnosti i sopostavimosti tematicheskikh kart lesnogo pokrova raznogo prostranstvennogo razresheniya na primere Srednego Povolzh'ya [Assessment of the accuracy and comparability of thematic maps of forest cover of different spatial resolution on the example of the Middle Volga region], *Sovremennyye problemy distantsionnogo zondirovaniya Zemli iz kosmosa*, **2016**, Vol. 13, № 1, P. 36–48.
8. Lupyan E.A., Savin I.Yu., Bartalev S.A., Tolpin V.A., Balashov I.V., Plotnikov D.E. Sputnikovyi servis monitoringa sostoyaniya rastitel'nosti («Vega») [Vegetation condition monitoring service ("Vega")], *Sovremennyye problemy distantsionnogo zondirovaniya Zemli iz kosmosa*, **2011**, Vol. 8, № 1, P. 190–198.
9. Parizhskoe soglasenie. OON [Paris Agreement. UN], **2015**, 30 p. URL: <https://unfccc.int/process-and-meetings/the-paris-agreement/the-paris-agreement>
10. Statakis D., Perakis K., Savin I.Yu. Deshifirovanie urbanizirovannykh territorii po sputnikovym dannym Landsat [Deciphering urban areas using satellite data Landsat], *Issledovanie zemli iz kosmosa*, **2012**, № 5, P. 22–29.
11. Terekhin E.A. Izmenenie narushennosti lesnykh ekosistem lesostepnoi zony Tsentral'nogo Chernozem'ya v kontse XX – nachale XXI veka [Changes in the disturbance of forest ecosystems in the forest-steppe zone of the Central Chernozem region at the end of the XX – beginning of the XXI century], *Issledovanie Zemli iz kosmosa*, **2020**, № 3, P. 26–37. DOI: 10.31857/S0205961420030069
12. Titkova T.B., Vinogradova V.V. Otklik rastitel'nosti na izmenenie klimaticheskikh uslovii v boreal'nykh i subarkticheskikh landshaftakh v nachale XXI veka [Vegetation response to changes in climatic conditions in boreal and subarctic landscapes at the beginning of the XXI century], *Sovremennyye problemy distantsionnogo zondirovaniya Zemli iz kosmosa*, **2015**, Vol. 12, № 3, P. 75–86.
13. Chernykh D.V., Biryukov R.Yu., Zolotov D.V., Pershin D.K. Prostranstvenno-vremennaya dinamika landshaftov vodosbornykh basseinov Altaiskogo regiona v poslednie 40 let [Spatial-temporal dynamics of the landscapes of the drainage basins of the Altai region in the last 40 years], *Geografiya i prirodnye resursy*, **2018**, № 3, P. 104–115 [https://doi.org/10.21782/GIPR0206-1619-2018-3\(104-115\)](https://doi.org/10.21782/GIPR0206-1619-2018-3(104-115))
14. Acheson J.M., McCloskey J. Causes of deforestation: The Maine case, *Human Ecology*, **2008**, Vol. 36, P. 909–922. <https://doi.org/10.1007/s10745-008-9204-3>
15. Alawamy J.S., Balasundram S.K., Hanif A.H.M., Sung C.T.B. Detecting and Analyzing Land Use and Land Cover Changes in the Region of Al-Jabal Al-Akhdar, Libya Using Time-Series Landsat Data from 1985 to 2017, *Sustainability (Switzerland)*, **2020**, Vol. 12(11), 4490 <https://doi.org/10.3390/su12114490>
16. Beck P.S.A., Goetz S. J. Satellite observations of high northern latitude vegetation productivity changes between 1982 and 2008: Ecological variability and regional differences, *Environmental Research Letters*, **2011**, 6, 045501 <https://doi.org/10.1088/1748-9326/7/2/029501>
17. Broucke S.V., Luyssert S., Davin E.L., Janssens I., van Lipzig N. New insights in the capability of climate models to simulate the impact of LUC based on temperature decomposition of paired site observations, *Journal of Geophysical Research: Atmospheres*, **2015**, Vol. 120, № 11, P. 5417–5436. <https://doi.org/10.1002/2015JD023095>
18. Bürgi M., Hersperger A.M., Schneeberger N. Driving forces of landscape change - Current and new directions, *Landscape Ecology*, **2005**, Vol. 19, № 8, P. 857–868. <https://doi.org/10.1007/s10980-004-0245-8>
19. Cao Q., Liu Y., Georgescu M., Wu J. Impacts of landscape changes on local and regional climate: a systematic review, *Landscape Ecology*, **2020**, Vol. 35, № 6, P. 1269–1290. <https://doi.org/10.1007/s10980-020-01015-7>
20. Chakraborty A., Ghosh A., Sachdeva K., Joshi, P.K. Characterizing fragmentation trends of the Himalayan forests in the Kumaon region of Uttarakhand, India, *Ecological Informatics*, **2017**, 38, P. 95–109. <https://doi.org/10.1016/j.ecoinf.2016.12.006>
21. Chen C., He X., Liu Z., Sun W., Dong H., Chu Y. Analysis of regional economic development based on land use and land cover change information derived from Landsat imagery, *Scientific Reports*, **2020**, Vol. 10, № 1, P. 1–16. <https://doi.org/10.1038/s41598-020-69716-2>
22. Cho H. S., Choi M. J. Effects of compact Urban development on air pollution: Empirical evidence from Korea, *Sustainability (Switzerland)*, **2014**, Vol. 6, № 9, P. 5968–5982. <https://doi.org/10.3390/su6095968>
23. Civerolo K., Hogrefe C., Lynn B., Rosenthal J., Ku J.Y., Solecki W., et al. Estimating the effects of increased urbanization on surface meteorology and ozone concentrations in the New York City metropolitan region, *Atmospheric Environment*, **2007**, Vol. 41, № 9, P. 1803–1818. <https://doi.org/10.1016/j.atmosenv.2006.10.076>
24. Cohen W. B., Yang Z., Stehman S.V., Schroeder T.A., Bell D.M., Masek J.G. et al. Forest disturbance across the conterminous United States from 1985–2012: The emerging dominance of forest decline, *Forest Ecology and Management*, **2016**, 360, P. 242–252. <https://doi.org/10.1016/j.foreco.2015.10.042>
25. Culas R.J. Deforestation and the environmental Kuznets curve: An institutional perspective, *Ecological Economics*, **2007**, 61(2–3), P. 429–437. <https://doi.org/10.1016/j.ecolecon.2006.03.014>
26. Deng C., Wu C. BCI: A biophysical composition index for remote sensing of urban environments, *Remote Sensing of Environment*, **2012**, 127, 247–259. <https://doi.org/10.1016/j.rse.2012.09.009>
27. Dong J., Xiao X., Sheldon S., Biradar C., Zhang G., Duong N.D., et al. A 50-m forest cover map in Southeast Asia from ALOS/PALSAR and its application on forest fragmentation assessment, *PLoS ONE*, **2014**, Vol. 9, № 1. <https://doi.org/10.1371/journal.pone.0085801>
28. Du J., He Z., Chen L., Yang J., Zhu X., Zhao W. Integrating lidar with Landsat data for subalpine temperate forest aboveground carbon estimation, *International Journal of Remote Sensing*, **2015**, Vol. 36, № 23, P. 5767–5789. <https://doi.org/10.1080/01431161.2015.1101651>
29. Echeverria C., Coomes D. A., Hall M., Newton, A.C. Spatially explicit models to analyze forest loss and fragmentation between 1976 and 2020 in southern Chile, *Ecological Modelling*, **2008**, Vol. 212(3–4), P. 439–449. <https://doi.org/10.1016/j.ecolmodel.2007.10.045>

30. FAO. The State of the World's Forests 2018 – Forest pathways to sustainable development. Rome, **2018**. 118 p.
31. Farooq S., Ahmad S. Urban sprawl development around Aligarh city: A study aided by satellite remote sensing and GIS, *Journal of the Indian Society of Remote Sensing*, **2008**, Vol. 36, № 1, P. 77–88. <https://doi.org/10.1007/s12524-008-0008-0>
32. Fauzi A., Sakti A., Yayusman L., Harto A., Prasetyo L., Irawan B., Kamal M., Wikantika K. Contextualizing mangrove forest deforestation in southeast Asia using environmental and socio-economic data products, *Forests*, **2019**, Vol. 10, № 11, P. 1–18. <https://doi.org/10.3390/f10110952>
33. Fayaz A., Shafiq M., Singh H., Ahmed P. Assessment of spatiotemporal changes in land use/land cover of North Kashmir Himalayas from 1992 to 2018, *Modeling Earth Systems and Environment*, **2020**, Vol. 6, № 2, P. 1189–1200. <https://doi.org/10.1007/s40808-020-00750-9>
34. Freitas S.R., Hawbaker T.J., Metzger J.P. Effects of roads, topography, and land use on forest cover dynamics in the Brazilian Atlantic Forest, *Forest Ecology and Management*, **2010**, Vol. 259, № 3, P. 410–417. <https://doi.org/10.1016/j.foreco.2009.10.036>
35. Galidaki G., Zianis D., Gitas I., Radoglou K., Karathanassi V., Tsakiri-Strati M., et al. Vegetation biomass estimation with remote sensing: focus on forest and other wooded land over the Mediterranean ecosystem, *International Journal of Remote Sensing*, **2017**, Vol. 38, № 7, P. 1940–1966. <https://doi.org/10.1080/01431161.2016.1266113>
36. Ghosh S. A city growth and land-use/land-cover change: a case study of Bhopal, India, *Modeling Earth Systems and Environment*, **2019**, Vol. 5, № 4, P. 1569–1578. <https://doi.org/10.1007/s40808-019-00605-y>
37. Global Land Programme (accessed 16.11.2020) <https://glp.earth/>
38. Gómez C., Wulder M.A., White J.C., Montes F., Delgado J.A. Characterizing 25 years of change in the area, distribution, and carbon stock of Mediterranean pines in Central Spain, *International Journal of Remote Sensing*, **2012**, Vol. 33, № 17, P. 5546–5573. <https://doi.org/10.1080/01431161.2012.663115>
39. Guidigan M.L.G., Sanou C.L., Ragatoa D.S., Fafa C.O., Mishra V.N. Assessing Land Use/Land Cover Dynamic and Its Impact in Benin Republic Using Land Change Model and CCI-LC Products, *Earth Systems and Environment*, **2019**, 3(1), P. 127–137. <https://doi.org/10.1007/s41748-018-0083-5>
40. Han S., Bian H., Tie X., Xie Y., Sun M., Liu A. Impact of nocturnal planetary boundary layer on urban air pollutants: Measurements from a 250-m tower over Tianjin, China, *Journal of Hazardous Materials*, **2009**, Vol. 162, № 1, P. 264–269. <https://doi.org/10.1016/j.jhazmat.2008.05.056>
41. Hao P., Niu Z., Zhan Y., Wu Y., Wang L., Liu, Y. Spatiotemporal changes of urban impervious surface area and land surface temperature in Beijing from 1990 to 2014, *GIScience and Remote Sensing*, **2016**, Vol. 53, № 1, P. 63–84. <https://doi.org/10.1080/15481603.2015.1095471>
42. Hou K., Li X., Wang J.J., Zhang J. An analysis of the impact on land use and ecological vulnerability of the policy of returning farmland to forest in Yan'an, China, *Environmental Science and Pollution Research*, **2016**, 23, P. 4670–4680. <https://doi.org/10.1007/s11356-015-5679-9>
43. Hoyos L.E., Cabido M.R., Cingolani A.M. A multivariate approach to study drivers of land-cover changes through remote sensing in the dry Chaco of Argentina, *ISPRS International Journal of Geo-Information*, **2018**, 7(5), P. 1–15. <https://doi.org/10.3390/ijgi7050170>
44. IGBP. Land use and Cover Change (accessed 16.11.2020) <http://www.igbp.net/researchprojects/igbpcoreprojectsphaseone/landuseandcoverchange.4.1b8ae20512db692f2a680009062.html>
45. Im J. Earth observations and geographic information science for sustainable development goals, *GIScience and Remote Sensing*, **2020**, Vol. 57, № 5, P. 591–592. <https://doi.org/10.1080/15481603.2020.1763041>
46. Ji L., Wylie B.K., Brown D.R.N., Peterson B., Alexander H.D., Mack M.C., et al. Spatially explicit estimation of aboveground boreal forest biomass in the Yukon River Basin, Alaska, *International Journal of Remote Sensing*, **2015**, Vol. 36, № 4, P. 939–953. <https://doi.org/10.1080/01431161.2015.1004764>
47. Johnson D.P., Stanforth A., Lulla V., Lubner G. Developing an applied extreme heat vulnerability index utilizing socioeconomic and environmental data, *Applied Geography*, **2012**, Vol. 35 (1–2), P. 23–31. <https://doi.org/10.1016/j.apgeog.2012.04.006>
48. Jusuf S.K., Wong N.H., Hagen E., Anggoro R., Hong Y. The influence of land use on the urban heat island in Singapore, *Habitat International*, **2007**, Vol. 31(2), P. 232–242. <https://doi.org/10.1016/j.habitatint.2007.02.006>
49. Kamwi J.M., Cho M.A., Kaetsch C., Manda S.O., Graz F.P., Chirwa P.W. Assessing the spatial drivers of land use and land cover change in the protected and communal areas of the Zambezi Region, Namibia, *Land*, **2018**, 7(4), <https://doi.org/10.3390/land7040131>
50. Khatami R., Mountrakis G., Stehman S.V. A meta-analysis of remote sensing research on supervised pixel-based land-cover image classification processes: General guidelines for practitioners and future research, *Remote Sensing of Environment*, **2016**, 177, P. 89–100. <https://doi.org/10.1016/j.rse.2016.02.028>
51. Kitsara G., Papaioannou G., Retalis A., Paronis D., Kerkides P. Estimation of air temperature and reference evapotranspiration using MODIS land surface temperature over Greece, *International Journal of Remote Sensing*, **2018**, Vol. 39, № 3, P. 924–948. <https://doi.org/10.1080/01431161.2017.1395965>
52. Knott J.A., Desprez, J.M., Oswalt, C.M., Fei S. Shifts in forest composition in the eastern United States, *Forest Ecology and Management*, **2019**, Vol. 433, P. 176–183. <https://doi.org/10.1016/j.foreco.2018.10.061>
53. Kolokotroni M., Giannitsaris I., Watkins R. The effect of the London urban heat island on building summer cooling demand and night ventilation strategies, *Solar Energy*, **2006**, Vol. 80, № 4, P. 383–392. <https://doi.org/10.1016/j.solener.2005.03.010>
54. Kumar A., Uniyal S.K., Lal B. Stratification of forest density and its validation by NDVI analysis in a part of western Himalaya, India using Remote sensing and GIS techniques, *International Journal of Remote Sensing*, **2007**, Vol. 28, № 11, P. 2485–2495. <https://doi.org/10.1080/01431160600693583>

55. Lai L., Huang X., Yang H., Chuai X., Zhang M., Zhong T., et al. Carbon emissions from land-use change and management in China between 1990 and 2010, *Science Advances*, **2016**, 2(11), P. 1–9. <https://doi.org/10.1126/sciadv.1601063>
56. Lele N., Joshi P.K., Agrawal S.P. Assessing forest fragmentation in northeastern region (NER) of India using landscape matrices, *Ecological Indicators*, **2008**, Vol. 8, № 5, P. 657–663. <https://doi.org/10.1016/j.ecolind.2007.10.002>
57. Levin N. Human factors explain the majority of MODIS-derived trends in vegetation cover in Israel: a densely populated country in the eastern Mediterranean, *Regional Environmental Change*, **2016**, Vol. 16, № 4, P. 1197–1211. <https://doi.org/10.1007/s10113-015-0848-4>
58. Li M., Zhu Z., Vogelmann J.E., Xu D., Wen W., Liu A. Characterizing fragmentation of the collective forests in southern China from multitemporal Landsat imagery: A case study from Kecheng district of Zhejiang province, *Applied Geography*, **2011**, Vol. 31, № 3, P. 1026–1035. <https://doi.org/10.1016/j.apgeog.2011.02.004>
59. Li S., Chen X. A new bare-soil index for rapid mapping developing areas using landsat 8 data, *International Archives of the Photogrammetry, Remote Sensing and Spatial Information Sciences - ISPRS Archives*, **2014**, Vol. 40, № 4, P. 139–144. <https://doi.org/10.5194/isprsarchives-XL-4-139-2014>
60. Li X., Qu Y. Evaluation of Vegetation Responses to Climatic Factors and Global Vegetation Trends using GLASS LAI from 1982 to 2010, *Canadian Journal of Remote Sensing*, **2018**, Vol. 44, № 4, P. 357–372. <https://doi.org/10.1080/07038992.2018.1526064>
61. Liu C., Shao Z., Chen M., Luo H. MNDISI: A multi-source composition index for impervious surface area estimation at the individual city scale, *Remote Sensing Letters*, **2013**, Vol. 4, № 8, P. 803–812. <https://doi.org/10.1080/2150704X.2013.798710>
62. Lu D., Mausel P., Brondizio E., Moran E. Change detection techniques, *International Journal of Remote Sensing*, **2004**, Vol. 25, № 12, P. 2365–2401. <https://doi.org/10.1080/0143116031000139863>
63. Lunetta R.S., Knight J.F., Ediriwickrema J., Lyon J.G., Worthy L.D. Land-cover change detection using multi-temporal MODIS NDVI data, *Remote Sensing of Environment*, **2006**, Vol. 105, № 2, P. 142–154. <https://doi.org/10.1016/j.rse.2006.06.018>
64. Manandhar R., Odeh I.O.A., Ancev T. Improving the accuracy of land use and land cover classification of Landsat data using post-classification enhancement, *Remote Sensing*, **2009**, Vol. 1, № 3, P. 330–344. <https://doi.org/10.3390/rs1030330>
65. Mannan A., Feng Z., Ahmad A., Liu J., Saeed S., Mukete B. Carbon dynamic shifts with land use change in margallah hills national park, Islamabad (Pakistan) from 1990 to 2017, *Applied Ecology and Environmental Research*, **2018**, Vol. 16, № 3, P. 3197–3214. https://doi.org/10.15666/aecer/1603_31973214
66. Meshesha T.W., Tripathi S.K., Khare D. Analyses of land use and land cover change dynamics using GIS and remote sensing during 1984 and 2015 in the Beressa Watershed Northern Central Highland of Ethiopia, *Modeling Earth Systems and Environment*, **2016**, 2(4), P. 1–12. <https://doi.org/10.1007/s40808-016-0233-4>
67. Moulds S., Buytaert W., Mijic A. Data Descriptor: A spatio-temporal land use and land cover reconstruction for India from 1960–2010, *Scientific Data*, **2018**, Vol. 5, P. 1–11. <https://doi.org/10.1038/sdata.2018.159>
68. Msofe N.K., Sheng L., Li Z., Lyimo J. Impact of land use/cover change on ecosystem service values in the Kilombero valley floodplain, southeastern Tanzania, *Forests*, **2020**, Vol. 11, № 1, P. 1–17. <https://doi.org/10.3390/f11010109>
69. Nabuurs G.J., Lindner M., Verkerk P.J., Gunia K., Deda P., Michalak R., Grassi, G. First signs of carbon sink saturation in European forest biomass, *Nature Climate Change*, **2013**, Vol. 3, № 9, P. 792–796. <https://doi.org/10.1038/nclimate1853>
70. Nery T., Sadler R., Solis A.M., White B., Polyakov M. Discriminating native and plantation forests in a Landsat time-series for land use policy design, *International Journal of Remote Sensing*, **2019**, Vol. 40, № 11, P. 4059–4082. <https://doi.org/10.1080/01431161.2018.1558375>
71. Nurda N., Noguchi R., Ahamed T. Change detection and land suitability analysis for extension of potential forest areas in Indonesia using satellite remote sensing and GIS, *Forests*, **2020**, Vol. 11, № 4, P. 1–22. <https://doi.org/10.3390/f11040398>
72. Obeidat M., Awawdeh M., Lababneh A. Assessment of land use/land cover change and its environmental impacts using remote sensing and GIS techniques, Yarmouk River Basin, north Jordan, *Arabian Journal of Geosciences*, **2019**, Vol. 12, № 22, <https://doi.org/10.1007/s12517-019-4905-z>
73. Pan Y., Birdsall R.A., Fang J., Houghton R., Kauppi P.E., Kurz W.A., et al. A large and persistent carbon sink in the world's forests, *Science*, **2011**, Vol. 333, № 6045, P. 988–993. <https://doi.org/10.1126/science.1201609>
74. Pereira O.J.R., Montes C.R., Lucas Y., Santin R.C., Melfi A.J. A multi-sensor approach for mapping plant-derived carbon storage in Amazonian podzols, *International Journal of Remote Sensing*, **2015**, Vol. 36, № 8, P. 2076–2092. <https://doi.org/10.1080/01431161.2015.1034896>
75. Pineda J.N.B., Bosque S.J., Gómez D.M., Franco P.R. Exploring the driving forces behind deforestation in the state of Mexico (Mexico) using geographically weighted regression, *Applied Geography*, **2010**, Vol. 30, № 4, P. 576–591. <https://doi.org/10.1016/j.apgeog.2010.05.004>
76. Potter C. Ten Years of Vegetation Change in Northern California Marshlands Detected Using Landsat Satellite Image Analysis, *Journal of Water Resource and Protection*, **2013**, Vol. 5, № 5, P. 485–494. <https://doi.org/10.4236/jwarp.2013.55048>
77. Pouliot D., Latifovic R., Zabcic N., Guindon L., Olthof I. Development and assessment of a 250m spatial resolution MODIS annual land cover time series (2000–2011) for the forest region of Canada derived from change-based updating, *Remote Sensing of Environment*, **2014**, Vol. 140, P. 731–743. <https://doi.org/10.1016/j.rse.2013.10.004>

78. Ramachandran R.M., Reddy C. S. Monitoring of deforestation and land use changes (1925–2012) in Idukki district, Kerala, India using remote sensing and GIS, *Journal of the Indian Society of Remote Sensing*, **2017**, Vol. 45, № 1, P. 163–170. <https://doi.org/10.1007/s12524-015-0521-x>
79. Reddy C.S., Satish K.V., Pasha S.V., Jha C.S., Dadhwal V.K. Assessment and monitoring of deforestation and land-use changes (1976–2014) in Andaman and Nicobar Islands, India using remote sensing and GIS, *Current Science*, **2016**, Vol. 111, № 9, P. 1492–1499. <https://doi.org/10.18520/cs/v111/i9/1492-1499>
80. Riitters K., Wickham J., Costanza J.K., Vogt P. A global evaluation of forest interior area dynamics using tree cover data from 2000 to 2012, *Landscape Ecology*, **2016**, Vol. 31, P. 137–148. <https://doi.org/10.1007/s10980-015-0270-9>
81. Riitters K., Wickham J., O'Neill R.O., Jones B., Smith E. Global-Scale Patterns of Forest Fragmentation, *Conservation Ecology*, **2000**, Vol. 4, № 2, <https://www.jstor.org/stable/26271763>
82. Riitters K.H., Wickham J.D., O'Neill R.V., Jones, K.B., Smith E.R., Coulston J.W., et al. Fragmentation of Continental United Forests, *Ecosystems*, **2002**, Vol. 5, № 8, P. 815–822.
83. Rinner C., Patychuk D., Bassil K., Nasr S., Gower S., Campbell M. The role of maps in neighborhood-level heat vulnerability assessment for the city of Toronto, *Cartography and Geographic Information Science*, **2010**, Vol. 37, № 1, P. 31–44. <https://doi.org/10.1559/152304010790588089>
84. Riutta T., Slade E.M., Morecroft M.D., Bebbler D.P., Malhi Y. Living on the edge: Quantifying the structure of a fragmented forest landscape in England, *Landscape Ecology*, **2014**, Vol. 29, № 6, P. 949–961. <https://doi.org/10.1007/s10980-014-0025-z>
85. Ruiz-Benito P., Gómez-Aparicio L., Paquette A., Messier C., Kattge J., Zavala M.A. Diversity increases carbon storage and tree productivity in Spanish forests, *Global Ecology and Biogeography*, **2014**, Vol. 23, № 3, P. 311–322. <https://doi.org/10.1111/geb.12126>
86. Sahana M., Hong H., Sajjad H., Liu J., Zhu A.X. Assessing deforestation susceptibility to forest ecosystem in Rudrapur district, India using fragmentation approach and frequency ratio model, *Science of the Total Environment*, **2018**, Vol. 627, P. 1264–1275. <https://doi.org/10.1016/j.scitotenv.2018.01.290>
87. Santamouris M., Papanikolaou N., Livada I., Koronakis I., Georgakis C., Argiriou A., Assimakopoulos D.N. On the impact of urban climate on the energy consumption of building, *Solar Energy*, **2001**, Vol. 70, № 3, P. 201–216. [https://doi.org/10.1016/S0038-092X\(00\)00095-5](https://doi.org/10.1016/S0038-092X(00)00095-5)
88. Sharma S., Roy P.S. Forest fragmentation in the Himalaya: A Central Himalayan case study, *International Journal of Sustainable Development and World Ecology*, **2007**, Vol. 14, № 2, P. 201–210. <https://doi.org/10.1080/13504500709469720>
89. Tadese M., Kumar L., Koech R., Kogo B.K. Mapping of land-use/land-cover changes and its dynamics in Awash River Basin using remote sensing and GIS, *Remote Sensing Applications: Society and Environment*, **2020**, Vol. 19, № 100352 <https://doi.org/10.1016/j.rsase.2020.100352>
90. Taubert F., Fischer R., Groeneveld J., Lehmann S., Müller M. S., Rödig E., et al. Global patterns of tropical forest fragmentation, *Nature*, **2018**, Vol. 554, № 7693, P. 519–522. <https://doi.org/10.1038/nature25508>
91. Tölle M.H., Engler S., Panitz H.J. Impact of abrupt land cover changes by tropical deforestation on Southeast Asian climate and agriculture, *Journal of Climate*, **2017**, Vol. 30, № 7, P. 2587–2600. <https://doi.org/10.1175/JCLI-D-16-0131.1>
92. Wade T.G., Riitters K.H., Wickham J.D., Jones K.B. Distribution and causes of global forest fragmentation, *Ecology and Society*, **2003**, Vol. 7, № 2, <https://doi.org/10.5751/es-00530-070207>
93. Wang N., Brown D.G., An L., Yang S., Ligmann-Zielinska A. Comparative performance of logistic regression and survival analysis for detecting spatial predictors of land-use change, *International Journal of Geographical Information Science*, **2013**, Vol. 27, № 10, P. 1960–1982. <https://doi.org/10.1080/13658816.2013.779377>
94. Wickham J.D., Riitters K.H., Wade T.G., Vogt P. A national assessment of green infrastructure and change for the conterminous United States using morphological image processing, *Landscape and Urban Planning*, **2010**, Vol. 94 (3–4), P. 186–195. <https://doi.org/10.1016/j.landurbplan.2009.10.003>
95. Wolken J.M., Hollingsworth T.N., Rupp T.S., Chapin F.S., Trainor S.F., Barrett T.M., et al. Evidence and implications of recent and projected climate change in Alaska's forest ecosystems, *Ecosphere*, **2011**, Vol. 2, № 11, <https://doi.org/10.1890/ES11-00288.1>
96. Wu J. Key concepts and research topics in landscape ecology revisited: 30 years after the Allerton Park workshop, *Landscape Ecology*, **2013**, Vol. 28, № 1, P. 1–11. <https://doi.org/10.1007/s10980-012-9836-y>
97. Wylie B., Rigge M., Brisco B., Murnaghan K., Rover J., Long J. Effects of disturbance and climate change on ecosystem performance in the Yukon River basin boreal forest, *Remote Sensing*, **2014**, Vol. 6, № 10, P. 9145–9169. <https://doi.org/10.3390/rs6109145>
98. Yang X., Lo C.P. Using a time series of satellite imagery to detect land use and land cover changes in the Atlanta, Georgia metropolitan area, *International Journal of Remote Sensing*, **2002**, Vol. 23, № 9, P. 1775–1798. <https://doi.org/10.1080/01431160110075802>
99. Yemshanov D., Koch F.H., Riitters K.H., McConkey B., Huffman T., Smith S. Assessing land clearing potential in the Canadian agriculture-forestry interface with a multi-attribute frontier approach, *Ecological Indicators*, **2015**, Vol. 54, P. 71–81. <https://doi.org/10.1016/j.ecolind.2015.02.019>
100. Zaiatz A.P.S.R., Zolin C.A., Vendrusculo L.G., Lopes T.R., Paulino J. Agricultural land use and cover change in the Cerrado/Amazon ecotone: A case study of the upper Teles Pires river basin, *Acta Amazonica*, **2018**, Vol. 48, № 2, P. 168–177. <https://doi.org/10.1590/1809-4392201701930>

101. Zha Y., Gao J., Ni S. Use of normalized difference built-up index in automatically mapping urban areas from TM imagery, *International Journal of Remote Sensing*, **2003**, Vol. 24, № 3, P. 583–594, <https://doi.org/10.1080/01431160304987>
102. Zhang C., Wang X., Liu Y. Changes in quantity, quality, and pattern of farmland in a rapidly developing region of China: a case study of the Ningbo region, *Landscape and Ecological Engineering*, **2019**, Vol. 15, № 3, P. 323–336. <https://doi.org/10.1007/s11355-019-00382-x>
103. Zhang H., Qi, Z. fang, Ye X. yue, Cai Y. bin, Ma W. chun, Chen M. nan. Analysis of land use/land cover change, population shift, and their effects on spatiotemporal patterns of urban heat islands in metropolitan Shanghai, China, *Applied Geography*, **2013**, Vol. 44, P. 121–133. <https://doi.org/10.1016/j.apgeog.2013.07.021>
104. Zhang L., Pan T., Zhang H., Li X., Jiang L. The effects of forest area changes on extreme temperature indexes between the 1900s and 2010s in Heilongjiang Province, China, *Remote Sensing*, **2017**, Vol. 9, № 12, <https://doi.org/10.3390/rs9121280>
105. Zhang Q., Li B., Thau D., Moore R. Building a better Urban picture: Combining day and night remote sensing imagery, *Remote Sensing*, **2015**, Vol. 7, № 9, P. 11887–11913. <https://doi.org/10.3390/rs70911887>
106. Zhu E., Deng J., Zhou M., Gan M., Jiang R., Wang K., Shahtahmassebi A.R. Carbon emissions induced by land-use and land-cover change from 1970 to 2010 in Zhejiang, China, *Science of the Total Environment*, **2019**, Vol. 646, P. 930–939. <https://doi.org/10.1016/j.scitotenv.2018.07.317>

FOREST PHENOLOGICAL TRENDS IN THE MIDDLE AND HIGH LATITUDE OF THE NORTHERN HEMISPHERE

Qi Shao^{1,2,3}, Chao Huang⁴, Jing Feng Huang^{1,2,3}

¹Institute of Applied Remote Sensing and Information Technology, Zhejiang University,

²Key Laboratory of Environment Remediation and Ecological Health, Ministry of Education, College of Environmental Resource Sciences, Zhejiang University

³Key Laboratory of Agricultural Remote Sensing and Information Systems, Hangzhou, Zhejiang Province

⁴Institute of Applied Ecology, Chinese Academy of Sciences

Vegetation phenology is the study of periodically recurring patterns of growth and development of plants, which affect terrestrial ecosystem carbon, energy budget balance, fire disturbance, and climate–biosphere interactions. The increases in surface temperature had already altered the extent of vegetation phenology. Vegetation phenology can make some responses to climate factors, and the current climate change has attracted more research for the trend of vegetation phenology and its causes. The purpose of this paper is to investigate the spatial and temporal trend of forest phenology at mid and high latitude in the Northern Hemisphere (50°N–90°N, 180°W–180°E) over the period 2001–2017 using Collection 6 MODIS Land Cover Dynamics (MCD12Q2) datasets. The results indicated that SOS has a significant advanced trend, EOS has a significant delayed trend and LOS showed a significant extended trend on the whole. The significant advancement of SOS and extension of LOS mainly occurred in central Russia, the north and southwest of North America. Meanwhile, EOS showed a delayed trend in the south of Russia, the north and southwest of Canada and Alaska.

Keywords: forest phenology, climate change, MODIS, remote sensing, Northern Hemisphere, GEE.

Introduction

The climate determines the phenology through its influence on temperature and precipitation. Climate change affects vegetation productivity changes, and it also causes changes in the biogeochemical cycle, which affect the structure of communities and ecosystems (Piao et al., 2008). According to the 2013 Report of IPCC (the Intergovernmental Panel on Climate Change), global warming is intensified with the impact of human activities (IPCC, 2014). From 1880 to 2012, the average surface temperature on a global scale increased by 0.85 °C, which affects vegetation phenology.

Vegetation phenology is a sensor of climate change (Wang, 2019). Vegetation has a better response to changes in the external environment, and this response is easy to observe, mainly in the phenological characteristics of the start of growing season, the end of season, etc. At the same time, phenological change affects the exchange of carbon, water and energy between vegetation and the atmosphere so that it is the driving force of global climate change (Loboda et al., 2017; Delbar et al., 2015; Richardson et al., 2013; White et al., 2009). Therefore, the study of vegetation phenology changes in the long-term sequence is very important.

Due to the advantages of remote sensing technology in large-area synchronous observation and periodicity at regional and global scales (Myneni et al., 1997; Zhang et al., 2003), the products based on remote sensing satellite data are produced. NDVI and EVI can well show the growth dynamics of vegetation. The most commonly used remote sensing phenological product sources are NDVI derived from the Advanced Very High Resolution Radiometer (AVHRR) (Tucker et al., 2001), NDVI derived from the Systeme Probatoire d'Observation de la Terre (SPOT), as well as NDVI and EVI derived from the Moderate-resolution Imaging Spectroradiometer (MODIS). Although the time range of AVHRR data is long, its spatial resolution is only 8 km. The SPOT NDVI dataset has a spatial resolution of 1 km. Compared with the former two, MODIS data has a higher spatial resolution, which is of great significance for the distribution study of forest phenological change trend.

Previous studies have reported hemispheric or local changes in growing seasons (Vorobev et al., 2019; Jeong et al., 2009; Jeong et al., 2011; Myneni et al., 1997; Shen et al., 2014; Zhou et al., 2001). In recent years, some researches indicated a global warming hiatus between 1998 and 2012 (Medhaug et al., 2017). Therefore, the hiatus of global warming has attracted widespread attention. For instance, Fu et al. (2015) demonstrated that the apparent response of leaf unfolding to climate warming has significantly decreased from 1980 to 2013 in seven dominant European tree species. The previous studies (Jeong et al., 2009; Jeong et al., 2011; Wang et al., 2019) found that the trend of vegetation growth season advancement has been stagnant during the global warming hiatus.

In some countries and regions, the advanced onset of vegetation growing season and the accumulation of forest fuel caused by climate warming have also led to an increasing number of large and severe wildfires (Westerling et al., 2006). Therefore, the study of forest phenological changes has an essential reference for understanding the occurrence of wildfire. Accurate trend information of forest phenology is essential to understand regional-to-global carbon budgets and climate change (Peng et al., 2017). However, there are few studies on forest phenological changes at present.

Purpose of work

The main goal of this study is to investigate the change trend of forest phenology in the middle and high latitudes of the Northern Hemisphere. Furthermore, the spatial distribution of the changing trend of forest phenology in different regions is analyzed, thus making a preliminary analysis of the response forest phenology to climate change.

Area of research

The Northern Hemisphere has the largest climate warming at middle and high latitudes, which is about two times faster than other areas. Moreover, the vegetation of terrestrial ecosystems in the mid-high latitudes of the Northern Hemisphere is very susceptible to climate change. Besides, this region is relatively less affected by human activities and can better reflect the impacts of climate change on vegetation phenology. Therefore, we selected the Northern Hemisphere with latitude greater than 50° to estimate forest phenology.

Materials and methods of research

Data

Phenology data from MCD12Q2

Vegetation phenology data is obtained from the Collection 6 (C6) MODIS Land Cover Dynamics Product (MCD12Q2), which offers global land surface phenology metrics at 500 m spatial resolution and annual time step since 2001. Phenometrics is derived from time series of MODIS observed land surface greenness, particularly time series of the 2-band Enhanced Vegetation Index calculated from MODIS nadir BRDF adjusted surface reflectance (NBAR-EVI2). It contains many science data sets (SDS), including greenup, dormancy, QA_Overall and so on. In this study, QA_Overall was used to quality control, SOS was showed by green up and EOS was showed by dormancy. LOS was calculated by the difference between SOS and EOS. The dataset was accessed and processed on the platform of Google Earth Engine (GEE).

Land cover from MCD12Q1

The vegetation classification data used in this study comes from the Moderate Resolution Imaging Spectroradiometer (MODIS) Land Cover Type Product (MCD12Q1), which provides a suite of science data sets that map global land cover at 500 m spatial resolution. It includes five legacy classification schemes, such as the International Geosphere-Biosphere Programme (IGBP), Uni-

iversity of Maryland (UMD), Leaf Area Index (LAI), BIOME-Biogeochemical Cycles (BGC), and Plant Functional Types (PFT). The dataset of IGBP classification schemes was chosen in this study. Evergreen needleleaf forests, evergreen broadleaf forests, deciduous needleleaf forests, deciduous broadleaf forests, mixed forests, closed shrublands, and open shrublands were selected as the study plots for this research. The legend and description were showed in table 1. A multiyear stable forest-covered region was generated from annual MCD12Q1 over the period from 2001 to 2017. The dataset was processed and downloaded on the GEE platform.

Table1

MCD12Q1 International Geosphere-Biosphere Programme (IGBP) legend

Value	Name	Description
1	Evergreen Needleleaf Forests	Dominated by evergreen conifer trees (canopy >2m). Tree cover >60%.
2	Evergreen Broadleaf Forests	Dominated by evergreen broadleaf and palmate trees (canopy >2m). Tree cover >60%.
3	Deciduous Needleleaf Forests	Dominated by deciduous needleleaf (larch) trees (canopy >2m). Tree cover >60%.
4	Deciduous Broadleaf Forests	Dominated by deciduous broadleaf trees (canopy >2m). Tree cover >60%.
5	Mixed Forests	Dominated by mixed canopy (2m) of evergreen (40%) and deciduous (60%) of each tree
6	Closed Shrublands	Dominated by woody perennials (1-2m height) >60% cover.
7	Open Shrublands	Dominated by woody perennials (1-2m height) 10-60% cover.

Data Analyses

The changing trend of each pixel in time series was calculated by the linear regression model (Xu et al., 2004) through IDL programming. The slope of each pixel was calculated by the unitary linear regression analysis method. The inter-annual rate of change and the inter-annual spatial distribution of each parameter in the study area were obtained from 2001 to 2017. The calculation formula is as follows:

$$SLOPE = \frac{n \times \sum_{i=1}^n i \times X_i - \sum_{i=1}^n i \times \sum_{i=1}^n X_i}{n \times \sum_{i=1}^n i^2 - (\sum_{i=1}^n X_i)^2}, \quad (1)$$

where i is serial number of year, X_i is the actual pixel value for a year. If $SLOPE$ is greater than 0, the parameter is increasing trend, and vice versa.

T-test was used to evaluate the significance of the results (Li,2019). It was calculated as follows:

$$t = \frac{b}{S_b}, \quad (2)$$

The b and S_b were calculated as follows:

$$b = \frac{\sum_{i=1}^n (X_i - \bar{X}) \times \sum_{i=1}^n (i - \bar{i})}{\sum_{i=1}^n (X_i - \bar{X})^2}, \quad (3)$$

$$S_b = \frac{S_x}{\sqrt{\sum_{i=1}^n (X_i - \bar{X})^2}}, \quad (4)$$

$$S_x = \sqrt{\frac{\sum_{i=1}^n (i - \hat{i})^2}{n-2}}, \quad (5)$$

where S_b is the standard deviation of regression coefficient, S_x is the standard error of estimation for regression equation.

Research results

The overall trend of forest phenology at the middle and high latitudes of the Northern Hemisphere was analyzed (fig.1). From 2001 to 2017, SOS (start of the growing season), EOS (end of growing season), and LOS (length of the growing season) had a significant trend at the $P < 0.01$ level. Consistent with the previous studies (Chen et al., 2020; Pulliainen et al., 2017; Tucker et al., 2001), we found that SOS was significantly advanced ($P < 0.01$), the advance rate was $0.70 \text{ days year}^{-1}$. In contrast to our result, an earlier study (Wang, 2019) reported that EOS has a postponement trend at the end of growing season in the Northern Hemisphere from 1982 to 2015, but the change is not significant. However, we found that EOS showed a significant delayed trend from 2001 to 2017 with a rate of $0.27 \text{ days year}^{-1}$. The small differences in results may be due to differences in the study area and time range. It has been previously reported that LOS showed a postponed trend with a more pronounced change range from 1948 to 1996 (Ahas et al., 2000). In our result, LOS was significantly extended ($P < 0.01$) from 2001 to 2017, the extended rate was $0.96 \text{ days year}^{-1}$.

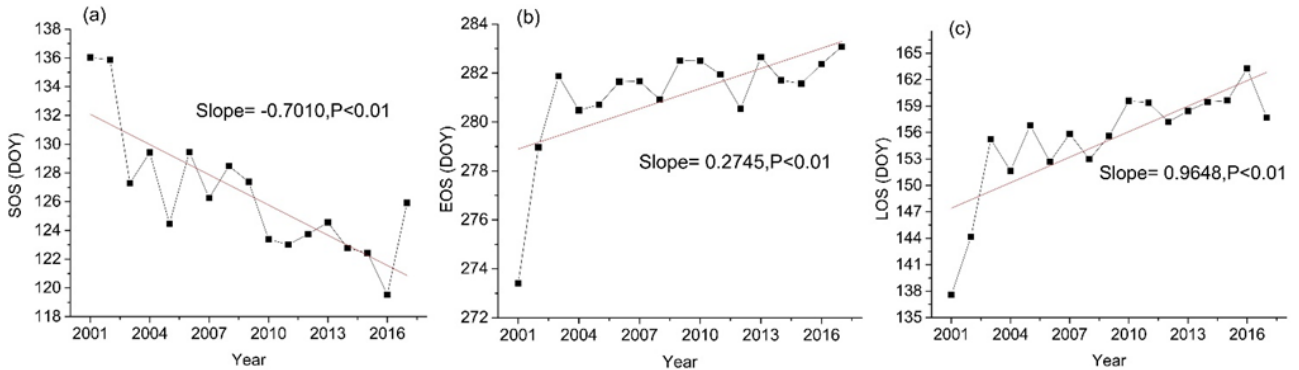


Fig.1. Vegetation phenology parameters trends. across forest area of mid and high latitude in the Northern Hemisphere(50°-90°N,180°W-180°E) from 1982 to 2014, including two snow parameters:(a) SOS (start of growing season),(b) EOS (end of growing season) and (c)LOS(length of growing season)

For the SOS, 79.41% of the area showed an advancement trend. 15.50% pixels were significantly advanced, which mainly distributed in central Russia, the north and southwest of North America. 20.59% of the pixels had a delayed trend and 0.32% were significantly delayed. The reason for this result may be the melting period of snow in the Northern Hemisphere high latitudes, which is significantly advanced with the warming of the climate, thus leading to the advancement of the spring phenology of vegetation (Pulliainen et al., 2017).

EOS showed an advanced trend of 32.06% on the study area; 67.94% of the area showed a delayed trend. The delayed pixels accounted for a greater proportion of the pixels than the earlier ones. Among them, 1.75% of pixels were significantly advanced and distributed in north central Russia. 10.51% pixels were significantly delayed, mainly distributed in the south of Russia, north and southwest of Canada and Alaska.

For the LOS, 22.19% of LOS has a short trend, and 77.81% of LOS showed an extended trend. Among them, 0.92% of pixels were significantly short and 19.54% of pixels were significantly extended. The spatial distribution is roughly similar to that of SOS. It is worth mentioning that the

significantly extended area of LOS is greater than that of EOS, resulting from a synergistic effect with the advancement of SOS.

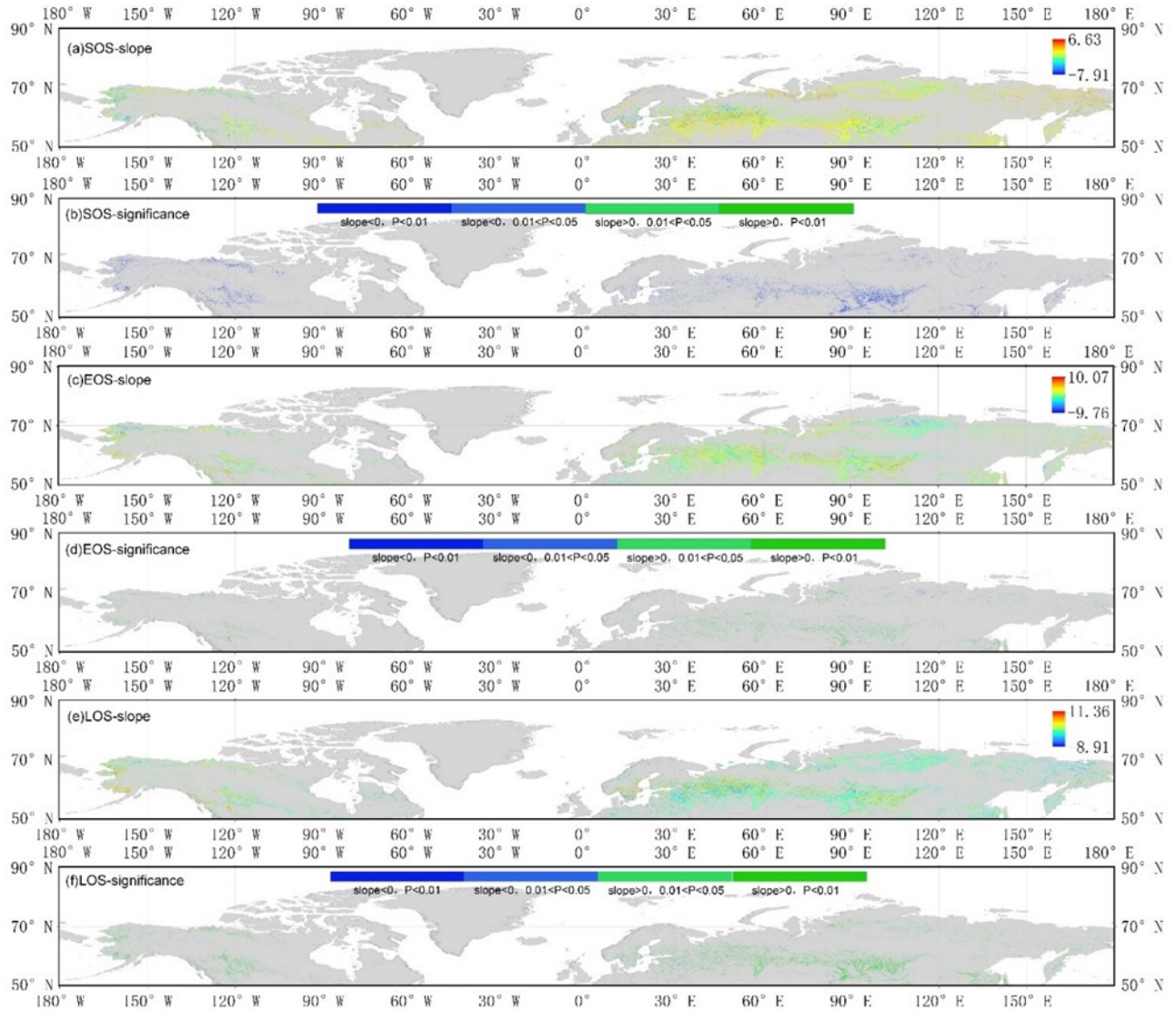


Fig. 2. Spatial patterns of vegetation phenology parameters trend across forest area of mid and high latitude in the Northern Hemisphere (50°-90°N, 180°W-180°E), including: (a) slope of SOS (start of growing season), (b) significance of SOS, (c) slope of EOS (end of growing season), (d) significance of EOS, (e) slope of LOS (length of growing season) and (f) significance of LOS (length of growing season)

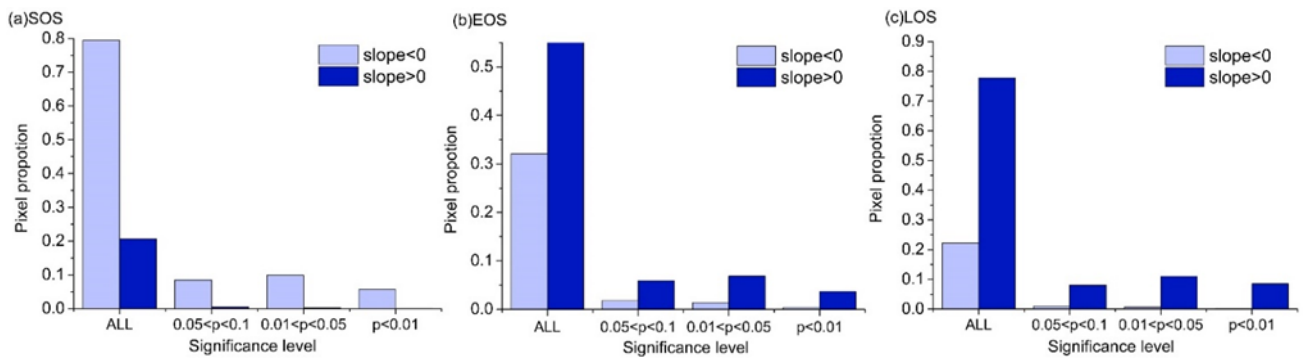


Fig. 3. The proportion of changing trend pixels at different significance levels in ALL pixels in the study area. ALL represents the total number at ALL significance levels, slope < 0 represents the advanced trend of parameters, and vice versa, including: (a) SOS, (b) EOS, (c) LOS

Conclusions

Based on long-term satellite data, our results found that SOS has a significant advanced trend, EOS and LOS has a significant delayed and extended tendency throughout the period 2001–2017 on the forest area of mid and high latitude in the Northern Hemisphere (50°N–90°N, 180°W–180°E) on the whole. The significantly advanced SOS and extended LOS are mainly distributed in central Russia, the north and southwest of North America. The significantly delayed EOS is mainly distributed in the south of Russia, the north and southwest of Canada and Alaska.

This work is funded by a “GIS and Remote Sensing for Sustainable Forestry and Ecology/SUFOGIS” of the Erasmus+. We thank GEE for providing the platform of accessing and processing data.

The European Commission support for the production of this publication does not constitute an endorsement of the contents which reflects the views only of the authors, and the Commission cannot be held responsible for any use which may be made of the information contained therein.

References

1. Ahas R., Jaagus J., Aasa A. The phenological calendar of Estonia and its correlation with mean air temperature. *International Journal of Biometeorol*, **2000**, 44, 159–166 <https://doi.org/10.1007/s004840000069>
2. Chen X., Yang Y. Observed earlier start of the growing season from middle to high latitudes across the Northern Hemisphere snow-covered landmass for the period 2001–2014. *Environmental Research Letters*, **2020**, 15, 34042. <https://iopscience.iop.org/article/10.1088/1748-9326/ab6d39>
3. Delbart N., Beaubien E., Kergoat L., Le Toan, T. Comparing land surface phenology with leafing and flowering observations from the PlantWatch citizen network. *Remote Sensing of Environment*, **2015**, 160, 273–280. <https://doi.org/10.1016/j.rse.2015.01.012>
4. Fu Y.H., Zhao H., Piao S., Peaucelle M., Peng S., Zhou G., et al. Declining global warming effects on the phenology of spring leaf unfolding. *Nature*, **2015**, 526, 104–107 <https://doi.org/10.1038/nature15402>
5. IPCC, 2014. Climate change 2014: impacts, adaptation, and vulnerability. Part A: Global and Sectoral Aspects. Contribution of Working Group II to the Fifth Assessment Report of the Intergovernmental Panel on Climate Change. In: Cambridge University Press, Cambridge, United Kingdom and New York, NY, USA.
6. Jeong S.J., Ho C.H., Gim H.J., Brown M.E. Phenology shifts at start vs. end of growing season in temperate vegetation over the Northern Hemisphere for the period 1982–2008. *Global Change Biology*, **2011**, 17, 2385–2399.
7. Jeong S.J., Ho C.H., Jeong J.H. Increase in vegetation greenness and decrease in springtime warming over East Asia. *Geophysical Research Letters*, **2009**, 36, L02710 <https://doi.org/10.1029/2008GL036583>
8. Loboda, T., O. Krankina O., I. Savin I., E. Kurbanov E., H. Joanne H. Land Management and the Impact of the 2010 Extreme Drought Event on the Agricultural and Ecological Systems of European Russia/ T. Loboda. // In book “Land-Cover and Land-Use Changes in Eastern Europe after the Collapse of the Soviet Union in 1991”. Eds. G. Gutman, R. Volker. - **2017**, Springer International Publishing. Pp. 173—192. https://doi.org/10.1007/978-3-319-42638-9_8 doi=10.1007/978-3-319-42638-9_8
9. Medhaug I., Stolpe M.B., Fischer E.M., Knutti R. Reconciling controversies about the “global warming hiatus”. *Nature*, **2017**, 545, 41–47 <https://doi.org/10.1038/nature22315>
10. Myneni R.B., Keeling C.D., Tucker C.J., Asrar G., Nemani R.R. Increased plant growth in the Northern high latitudes from 1981 to 1991. *Nature*, **1997**, 386, 698–702 <https://doi.org/10.1038/386698a0>
11. Peng D., Wu C., Li C., Zhang X., Liu Z., Ye H., et al. Spring green-up phenology products derived from MODIS NDVI and EVI: Intercomparison, interpretation and validation using National Phenology Network and AmeriFlux observations. *Ecological Indicators*, **2017**, 77, 323–336 <https://doi.org/10.1016/j.ecolind.2017.02.024>
12. Piao S.L., Ciais P., Friedlingstein P., Peylin P., Reichstein M., Luyssaert S., et al. Net carbon dioxide losses of Northern ecosystems in response to autumn warming, *Nature*, **2008**, 451, 49–52. <https://doi.org/10.1038/nature06444>
13. Pulliainen J., Aurela M., Laurila T., Aalto T., Takala M., Salminen M., et al. Early snowmelt significantly enhances boreal springtime carbon uptake. *Proceedings of the National Academy of Sciences of the United States of America*, **2017**, 114, 11081–11086 <https://doi.org/10.1073/pnas.1707889114>
14. Richardson A.D., Keenan T.F., Migliavacca M., Ryu Y., Sonnentag O., Toomey M. Climate change, phenology: and phenological control of vegetation feedbacks to the climate system. *Agricultural and Forest Meteorology*, **2013**, 169, 156–173 <https://doi.org/10.1016/j.agrformet.2012.09.012>
15. Shen M.G., Zhang G., Cong N., Wang S., Kong W., Piao S. Increasing altitudinal gradient of spring vegetation phenology during the last decade on the Qinghai–Tibetan Plateau. *Agricultural and Forest Meteorology*, **2014**, 189, 71–80 <https://doi.org/10.1016/j.agrformet.2014.01.003>
16. Tucker C.J., Slayback D.A., Pinzon J.E., Los S.O., Myneni R.B., Taylor M.G. Higher Northern latitude normalized difference vegetation index and growing season trends from 1982 to 1999. *International Journal of Biometeorology*, **2001**, 45, 84–190 <https://doi.org/10.1007/s00484-001-0109-8>

17. Vorobev O.N., Kurbanov E.A., Demisheva E.N., Menshikov S.A., Smirnova L.N. Algorithm for reviling the phenological parameters of forest cover on the base of time series of satellite data. *Vestnik of Volga State University of Technology. Ser. Forest. Ecology. Nature Management*. **2019**. 41, 5-20 (in Russian)
18. Wang X., Xiao J., Li X., Cheng G., Ma M., Zhu G., et al. No trends in spring and autumn phenology during the global warming hiatus. *Nature Communications*, **2019**, 2389 <https://doi.org/10.1038/s41467-019-10235-8>
19. Wang X.Y. Study on the simulation and influence mechanism of regional vegetation phenology based on multi-source data. University of Chinese Academy of Sciences, **2018** (In Chinese).
20. Westerling A.L., Hidalgo H.G., Cayan D.R., Swetnam T.W. Warming and earlier spring increase western US forest wildfire activity. *Science*, **2006**, 313, 940–943 <https://doi.org/10.1126/science.1128834>
21. White M.A., De Beurs K.M., Didan K., Inouye D.W., Richardson A.D., et al. Intercomparison, interpretation, and assessment of spring phenology in North America estimated from remote sensing for 1982–2006. *Global Change Biology*, **2009**, 15, 2335–2359 <http://dx.doi.org/10.1111/j.1365-2486.2009.01910.x>
22. Xu Y., Lu P., Yu Q. Review and Prospect in the Researches of Influence of Climate Change on Plant Phenology. *Resources Science*, **2004**, 26, 129-136 <https://europepmc.org/article/cba/461782>
23. Zhang X., Friedl M.A., Schaaf C.B., Strahler A.H., Hodges J.C.F., Gao F., et al. Monitoring vegetation phenology using MODIS. *Remote Sensing of Environment*. **2003**, 84, 471–475 [https://doi.org/10.1016/S0034-4257\(02\)00135-9](https://doi.org/10.1016/S0034-4257(02)00135-9)
24. Zhou L., Tucker C.J., Kaufmann R.K., Slayback D., Shabanov N.V., Myneni R.B. Variations in Northern vegetation activity inferred from satellite data of vegetation index during 1981 to 1999. *Journal of Geophysical Research Atmospheres*, **2001**, 106, 20069–20083. <https://doi.org/10.1029/2000JD000115>

ОЦЕНКА ИЗМЕНЕНИЙ В ЛЕСАХ ЮГА СРЕДНЕРУССКОЙ ВОЗВЫШЕННОСТИ ПО СПУТНИКОВЫМ ДАННЫМ

Э.А. Терехин

Белгородский государственный национальный исследовательский университет

Оценка изменений в лесах, обусловленных влиянием негативных факторов, является одной из ключевых задач мониторинга лесных земель. В статье изложен новый подход к автоматизированному геоинформационному картографированию участков лесов с нарушенным древостоем. Метод основан на оценке изменений в высотах лесных насаждений с использованием спектрального отклика. Исследование выполнено на примере лесных массивов юга Среднерусской возвышенности, охватывающего территорию Белгородской области. Для оценки высот предложено использовать логистическую модель, описывающую зависимость коэффициентов спектральной яркости SWIR-диапазона от высоты древостоя. Для повышения точности оценки высот предложено использовать виды моделей, использующие спектральные характеристики с конкретных спутниковых сенсоров. Критерием индикации участков нарушенности древостоя является резкое снижение высоты лесных насаждений, обусловленное влиянием негативных факторов. Ограничениями применения метода являются региональные особенности лесных экосистем, наличие участков теней от лесных массивов, расположенных на крутых склонах. С использованием предложенного подхода выполнено геоинформационное картографирование изменений в лесах юга Среднерусской возвышенности в период середины 1980-х – конец 2010-х гг. Подготовлена серия картосхем, пространственно характеризующих произошедшие изменения. С использованием средств геоинформационного анализа выполнена оценка доли нарушенных лесных экосистем в каждом административном районе Белгородской области. В большинстве районов произошло снижение доли нарушенных лесных участков. Установлено, что в исследуемый период доля нарушенных лесных участков на юге Среднерусской возвышенности была сравнительно невелика и составила 1,84 % от общей площади лиственных лесов в середине 1980-х – конце 1990-х гг. и 0,85% в период 2000-2017 гг.

Ключевые слова: лесные экосистемы, лесостепь, нарушенность лесов, геоинформационное картографирование, спутниковые данные, Landsat

ASSESSMENT OF CHANGES IN THE FOREST OF CENTRAL RUSSIAN UPLAND USING REMOTE SENSING DATA

E.A. Terekhin

Belgorod State National Research University

The assessment of changes in forests caused by the influence of negative factors is one of the key objectives of forest monitoring. The article presents a new approach to automated mapping of forest areas with disturbed stands. The method is based on the estimation of changes in the heights of forest stands using a spectral response. The research was carried out using forest areas in the south of the Central Russian Upland, in the Belgorod Region. In order to assess the heights of the stand, it was proposed to use a logistic model that describes the dependence of the SWIR range spectral response on the height of the forest stand. In order to improve the accuracy of estimating stand heights, it was proposed to use the types of models that use spectral characteristics from specific satellite sensors. The criterion for identifying areas of disturbance in the stand is a significant decrease in the height of forest stands, occurring as a result of negative factors impact. The regional features of forests and shadowed areas on steep slopes can be considered to be the major limitations of the method. The proposed approach enabled the authors to carry out geoinformation mapping of the changes in the forests in the south of the Central Russian Upland over the period from the mid-1980s to the end of 2010s. Schematic maps characterizing the occurring changes have been prepared. Using geoinformation analysis, the share of disturbed forest ecosystems in each administrative district of the Belgorod Region has been estimated. In many districts, the share of disturbed forest ecosystems has decreased. During the reference period the share of disturbed forest areas in the south of the Central Russian Upland was relatively small. It was 1.84% of the total deciduous forest area in the mid-1980s - late 1990s and 0.85% in the period 2000-2017.

Key words: forest ecosystems, forest-steppe, forest disturbance, GIS-mapping, satellite data, Landsat

Введение. Оценка изменений в лесах, обусловленных воздействием негативных факторов, является ключевой задачей мониторинга покрытых лесом земель. В значительной степени она связана с пространственно-временным анализом изменений в лесах, обусловленных влиянием сплошных рубок, пожаров, насекомых-вредителей. В связи с этим актуальность приобретают разработка и совершенствование подходов к выявлению таких изменений, что во многом связано с использованием возможностей данных дистанционного зондирования Земли. Это направление достаточно интенсивно развивается в настоящее время, что во многом обусловлено повышением доступности материалов разновременной спутниковой съёмки и развитием технологий её обработки (Курбанов и др., 2014; Senf et al., 2017; Novo-Fernández, 2018; Ховратович и др., 2019). На текущий момент предложен ряд подходов к автоматизированному картографированию изменений в лесах на разных территориальных уровнях: в первую очередь глобальном и региональном (Healey et al., 2005; Kennedy et al., 2010; Барталев, Лупян, 2013; Курбанов и др., 2015; Potapov et al., 2015). Современные методы выявления изменений используют различные алгоритмы: применение пороговых значений спектральных признаков при выделении исследуемых классов объектов, сегментацию изображений, методы индикации различий на основе сравнения пар разновременных снимков, методы статистического определения границ, включая методы многомерного анализа, использование моделей регрессии.

Тем не менее, данная проблема остаётся во многом открытой в связи с региональными и локальными особенностями лесных экосистем, обусловленными породным составом, фазовыми, а также с появлением новых типов спутниковых данных (Banskota et al., 2014; Zhu, 2017). Эффективное автоматизированное картографирование изменений в лесах на субрегиональном и локальном уровнях обуславливает необходимость разработки регионально адаптированных подходов к автоматизированному определению характеристик лесных массивов и изменений, происходящих в них.

Появление регулярно получаемых многозональных снимков высокого радиометрического разрешения, в первую очередь, Landsat-8, позволило на новом уровне подойти к проблеме количественного анализа биометрических параметров лесных экосистем на основе их спектрально-отражательных признаков. Обусловлено это более высокими информационными возможностями данных Landsat OLI по сравнению с сенсорами предыдущего поколения.

На территории юга Среднерусской возвышенности, охватывающего Белгородскую область и расположенного преимущественно в зоне лесостепи, преобладают лесные насаждения лиственного породного состава. Основная часть лесов отнесена к категории водоохранных и защитных, играющих важное экологическое значение. Большинство лесов относится к нагорным дубравам. Вследствие длительного аграрного освоения в прошедшие столетия площадь земель, покрытых лесом, значительно сократилась и в настоящее время леса представлены преимущественно отдельными сравнительно небольшими лесными массивами. Покрытые лесом земли характеризуются высокой фрагментированностью (Украинский и др., 2017). Вместе с этим в последние десятилетия в регионе наблюдаются тенденции увеличения лесистости (Терехин, Чендев, 2018).

Цель исследования состояла в оценке изменений в лиственных лесах юга Среднерусской возвышенности (территория Белгородской области), обусловленных воздействием нарушающих факторов, разработке новых подходов к автоматизированному картографированию участков нарушенных лесов на основе количественного анализа биометрических параметров лесных массивов и их спектрального отклика. Анализируемый временной интервал включал период с середины 1980-х по конец 2010-х гг.

Задачами исследования являлись:

1. Автоматизированное картографирование изменений в лесах, обусловленных ухудшением состояния древостоя, на юге Среднерусской возвышенности в период середины 1980-х – кон. 2010-х гг.
2. Пространственно-временная оценка участков нарушенных лесных экосистем.
3. Оценка доли нарушенных лесов от общей площади лесных массивов в пределах административных районов Белгородской области.

Материалы, объект и методы исследования. Объектом исследования выступали лиственные леса Белгородской области (рис. 1), суммарной площадью 212651, 1 га при средней площади 73,9 га.



Рис. 1. Местоположение территории исследования

Исследование охватывало 2875 лесных массивов региона, что составляет подавляющую часть лиственных лесов Белгородской области. Для автоматизированного выявления изменений в лесах был предложен новый подход, основанный на количественном анализе биометрических параметров лесных насаждений с использованием их спектрального отклика. Он заключается в выявлении участков лесов с нарушенным древостоем на основе оценки изменений в высотах лесных насаждений, которые в свою очередь измеряются на основе их коэффициентов спектральной яркости. Оценка спектрально-отражательных свойств была осуществлена на основе разновременных космических снимков Landsat TM, ETM+, OLI, полученных с середины 1980-х гг. по конец 2010-х гг.

Снимки серии Landsat являются практически единственным типом спутниковых данных, позволяющих провести данное исследование благодаря длинному периоду спутниковой съёмки и возможности формирования полного покрытия изображений на всю область на конкретные сроки.

В рамках ранее проведённых работ (Терехин, 2012) установлено, что возраст и высота лесных насаждений оказывают статистически значимое влияние на коэффициенты спектральной яркости (КСЯ) лесных экосистем. Наиболее чувствительными к изменениям в возрасте и высоте лесных насаждений являются коэффициенты отражения инфракрасной зоны спектра (1,55-1,75 мкм) – SWIR-диапазон, соответствующий каналу 5 сенсоров Landsat TM,

ETM+ и каналу 6 сенсора Landsat OLI. Зависимость между исследуемыми показателями может быть использована для количественной оценки высоты лесных насаждений на основе их спектрального отклика. Повышение высот лесных насаждений является следствием нормального развития лесных массивов. Соответственно участки их резкого снижения являются следствием воздействия нарушающих факторов, например, сплошных рубок. Оценка высоты в свою очередь может быть проведена на основе коэффициентов спектральной яркости, достаточно тесно коррелирующих с ней.

Для оценки высоты лесных насаждений использована предложенная зависимость между высотой древостоя и его коэффициентами спектральной яркости SWIR-диапазона. Она имеет вид логистической кривой и получена на основе фактических данных о характеристиках высот лесных насаждений, типичных для региона, и соответствующих им значений КСЯ, измеренных на основе августовских снимков Landsat. Для повышения точности проводимых вычислений использовали два вида зависимости. Первый – полученный на основе данных Landsat TM/ETM+, второй – на основе данных Landsat OLI.

На основе снимков Landsat ETM+ она имеет вид

$$y = 28 - \frac{27,8}{(1 + e^{-90,045x})^{190788,0}}, \quad (1)$$

где y – значения высот, x – значения коэффициентов спектральной яркости SWIR1-диапазона (5-й канал сенсора Landsat TM/ETM+).

На основе данных Landsat OLI она имеет следующие параметры:

$$y = 28 - \frac{27,8}{(1 + e^{-92,3x})^{665276,0}}, \quad (2)$$

где y – значения высот, x – значения коэффициентов спектральной яркости SWIR1-диапазона (6-й канал сенсора Landsat OLI).

Коэффициенты спектральной яркости, используемые в уравнениях 1 и 2, являются безразмерными величинами, принимающими значения в диапазоне от 0 до 1. Они рассчитаны на основе атмосферно и радиометрически скорректированных спутниковых снимков.

Картографирование высоты лесных насаждений было выполнено на три временных среза: середина 1980-х гг., начало 2000-х, конец 2010-х гг. На каждый из них было сформировано полное покрытие территории Белгородской области снимками Landsat, полученными в период августа, являющегося наименее безоблачным месяцем (табл. 1). Растровые модели высот лесных насаждений на периоды середины 1980-х и начала 2000-х гг. вычисляли на основе уравнения (1), растры высот на 2017-2018 гг. – на основе уравнения (2).

Таблица 1

Спутниковые данные Landsat, используемые для оценки высот насаждений и автоматизированного картографирования изменений в лесах на юге Среднерусской возвышенности

Path/Row	Период съёмки и даты получения снимков		
	1980-е гг.	2000-е гг.	2010-е гг.
178/025	07.08.1986	13.08.2000	31.08.2018
177/025	29.08.1985	22.08.2000	24.08.2018
177/024	29.08.1985	22.08.2000	24.08.2018
176/025	28.08.1987	10.08.2001	14.08.2017

Все снимки Landsat прошли этап атмосферной и радиометрической коррекции (Chander et al., 2009; Landsat 8 Data Users Handbook, 2019). Для автоматизированного картографирования высот лесных насаждений и участков нарушенности был использован предварительно подготовленный векторный слой всех лиственных лесов региона, созданный методом ручной оцифровки лесных массивов на основе снимков Landsat. Его использование позво-

лило провести анализ спектрального отклика в пределах контуров лесных участков и оценить особенности динамики отражательных свойств для каждого из них.

Получение экспериментальных результатов было проведено в два этапа. На первом из них осуществили картографирование высот лесных насаждений на каждый временной срез. Для этого в программе ArcGIS был написан алгоритм, использующий на входе спутниковые сцены Landsat каждого временного среза и векторную маску исследуемых лесных массивов. Сущность алгоритма заключается в пересчёте значений КСЯ в значения высот лесных насаждений, растры которых формируются на его выходе. Несмотря на определённые погрешности измерений, обусловленные вариацией спектральных свойств лесных экосистем на космических снимках, данный подход достаточно эффективен при выявлении участков существенных изменений (снижений) высот, обусловленных появлением ареалов нарушенности древостоя. На втором этапе с использованием другого алгоритма, также подготовленного в ArcGIS, были вычислены растры участков нарушенности, идентификация которых производилась методом оценки изменения высот насаждений в каждый исследуемый временной интервал: 1985-2000 гг. и 2000-2017 гг. К участкам изменений в древостое в автоматическом режиме относили фрагменты растров, на которых снижение высот составляло 12 м и более между начальной и конечной анализируемой датой, например, 1985 г. и 2000 г.

Ошибки, связанные с использованием предложенного подхода, обусловлены следующими причинами: тенями от лесных массивов, расположенных на относительно крутых склонах, и наличие небольшой облачности на некоторых фрагментах спутниковых изображений. Они были отредактированы вручную в процессе проверки полученных результатов и их сопоставления с разновременными спутниковыми данными Landsat, на которых участки изменений в лесах достаточно выявляются при визуальном просмотре. Полученные материалы позволили создать картосхемы лесов с нарушениями древостоя, провести пространственный анализ изменений в лесах.

Результаты. Применение предложенного метода позволило в автоматизированном режиме провести картографирование участков негативных изменений в лесах, появившихся в период с середины 1980-х по конец 2010-х гг., для подавляющей части лиственных лесных насаждений Белгородской области (2785 лесных массивов). Сравнение результатов автоматизированного картографирования с фактическими изменениями (рис. 2, 3) показало, что предложенный подход может быть достаточно эффективно применён для выявления участков лесов с нарушениями древостоя.



Рис. 2. Пример изменений в древостое лиственных лесов юга Среднерусской возвышенности на снимках Landsat в начале 2000-х гг. и в конце 2010-х гг.

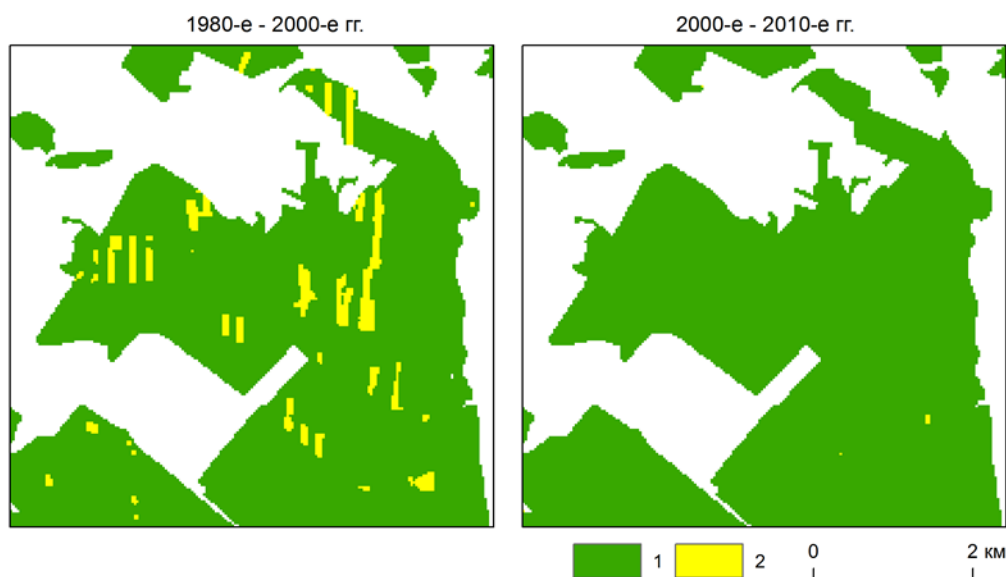


Рис. 3. Пример автоматизированного дешифрирования участков лесных массивов с нарушенным древостоем на юге Среднерусской возвышенности в период с середины 1980-х г. по конец 2010-х гг.
1 – леса без нарушений древостоя, 2 – нарушенные леса

Наиболее эффективно его использование при дешифрировании участков негативных изменений сложной формы, когда размер участков сопоставим с размером пикселей снимка. Преимуществом подхода является также то, что он учитывает различия в спектральных характеристиках сенсоров Landsat TM и OLI, т.к. использует раздельную оценку высот насаждений на основе уравнений, вычисленных с учётом спектрально-отражательных свойств снимков с каждого сенсора.

Главным ограничением используемого подхода является его изначальная адаптация к лесам Среднерусской возвышенности, в которых преобладают лиственные породы: дуб и ясень. Но одновременно в этом заключается и его преимущество при картографировании изменений в лесах региона. Кроме того, обязательным условием предложенного метода является точная взаимная привязка разновременных космических снимков

Анализ полученных результатов позволил установить ряд тенденций в изменении состояния лесных массивов юга Среднерусской возвышенности. Основной особенностью изменения состояния лесов лиственного породного состава в период с середины 1980-х по конец 2010-х гг. является снижение площади участков с нарушениями древостоя. Необходимо отметить, что выявленная особенность характерна для лиственных лесов и не учитывает хвойные (сосновые) леса региона, которые не являлись объектом исследования. В целом на основе полученных данных, по региону в период с середины 1980-х по конец 1990-х гг. доля участков с нарушенным древостоем в лиственных лесах составила 1,83 %. В период 2000-2017 гг. этот показатель был равен 0,85 %. В большинстве административных районов Белгородской области в исследуемый период произошло снижение доли нарушенных лесных участков (рис. 4).

Таким образом, основная часть лиственных лесов региона в последние десятилетия характеризовалась относительно невысокой долей нарушенности древостоя, обусловленной воздействием негативных факторов.

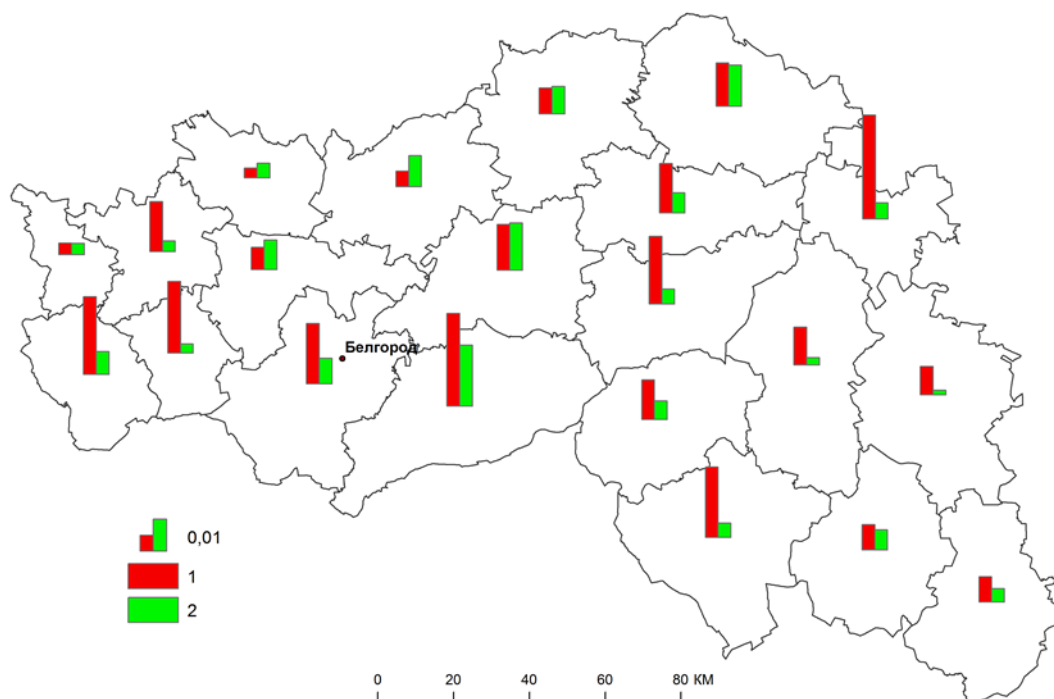


Рис. 4. Изменение доли нарушенных лесных участков от общей площади лесных массивов в районах Белгородской области в период с середины 1980-х гг. по конец 2010-х гг.: 1 – доля нарушенных лесных участков в период 1985-2000 гг., 2 – доля нарушенных лесных участков в период 2000-2017 гг.

Выводы. Предложен способ автоматизированного выявления негативных изменений в лесах, основанный на количественной оценке высот лесных насаждений с использованием их спектрального отклика. Метод использует количественную зависимость, описывающую влияние высот лесных насаждений на их коэффициенты спектральной яркости SWIR-диапазона. С использованием предложенного метода выполнено автоматизированное картографирование изменений в лесных массивах юга Среднерусской возвышенности, обусловленных нарушениями древостоя, в период середина 1980-х – конец 2010-х гг. Изучены пространственно-временные особенности произошедших изменений.

Исследование выполнено при финансовой поддержке РФФИ в рамках научного проекта № 18-35-20018

Библиографический список

1. Барталев С.А., Лупян Е. А. Исследования и разработки ИКИ РАН по развитию методов спутникового мониторинга растительного покрова // Современные проблемы дистанционного зондирования Земли из космоса . 2013. Т. 10. № 1. С. 197-214.
2. Воробьев О.Н., Курбанов Э.А., Полевщикова Ю. А., С. А. Лежнин С.А. Оценка динамики и нарушенности лесного покрова в Среднем Поволжье по снимкам Landsat // Современные проблемы дистанционного зондирования Земли из космоса. 2016. Т. 13 № 4 С. 124-134.
3. Курбанов Э.А., Воробьев О.Н., Губаев А.В., Лежнин С.А., Полевщикова Ю.А., Демишева Е.Н. Четыре десятилетия исследований лесов по снимкам Landsat // Вестник Поволжского государственного технологического университета. Сер.: Лес. Экология. Природопользование. 2014. № 1(21). С. 18-32.
4. Курбанов Э.А., Воробьев О.Н., Лежнин С.А., Губаев А.В., Полевщикова Ю.А. Тематическое картирование растительного покрова по спутниковым снимкам: валидация и оценка точности :: монография. Йошкар-Ола: ПГТУ. 2015. 131 с.
5. Терехин Э.А. Анализ каналов спутниковых данных Landsat ТМ для оценки характеристик лесных насаждений Лесостепной провинции Среднерусской возвышенности // Исследование Земли из космоса . 2012. № 2 . С. 53-61.
6. Терехин Э.А., Чендев Ю. Г. Оценка изменения лесистости в современный период на юге Среднерусской возвышенности с использованием материалов разновременных космических съемок // Современные проблемы дистанционного зондирования Земли из космоса – 2018. – Т. 15. – № 3. – С.114-126.

7. Украинский П.А., Терехин Э. А., Павлюк Я.В., Фрагментация лесов верхней части бассейна реки Ворскла с конца XVIII века // Вестник Московского университета. Серия 5: География. 2017. № 1. С. 82-91.
8. Ховратович Т.С., Барталев С.В., Кашницкий А. В. Метод детектирования изменений лесов на основе подпиксельной оценки проективного покрытия древесного полога по разновременным спутниковым изображениям // Современные проблемы дистанционного зондирования Земли из космоса. 2019. Т. 16 № 4. С. 102-110.
9. Banskota A., Kayastha N., Falkowski M. J., Wulder M. A., Froese R. E., White J. C. Forest Monitoring Using Landsat Time Series Data: A Review // Canadian Journal of Remote Sensing. 2014. Vol. 40, No. 5. P. 362-384.
10. Chander G., Markham B. L., Helder D. L. Summary of current radiometric calibration coefficients for Landsat MSS, TM, ETM+, and EO-1 ALI sensors // Remote Sensing of Environment. 2009. Vol. 113, No. 5. P. 893-903.
11. Healey S., Cohen W., Zhiqiang Y., Krankina O. Comparison of Tasseled Cap-based Landsat data structures for use in forest disturbance detection // Remote Sensing of Environment. 2005. Vol. 97, № 3. P. 301-310.
12. Kennedy R.E., Yang Z., Cohen W. B. Detecting trends in forest disturbance and recovery using yearly Landsat time series: 1. LandTrendr – Temporal segmentation algorithms // Remote Sensing of Environment. 2010. Vol. 114, No. 12. P. 2897-2910.
13. Landsat 8 Data Users Handbook. Department of the Interior U.S. Geological Survey. Sioux Falls, South Dakota. 2019. 106 p.
14. Novo-Fernández A., Franks S., Wehenkel C., López-Serrano P. M., Molinier M., López-Sánchez C. A. Landsat time series analysis for temperate forest cover change detection in the Sierra Madre Occidental, Durango, Mexico // International Journal of Applied Earth Observation and Geoinformation. 2018. Vol. 73. P. 230-244.
15. Potapov P.V., Turubanova S. A., Tyukavina A., Krylov A. M., J. L. McCarty, V. C. Radeloff, M. C. Hansen Eastern Europe's forest cover dynamics from 1985 to 2012 quantified from the full Landsat archive / P. V. Potapov, S. A. Turubanova, A. Tyukavina, A. M. Krylov, J. L. McCarty, V. C. Radeloff, M. C. Hansen // Remote Sensing of Environment – 2015. – Vol. 159. – P. 28-43.
16. Senf C., Pflugmacher D., Hostert P., Seidl R. Using Landsat time series for characterizing forest disturbance dynamics in the coupled human and natural systems of Central Europe // ISPRS Journal of Photogrammetry and Remote Sensing. 2017. Vol. 130. P. 453-463.
17. Zhu Z. Change detection using landsat time series: A review of frequencies, preprocessing, algorithms, and applications // ISPRS Journal of Photogrammetry and Remote Sensing. 2017. Vol. 130. P. 370-384.

References

1. Bartalev S.A., Loupian E.A. Issledovaniya i razrabotki IKI RAN po razvitiyu metodov sputnikovogo monitoringa rastitel'nogo pokrova [R&D on methods for satellite monitoring of vegetation by the Russian Academy of Sciences' Space Research Institute], *Sovremennyye problemy distantsionnogo zondirovaniya Zemli iz kosmosa*, **2013**, Vol. 10, No. 1, pp. 197-214.
2. Vorob'ev O.N., Kurbanov E. A., Polevshchikova Yu. A., Lezhnin S. A. Otsenka dinamiki i narushennosti lesnogo pokrova v srednem povolzh'e po snimkam landsat [Assessment of dynamics and disturbance of forest cover in the Middle Povolzh'ye by Landsat images], *Sovremennyye problemy distantsionnogo zondirovaniya Zemli iz kosmosa*, **2016**, Vol. 13, No. 4, pp. 124-134.
3. Kurbanov E.A., Vorob'ev O.N., Lezhnin S.A., Gubaev A.V., Polevshchikova Yu.A. Tematicheskoe kartirovanie rastitel'nogo pokrova po sputnikovym snimkam: validatsiya i otsenka tochnosti [Thematic mapping of vegetation by satellite imagery: validation and accuracy assessment]: monografiya, Yoshkar-Ola, **2015**, 131 p.
4. Terekhin E.A. Analiz kanalov sputnikovyykh dannykh landsat TM dlya otsenki kharakteristik lesnykh nasazhdeniy Lesostepnoy provintsii Srednerusskoy vozvyshennosti [The Analysis of Landsat TM Data for the Forest Parameters Estimation in the Forest Steppe Province of Central Russian Upland], *Issledovaniye Zemli iz kosmosa*, **2012**, No. 2, pp. 53-61.
5. Terekhin E.A., Chendev Y. G. Otsenka izmeneniya lesistosti v sovremennyy period na yuge Srednerusskoy vozvyshennosti s ispol'zovaniyem materialov raznovremennykh kosmicheskikh s"yomok [Estimation of forest cover changes during modern period in the south of the Central Russian Upland using multiyear remote sensing data], *Sovremennyye Problemy Distantsionnogo Zondirovaniya Zemli iz Kosmosa*, **2018**, Vol. 15, No. 3, pp. 114-126.
6. Ukrainskiy P.A., Terekhin E.A., Pavlyuk Y.V. Fragmentatsiya lesov verkhney chasti basseyna reki Vorskla s kontsa XVIII veka [Fragmentation of forests in the upper part of the Vorskla river basin since the end of the 18th century], *Moscow University Bulletin. Series 5. Geography*, **2017**, No. 1, pp. 82-91.
7. Khovratovich T.S., Bartalev S.A., Kashnitskiy A. V. Metod detektirovaniya izmeneniy lesov na osnove podpiksel'noy otsenki proyektivnogo pokrytiya drevesnogo pologa po raznovremennym sputnikovym izobrazheniyam [Forest change detection based on sub-pixel estimation of crown cover density using bitemporal satellite data], *Sovremennyye problemy distantsionnogo zondirovaniya Zemli iz kosmosa*, **2019**, Vol. 16, No. 4, pp. 102-110.
8. Banskota A., Kayastha N., Falkowski M., Wulder M.A., Froese R.E., White J.C. Forest monitoring using Landsat time-series data—A review, *Canadian Journal of Remote Sensing*, **2014**, Vol. 40, pp. 362–384.
9. Chander G., Markham B.L., Helder D.L. Summary of current radiometric calibration coefficients for Landsat MSS, TM, ETM+, and EO-1 ALI sensors, *Remote Sensing of Environment*, **2009**, Vol. 113, No. 5, pp. 893–903.
10. Healey S., Cohen W., Zhiqiang Y., Krankina O. Comparison of Tasseled Cap-based Landsat data structures for

- use in forest disturbance detection, *Remote Sensing of Environment*, **2005**, Vol. 97, No. 3, pp. 301-310.
11. Kennedy R.E., Yang Z., Cohen W.B. Detecting trends in forest disturbance and recovery using yearly Landsat time series: 1. LandTrendr – Temporal segmentation algorithms, *Remote Sensing of Environment*, **2010**, Vol. 114, No. 12, pp. 2897-2910.
 12. Landsat 8 Data Users Handbook. Department of the Interior U.S. Geological Survey. Sioux Falls, South Dakota. **2019**. 106 p.
 13. Novo-Fernández A., Franks S., Wehenkel C., López-Serrano P.M., Molinier M., López-Sánchez C.A., Landsat time series analysis for temperate forest cover change detection in the Sierra Madre Occidental, Durango, Mexico, *International Journal of Applied Earth Observation and Geoinformation*, **2018**, Vol. 73, pp. 230-244.
 14. Potapov P.V., Turubanova S.A., Tyukavina A., Krylov A.M., McCarty J.L., Radeloff V.C., Hansen M.C. Eastern Europe's forest cover dynamics from 1985 to 2012 quantified from the full Landsat archive, *Remote Sensing of Environment*, **2015**, Vol. 159, pp. 28-43.
 15. Senf C., Pflugmacher D., Hostert P., Seidl R. Using Landsat time series for characterizing forest disturbance dynamics in the coupled human and natural systems of Central Europe, *ISPRS Journal of Photogrammetry and Remote Sensing*, **2017**, Vol. 130, pp. 453-463.
 16. Zhu Z. Change detection using Landsat time series: a review of frequencies, preprocessing, algorithms, and applications, *ISPRS Journal of Photogrammetry and Remote Sensing*, **2017**, Vol. 130, pp. 370-384.

ОЦЕНКА ЗАРАСТАНИЯ СЕЛЬСКОХОЗЯЙСТВЕННЫХ ЗЕМЕЛЬ ДРЕВЕСНЫМИ ПОРОДАМИ ПО СПУТНИКОВЫМ ДАННЫМ LANDSAT НА ПРИМЕРЕ УЧАСТКА БАКАЛИНСКОГО РАЙОНА РЕСПУБЛИКИ БАШКОРТОСТАН

М.В. Мартынова, Р.Р. Султанова, А.К. Габделхаков, З.З. Рахматуллин, Г.Е. Одинцов
Башкирский государственный аграрный университет

Выполнена оценка зарастания земель, вышедших из сельскохозяйственного пользования, древесной растительностью, определены её состав и густота на основе полевых исследований, а также с использованием разновременных снимков Landsat 5,8 путём расчёта вегетационного индекса ARVI. Объект исследования – земельный участок, расположенный в с. Нагайбаково Бакалинского района Республики Башкортостан. При помощи дискретной шкалы значений индекса ARVI травяной покров и древесная растительность были отделены от участков с открытой почвой. Комбинации спектральных каналов 5, 4, 3 для снимков со спутника Landsat 8 и каналов 4, 3, 2 для снимков со спутника Landsat 5 позволяют определить наличие древесной растительности на землях сельскохозяйственного назначения. На участке зарастания присутствует густая травянистая растительность с индексом ARVI от 0,2 до 0,3. На снимках 2001 и 2019 гг. проявляются участки с присутствием деревьев, индекс ARVI которых находится в диапазоне 0,3-0,9. Открытые почвы с индексом ARVI от 0 до 0,2 на снимках Landsat имеют тёмно-коричневую окраску. Установлено, что площадь зарастания древесными породами сельскохозяйственного участка составляет 2,5 га. Видовой состав и густота изучаемого насаждения определены комбинацией глазомерного и инструментального методов лесной таксации. Использование осенних снимков (конец сентября - начало октября) является наиболее удачным решением для определения породного состава древесной растительности. Используя дискретную шкалу и полученный индекс ARVI, находящийся в диапазоне 0,3-0,9 для хвойных, получаем возможность подтвердить данное утверждение.

Ключевые слова: лес, сельскохозяйственные земли, древесная растительность, Landsat, индекс ARVI, ДЗЗ, ArcGIS

ASSESSMENT OF REFORESTATION ON ABANDONED AGRICULTURAL LANDS USING LANDSAT DATA ON THE EXAMPLE OF A SITE IN THE BAKALINSKY REGION OF THE REPUBLIC BASHKORTOSTAN

M.V. Martynova, R.R. Sultanova, A.K. Gabdelkhakov, Z.Z. Rakhmatullin, G.E. Odintsov
Bashkir State Agrarian University

The paper assesses the lands excluded from agricultural use in terms of woody vegetation, composition and density determined based on field studies, as well as using Landsat 5,8 multi-time images by calculating the vegetation index ARVI. The area under study is located near the village of Nagaybakovo in the Bakalinsky district of the Republic of Bashkortostan. Grass cover and woody vegetation were differentiated from open soil areas using a discrete scale of ARVI values. The combinations of spectral channels 5, 4, 3 for Landsat 8 satellite images and channels 4, 3, 2 for Landsat 5 satellite images make it possible to detect woody vegetation on agricultural lands. The overgrown area has dense grassy vegetation with an ARVI index from 0.2 to 0.3. In the images obtained in 2001 and 2019 there are spots with the presence of trees, and the ARVI index ranges between 0.3 and 0.9. Open soil area with an ARVI index ranging from 0 to 0.2 in Landsat images is characterized by dark brown color. In the course of research it has been found out that the agricultural area overgrown with tree species accounts to 2.5 hectares. The species composition and the density of the area under study are determined by a combination of visual and instrumental methods of forest inventory. Using the autumn images (late September - early October) is best for determining species composition of woody vegetation. Using a discrete scale and the resulting ARVI index ranging from 0.3 to 0.9 for conifers proves this assumption.

Keywords: forest, agricultural land, woody vegetation, Landsat, ARVI index, remote sensing, ArcGIS

Введение. Для второй половины XX в. было характерно то, что почти в 80 странах мира наблюдалось стабильное уменьшение земель сельскохозяйственного назначения. Почти за сорок лет из оборота было выведено 223 млн га сельскохозяйственных угодий. Ввиду

социально-экономических преобразований, которые пришлось на период 1990-х годов, Россия также потеряла около 58,3 млн га сельскохозяйственных угодий. Также существенные потери сельскохозяйственных земель наблюдались в Австралии (40,8 млн га), США (35,6 млн га) и Западной Европе (25,1 млн га) (Агроэкологическое состояние..., 2008).

Если же обратиться к современной истории, то в период с 2010 по 2018 г. общая площадь земель сельскохозяйственного назначения в Российской Федерации сократилась на 17,5 млн га. Согласно данным Росреестра, только в 2018 году органами государственной власти Российской Федерации, субъектов Российской Федерации и органами местного самоуправления из земель сельскохозяйственного назначения 770,3 тыс. га, в том числе 647,8 тыс. га было переведено в земли лесного фонда (Доклад о состоянии и использовании земель..., 2020).

Вопросы перевода земель сельскохозяйственного назначения под другие виды землепользования также находят свое отражение в зарубежных исследованиях. В регионе Трентино, который расположен в восточной части Альп на территории Италии, такое исследование было проведено в два этапа с использованием ортофотоснимков 1973 и 1999 годов (De Natale et al., 2007). На их основе была проведена оценка площади новых лесных массивов, проанализированы их экологические и ландшафтные особенности. Во Франции доминирующей древесной породой, зарастающей на землях сельскохозяйственного назначения, является ясень (Sheeren et al., 2011). Точность его распознавания на спутниковых изображениях на основе метода опорных векторов составила более 90 %. В восточной части Балтийской территории состав древостоев, зарастающих на сельскохозяйственных полях, изменился с лиственных пород на ель европейскую (*Picea abies*), что объясняется благоприятной влажностью почвы и развитием плотного травяного покрова (Rüsiņa et al., 2020).

В настоящее время в Республике Башкортостан наблюдается такая же ситуация. Около десятков тысяч гектар заброшенных сельскохозяйственных угодий, которые на протяжении более 10 лет не подвергались распашке, сенокосению и выпасу скота, зарастают древесной растительностью (Государственный доклад..., 2020). Причиной такой тенденции является неиспользование сельскохозяйственных земель по назначению и бездействие со стороны правообладателей земельных участков, сопряжённое с несоблюдением обязательных требований и мероприятий по защите земель от зарастания. Между тем в Республике Башкортостан, в отличие от других регионов, практически отсутствуют исследования, рассматривающие данную проблему. В Республике Марий Эл результаты исследования на эту тему показали, что на землях бывших сельскохозяйственных угодий происходит рост и формирование высокопродуктивных берёзовых и сосновых насаждений (Курбанов и др., 2010а, Курбанов и др., 2010б). Эффект от перевода таких земель в лесной, однозначно, будет иметь положительный эффект, что также регламентируется нормативно-правовыми актами (Об обеспечении плодородия земель..., 2014; Об утверждении Правил обеспечения сохранения..., 2018). Тем не менее, ведение лесного хозяйства на таких участках вызывает определённые трудности (Морозов, Николаева, 2013). Это обоснованно тем, что зарастание происходит постепенно, а его скорость зависит от площади заброшенного участка.

Кроме того, такие естественные процессы на бывших сельскохозяйственных землях могут привести к тому, что и через несколько десятков лет участок не будет полностью покрыт древесной растительностью. В этом случае не обойтись без применения технологии искусственного лесовозобновления, что в результате приведёт к созданию разновозрастного насаждения. Всё это свидетельствует об актуальности рассматриваемого вопроса для республики Башкортостан.

Целью работы является оценка зарастания сельскохозяйственных земель древесной растительностью, определение её породного состава с использованием разновременных снимков Landsat и натурных обследований. Для достижения цели были поставлены следующие задачи:

- подобрать участок с использованием базы данных Landsat;
- провести натурные обследования на выбранном участке путём глазомерно-измерительной таксации;
- оценить степень зарастания исследуемого участка древесной растительностью по разновременным изображениям Landsat в программной среде ArcGIS;
- сравнить результаты полученных наземных и спутниковых данных, сделать выводы.

Характеристика объекта исследования. Объект исследования расположен на земельном участке, принадлежащем ООО «Нива», Бакалинского района (село Нагайбаково) Республики Башкортостан (рис. 1).



Рис. 1. Объект исследования (карта Яндекс)

Методика исследований состояла из двух этапов: полевые и камеральные работы. Полевые исследования на рассматриваемом участке проводились в период с мая по октябрь 2018 года. При глазомерно-измерительной таксации было использовано комбинирование глазомерных и инструментальных методов. На пробной площади был определён породный состав, у средних учётных деревьев замерены высоты и диаметры на 1,3 м высоты.

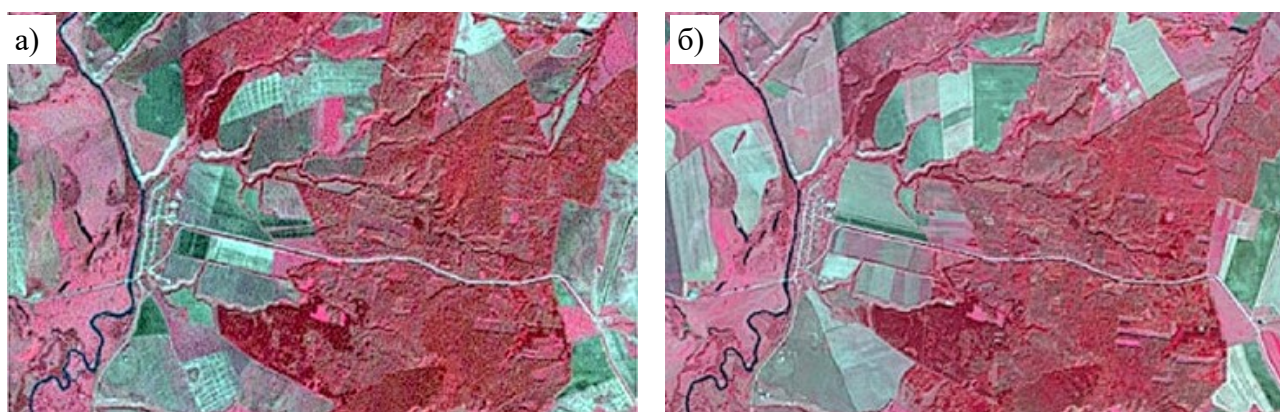
Во время камеральных работ подобраны изображения за 2001 (Landsat 5) и 2019 гг. (Landsat 8), сделанные в сентябре–октябре соответствующего года. Все снимки были атмосферно скорректированы в пакете ArcGIS 10.5. При расчёте индекса ARVI (Атмосфероустойчивый вегетационный индекс – *англ.* Atmospherically Resistant Vegetation Index) на исследуемую площадь был использован широкий инструментарий программы ArcMap. Значения данных индексов варьируют от -1 до 1. Определение видового состава проведено полевым методом ввиду недостаточного разрешения снимков со спутников Landsat.

Результаты исследований. Первый этап обработки данных снимков заключался в использовании комбинации спектральных каналов NIR, Red и Green для определения наличия на исследуемом участке древесной растительности. В табл. 1 приведена информация о наземном покрове, которую возможно извлечь из комбинации спектральных каналов Landsat.

Информация, получаемая при комбинации каналов (Костикова, 2005)

Комбинация спектральных каналов Landsat 5	Комбинация спектральных каналов Landsat 8	Потенциальная информация о наземном покрове
4, 3, 2	5, 4, 3	Стандартная комбинация «искусственные цвета». Растительность отображается в оттенках красного, городская застройка – зелено-голубых, а цвет почвы варьируется от темно- до светло- коричневого. Лёд, снег и облака выглядят белыми или светло-голубыми (лёд и облака по краям). Хвойные леса будут выглядеть более темно-красными или даже коричневыми по сравнению с лиственными. Эта комбинация очень популярна и используется главным образом для изучения состояния растительного покрова, мониторинга дренажа и почвенной мозаики, а также для изучения агрокультур. В целом насыщенные оттенки красного являются индикаторами здоровой и (или) широколиственной растительности, в то время как более светлые оттенки характеризуют травянистую или редколесья/кустарниковую растительность.

По результатам синтезирования каналов Landsat получились сцены на исследуемый участок за разные годы (рис. 2).



По результатам проведённой обработки можно отметить следующее: на снимке 2001 года древесная растительность на исследуемом участке не обнаружена. На снимках 2019 года древесная растительность на исследуемом участке, состоящая из хвойных и лиственных пород, отображается более чётко. Об этом свидетельствует более тёмный цвет растительности, расположенной по краям зарастающего участка (рис. 2).

При помощи дискретной шкалы значений индекса ARVI (рис. 3) возможно чёткое выделение растительного покрова от прочих природных объектов.



Рис. 3. Дискретная шкала индекса ARVI

Как видно из рисунка 4, на участке зарастания присутствует густая травянистая растительность с индексом ARVI от 0,2 до 0,3; на снимках 2001 и 2019 годов проявляются участки с присутствием деревьев, чей индекс находится в промежутках 0,3-0,9. Открытые почвы с индексом ARVI от 0 до 0,2 имеют тёмно-коричневую окраску.

По результатам расчёта индекса ARVI можно сделать вывод, что зарастающий участок (фиолетовый треугольник) имеет прямое происхождение от стены леса (красная линия), которая граничит с изучаемым участком.

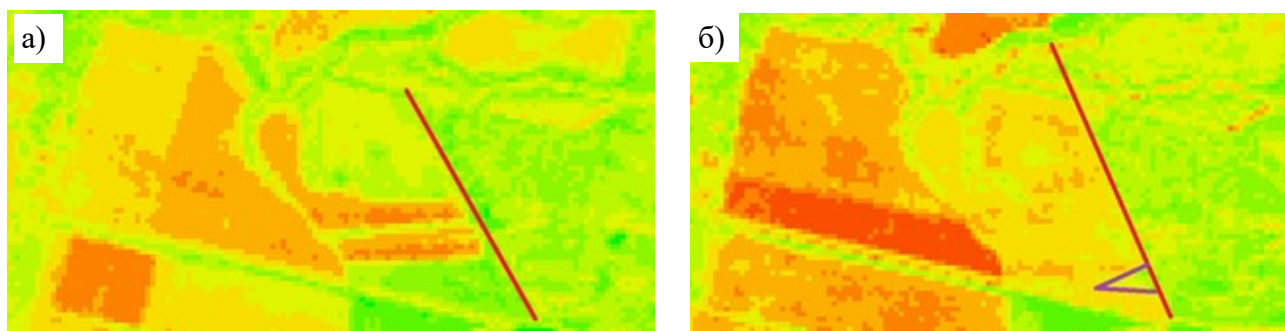


Рис. 4. Сцены изучаемой территории по индексу ARVI: а) 2001 г., б) 2019 г.

Второй этап обработки состоял в определении породного состава древесной растительности, зарастающей на обследуемом участке. Для этого была использована комбинация каналов Red, Green и Blue (табл. 2).

Таблица 2

Информация, получаемая при комбинации каналов Landsat (Костикова, 2005)

Комбинация каналов Landsat 5	Комбинация каналов Landsat 8	Информация о наземном покрове
3, 2, 1	4, 3, 2	Комбинация «естественные цвета». В этой комбинации используются каналы видимого диапазона, поэтому объекты земной поверхности выглядят похожими на то, как они воспринимаются человеческим глазом. Здоровая растительность выглядит зелёной, убранные поля – светлыми, нездоровая растительность – коричневой и жёлтой, дороги – серыми, береговые линии – белёсыми. Эта комбинация каналов дает возможность анализировать состояние водных объектов и процессы седиментации, оценивать глубины. Также используется для изучения антропогенных объектов.

По результатам такого синтеза каналов получились следующие снимки (рис. 5):



Рис. 5. Комбинации каналов Red, Green и Blue снимков Landsat: а) 2001 г., б) 2019 г.

На рисунке 5 видно, что стена леса, которая граничит с нашим исходным участком, имеет смешанный состав, то есть встречаются как лиственные, так и хвойные породы. Это можно отметить по пожелтевшей листве и зелёной хвое, что соотносится с натурными исследованиями. Для подтверждения наличия хвойной растительности на прилегающем лесном массиве к зарастающему участку был также обработан снимок, сделанный в январе (рис. 6).

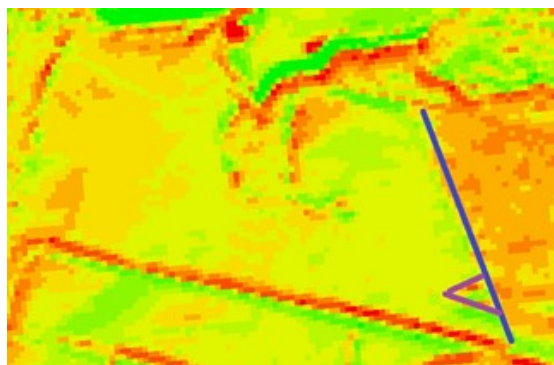


Рис. 6. Индекс ARVI на снимке Landsat (январь 2019)

Для определения хвойной растительности была использована шкала ARVI для снимков, сделанных в зимние месяцы (рис. 7) (Вегетационные индексы. Основы, формулы...).

Значение индекса ARVI для этого участка составляет 0,3–0,9, что является подтверждением факта наличия древесно-кустарниковой растительности.

Определение площади проведено с помощью инструментов «Переклассификация» и «Таблица атрибутов». Снимок, полученный при расчёте индекса ARVI, позволил отделить пиксели, содержащие древесную растительность, от остальных видов земель. Зная площадь одного такого пикселя, получили данные по площади зарастающего участка.

При определении видового состава и густоты древесной растительности, ввиду низкого разрешения снимков со спутников Landsat, были использованы устоявшиеся методы, применяемые в лесной таксации.

По итогам выполненных работ было установлено, что площадь зарастания древесными породами сельскохозяйственного участка составляет 2,5 га. Из них 60 % составляет сосна обыкновенная, а 40 % – лиственные породы (в основном берёза повислая). Полнота составила 0,6.

Выводы. Комплексное использование данных ДЗЗ и ГИС технологий позволяет провести оценку зарастания земель сельскохозяйственного назначения древесной растительностью. Комбинации спектральных каналов 5, 4, 3 для снимков со спутника Landsat 8 и каналов 4, 3, 2 для снимков со спутника Landsat 5 дают возможность определить наличие древесной растительности на землях сельскохозяйственного назначения.

Анализ космических снимков показал, что на исследуемом участке присутствует густая травянистая растительность с индексом ARVI от 0,2 до 0,3, для участков с наличием древесной растительности индекс находится в промежутках 0,3–0,9. Возможности ГИС-технологий позволили определить площадь зарастания, которая составила 2,5 га. Видовой состав и густота были установлены с помощью натурных исследований.

The European Commission support for the production of this publication does not constitute an endorsement of the contents which reflects the views only of the authors, and the Commission cannot be held responsible for any use which may be made of the information contained therein.

Библиографический список

1. Агроэкологическое состояние и перспективы использования земель России, выбывших из активного сельскохозяйственного оборота / под ред. акад. Г. А. Романенко. Москва: ФГНУ «Росинформагротех», 2008. 64с.
2. Государственный доклад о состоянии природных ресурсов и окружающей среды Республики Башкортостан в 2019 году / Министерство природопользования и экологии Республики Башкортостан. Уфа, 2020. 286 с.
3. Доклад о состоянии и использовании земель сельскохозяйственного назначения Российской Федерации в 2018 году. Москва: ФГБНУ «Росинформагротех», 2020. 340 с.
4. Об обеспечении плодородия земель сельскохозяйственного назначения в Республике Башкортостан: закон Республики Башкортостан от 26.09.2014 г. № 131-з
5. Об утверждении Правил обеспечения сохранения и восстановления плодородия земель сельскохозяйственного назначения в Республике Башкортостан: постановление Правительства Республики Башкортостан от 1 августа 2018 года N 369.



Рис. 7. Индекс ARVI на снимке Landsat (январь 2020)

6. Вегетационные индексы. Основы, формулы, практическое использование [Электронный ресурс]. Режим доступа: http://mapexpert.com.ua/index_ru.php?id=20&table=news. – 18.11.2020.
7. Костикова А. Интерпретация комбинаций каналов данных Landsat TM / ETM+ [Электронный ресурс]. Режим доступа: <https://gis-lab.info/qa/landsat-bandcomb.html>. – 15.10.2020.
8. Курбанов Э.А., Воробьев О.Н., Губаев А.В., Лежнин С.А., Незамаев С.А., Александрова Т.А. Оценка зарастания земель запаса Республики Марий Эл лесной растительностью по спутниковым снимкам // Вестник МарГТУ. Сер.: Лес. Экология. Природопользование. 2010а. Т. 2, № 9. С. 14-20.
9. Курбанов Э.А., Воробьев О.Н., Губаев А.В., Лежнин С.А. Использование космических снимков ALOS для выявления площадей бывших сельскохозяйственных угодий, зарастающих лесом // Геоматика. 2010б. №4. С. 68–72.
10. Морозов А.М, Николаева И.О. Особенности лесообразовательного процесса на пашне и сенокосе // Вестник Алтайского государственного аграрного университета. 2013. № 5. С. 82-86.
11. De Natale F., Gasparini P., Carriero A. A study on tree colonization of abandoned land in the Italian Alps: extent and some characteristics of new forest stands in Trentino. Sustainable Forestry – From monitoring and modelling to knowledge management and policy science. CAB International, 2007. P. 269–284.
12. Rūsiņa S., Prižavotte D., Nikodemus O., Brūmelis G., Gustiņa L., Kasparinskis R. Land-use legacies affect Norway spruce *Picea abies* colonization on abandoned marginal agricultural land in Eastern Baltics // New forests. 2020. DOI: 10.1007/s11056-020-09809-y.
13. Sheeren D., Fauvel M., Ladet S., Jacquin A., Bertoni G., Gibon A. Mapping ash tree colonization in an agricultural mountain landscape: Investigating the potential of hyperspectral imagery // IEEE International Geoscience and Remote Sensing Symposium, IGARSS 2011. Vancouver, BC, Canada, 2011, July 24-29.

References

1. Agroekologicheskoe sostoyanie i perspektivy ispol'zovaniya zemel' Rossii, vybyvshikh iz aktivnogo sel'skokhozyaystvennogo oborota [Agroecological state and prospects for the use of Russian lands that have been removed from active agricultural use] / pod red. akad. G. A. Romanenko, Moscow: FGUN «Rosinformagrotekh», **2008**, 64 p.
2. Gosudarstvennyi doklad o sostoyanii prirodnkh resursov i okruzhayushchei sredy Respubliki Bashkortostan v 2019 godu [State report on the state of natural resources and the environment of the Republic of Bashkortostan in 2019] / Ministerstvo prirodopol'zovaniya i ekologii Respubliki Bashkortostan, Ufa, **2020**, 286 p.
3. Doklad o sostoyanii i ispol'zovanii zemel' sel'skokhozyaystvennogo naznacheniya Rossiiskoi Federatsii v 2018 godu [Report on the state and use of agricultural land in the Russian Federation in 2018], Moscow: FGBNU «Rosinformagrotekh», **2020**, 340 p.
4. Ob obespechenii plodorodiya zemel' sel'skokhozyaystvennogo naznacheniya v Respublike Bashkortostan: zakon Respubliki Bashkortostan ot 26.09.2014 g. № 131-z [On ensuring the fertility of agricultural lands in the Republic of Bashkortostan: the law of the Republic of Bashkortostan dated 09/26/2014 № 131-z]
5. Ob utverzhdenii Pravil obespecheniya sokhraneniya i vosstanovleniya plodorodiya zemel' sel'skokhozyaystvennogo naznacheniya v Respublike Bashkortostan: postanovlenie Pravitel'stva Respubliki Bashkortostan ot 1 avgusta 2018 goda N 369 [On approval of the Rules for ensuring the preservation and restoration of the fertility of agricultural lands in the Republic of Bashkortostan: Resolution of the Government of the Republic of Bashkortostan of August 1, 2018 N 369]
6. Vegetatsionnye indeksy. Osnovy, formuly, prakticheskoe ispol'zovanie [Vegetation indexes. Basics, formulas, practical use], URL: http://mapexpert.com.ua/index_ru.php?id=20&table=news. – 18.11.2020.
7. Kostikova A. Interpretatsiya kombinatsii kanalov dannykh Landsat TM / ETM+ [Interpreting a combination of Landsat TM data channels / ETM+], URL: <https://gis-lab.info/qa/landsat-bandcomb.html>. – 15.10.2020.
8. Kurbanov E.A., Vorob'ev O.N., Gubaev A.V., Lezhnin S.A., Nezamaev S.A., Aleksandrova T.A. Otsenka zarastaniya zemel' zapasa Respubliki Marii El lesnoi rastitel'nost'yu po sputnikovym snimkam [Assessment of overgrowth of the reserve lands of the Republic of Mari El with forest vegetation based on satellite images], *Vestnik MarGTU. Ser.: Les. Ekologiya. Prirodopol'zovanie*, **2010a**, T. 2, № 9, P. 14-20.
9. Kurbanov E.A., Vorob'ev O.N., Gubaev A.V., Lezhnin S.A. Ispol'zovanie kosmicheskikh snimkov ALOS dlya vyyavleniya ploshchadei byvshikh sel'skokhozyaystvennykh ugodii, zarastayushchikh lesom [Use of ALOS satellite images to identify areas of former agricultural lands overgrown with forest], *Geomatika*, **2010b**, №4, P. 68–72.
10. Morozov A.M, Nikolaeva I.O. Osobennosti lesoobrazovatel'nogo protsessa na pashne i senokose [Features of the forest formation process in arable land and hayfields], *Vestnik Altaiskogo gosudarstvennogo agrarnogo universiteta*, **2013**, № 5, S. 82-86.
11. De Natale F., Gasparini P., Carriero A. A study on tree colonization of abandoned land in the Italian Alps: extent and some characteristics of new forest stands in Trentino, Sustainable Forestry – From monitoring and modelling to knowledge management and policy science, *CAB International*, **2007**, P. 269–284.
12. Rūsiņa S., Prižavotte D., Nikodemus O., Brūmelis G., Gustiņa L., Kasparinskis R. Land-use legacies affect Norway spruce *Picea abies* colonization on abandoned marginal agricultural land in Eastern Baltics, *New forests*, **2020**. DOI: 10.1007/s11056-020-09809-y.
13. Sheeren D., Fauvel M., Ladet S., Jacquin A., Bertoni G., Gibon A. Mapping ash tree colonization in an agricultural mountain landscape: Investigating the potential of hyperspectral imagery, *IEEE International Geoscience and Remote Sensing Symposium, IGARSS*, **2011**.

ESTIMATION OF URBAN ENVIRONMENT IN TAIPEI LIVING CIRCLE BASED ON REMOTE SENSING ECOLOGICAL INDEX

Yibo Wang

Volga State Technological University

The development of urbanization affects the natural environment in many fields such as resources, economy, society, culture, and technology. With the continuous development of urbanization, the interference of human activities has greatly changed the structure of the original land. This article takes Taipei Living Circle in the northern part of Taiwan Island as an example. Based on the Remote Sensing Ecological Index (RSEI), the ecological quality of the ground objects from 1988 to 2019 was evaluated. The remote sensing ecological index is divided into five grades and combined with the land use transfer matrix to analyze the impact of land-use changes in the region on the ecology, so as to analyze and evaluate the ecological environment changes in the study area. Research shows that from 1988 to 2019, the remote sensing ecological index was 0.559, 0.571, 0.546, and 0.396 respectively. The areas with improved ecological quality are concentrated in high-altitude areas, in mountainous areas, while the areas with reduced ecological quality are concentrated in the expansion of the city in the Taipei Life Circle. The process of transformation has a significant impact on the ecological environment. From 1988 to 2019, areas with improved ecological quality were concentrated in high-altitude areas in mountainous areas, and areas with reduced ecological quality were concentrated in urban expansion. The forested areas exert significant influence on the quality of environment. Reasonable protection and utilization of mountain forest resources play an important role in the sustainable development of Taipei Living Circle.

Key words: urbanization, ecological quality, RSEI, sustainable development, Taipei Living Circle, environmental change.

Introduction

Remote sensing technology has been widely used in the field of ecological environment and has become an effective means of evaluating the regional ecological environment. Land use and land cover changes are often used to explore the impact on the environment (Cooper et al., 2006). The development of urbanization affects the natural environment in many fields such as resources, economy, society, culture, and technology. With the development of human society and the rapid expansion of the scale of cities, people's demand for land resources is increasing (Grimm et al., 2008). The continuous development of urbanization and the interference of human activities have greatly changed the structure of the original land (Jimenez et al., 2018), and have a certain impact on the surrounding ecology. Sustainable urban development is used to coordinate the relationship between people and nature, so as to achieve a relative balance between the various parts of society, economy, and natural environment (Aminzadeh, Khansefid, 2010). In response to the continuous acceleration of global urbanization, remote sensing is used to conduct multi-angle research into the cities. The direct application of remote sensing data has been widely used in the urban thermal environment (Estoque et al., 2017), urban smog (Liu et al., 2017), urban green space (Vorobyev et al., 2015). On this basis, the use of economic (McDonnell, MacGregor, 2016), lighting (Xu et al., 2018) and other data directly reflect remote sensing research of the environment.

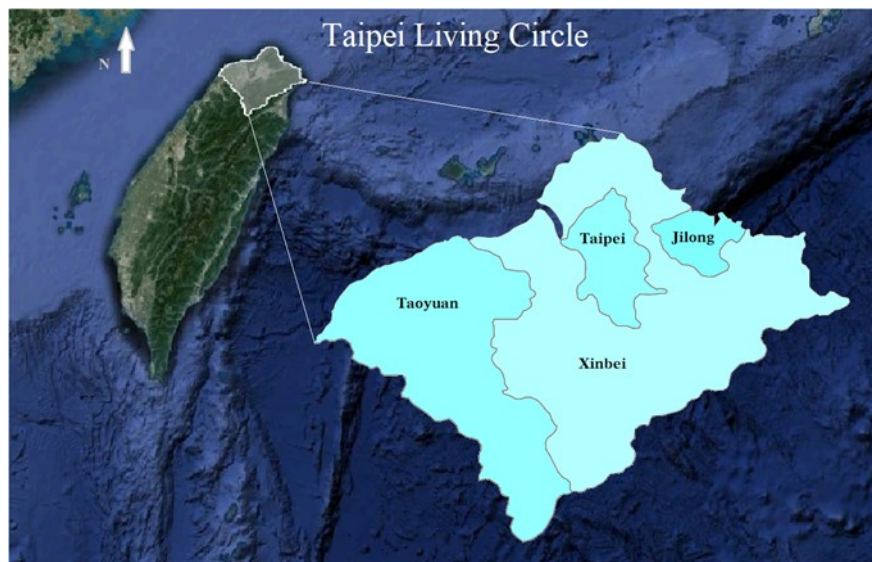
The formation and the development of ecosystem are affected by many factors, so the ecological quality status needs to be described from multiple aspects. It is not objective to use only one or two aspects of ecological factors to reflect changes in the ecological environment (Wei et al., 2017). The Remote Sensing Ecological Index (RSEI) is completely based on remote sensing information and integrates a variety of environmental factors including greenness, humidity, heat, and dryness (Xu, 2013). This index is comparable with traditional ecological quality index calculations. Since the data is obtained entirely through remote sensing, the difficulty of data collection is greatly reduced. Data can also be visualized to facilitate comparison between different periods. The principal component analysis method is used to assign weights, thereby improving the objec-

tivity of the evaluation results. And it has been better used in urban (Yang et al., 2019), desert (Jiang et al., 2019), wetland (Wen et al., 2020), and other settings. Combined with the actual situation of Taiwan Island, RSEI, land use and land cover changes, it is possible to understand the impact of different types of ground features on environmental quality.

Joining the land-use change and remote sensing ecological index in the Metropolitan Taipei in the northern part of Taiwan Island, China from 1988 to 2019, we analyzed the impact of the changes on the ecological environment. It also helps understand the impact of different types of ground features on environmental quality and help urban areas achieve the goal of sustainable development most effectively.

Study area and research methods

The study area was selected as the Taipei Living Circle in the northern part of Taiwan Island. This area is located in the northern part of Taiwan Island, northwest of the Pacific Ocean. Geographical location $24^{\circ}11'41''\text{N}\sim 25^{\circ}17'59''\text{N}$, $120^{\circ}59'10''\text{E}\sim 122^{\circ}01'26''\text{E}$, including Taipei City, New Taipei City, Keelung City and Taoyuan City (fig. 1). The total area is $3,677\text{ km}^2$. The climate is subtropical: it is warm and humid all year round, with frequent typhoons (Chang et al., 2013; Jimenez, 2018).



The main remote sensing data used in this article is the Landsat series of satellite images provided by the US Geological Survey (<https://eros.usgs.gov/>). According to the quality of remote sensing data and cloud conditions, a total of 5 images ranging from 1988 to 2019 were selected. In the period of image data, the selected remote sensing image is of good quality with no cloud coverage or the cloud coverage is less than 5%.

Among them, Landsat 5 data were selected in 1988, 1995, and 2007. Images of 2018, 2019 were acquired from Landsat 8 data. Taiwan carries out a new round of cultivation every February and July-August, at this time the characteristics of the fields are most obvious. In order to better extract the field information, we chose the remote sensing images from that period (table 1).

The images produced in the experiment are processed by ENVI and ArcGIS. Image feature classification is provided by eCognition 9.01. SPSS Modeler 14 for satellite image data mining. In eCognition 9.01, the preprocessed 1988, 1995, 2007, and 2019 remote sensing images are segmented (Florence et al., 2011; Kurtz et al., 2012) and classified according to nine types of ground features: coniferous forest, broad-leaved forest, bamboo forest, field, shrub, water, wetland, city,

Table 1

Image data information in the study area

Years	Satellite	Sensor	Resolution	Date
1988	Landsat 5	TM	30	1988.02.23
1995	Landsat 5	TM	30	1995.07.20
2007	Landsat 5	TM	30	2007.07.21
2019	Landsat 8	OLI	30	2019.07.22

grassland, and bare land. General training sample data sets are used. SPSS Modeler 14 is used to implement data mining. We used the C5.0 model with the Boosting algorithm and set the number of experiments to 10. The interactive verification was selected, and there were 5 folds selected to train the training samples to generate a classification decision tree (Ma et al., 2015). In ENVI 5.3, the decision tree is used to classify the data in 1988, 1995, 2007, and 2019.

The Remote Sensing Ecological Index (RESI) constructed in this paper is to extract the four indicators of humidity, greenness, dryness, and heat from the four aspects of regional humidity, vegetation coverage, surface exposure, and temperature from the remote sensing images to come to the cities in the Taipei metropolitan area Ecological quality. Greenness, humidity, and heat are used for normalized difference vegetation index (NDVI), humidity index (Wet), and land surface temperature (LST), respectively. The land building index (IBI) and the soil index (SI) can respectively express the construction land and bare land conditions. This study uses the average of the two indicators to represent the dryness index (NDBSI). Calculation formula of humidity index is as follows:

$$WET = C_1\rho_B + C_2\rho_G + C_3\rho_R + C_4\rho_{NIR} + C_5\rho_{SWIR1} + C_6\rho_{SWIR2}, \quad (1)$$

In the formula ρ_{NIR} , ρ_R , ρ_B , ρ_G , ρ_{SWIR1} , ρ_{SWIR2} corresponds to the surface reflectivity of 4, 3, 1, 2, 5, and 7 bands in the TM image, and corresponds to the surface reflectivity of 5, 4, 2, 3, 6, 7 bands in the OLI image, respectively. C_1 , C_2 , C_3 , C_4 , C_5 , C_6 - the coefficients are 0.0315, 0.2021, 0.3102, 0.1594, -0.6806, -0.6109 in TM images. In OLI images, they are 0.1511, 0.1973, 0.3283, 0.3407, -0.7117, and -0.4559.

Green index calculation formula is as follows:

$$NDVI = \frac{\rho_{NIR} - \rho_R}{\rho_{NIR} + \rho_R}, \quad (2)$$

Calculation formula of dryness index is presented below:

$$NDBSI = \frac{IBI + SI}{2}, \quad (3)$$

$$IBI = IBI_{min} * IBI_{max}, \quad (4)$$

$$IBI_{min} = \frac{2\rho_{SWIR1}}{\rho_{SWIR1} + \rho_{NIR}} - \rho_{NIR}(\rho_{NIR} + \rho_R) - \frac{\rho_G}{\rho_G + \rho_{SWIR1}}, \quad (5)$$

$$IBI_{max} = \frac{2\rho_{SWIR1}}{\rho_{SWIR1} + \rho_{NIR}} + \rho_{NIR}(\rho_{NIR} + \rho_R) + \frac{\rho_G}{\rho_G + \rho_{SWIR1}}, \quad (6)$$

$$SI = \frac{[(\rho_{SWIR1} + \rho_{NIR}) - (\rho_{NIR} + \rho_R)]}{[(\rho_{SWIR1} + \rho_{NIR}) + (\rho_{NIR} + \rho_R)]}, \quad (7)$$

Formula for calculating the heat index is as follows:

$$L = gain * DN + basi, \quad (8)$$

$$P_V = \frac{NDVI - NDVI_{Soil}}{NDVI_{veg} - NDVI_{Soil}} , \quad (9)$$

$$\varepsilon_{surface} = 0.9625 + 0.0614P_V - 0.0461P_V^2 , \quad (10)$$

$$\varepsilon_{building} = 0.9589 + 0.086P_V - 0.0671P_V^2 , \quad (11)$$

$$B(LST) = \frac{[L - L_{up} - T * (1 - \varepsilon)L_{down}]}{T} * \varepsilon , \quad (12)$$

$$LST = \frac{K_2}{\ln \left[\frac{K_1}{B(TS)} + 1 \right]} - 273 , \quad (13)$$

The L represents the sensor radiation value obtained by the image calibration of the 6th band of the TM image and the 10th band of the OLI image through ENVI software radiation calibration. DN is the pixel gray value, the gain is the gain value of the band, and bias is the offset value. These three values are obtained through remote sensing image header files. P_V indicates vegetation coverage.

$NDVI_{Soil}$ represents the NDVI value of the area without vegetation coverage, and the empirical value is 0.05. $NDVI_{veg}$ is the NDVI value of vegetation pixels, and the empirical value is 0.7.

$\varepsilon_{surface}$ and $\varepsilon_{building}$ represent the pixel specific emissivity of natural surfaces and urban areas, respectively, and the water cell pixel specific emissivity takes a value of 0.995 (Yu et al., 2014).

$B(LST)$ is the blackbody radiance value.

L_{up} , L_{down} , T represents the upward radiance of the atmosphere, the downward radiance of the atmosphere and the transmittance of the thermal infrared band.

Because there are many different standards for obtaining weight values, the final image results will also be different, so this experiment uses principal component analysis to obtain the combined value, which can determine the weight according to the value of the data itself. RSEI synthesizes the contents of the four component indicators, and it can determine the only certain value at a certain time point after the change of the main component (Zhang et al, 2019).

RSEI ecological index formula is as follows:

$$RSEI = \frac{RESI_0 - RSEI_{0-min}}{RSEI_{0-max} - RSEI_{0-min}} , \quad (14)$$

$$RESI_0 = 1 - PC1 , \quad (15)$$

$RSEI$ is the normalized remote sensing ecological index. $RESI_0$ is the original ecological index at i pixel. $RSEI_{0-max}$ and $RSEI_{0-min}$, these are the maximum and minimum values of the original ecological index. PC1 is the load value of the first principal component.

In order to further analyze the ecological quality evaluation results, combined with the distribution characteristics of the RSEI index in northern Taiwan, the reclassification is used to divide the RSEI values from 0-1 into equidistant and divided into five grades: poor, fair, average, good, and excellent.

Based on the study of classification of the dynamic changes of the ecological quality in the Taipei Living Circle, this paper makes further analysis of the causes of different ecological quality changes. By combining areas with different ecological qualities in various years and land use types, we explore the changes in land use types under different ecological qualities.

We carried out interpolation analysis and processing of RSEI remote sensing ecological quality value images in 1988 and 2019. The remote sensing images we reclassified after the difference

processing in ArcGIS, and divided into five categories: 2, 1, 0, -1, -2. They represent ecological quality significantly improved area, ecological quality improved area, ecological quality constant area, ecological quality deteriorated area, and ecological quality significantly deteriorated area. By combining the areas where different ecological qualities are located each year and the types of land use, the changes in land use types under different ecological qualities are explored.

Results and discussion

Forests occupy the main part of Taipei Living Circle, of which deciduous forests are mainly distributed in mountainous areas (fig. 2). The building area comprising cities, bare land, and grassland is growing year by year. It is mostly concentrated in the Taipei Basin and Taoyuan. Agricultural areas comprising fields and shrubs have also increased. Building areas and agricultural areas have increased by overlapping onto the areas originally covered with bamboo forests, deciduous forests, and coniferous forests. Water and wetlands remain basically unchanged.

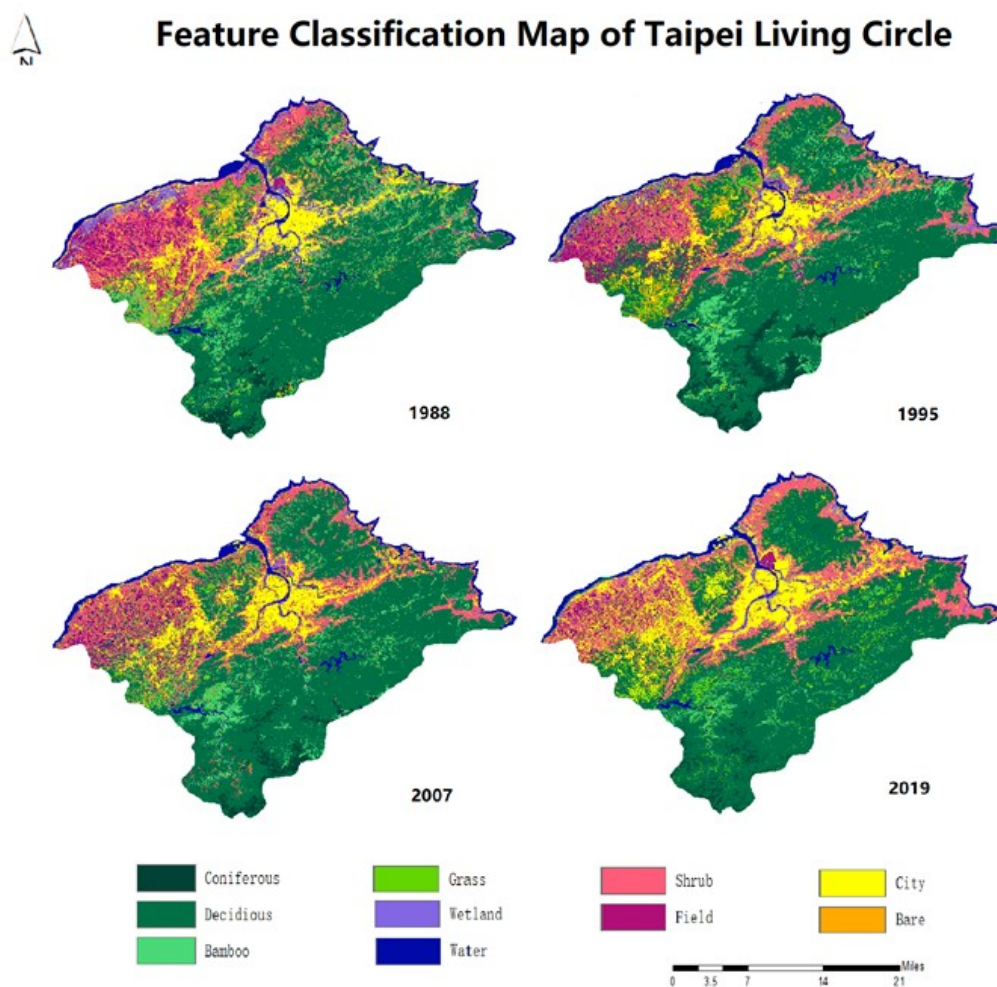


Fig 2. Maps of feature classification for 1988-2019

According to calculations, the RESI values in 1988, 1995, 2007 and 2019 are 0.559, 0.571, 0.546, 0.396 (table 2). The larger the value, the better the quality of the ecological environment in that year. The overall trend in the past four years has been a gradual decline. Based on the four-year data, it can be seen that four ecological indicators have varying degrees of influence on the final RSEI index. Among them, WET, NDVI, NDSI, and LST contributed more evenly to the final results.

Table 2

RSEI index parameter statistics

Date	1988		1995		2007		2019	
Type	Average	SD	Average	SD	Average	SD	Average	SD
WET	0.722	0.021	0.775	0.018	0.716	0.030	0.642	0.021
NDVI	0.404	0.005	0.524	0.154	0.879	0.042	0.518	0.043
NDBSI	0.145	0.162	0.301	0.333	0.151	0.163	0.121	0.159
LST	0.251	0.283	0.255	0.284	0.207	0.218	0.259	0.294
RESI	0.559	0.059	0.571	0.067	0.546	0.078	0.396	0.117

RSEI ecological quality value is a way of expressing, evaluating, and judging the level of the regional ecological environment. From the perspective of effect, the impact of land-use change on the regional ecological environment mainly includes positive and negative correlations. Among them, the positive correlation is mainly manifested in the improvement of soil quality. Bare land and unused wasteland are converted into cultivated land and forest land by human activities. With the improvement of water resources, the ecological habits of land plants have been further improved (Nakamura et al., 2008). Vegetation coverage has been improved, thereby improving the ecological quality of the natural environment. Correspondingly, the negative correlation mainly includes land quality degradation, desertification, and salinization. The area of cultivated land, garden land, or forest land is gradually reduced or replaced by non-permeable grounds such as urban construction land and urban roads. Water resources pollution and over-exploitation, ecological habits of land plants have further deteriorated, and the vegetation coverage has declined seriously. As a result, the ecological quality of the natural environment deteriorates.

Table 3

RSEI level statistics

Date	1988		1995		2007		2019	
Type	Area, km ²	%	Area, km ²	%	Area, km ²	%	Area, km ²	%
Poor	26,405	0.61	45,430	1.06	67,951	1.59	121,206	2.83
Fair	819,400	19.16	1,148,652	26.85	1,444,596	33.77	1,532,365	35.83
Average	3,329,216	77.83	2,458,707	57.49	2,442,375	57.11	2,362,187	55.22
Good	102,188	2.39	580,764	13.57	320,336	7.48	261,456	6.11
Excellent	87	0.01	43,743	1.03	2,038	0.05	84	0.01

It can be seen that most research areas found within the average interval in 1988, accounted for more than 77% of the total area (table 3). Followed by the fair area, which accounted for about one-fifth. The ecological excellent area and poor area account for a small proportion. The average interval accounted for the largest proportion in 1995, exceeding 57%. Fair area and good area accounted for 26.85% and 13.58% respectively. Ecological Excellent area and poor area account for less. The average interval in 2007 is basically the same as the Average interval in 1995. The Fair area has increased compared to before, with the ratio reaching one third. The good area is reduced by 50%, and the total proportion is 7.5%. The poor region increased slightly, and the excellent region decreased slightly. The region with the largest share in 2019 is still the average region, exceeding 55%.

The fair area and poor area both increased slightly. The proportion of the good area and excellent area has decreased. Comparing the four-year data, we can see that environmental quality has a significant downward trend. Among them, the proportion of poor area and fair area is constantly rising. The corresponding areas in the figure are concentrated on impervious surfaces such as urban roads and agricultural land such as farmland shrubs. Due to the advancement of urbanization, the expansion of urban areas has led to a decline in the value of environmental quality in the re-

gion. The average area has been declining continuously in the four-year period. There is also a downward trend in good and excellent region types (fig. 3).

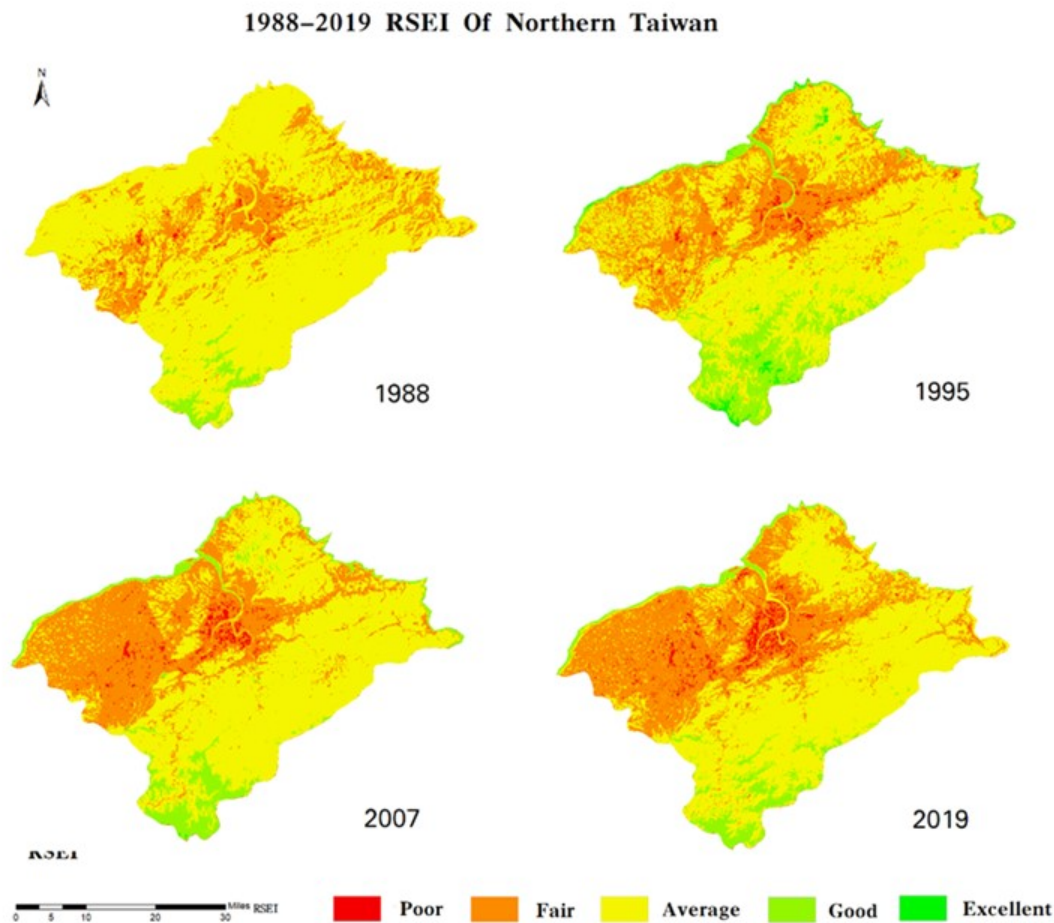


Fig 3. RSEI index area for 1988-2019

The average area occupies the largest area ratio in four years, and the proportion is more than 50%. The poor area and excellent area account for only a small percentage of the four-year data. The area of change is mainly concentrated in the fair area and good area. According to the DEM comparison of the study area, the areas with ecological quality changes are mostly concentrated in plains or hills with a terrain of less than 500 m, which corresponds to changes in urban expansion. The mountainous areas, which account for the largest proportion of the study area, basically maintain good ecological quality.

Through the analysis of the feature type transfer matrix of ecological quality significantly improved area, improved area, constant area, deteriorated area, significantly deteriorated area, the relationship between the ecological quality index and urbanization is obtained (fig. 4). In the ecological quality improved area, broad-leaved forest occupies the largest proportion, indicating that the area of broad-leaved forest plays an important role in ecological quality. At the same time, it is found that although grassland, shrubs, and other areas are all green, their impact on ecological quality is less than that of woodland. According to the invariable areas of ecological regions, the mutual conversion between different types can reach a relative balance of ecological quality. According to the analysis of the ecological quality deteriorated area, the increase in the area of cities and fields has a significant negative effect on ecological quality. Substituting shrub areas for forest areas will slightly reduce the ecological quality. Cities have the most obvious response to ecological quality. The main reason for the loss of wetlands and water bodies is the increase in the urban

areas. The main reason is that most wetlands are located in low-altitude areas and the area is close to the city. The area of water loss is mainly the area of shallow waters near the city.

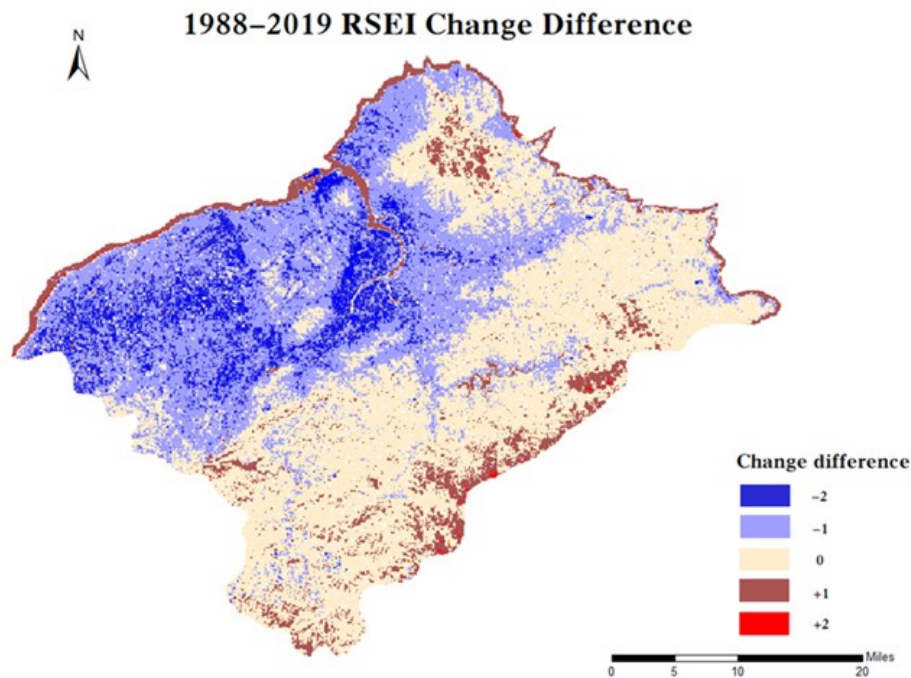


Fig 4. RSEI change difference for 1988-2019

The mountains with higher altitudes are mostly covered by forest, among which broad-leaved forests have a greater influence on the ecological quality than bamboo forests and coniferous forests. And most of the broad-leaved forests are located in areas where human activities are limited, making the broad-leaved forests basically unchanged. Part of the broad-leaved forest near the city turned into shrubs. The reason is that it has become grassland and some trees have been replaced with cash crops under the influence of urban development. The amount of bare land is reduced, and it is transformed into an urban impervious surface, and its impact on environmental quality remains basically unchanged.

The land use/land class maps of 1988 and 2019 years were combined using the spatial connection tool. We generated several matrix tables to estimate the ecological quality: significantly improved area transition matrix (table 4), improved area transition matrix (table 5), constant area transition matrix (table 6), deteriorated area transition matrix (table 7), and significantly deteriorated area transition matrix (table 8).

Table 4

Ecological quality significantly improved area

1988 2019	water	field	city	grass	wet- land	shrub	decidu- ous	bam- boo	conif- erous	bare	Output
water		1557	809	0	0	6	0	0	18	1	2391
field	0		1	0	2	0	0	0	0	0	3
city	0	13		0	0	4	0	0	0	0	17
grass	0	0	0		0	1	228	38	0	0	267
wetland	0	1	4	0		0	0	0	0	0	5
shrub	0	3	2	0	1		3	1	0	0	10
deciduous	320	363	287	128	0	23		381	84	0	1,586
bamboo	0	0	0	0	0	0	20		0	0	20
coniferous	0	0	0	0	0	0	9	10		0	19
bare	0	0	0	0	0	0	0	0	0		0
Input	320	1,937	1,103	128	3	34	260	430	102	1	

Table 5

Ecological quality improved area

1988 2019	water	field	city	grass	wet- land	shrub	decidu- ous	bam- boo	conif- erous	bare	Output
water		3,900	1,513	11	310	295	535	74	4,150	4	10,792
field	4		15	4	4	22	0	1	0	0	50
city	1,706	296		22	21	98	54	27	18	6	2,248
grass	38	34	43		0	102	1,305	363	37	0	1,922
wetland	233	106	53	0		12	23	7	17	1	452
shrub	44	100	109	1	7		234	146	16	1	658
deciduous	2,096	940	1,319	2,407	1	2,386		10,948	26,301	44	46,442
bamboo	14	1	2	32	0	7	5,934		374	0	6,364
coniferous	0	1	34	44	0	55	1408	317		0	1,859
bare	3	0	0	0	0	0	0	0	0		3
Input	4,138	5,378	3,088	2,521	343	2,977	9,493	11,883	30,913	56	

Table 6

Ecological quality constant area

1988 2019	water	field	city	grass	wet- land	shrub	decidu- ous	bamboo	conif- erous	bare	Output
water		495	1,226	63	114	445	1,913	391	2,273	9	6,929
field	83		684	318	169	905	448	684	18	291	3,600
city	515	941		1,987	941	6,748	6,226	4,669	561	329	22,917
grass	346	524	1,561		4	5,983	41,806	23,982	349	271	74,826
wetland	236	702	1,878	16		989	1,681	976	228	15	6,721
shrub	314	2,895	8,585	150	3,024		78,676	28,532	2,582	143	124,901
deciduous	1,213	2,893	19,016	40,003	105	44,921		160,249	65,217	1,312	334,929
bamboo	63	16	294	1,342	1	1034	80,865		916	23	84,554
coniferous	3	0	162	819	0	287	37,157	3664		0	42,092
bare	0	0	109	9	0	44	79	2	0		243
Input	2,773	8,466	33,515	44,707	4,358	61,356	24,885	223,149	72,144	2,393	

Table 7

Ecological quality deteriorated area

1988 2019	water	field	city	grass	wet- land	shrub	decidu- ous	bam- boo	co- nifer- ous	bare	Output
water		2,650	6,925	320	1,427	2,586	965	303	940	109	16,225
field	225		19,665	5,840	12,363	33,384	3,430	1,619	568	2,565	79,659
city	1,815	36,768		19,257	41,462	80,033	13,839	8,549	953	8,553	211,229
grass	437	9,935	7,670		14	35,474	18,456	16,900	235	1,453	90,574
wetland	2,106	11,103	17,089	31		11,920	4,544	2,619	639	579	50,630
shrub	1,987	35,668	28,617	782	31,811		100,119	21,894	2,884	821	224,583
deciduous	1,312	12,255	15,850	44,371	198	46,249		22,929	1,845	1,414	146,423
bamboo	24	27	77	360	4	408	3,015		20	15	3,950
coniferous	0	0	44	71	0	17	536	118		0	786
bare	0	0	83	34	0	22	14	7	0		160
Input	7,906	108,406	96,020	71,066	87,279	210,093	144,918	74,938	8,084	15,509	

Table 8

Ecological quality significantly deteriorated area

1988 2019	water	field	city	grass	wet- land	shrub	decidu- ous	bamboo	conif- erous	bare	Output
water		884	770	49	323	608	97	10	96	35	2,872
field	468		13,406	2,048	9,513	21,983	1,685	299	357	1,758	51,517
city	4,830	40,731		4,559	30,540	33,007	3,284	760	721	4,547	122,979
grass	272	7,309	1,415		10	9,705	1,886	373	117	136	21,223
wetland	847	4,553	3,197	0		3,116	417	38	117	149	12,434
shrub	1,107	22,254	2,832	36	3,700		1,535	191	371	111	32,137
deciduous	839	4,827	932	1,602	51	2,795		236	155	77	11,514
bamboo	4	11	4	4	5	16	21		3	1	69
coniferous	0	0	0	1	0	0	49	10		0	60
bare	0	0	7	6	0	3	0	2	0		18
Input	8,367	80,569	22,563	8,305	44,142	71,233	8,974	1,919	1,937	6,814	

In areas with the improved ecological quality, broad-leaved forests account for the largest proportion, which indicates that the area of broad-leaved forests plays an important role in ecological quality. At the same time, it was found that although grassland, shrubs, and other areas are also green areas, their impact on ecological quality is less than that of woodland. Through unchanging ecological regions, we know that the conversion between different types of characteristics can achieve a relative balance of ecological quality to a certain extent. It can be seen from the analysis of areas with degraded ecological quality that the increase in urban and field area has a significant negative correlation with ecological quality. Substituting bush areas for forest areas will result in a slight decline in ecological quality.

The remote sensing image was selected when the field had just been planted. During this period, the crops in the field have not fully grown, and the bare land constitutes a large area, which will greatly reduce the ecological quality. The main reason for the loss of wetlands and water bodies is the increase in urban areas. Most wetlands are located in low-altitude areas and the area is closer to the city. The decrease in the water area is mainly observed in wet areas near cities.

High-altitude mountainous areas are mostly forests, and the number of broad-leaved forests and their impact on environmental quality is greater than that of bamboo forests and coniferous forests. Moreover, human activities in most broad-leaved forest areas are restricted, so broad-leaved forests remain basically unchanged. The broad-leaved forest near the city was partially turned into shrubs. The reason is that due to the impact of urban development, grasslands and some trees have been replaced by cash crops. The number of bare lands has been reduced, and it has become an impermeable surface of the city, which has basically no impact on environmental quality.

Conclusions

Through the Landsat 5/TM and Landsat 8/OLI images of Taipei Living Circle from 1988 to 2019, the RSEI model combined with the Feature classification map was used to quantitatively evaluate the ecological quality and changes of Taipei Living Circle, and monitor the changes. An analysis of the results leads to several conclusions.

1. Taipei Living Circle in 1988, 1995, 2006, and 2019, the remote sensing ecological index was 0.559, 0.571, 0.546, and 0.396 respectively. It showed a slight increase in the early period and a downward trend in the later period. From an overall perspective, ecological quality shows a trend of degradation.

2. From the RSEI level statistics, the average accounts for the majority, exceeding 50%. The comparison of data from 1988 and 2019 revealed that the fair area and poor area increased by 807,766, the average area decreased by 845,805, and the good area and excellent area increased by 102,275. Both the areas with a better environment and the areas with the worse environment have increased, the average area accounting for the largest area has decreased, and the overall environmental performance has decreased.

3. The forest area covered with coniferous forest, deciduous forest, and bamboo forest has reduced by 10% to 252,148 km². Agricultural land (fields and shrubs) decreased by 7.7% to 66,958 km². The water area comprising water and wetlands decreased by 18.2 % to 67,846 km². The building area comprising urban, grass, and bare land increased by 72.7% to 377,547 km².

4. Through the transfer matrix of land-use types of different RSEI levels, it can be seen that forests and water bodies have a positive effect on the environment, while agricultural building areas have a negative effect on the environment. Forest has the greatest impact on the ecological index, and the area of broad-leaved species determines the influence of the entire area. Although grasslands, shrubs, and other areas are also green areas, their impact on ecological quality is less visible than that of forest land. Since the remote sensing image was taken at the sawing period, the vegetation in the field has not fully grown, and the reflected ecological index value is low.

References

1. Aminzadeh B., Khansefid M. A case study of urban ecological networks and a sustainable city: Tehran's metropolitan area. *Urban Ecosystems*, **2010**, 13, 23-36 <https://doi.org/10.1007/s11252-009-0101-3>
2. Chang C.P., Yang Y.T., Kuo H.C. Large Increasing Trend of Tropical Cyclone Rainfall in Taiwan and the Roles of Terrain. *Journal of Climate*, **2013**, 26, 4138–4147, <https://doi.org/10.1175/JCLI-D-12-00463.1>.
3. Cooper A., Shine T., McCann T., Tidane D.A. An ecological basis for sustainable land use of Eastern Mauritanian wetlands. *Journal of Arid Environments*, **2006**, 67, 116-141 <https://doi.org/10.1016/j.jaridenv.2006.02.003>
4. Estoque R.C., Murayama Y., Myint S.W. Effects of Landscape Composition and Pattern on Land Surface Temperature: An Urban Heat Island Study in the Megacities of Southeast Asia. *Science of the Total Environment*, **2017**, 577, 349-359. <https://doi.org/10.1016/j.scitotenv.2016.10.195>
5. Florence L. Guy F, Olivier A. The morphological pyramid and its applications to remote sensing: Multiresolution data analysis and features extraction. *Image Analysis & Stereology*, **2011**, 21, 49-53.
6. Grimm N.B., Faeth S.H., Golubiewski N.E., Redman C.L. Wu J., Bai X., et al. Global change and the ecology of cities. *Science*, **2008**, 319, 756-760 <https://doi.org/10.1126/science.1150195>
7. Jiang C. L., Wu L., Liu D., Wang S. M. Dynamic monitoring of eco-environmental quality in arid desert area by remote sensing: Taking the Gurbantunggut Desert China as an example. *The journal of applied ecology*, **2019**, 30, 877–883. <https://doi.org/10.13287/j.1001-9332.201903.008>
8. Jimenez A.A., Vilchez F.F., González O.N., Flores S.M. Analysis of the Land Use and Cover Changes in the Metropolitan Area of Tepic-Xalisco (1973–2015) through Landsat Images. *Sustainability*, **2018**, 10, 1860.
9. Kurtz C., Passat N., Gancarski P., Puissant A. Extraction of complex patterns from multiresolution remote sensing images: A hierarchical top-down methodology. *Pattern Recognition*, **2012**, 45, 685-706 <https://doi.org/10.1016/j.patcog.2011.07.017>
10. Liu Y, Arp H.P.H, Song X., Song Y. Research on the relationship between urban form and urban smog in China. *Environment and Planning B: Urban Analytics and City Science*, **2017**, 44: 328-342. <https://doi.org/10.1177/0265813515624687>
11. Ma L.G., Deng J., Yang H., Hong Y., Wang K. Urban landscape classification using Chinese advanced high-resolution satellite imagery and an object-oriented multi-variable model. *Frontiers of Information Technology & Electronic Engineering*, **2015**, 16, 238-249.
12. McDonnell M.J., MacGregor-Fors I. The ecological future of cities. *Science*, **2016**, 352, 936-938 <https://doi.org/10.1126/science.aaf3630>
13. Nakamura K., Kayaba Y., Nishihiro J., Takamura N. Effects of submerged plants on water quality and biota in largescale experimental ponds. *Landscape and Ecological Engineering*, **2008**, 4, 1-9.
14. Vorobyev O.N, Kurbanov E.A., Gubayev A.V. Polevshikova Y.A., Demisheva E.N., V.O. Koptelov. Remote sensing monitoring of urban forests. *Vestnik of Volga State University of Technology: Human. Ecology. Nature management*. **2015**, 25, 5-21.
15. Wei S.R., Jin X., Wang K., Liang H. Response of lake area variation to climate change in Qaidam Basin based on remote sensing. *Earth Science Frontiers*, **2017**, 24, 427-433. DOI: 10.13745/j.esf.yx.2016-10-1
16. Wen X., Ming Y., Gao Y., Hu X. Dynamic Monitoring and Analysis of Ecological Quality of Pingtan Comprehensive Experimental Zone, a New Type of Sea Island City, Based on RSEI. *Sustainability*, **2019**, 12, 1-14. <https://doi.org/10.3390/su12010021>

17. Xu H. A Remote Sensing Index for Assessment of Regional Ecological Changes. *China Environmental Science*, **2013**, 33, 889-897.
18. Xu Y., Knudby A., Côté-Lussier C. Mapping ambient light at night using field observations and high-resolution remote sensing imagery for studies of urban environments. *Building and Environment*, **2018**, 145, 104-114, <https://doi.org/10.1016/j.buildenv.2018.09.002>
19. Yang J.Y., Wu T., Pan X.Y., Du H.T., Li J.L., Zhang L., et al. Ecological quality assessment of Xiongan New Area based on remote sensing ecological index. *Chinese Journal of Applied Ecology*. **2019**, 30, 277-284 <https://doi.org/10.13287/j.1001-9332.201901.017>
20. Yang JY, Wu T, Pan XY, et al. Ecological quality assessment of Xiongan New Area based on remote sensing ecological index. *Ying Yong Sheng Tai Xue Bao*. **2019**; 30: 277-284. <https://doi.org/10.13287/j.1001-9332.201901.017>
21. Yu X., Guo X., Wu Z.. Land Surface Temperature Retrieval from Landsat 8 TIRS-Comparison between Radiative Transfer Equation-Based Method, Split Window Algorithm and Single Channel Method. *Remote Sensing*, **2014**, 6, 9829-9852. <https://doi.org/10.3390/rs6109829>
22. Zhang C., Xu H.Q., Zhang H., Tang F., Lin Z. Fractional vegetation cover change and its ecological effect assessment in a typical reddish soil region of southeastern China: Changting County Fujian Province. *Chinese Journal of Natural Resources*, **2015**, 30, 917-928. DOI:10.1115/1.4031791

MONITORING OF FOREST ECOSYSTEMS DISTURBANCES IN MARI EL REPUBLIC

Jun Ma

Volga State University of Technology

Natural factors and anthropogenic impact frequently result in different levels of forest disturbances, which have an important influence on forest resource management and climate change. Under the background of global warming, large-scale forest disturbance monitoring and its impact have become the hotspot and the focus of research worldwide. Remote sensing can obtain large-area forest cover data on a regular basis, thus becoming an important means of regular and continuous forest disturbance monitoring. Forest monitoring based on time series data has become the main research method. Therefore, based on in-depth analysis of the relevant methods of forest disturbance monitoring and their indexes, according to time series analysis technique, the author carried out research in Mari El Republic to detect forest disturbances from 10 Landsat images taken between 1985 and 2019. The vegetation index time series methods are adopted to extract the forest disturbance information. Based on the spatial and temporal resolutions of remote sensing data, the laws and driving factors of forest disturbance in the study area were analyzed. The results show that from 1985 to 2019 the number of forest pixels in Mari-El Republic did not change much, and the total area remained floating within a certain range. Forest disturbance pixel number and area of disturbance have an increasing trend year by year, of which the most obvious increase is observed in the period from 2007 to 2011. Finally, the prospects for future research are discussed.

Keywords: remote sensing, Landsat data, forest disturbance, vegetation index, time series, change detection.

Introduction

Forest is a type of land ecology system and an essential part of the Earth's biosphere. The carbon recycling and storage of forests play an important role in global land carbon cycle and climate change (He et al., 2001; Schimel, 1995). Due to the occurrence of forest disturbance events such as deforestation, fire (Kurbanov et al., 2017), drought (Millar, Stephenson, 2015) and insect outbreaks (Kautz et al., 2017). The forest communities are replaced by sparse forests, low shrubs and even grasslands, and the carbon originally stored in organisms is re-released into the atmosphere. These events have changed the composition, structure and function of forest systems. It seriously affects the ecological balance and stability of the region and to a certain extent affects the regional and global carbon budget, and may have an impact on the global climate system.

Under the background of global warming, forest disturbance monitoring and its impact have become the hotspot and the focus of research worldwide (Dale et al., 2000). Forest disturbance monitoring research is of great significance for revealing the temporal and spatial evolution of forests. It also provides basic theoretical and technical support for the global forest carbon sink estimation research, and has become an important topic in the field of global change research (Huang et al., 2010). The traditional forest resources and their changes are mainly based on ground surveys, which have problems such as large workload, high labor intensity, high cost, long cycle, low efficiency and poor timeliness. Moreover, the survey accuracy is not high enough to meet the needs of today's monitoring of forest resource changes, especially for large-scale forest disturbance monitoring. Remote sensing, with its wide coverage and repeatable access, can quickly monitor changes that occur, plan forestry activities to care for young plantations, and improve forecasts for the development of forest landscapes and territories (Kurbanov et al., 2010). It also plays an important role in the monitoring of forest changes and disturbances, thus also addressing the above stated problem.

Many experts and scholars have used satellite remote sensing technology to carry out a large number of forest disturbance monitoring studies, and their methods are mainly divided into two categories: threshold segmentation and image classification (Healey et al., 2005). Many researchers point to the need for long-term monitoring and development of technology to assess the eco-

system response to natural disturbances (droughts and fires) from satellite image (Kurbanov et al., 2011).

The purpose of this research is to provide the basis for the local forest protection, and to provide data and support method for forest resource inventory and management.

Study area and materials

The study area Of Mari El; Republic of Russia is located between 45°37' E and 50°12' E, 55°48' N and 57°20' N, where it occupies 23 thousand km² (fig.1). The territory is a hilly plain with elevation range from 45 to 275 m above the sea level. The climate is moderately-continental with distinct and stable weather in winter and summer and variable weather in spring and fall. The mean annual temperature varies from +2.20 C in the north-eastern part to +3.10 C in the south-west. In recent years, winter months have been warmer than they used to be. The average amount of precipitation is 450-500 mm, including 200-250 mm during vegetation period.

According to a forest resource study conducted in 2017, the forested area of Mari El Republic covers 1,117 thousand ha (Vorobev, Kurbanov, 2017) and the forest cover is 55.4%. The main forest-forming species are pine (*Pinus sylvestris*), spruce (*Picea Abies*), birch (*Betula pendula*), linden (*Tilia cordata*) and aspen (*Populus tremula*). The region can be subdivided into three ecological zones: southern taiga, mixed forest and forest-steppe. The Volga River serves as the natural western border of physiographic and natural conditions. This area has a high rate of forest coverage, and the forest disturbance has changed significantly since 1985 (Kurbanov et al., 2017). Therefore, Mari El Republic serves as a good site for detecting changes in disturbance regimes caused by natural and social conditions, as well forest management policies.

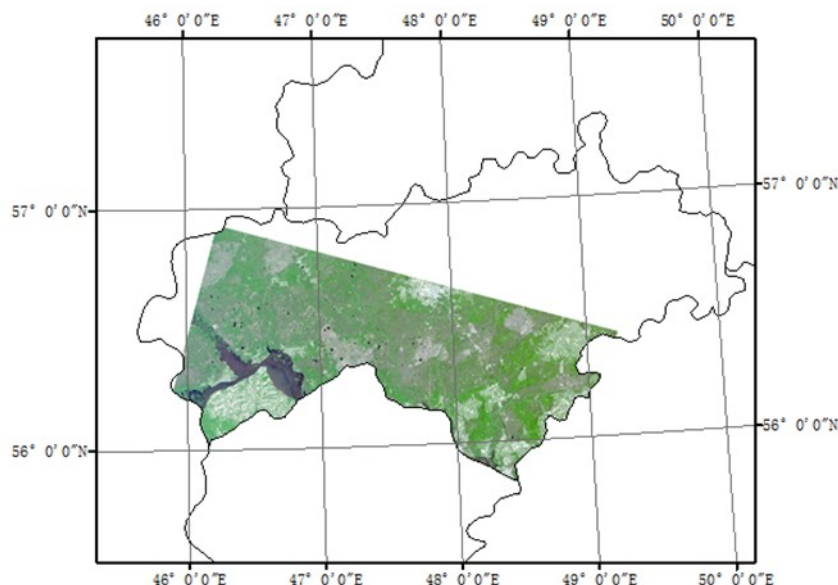


Fig. 1. Location map of study area

Materials and Method

Remote Sensing Images. Landsat remote sensing data acquisition and processing selection during 1985-2019, Landsat images with a spatial resolution of 30 m were used as the main data source to extract forest disturbance information in the study area (Kurbanov et al., 2014). The image data came from the USGS website. The study takes 3-5 years and selects the vegetation growth period (June to early October). In some years, due to cloud coverage, the images are selected for 6 years. A total of 10 scene images were selected as the source data (table 1).

Table 1

Remote sensing data

No.	Date	Sensor	Sources	Level	Cloud/%
1	10.08.1985	Landsat TM	USGS	L1T	0
2	30.05.1988	Landsat TM	USGS	L1T	0
3	25.05.1992	Landsat TM	USGS	L1T	0
4	05.07.1995	Landsat TM	USGS	L1T	1
5	11.06.1998	Landsat TM	USGS	L1T	0
6	29.05.2002	Landsat ETM +	USGS	L1T	2
7	27.05.2007	Landsat ETM +	USGS	L1T	1
8	01.07.2011	Landsat TM	USGS	L1T	0
9	19.05.2013	Landsat OLI	USGS	L1T	0
10	05.06.2019	Landsat OLI	USGS	L1T	2

Preprocessing of Remote Sensing Images. The Landsat ETM images obtained in 2007 have lost data bands. In this paper, the ENVI5.3 plug-in “landsat_gapfill.sav” is used, and the missing bands are repaired by interpolation using a mask. Since the reflectivity of the water body in the fourth band of Landsat is very low, in order to eliminate the influence of directional reflection and prevent the water body from interfering with the recognition of cloud shadows and conducive to radiation calibration and atmospheric correction, before the cloud shadow recognition Water mask. In the study, MNDWI (Wang et al., 2013) was used to extract water. For cloud pixels, this study uses “Fmask 4.0” to extract and make a mask (Qiu et al., 2019). After grinding the cloud and cloud shadow, a certain empty value was generated, which needs to be filled with time interpolation. The Landsat calibration tool of 5.3 was used in conjunction with metadata and data header information to convert the DN value of the Landsat TM/ETM+/OLI data into radiance values. In this radiation calibration, the calibration coefficient proposed in the study (Chander et al., 2009) is used: The Landsat 5/7/8 TM /ETM /OLI image data used in the research institute were using atmospheric radiation correction software Landsat ecosystem disturbance adaptive processing system (LEDAPS).The geometric correction uses the area gray matching method to automatically generate matching points, and adopts the quadratic polynomial method based on control points to complete the geometric correction of the L2 product, so that the registration accuracy is controlled within 0.5 pixels.

Forest extraction. Objects in object-oriented classification technology are represented as collected adjacent pixels, and then through these objects we identify the spectral elements of interest (Walker, Briggs, 2007). This method can make good use of high-resolution panchromatic and multi-spectral bands with rich color information, multi-segment texture, spatial and spectral information segment and classification of features. The final classification result is highly accurate. At the same time, the final classification result can also be output in the form of a vector. This paper uses the “Feature Extraction” module to extract forest area information from high-resolution panchromatic or multi-spectral data based on image space and image spectral characteristics, that is, object-oriented.

Then the extracted 1985 forest area is used as a mask file for subsequent operations, which can improve the detection accuracy and reduce the amount of calculation. The scale level of this study is 40, the merge level is 85 and the attributes are >0.77 in the spectral mean. There are three pixel values in the output raster image: 0, 1, 2, where the value 1 represents the forest area. The Forest extractions are shown in fig. 2.

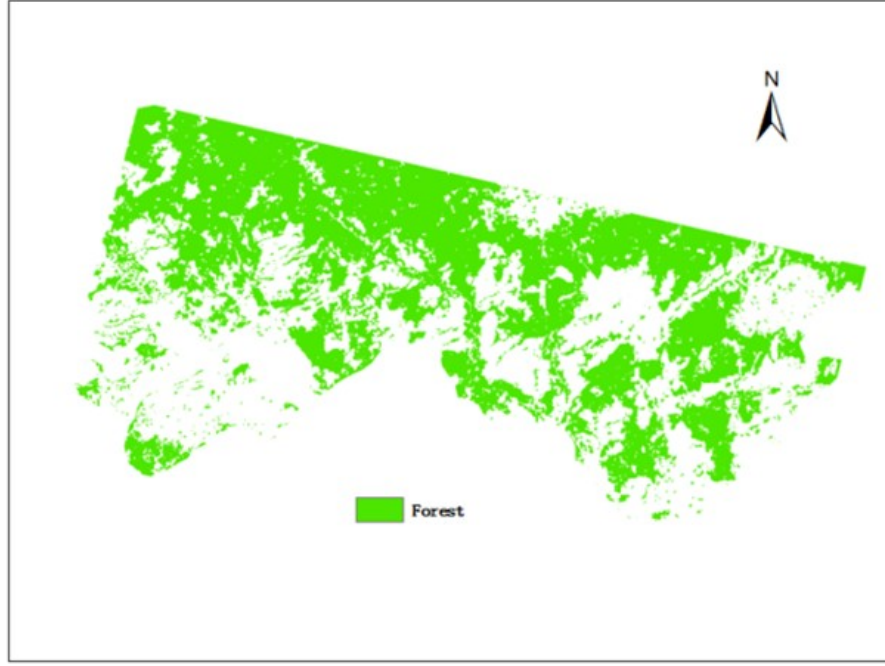


Fig. 2. Forest extractions

Forest canopy change detection. NDVI is an important indicator reflecting the ecological environment and one of the most widely used vegetation indices. However, under sparse vegetation cover conditions, NDVI is susceptible to soil background interference (Wulder et al., 2004), and for dense vegetation, NDVI also exhibits saturation effects (Asrar et al., 1984). Maselli (2004) used NDVI index to conduct long-term monitoring of forest conditions in Mediterranean protected areas and analyzed changes in ecosystem function in the region. Its formula is as follows:

$$NDVI = \frac{NIR - R}{NIR + R}, \quad (1)$$

where R is the reflection value of the red light band, and NIR is the reflection value of the near infrared band.

In this study, the image difference method is used to extract the forest change information using the $NDVI$ interpolation results $\Delta NDVI$ of the two scenes before and after the image. The image after the " i " scene image is the " p " scene image and the formula is:

$$\Delta NDVI = NDVI_i - NDVI_p$$

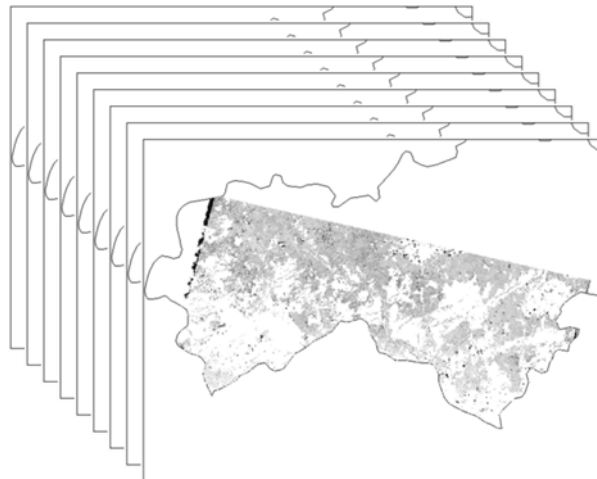


Fig. 3. Examples of the $\Delta NDVI$ Images

Data standardization. In order to minimize the impact of seasonal changes and directional reflection on the consistency of data, this study uses the mature forest standardization method (Hansen et al., 2008) to standardize the bands and indices used:

$$I_r = \frac{(I - I_\mu)}{I_\sigma}, \quad (3)$$

where I_r is the normalized band or index; I_μ and I_σ are the average and standard deviation of the mature forest area in the band or index, respectively. Among them, the mature forest area is extracted using data, and according to the surface classification system, the part with a pixel value of 1 to 7 is selected as the forest pixel, including evergreen coniferous forest.

Broad-leaved forests, deciduous coniferous forests, deciduous broad-leaved forests, mixed forests, dense shrub forests and sparse shrub forests, the rest non-forest pixels, and forest pixels are extracted through image masks.

Vegetation change tracking algorithm. Vegetation Change Tracker (VCT) is an algorithm for automatic monitoring of forest disturbances based on Landsat time series data at two-year intervals. It fully utilizes time series information to automatically monitor and track land cover changes (Li et al., 2009). Before tracking the vegetation change of the time series index, we selected 4 index values per year, calculated the average value of multiple pixels in the window according to the size of the season setting window and extracted it to obtain the image. We drew the trajectory of the time series of the meta-index, and then tracked the trajectory of the time series of each pixel index, established decision rules according to the time characteristics of the forest change process of the index, and finally determined whether there is forest disturbance in the pixel.

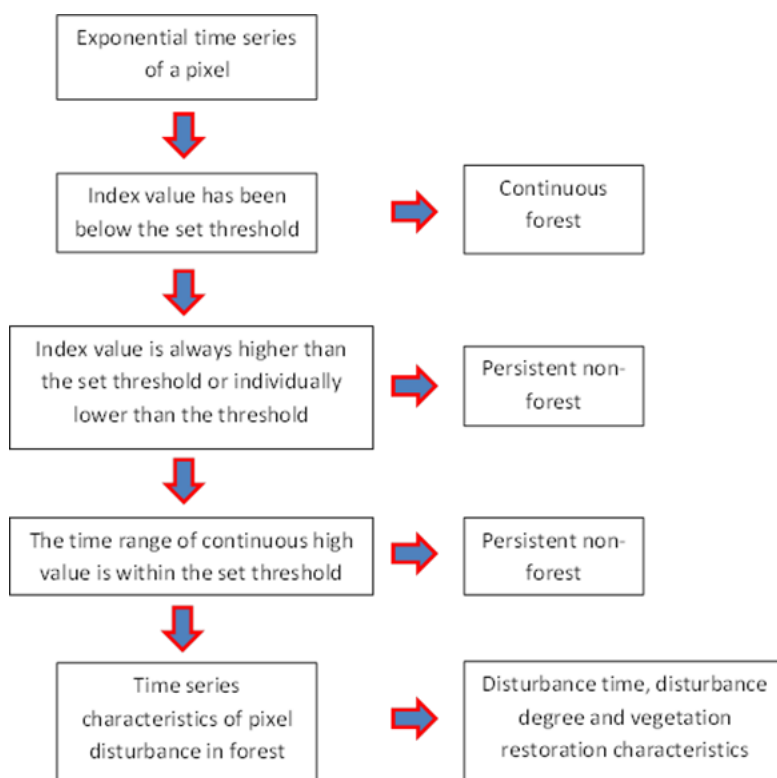


Fig. 4. Major steps and decision rules of VCT algorithm

1) When the forest is not disturbed, the normalized index value only fluctuates around the zero value. The index of a pixel has been at a low (high) value in the time series, and within the set threshold range, then the pixel did not disturb the forest during the monitoring period, and it was determined as a continuous forest.

2) The index value of non-forest pixels is high (low), the continuous non-forest pixels appear in the time series as the index value is always at a high (low) value, and the index of a pixel is in the set threshold in the time series. Outside the range, the pixel is determined to remain non-forest. However, there may also be occasions where the index value is lower (higher) than the threshold for a very small part of the time (Li et al., 2009). When this period of time does not continue for more than a year, the pixel is considered to be a continuous non-forest pixel.

3) The recognition degree of farmland is low, and the index value often shows seasonal fluctuations between high and low values in the time series. The seasonal change is more obvious. The index value is higher in a short period of time. In order to distinguish farmland from disturbing pixels, we used Judging by the time range of continuous high values (Zhao et al., 2015), when the time of continuous high values is within one year, the pixel is considered to be farmland, that is, non-forest pixels, otherwise it is a pixel that has been disturbed. The influence of seasonal fluctuations of index values on the monitoring results of forest disturbances in the time series is reduced.

Extract forest disturbance information. The threshold segmentation method is a common method in image segmentation. This method uses the gray level difference between the target and the background, and then divides the pixel level into different categories by setting a certain threshold, and finally can separate the target and the background.

We used the histogram of the NDVI difference image to find the segmentation threshold. The scene image is composed of multiple forest interference characteristic areas, and the histogram presents a multi-peak phenomenon. Each peak corresponds to a forest interference characteristic area, and the adjacent peak is divided by the valley point convex threshold, by visual method. A, B, and C "inflection points" are visible in the histogram. The pixel values corresponding to these three "inflection points" are segmentation thresholds. Therefore, the forest interference area is divided into slight interference area, medium interference area and severely interference area. [MIN, A]: Slightly disturbance zone, [A, B]: Medium disturbance zone, [B, C]: Severely disturbance zone. After determining the segmentation threshold, we edited and output the gray segmentation results to obtain statistical results, and finally used the 3×3 window to filter the small interference spots, so as to obtain the final forest interference products year by year. Fig. 5, fig. 6 and fig. 7 take Histograms of NDVI 2019-NDVI 2013 as an example, In the example of Histograms of NDVI 2019-NDVI 2013, MIN is -1.9894764, the value of point A is -0.1403, the value of point B is -0.0252, and the value of point C is -0.0109. The other NDVI difference images are defined according to this method. The three "inflection points" A, B, and C have been obtained. The value of the "inflection point" is obtained according to the visual observation of the histogram.

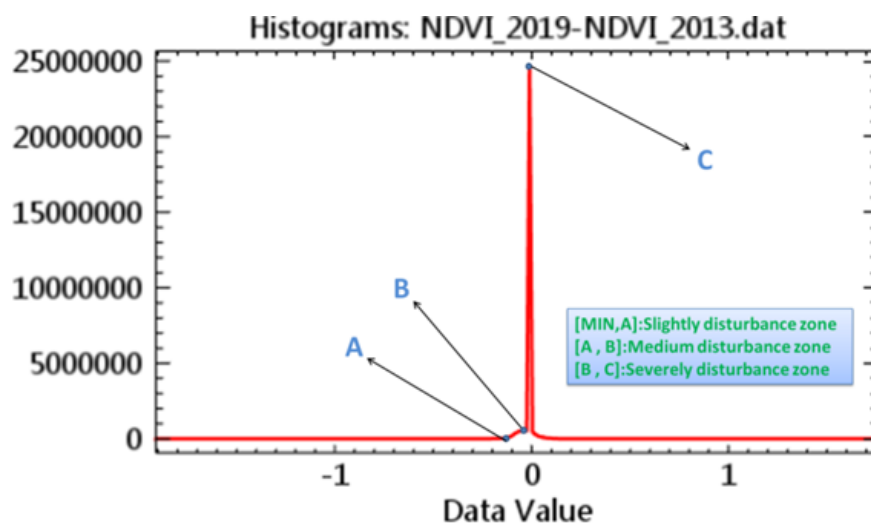


Fig. 5. Histograms of NDVI 2019-NDVI 2013

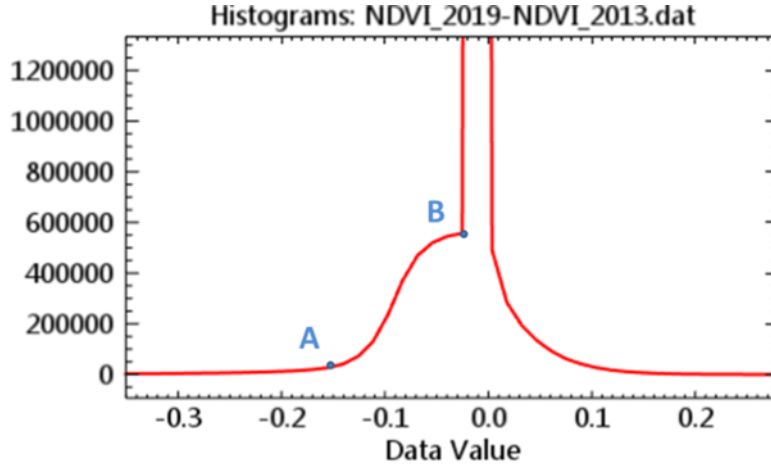


Fig. 6. Detail histogram of NDVI 2019 - NDVI 2013 (1)

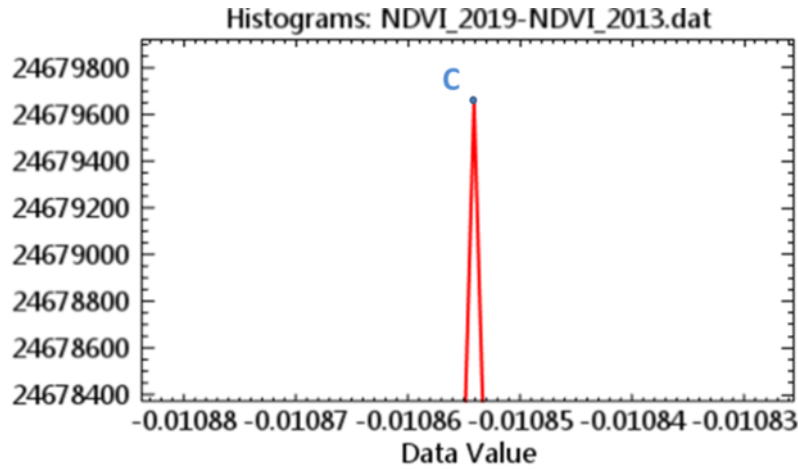


Fig. 7. Detail histogram of NDVI 2019-NDVI 2013 (2)

Accuracy evaluation. In this study, the confusion matrix is used to obtain the detection accuracy. Among them, Overall Accuracy (OA) represents the combination of correctly classified pixels divided by the total number of pixels (Fitzgerald, Lees, 1994). Kappa is a multivariate statistical method for evaluating classification accuracy and it refers to the proportion of errors reduced by the evaluated classification compared to completely random classification. The classifier correctly divides the pixels of the entire image into the number of pixels in a specific category and the ratio of the total number of actual references in a specific category is called the mapping accuracy (Manandhar et al., 2009). The ratio of the total number of pixels correctly classified into a specific category is called user accuracy. The calculation is as follows:

$$OA = \frac{x_{ii} + x_{jj}}{N} \times 100\% , \quad (4)$$

$$Kappa = \frac{N \sum_i^r x_{ii} - \sum (x_{i+} x_{+i})}{N^2 - \sum (x_{i+} x_{+i})} , \quad (5)$$

$$P_{Ai} = \frac{x_{ii}}{x_{+i}} \times 100\% , \quad (6)$$

$$U_{Aj} = \frac{x_{ii}}{x_{i+}} \times 100\% , \quad (7)$$

where OA is the overall accuracy; in the Kappa coefficient, r is the number of rows of the error matrix; x_{ii} is the value on the i row and i column (main diagonal); x_{i+} and x_{+i} are the sum and the

sum of column i ; N is the total number of samples; P_{Ai} is the cartographer accuracy of class i ; U_{Aj} is the user accuracy of class j .

Results and discussion

Accuracy evaluation results. The Mari-El forest disturbance monitoring confusion matrix from 1985 to 2019 is shown in table 2. The disturbance points are classified. The number of 326 refers to 386 pixel points, but many non-disturbance points are sacrificed, and 46 are misclassified, which is not stable enough. The overall accuracy for unbalanced classification in Table 3 is 99.26%, and the kappa coefficient is 0.89, which meets the accuracy requirements of disturbance monitoring.

Table 2

1985 to 2019 Mari-El forest disturbance monitoring confusion matrix

Number of pixels	Disturbed point	Undisturbed point
Disturbed point	326	46
Undisturbed point	53	10935

Table 3

1985 to 2019 Mari-El forest disturbance monitoring accuracy

Project	Disturbed point	Undisturbed point
Cartographer accuracy/%	87.19	99.13
User precision/%	89.2	99.45
Overall accuracy/%	99.26	
Kappa	0.89	

The methods proposed in this study aiming at the characteristics of low spatial resolution and unbalanced classification can not only effectively improve the classification accuracy and solve the problem of unbalanced classification. Iterative training can also provide a more stable and robust monitoring model. In the accuracy test, the kappa coefficient is 0.89. The plotter precision and user precision of the disturbance point are 87.19% and 89.2% respectively, which shows good stability. Both precisions of the non-disturbance point are above 99%, which guarantees the user precision of the disturbance point and a high kappa coefficient.

Mari-El Forest Disturbance from 1985 to 2019. According to the analysis results of the forest disturbance results map (fig. 8)

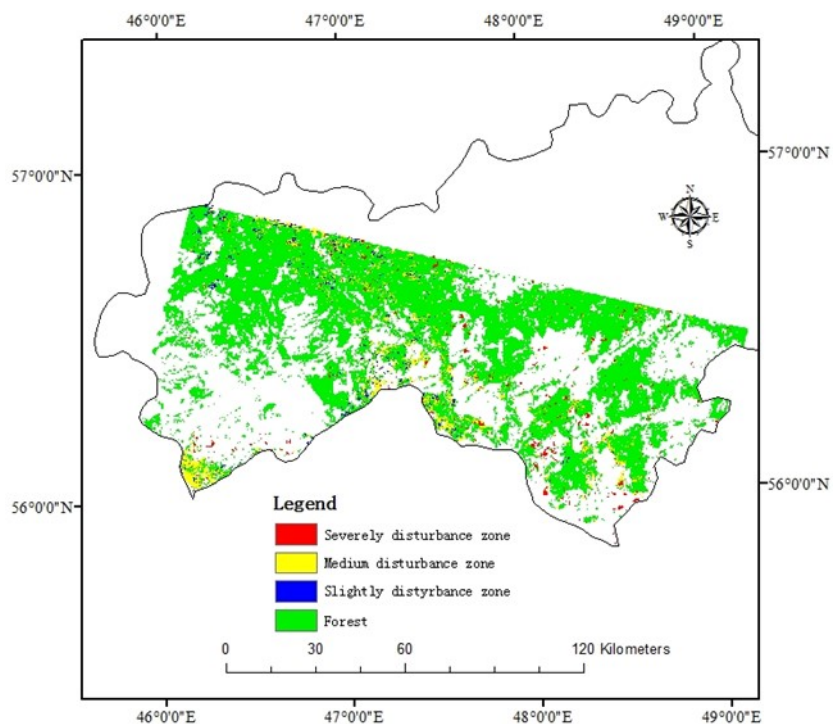


Fig. 8. Mari-El Forest Disturbance Map from 1985 to 2019

and the forest disturbance detail map (fig. 9) of the study area from 1985 to 2019, the forests of Mari-El Republic have suffered a large disturbance.

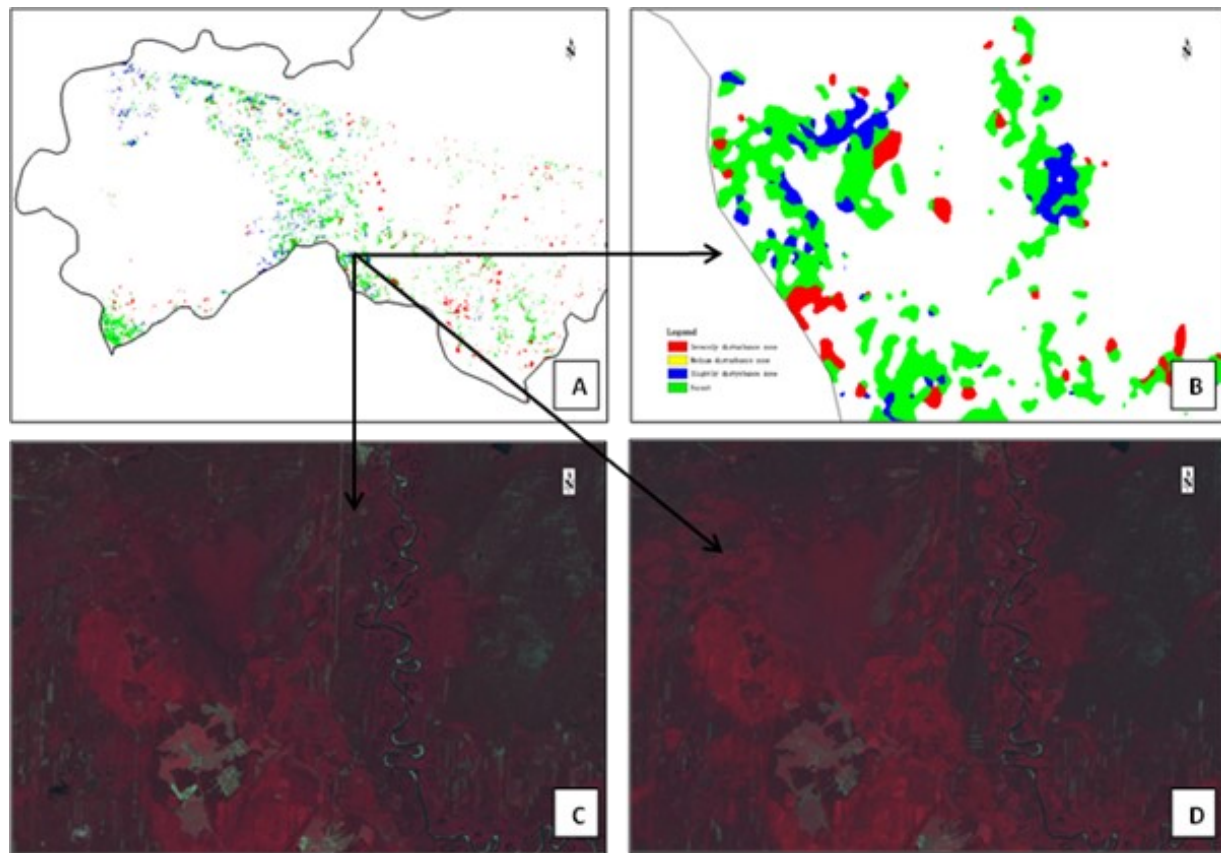


Figure 9. Disturbance maps of Mari El: A) forest disturbance map; B) forest disturbance detail map; C) Landsat CIR map in 2002; D) is Landsat CIR map in 2007

Through the map of forest disturbance changes from 1985 to 2019. It was estimated that from 1985 to 2019, the number of forest pixels in Mari-El Republic did not change significantly, and the total area remained floating within a certain range. Forest disturbance pixel number and area of disturbance have an increasing trend year by year, of which the most obvious increase is from 2007 to 2011. Area of forest disturbance is 1,117.49 km², accounting for 8.42% of the total forest area. The annual statistics is shown in Table 4. The highest disturbance accounted for 8.42% in 2007-2011, and the lowest disturbance accounted for 0.41% in 1988-1992.

Table 4

The area of forest disturbance changes in different years

Year	Forest pixel number	Area of Forest, km ²	Area of disturbance, km2	%
2019	14587720	13128.95	375.43	2.86
2013	14405930	12965.34	446.45	3.44
2011	14743575	13269.22	1117.49	8.42
2007	14677232	13209.51	302.35	2.29
2002	14489206	13040.29	278.80	2.14
1998	14009290	12608.36	84.02	0.67
1995	14334776	12901.30	53.93	0.42
1992	14252640	12827.38	52.26	0.41
1988	14405260	12964.73	462.38	3.57

Analysis of the forest disturbances in the Mari El from 1985 to 2019. The forests of Mari-El continued to be disturbed from 1985 to 2019 (Table 5). The forest area transfers changed significantly every two periods. This shows that during this period, the forest is still affected by various factors, and disturbances continue to occur. From the time dimension, the area of forest transfer from 2007 to 2011 is much larger. The loss of forest area is quite serious, mainly due to regional disturbances. Field investigations revealed that a serious forest fire occurred in 2010.

After 2010, the area transferred from the forest showed a downward trend, and the area transferred to forest showed a rapid upward trend, indicating that the local forest restoration and environmental protection policies after the disaster also have a certain inhibitory effect on forest disturbances, which owe to the protection of forest and its ecological environment. Overall, the disturbance mainly occurs when it is mainly logging and forest fires. Therefore, forest disturbance mainly occurs near roads and water areas, and is constrained by terrain and traffic. Urbanization has gradually become a forest disturbance in this area and the driving factor that cannot be ignored.

Table 5

Forest disturbance changes in Mari-El from 1985 to 2019

Year	Severely disturbance zone	Medium disturbance zone	Slightly disturbance zone
2019	0.61	1.18	1.89
2013	1.04	1.77	1.44
2011	4.03	1.18	0.49
2007	1.06	2.29	1.72
2002	1.07	2.64	2.09
1998	0.55	0.23	0.15
1995	0.76	1.87	1.40
1992	1.16	2.87	0.57
1988	1.89	1.37	2.13

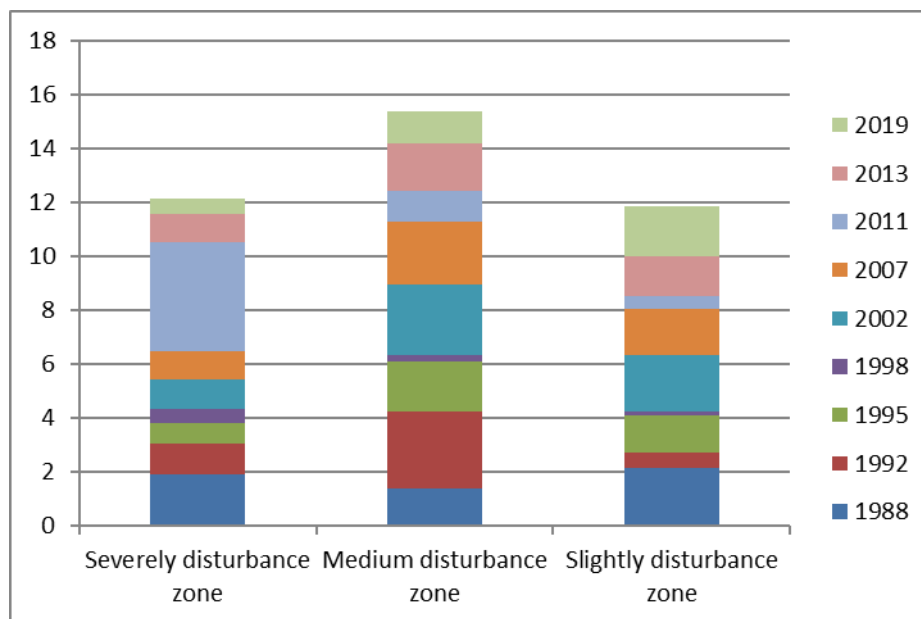


Figure 10. Trend map of forest disturbance Mari-El from 1985 to 2019

Conclusions

This paper reviews and summarizes the update and development of remote sensing data, remote sensing monitoring methods and monitoring indexes of forest disturbances. It summarizes and compares several current disturbance monitoring indexes. And this study is also based on the Landsat TM/ETM+/OLI remote sensing image with a resolution of 30 m, using object-oriented classification method to extract forest area and NDVI image difference method. The research results show that the NDVI image difference extraction forest disturbance method has high accuracy in extracting boreal forests, and has the advantages of simple and convenient operation, and is a cost and time-effective method.

According to the interference monitoring results of Mari-El forests between 1985 and 2019, the forests in this area are still continuously disturbed by various factors. Among them, the disturbances were the largest in 2007-2011 and the least in 1988-2002. The area of thermal forests was year by year. With the decreasing trend, the situation of forest protection is still severe. Since the changes in forest area are closely related to regional and environmental protection policies, according to the continuous increase in forest area in 2011, regional land use and environmental protection policies can suppress the extent of human activities that interfere with forests area. This results in protection and restoration of ecological environment.

The method of automatic extraction of forest samples used in this study can effectively and quickly extract a large number of accurate forest samples, improve the detection accuracy and reduce the amount of calculation for the extraction of forest disturbance areas. It can be used in related research. Although the NDVI image difference extraction method for forest disturbances has a high efficiency and reliable basis for forest disturbance monitoring, it is prone to misdetect agricultural land during the growth period of crops. So the next research needs to consider this aspect. The method is optimized, and the thresholds of forest segmentation in different regions are different. We need to refer to relevant literature and field research to continuously debug to find the optimal threshold, and further clarify the type of forest disturbance in the region and analyze the causes of forest disturbance.

Recommendations

It can be seen that although forest disturbance remote sensing monitoring technology has been well applied in recent years, there are still some shortcomings, and further research can be carried out in the following three aspects:

- 1) Strengthening the comparative study of the disturbance monitoring index. Due to the fact that the construction methods and theoretical basis of different indexes are different, the monitoring effects for different types of disturbances are also different. Therefore, for the specific forest disturbance types, it is helpful to further distinguish and identify the causes of disturbances by comparing the monitoring effects of different indices.

- 2) Conducting long-term sequence disturbance monitoring analysis. For a long time, forest disturbance research has been based on the study of changes in remote sensing data of Phase 2 or Phase 3. It is not only time-consuming and laborious, but also has a significant reduction in accuracy during long-term sequence analysis, so that it cannot meet the application requirements. By combining the long-term sequence disturbance analysis method with the appropriate disturbance monitoring index, the monitoring efficiency of forest disturbance can be further improved.

- 3) Establishing and improving the disturbance monitoring model applicable to regional forests. Frequent changes in forests have caused great disturbances in the estimation of terrestrial carbon sinks, while most of the existing forest carbon stocks use forest resource inventory data, and forest disturbance monitoring based on remote sensing data is underdeveloped. Therefore, it is of great

theoretical significance and practical value to study the disturbance monitoring model applicable to regional forests.

This project/achievement/thesis was funded by "China Scholarship Fund".

This article was completed under the careful guidance of my mentors prof. E.A. Kurbanov, who has given me a lot of help in academic direction determination, topic selection, experimental methods, data processing, theoretical analysis, and finalization of the thesis. During the two-year graduate career, under the guidance of Professor Eldar Kurbanov, I have gained a lot of practical knowledge and techniques, the morality and character of being a person, and more importantly, a serious attitude to everything I do.

References

1. Asrar G.Q., Fuchs M., Kanemasu E.T., Hatfield J.L. Estimating absorbed photosynthetic radiation and leaf area index from spectral reflectance in wheat 1. *Agronomy journal*, **1984**, 76, 300-306. <https://doi.org/10.2134/agronj1984.00021962007600020029x>
2. He C., Wang S., Xu J., Zhou C. Using remote sensing to estimate the change of carbon storage: A case study in the estuary of Yellow River delta. *International Journal of Remote Sensing*, **2002**, 23, 1565-1580. <https://doi.org/10.1080/014311602753590887>
3. Chander G., Markham B.L., Helder D.L. Summary of current radiometric calibration coefficients for Landsat MSS, TM, ETM+, and EO-1 ALI sensors. *Remote sensing of environment*, **2009**, 113, 893-903. <https://doi.org/10.1016/j.rse.2009.01.007>
4. Dale V.H., Joyce L.A., McNulty S., Neilson R.P. The interplay between climate change, forests, and disturbances. *Science of the total environment*, **2000**, 262, 201-204 [https://doi.org/10.1016/S0048-9697\(00\)00522-2](https://doi.org/10.1016/S0048-9697(00)00522-2)
5. Fitzgerald R.W., Lees B.G. Assessing the classification accuracy of multisource remote sensing data. *Remote sensing of Environment*, **1994**, 47, 362-368. [https://doi.org/10.1016/0034-4257\(94\)90103-1](https://doi.org/10.1016/0034-4257(94)90103-1)
6. Hansen M.C., Roy D.P., Lindquist E., Adusei, B., Justice C.O., Altstatt A. A method for integrating MODIS and Landsat data for systematic monitoring of forest covers and changes in the Congo Basin. *Remote Sensing of Environment*, **2008**, 112, 2495-2513. <https://doi.org/10.1016/j.rse.2007.11.012>
7. Huang C., Goward S.N., Masek J.G., Thomas N., Zhu Z. and Vogelmann J.E. An automated approach for reconstructing recent forest disturbance history using dense Landsat time series stacks. *Remote Sensing of Environment*, **2010**, 114, 183-198. <https://doi.org/10.1016/j.rse.2009.08.017>
8. Healey S.P., Cohen W.B., Zhiqiang Y., Krankina O.N. Comparison of Tasseled Cap-based Landsat data structures for use in forest disturbance detection. *Remote sensing of environment*, **2005**, 97, 301-310. <https://doi.org/10.1016/j.rse.2005.05.009>
9. Kurbanov E.A., Vorobev O.N., Leznin S.A., Polevshikova Y.A. and Demisheva E.N. Assessment of burn severity in Middle Povolzhje with Landsat multitemporal data. *International Journal of Wildland Fire*, **2017**, 26, 772-782. <https://doi.org/10.1071/WF16141>
10. Kurbanov E.A., Vorobev O.N., Gubaev A.V., Lezhnin S.A., Nezamaev S.A., Aleksandrova T.A. Estimation of reforestation on abandoned agricultural lands in Republic Mari El by satellite images. *Vestnik MarGTU. Seriya "Les. Ekologiya. Prirodopol'zovanie"*, **2010**, 9, 14-20.
11. Kurbanov E.A., Nureeva T.V., Vorobev O.N., Gubaev A.V., Lezhnin S.A., Miftakhov T.F. et al. Remote monitoring of disturbances in forest cover, reforestation and afforestation of Mari Zavolzhje. *Vestnik MarGTU. Seriya "Les. Ekologiya. Prirodopol'zovanie. Ser.: Les. Ekologiya. Prirodopol'zovanie"*, **2011**, 3, 17-24.
12. Kurbanov E.A., Vorobev O.N., Gubaev A.V., Lezhnin S.A., Polevshchikova Yu.A., Demisheva E.N. Four decades of forest research with the use of Landsat images. *Vestnik MarGTU. Seriya "Les. Ekologiya. Prirodopol'zovanie"*, **2014**, 1, 18-32.
13. Kautz M., Meddens A.J., Hall R.J., Arneeth A. Biotic disturbances in Northern Hemisphere forests – a synthesis of recent data, uncertainties and implications for forest monitoring and modelling. *Global Ecology and Biogeography*, **2017**, 26, 533-552. <https://doi.org/10.1111/geb.12558>
14. Li M., Huang C., Zhu Z., Shi H., Lu H., Peng S. Assessing rates of forest change and fragmentation in Alabama, USA, using the vegetation change tracker model. *Forest Ecology and Management*, **2009**, 257, 1480-1488. <https://doi.org/10.1016/j.foreco.2008.12.023>
15. Li M., Huang C., Zhu Z., Wen W., Xu D. and Liu A. Use of remote sensing coupled with a vegetation change tracker model to assess rates of forest change and fragmentation in Mississippi, USA. *International Journal of Remote Sensing*, **2009**, 30, 6559-6574. <https://doi.org/10.1080/01431160903241999>
16. Maselli F. Monitoring forest conditions in a protected Mediterranean coastal area by the analysis of multiyear NDVI data. *Remote sensing of environment*, **2004**, 89, 423-433. <https://doi.org/10.1016/j.rse.2003.10.020>
17. Manandhar R., Odeh I.O., Ancev T. Improving the accuracy of land use and land cover classification of Landsat data using post-classification enhancement. *Remote Sensing*, **2009**, 1, 330-344. <https://doi.org/10.3390/rs1030330>
18. Millar C.I., Stephenson N.L. Temperate forest health in an era of emerging mega disturbance. *Science*, **2015**, 349, 823-826. <https://doi.org/10.1126/science.aaa9933>
19. Qiu S., Zhu Z. and He B. Fmask 4.0: Improved cloud and cloud shadow detection in Landsats 4–8 and Sentinel-2 imagery. *Remote Sensing of Environment*, **2019**, 231, 111205. <https://doi.org/10.1016/j.rse.2019.05.024>

20. Schimel D.S. Terrestrial ecosystems and the carbon cycle. *Global Change Biology*, **1995**, *1*, 77-91. <https://doi.org/10.1111/j.1365-2486.1995.tb00008.x>
21. Vorobev O.N., Kurbanov E.A. Remote monitoring of vegetation regeneration dynamics on burnt areas of Mari Zavolzhje forests. *Sovremennye Problemy Distantionnogo Zondirovaniya Zemli Iz Kosmosa*. **2017**, *14*, 2. <https://doi.org/10.21046/2070-7401-2017-14-2-84-97>
22. Wang Y., Huang F., Wei Y.. Water body extraction from LANDSAT ETM+ image using MNDWI and KT transformation. In 2013 21st International Conference on Geoinformatics, Kaifeng, China, 20-22, June, **2013**, IEEE, 1-5. <https://doi.org/10.1109/Geoinformatics.2013.6626162>
23. Walker J.S., Briggs J.M. An object-oriented approach to urban forest mapping in Phoenix. *Photogrammetric Engineering & Remote Sensing*, **2007**, *73*, 577-583. <https://doi.org/10.14358/PERS.73.5.577>
24. Wulder M.A., Skakun R.S., Kurz W.A., White J.C. Estimating time since forest harvest using segmented Landsat ETM+ imagery. *Remote sensing of environment*, **2004**, *93*, 179-187. <https://doi.org/10.1016/j.rse.2004.07.009>
25. Zhao F., Huang C., Zhu Z. Use of vegetation change tracker and support vector machine to map disturbance types in greater yellow stone ecosystems in a 1984–2010 Landsat time series. *IEEE Geoscience and Remote Sensing Letters*, **2015**, *12*, 1650-1654. <https://doi.org/10.1109/LGRS.2015.2418159>

ОЦЕНКА ЗАРАСТАНИЯ ЗАЛЕЖЕЙ ЯРАНСКОГО РАЙОНА КИРОВСКОЙ ОБЛАСТИ ПО СПУТНИКОВЫМ ДАННЫМ

С.А. Лежнин

Поволжский государственный технологический университет

В статье представлены результаты исследования зарастания земель залежей Яранского района Кировской области древесно-кустарниковой растительностью, выполненного с использованием спутниковых снимков высокого разрешения Sentinel. Во многих регионах Российской Федерации, в том числе и в Кировской области, отсутствие актуальной картографической основы является лимитирующим фактором при решении задач мониторинга зарастающих земель. Применение современных технологий позволяет проводить мониторинг больших территорий заброшенных сельскохозяйственных угодий с минимальными финансовыми трудовыми затратами. Для определения площади зарастания залежей древесно-кустарниковыми породами были отобраны спутниковые снимки высокого разрешения Sentinel-2 за три периода: весенние снимки (начало мая 2019 г.), летние снимки (июль 2019 г.) и осенние снимки (сентябрь 2019 г.). Снимки были объединены в композиты с различным набором спектральных каналов (2 – синий канал; 3 – зеленый; 4 – красный; 8 – ближний инфракрасный) для выявления оптимального сочетания каналов и времени съемки. Тематическое картографирование молодняков древесных пород на заброшенных сельскохозяйственных землях Яранского района выявило значительные площади зарастания на 2019 год. Наилучшую точность классификации показала летняя карта в сочетании спектральных каналов 8-4-2. Доля лиственных молодняков на залежах составила 16,35 % от общей площади сельскохозяйственных земель района, тогда как площадь хвойных молодняков – 11,31 %. Общая площадь сельскохозяйственных земель Яранского района составила 192380,1 га, часть из которых (около 33 %) зарастает древесной растительностью. Проверка точности тематической карты лесовозобновления на исследуемых землях показала высокую точность классификации, которая составила 77 %.

Ключевые слова: залежи, спутниковые снимки, спектральный канал, тематические карты, оценка точности, Sentinel.

THE USE OF SATELLITE DATA IN THE ASSESSMENT OF REFORESTATION ON THE ABANDONED AGRICULTURAL LANDS IN YARANSK DISTRICT OF THE KIROV REGION

S.A. Lezhnin

Volga State University of Technology

The paper assesses the deposits on overgrown areas in Yaransk district of the Kirov region using modern Sentinel high-resolution satellite images. In many regions of the Russian Federation, including the Kirov region, the lack of up-to-date cartographic data acts as a constraint when monitoring the overgrown lands. The use of modern technologies is cost-effective and labour-saving particularly when monitoring large areas. In order to determine the agricultural areas overgrown with trees and shrubs, high-resolution satellite images Sentinel-2 referring to three time periods were selected: spring images (early May 2019), summer images (July 2019) and autumn images (September 2019). The images were combined into composites with a different set of spectral channels (2 - blue channel; 3 - green channel, 4 - red channel; 8 - near infrared) to identify the optimal combination of channels and shooting time. Thematic mapping of young tree species on abandoned agricultural lands in Yaransk district revealed significant areas of overgrowth in 2019. The best accuracy was achieved by the summer map with spectral channel combination 8-4-2. The share of deciduous young stands on deposits amounted to 16.35% of the total area of agricultural land in the district, while the area of coniferous young stands was 11.31%. The total area of agricultural land in Yaransk district was 192,380.1 hectares, partly (about 33%) overgrown with woody vegetation. The accuracy of thematic reforestation map developed using satellite data was compared against the field data and proved to be 77% accurate.

Key words: abandoned lands, satellite images, spectral channel, thematic maps, accuracy assessment, Sentinel.

Введение. В настоящее время система обеспечения федеральных органов исполнительной власти, органов исполнительной власти субъектов Российской Федерации и органов местного самоуправления оперативной информацией о состоянии сельскохозяйственных земель во многих случаях не является достоверной и не отражает реальное состояние земель. Обширные территории, занимаемые сельскохозяйственными землями, сложно поддаются контролю из-за отсутствия цифровых карт сельскохозяйственной освоенности территорий, неразвитой сети пунктов оперативного мониторинга, наземных станций, в том числе и метеорологических, отсутствия авиационной поддержки ввиду высокой стоимости ее содержания. Выведение сельскохозяйственных земель из пользования является одним из доминирующих процессов изменения землепользования в Европе (Levers et al., 2018).

Согласно данным Росреестра, площадь залежных земель в Кировской области увеличилась с 42,5 тыс. га в 2009 году до 51,8 тыс. га в 2018 году, что составляет примерно 1 тыс. га в год (О состоянии окружающей среды...). На этих землях в силу различного рода природных процессов и хозяйственной деятельности человека происходит активное зарастание больших территорий земель сельхозназначения (земель запаса) древесно-кустарниковой растительностью. Во многих регионах Российской Федерации, в том числе и в Кировской области, отсутствие актуальной картографической основы не дает возможности решать задачи мониторинга таких участков. Поэтому применение современных технологий, позволяющих проводить мониторинг на больших территориях с минимальными финансовыми трудозатратами, является актуальной задачей.

Прекращение сельскохозяйственной деятельности может иметь как положительные, так и отрицательные результаты, а последствия различаются в зависимости от местоположения и масштаба (Milenov et al., 2014; Romo-Leon et al., 2014). Негативные последствия могут быть связаны с продовольственной безопасностью и местным жизнеобеспечением, тогда как положительные – связаны с эффектом растительного покрова, который повышает депонирование углерода за счёт увеличения древесной биомассы и создания новых мест обитания, подходящих для многих видов фауны (Levers et al., 2018).

Недавние исследования по этой теме в Европе показали, что образование залежей в основном происходит в менее продуктивных, отдалённых и горных участках, а также районах с эрозией почвы или иными неблагоприятными условиями (Song, 2019; Kolečka et al., 2016). Другими факторами этих процессов являются: миграция населения из сельской местности в города, особенности владения землями и налоговые режимы (Stefanski et al., 2014). Тем не менее, Gradinaru и др. (2015) указывают на сохранение сельскохозяйственных земель вокруг городов, что обусловлено ростом цен на землю и фрагментацией сельскохозяйственных угодий.

Согласно некоторым исследованиям, естественное зарастание может зависеть от площади бывшего поля и последующего использования пашни. При размере участка от 2 до 10 га густота деревьев составляет 5-8 тыс. на 1 га. При этом формируются в основном сосновые насаждения с примесью берёзы и иногда смешанные с преобладанием берёзы. При размере участков 20-25 га количество деревьев снижается примерно до 1,5-2 тыс. на 1 га. Если зарастание пашни происходит без использования ее как пастбища или сенокоса, то на ней успешно начинают расти сосновые насаждения. Если же пашня выводится из оборота через последующее использование ее как сенокос или пастбище, то она заселяется лиственными породами: в основном берёзой или осинкой (Беляев и др., 2013; Лежнин, 2019).

Берёза является одной из наиболее активных пионерных и почвоулучшающих пород, она не уступает по продуктивности хвойным породам, а во многих случаях и превосходит их (Балашкевич, 2006; Гульбе, 2006; Москаленко, Бобровский, 2014). Активное зарастание за-

лежей берёзой также подтверждено исследованиями на территории Республики Марий Эл (Курбанов и др., 2010; Курбанов и др., 2009; Лежнин, Музурова, 2019).

Несмотря на то, что мониторинг использования земель является приоритетным для многих национальных программ мониторинга сельского хозяйства (Alcantara et al., 2012), до настоящего времени отсутствуют согласованные карты земель запаса и надежные подходы для создания таких карт на основе спутниковых данных.

Картографирование заброшенных земель традиционными методами (например, полевые работы, оцифровка аэрофотоснимков) может занимать много времени, быть дорогостоящим и требовать значительной рабочей силы. В этом контексте спутниковые снимки оказываются более эффективным источником данных. Результаты многих исследований показали, что зарастающие залежи могут быть нанесены на карту с помощью данных ДЗЗ с точностью выше 80 %. Более высокая точность достигается, когда в модели включены сцены, охватывающие начало вегетационного периода (Grădinaru et al., 2017).

Yin et al. (2018) и Prishchepov et al. (2012), которые картографировали заброшенные сельхозугодья по снимкам Landsat, достигли относительно высокой точности классификации: 91 и 80 % соответственно. Однако распознавание зарастания на залежах – более трудоёмкий процесс по сравнению с другими видами землепользования, например, наличие рядом садов, лесопитомников или парков может негативно повлиять на результаты (Wittke et al., 2019; Стыценко, 2017).

В апреле 2018 г. в Минсельхозе России была введена в эксплуатацию Единая федеральная информационная система о землях сельскохозяйственного назначения и землях, используемых или предоставленных для ведения сельского хозяйства в составе земель иных категорий (ЕФИС ЗСН), одной из частей которой стал блок работы с данными дистанционного зондирования Земли (ДЗЗ) (Спутниковый мониторинг..., 2019). Существенная роль при создании ЕФИС ЗСН отведена использованию технологий спутникового мониторинга. Так, одной из составных частей ЕФИС ЗСН стал специализированный блок работы с данными ДЗЗ, получивший название «Аналитик ДЗЗ ЕФИС ЗСН» (Буланов и др., 2018; Козубенко и др., 2018). Блок разработан на базе сервисов спутникового мониторинга растительности семейства ВЕГА (Лупян и др., 2011), входящего в состав Центра коллективного пользования системами архивации, обработки и анализа спутниковых данных ЦКП «ИКИ-Мониторинг». Основной задачей реализованных в блоке ДЗЗ функций является оперативное получение объективной информации о состоянии и использовании сельскохозяйственных земель и посевов, а также верификация данных, предоставляемых подведомственными Минсельхозу России учреждениями.

Целью работы являлась оценка древесно-кустарниковых пород, сформировавшихся на залежах Яранского района Кировской области с помощью спутниковых снимков Sentinel.

Для достижения цели были решены следующие **задачи**:

- проведены полевые исследования с закладками тестовых участков (ТУ) на исследуемой территории;
- созданы тематические карты зарастающих залежей;
- проведена оценка площадей молодняков, произрастающих на территории залежей.

Методика исследования включает в себя несколько этапов: проведение полевых работ, подбор спутниковых снимков на территорию исследования, проведение тематического картирования и оценку точности полученных карт.

Расположение ТУ на исследуемой территории было выбрано в результате анализа материалов лесной инвентаризации и кадастровых карт, изучения спутниковых снимков и материалов аэрофотосъемки. Кроме того, использовались картографические интернет-ресурсы (Яндекс и Google карты, Bing maps). Предварительный отбор местности для закладки пробных площадок для оценки зарастания проводился на бывших сельскохозяйственных землях, которые расположены на большом расстоянии от населенных пунктов и не были в пользовании в последние несколько лет или десятилетий (рис. 1).



Рис. 1. Распределение тестовых участков на территории исследования

Координаты тестовых участков фиксировались с помощью GPS-приемника, разрабатывался абрис их расположения относительно ближайшего лесного насаждения или других заметных объектов (дороги, линии электропередач, постройки и т.п.).

Для определения площади зарастания полей древесно-кустарниковыми породами были отобраны спутниковые снимки высокого разрешения Sentinel-2 за три временных периода: весенние снимки (начало мая 2019 г.), летние снимки (июль 2019 г.) и осенние снимки (сентябрь 2019 г.). Все подобранные снимки прошли процедуру атмосферной и геометрической коррекции.

В данной работе использовались композиты с различным набором спектральных каналов (2 – синий канал; 3 – зеленый; 4 – красный; 8 – ближний инфракрасный) для выявления оптимального сочетания каналов и времени съёмки (табл. 1).

Таблица 1

Снимки Sentinel-2, использованные в исследовании

Условное обозначение снимка	Дата съемки	Сочетание спектральных каналов
Spring_432	Май 2019	4-3-2
Spring_842		8-4-2
Spring_843		8-4-3
Summer_432	Июль 2019	4-3-2
Summer_842		8-4-2
Summer_843		8-4-3
Autumn_432	Сентябрь 2019	4-3-2
Autumn_842		8-4-2
Autumn_843		8-4-3

Результаты исследования. Подобранные снимки были синтезированы в трёх различных сочетаниях спектральных каналов (4-3-2, 8-4-2, 8-4-3) и выделены в виде маски по границе Яранского района (рис. 2).

Рис. 2. Комбинирование спектральных каналов сцен весенних снимков Sentinel-2 на территорию Яранского района: а) 4-3-2, б) 8-4-2, в) 8-4-3

До начала работ со снимками из территории исследования были исключены водные объекты, земли населенных пунктов и лесного фонда. После первоначальной классификации были получены карты Яранского района, состоящие из 25 тематических классов. Подбранное количество классов является оптимальным для максимально достоверного разделения классов наземного покрова на лесовозобновление и собственно сельскохозяйственные земли. В последующем все классы тематической карты распределялись на 4 категории: лесные участки, не входящие в лесной фонд; обрабатываемые сельскохозяйственные земли; лиственное лесовозобновление и хвойное лесовозобновление. В случае если какой-либо класс не мог быть достоверно отнесён к одной из категорий, то для него создавалась отдельная векторная маска, внутри которой осуществлялась дополнительная классификация с выделением уже 14 классов. Итогом всего процесса тематического картографирования стали карты лесовозобновления на заброшенных сельскохозяйственных землях Яранского района Кировской области за три временных периода и в трех сочетаниях спектральных каналов (рис. 3).

Как видно из рисунка 3, основная часть лесовозобновления на залежных землях приходится на центральную и юго-восточную часть Яранского района. Этот факт можно объяснить большим количеством взрослых древостоев на этой территории, которые ранее входили в сельские лесничества, но в данный момент не входят в состав лесного фонда. Обсеменение заброшенных полей обычно происходит вдоль границы лесных насаждений, тогда как в северной и северо-западной частях района таких лесных участков меньше, поэтому обсеменение этих заброшенных земель происходит в меньшей степени.

Итоговое распределение площадей полученных тематических классов по временным периодам представлено в таблице 2.

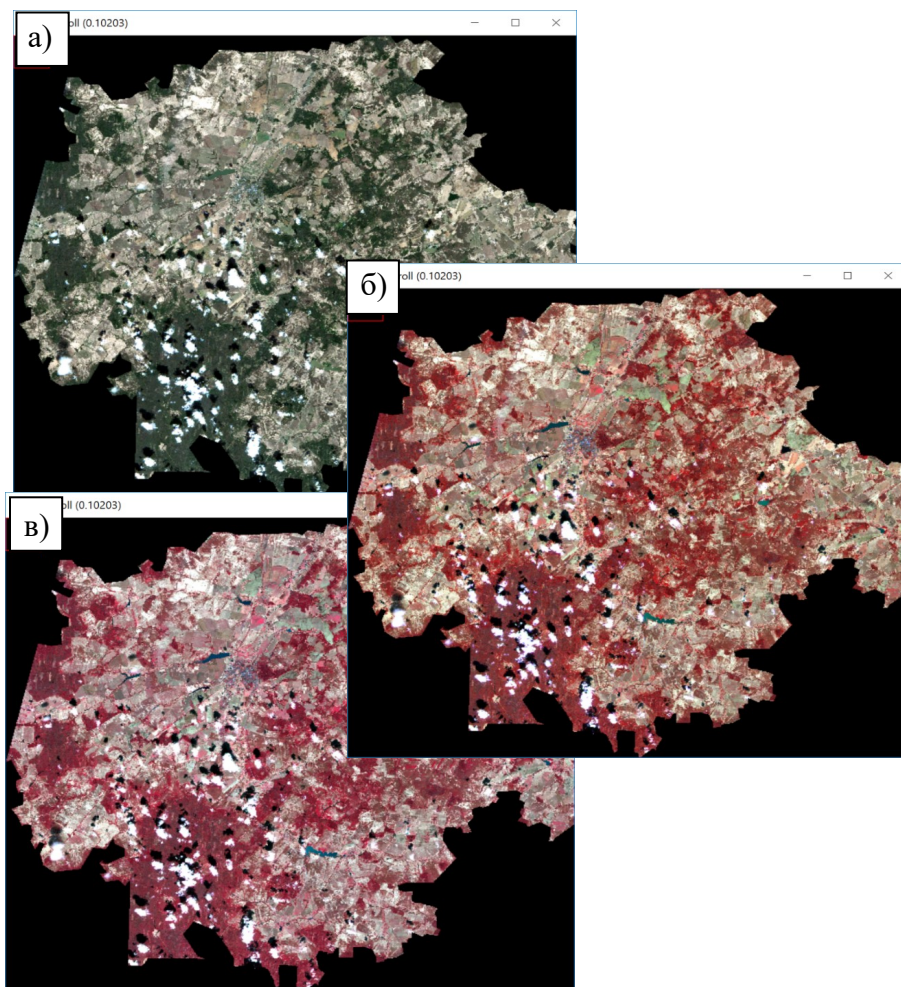


Рис. 2. Комбинирование спектральных каналов сцен весенних снимков Sentinel-2 на территорию Яранского района: а) 4-3-2, б) 8-4-2, в) 8-4-3

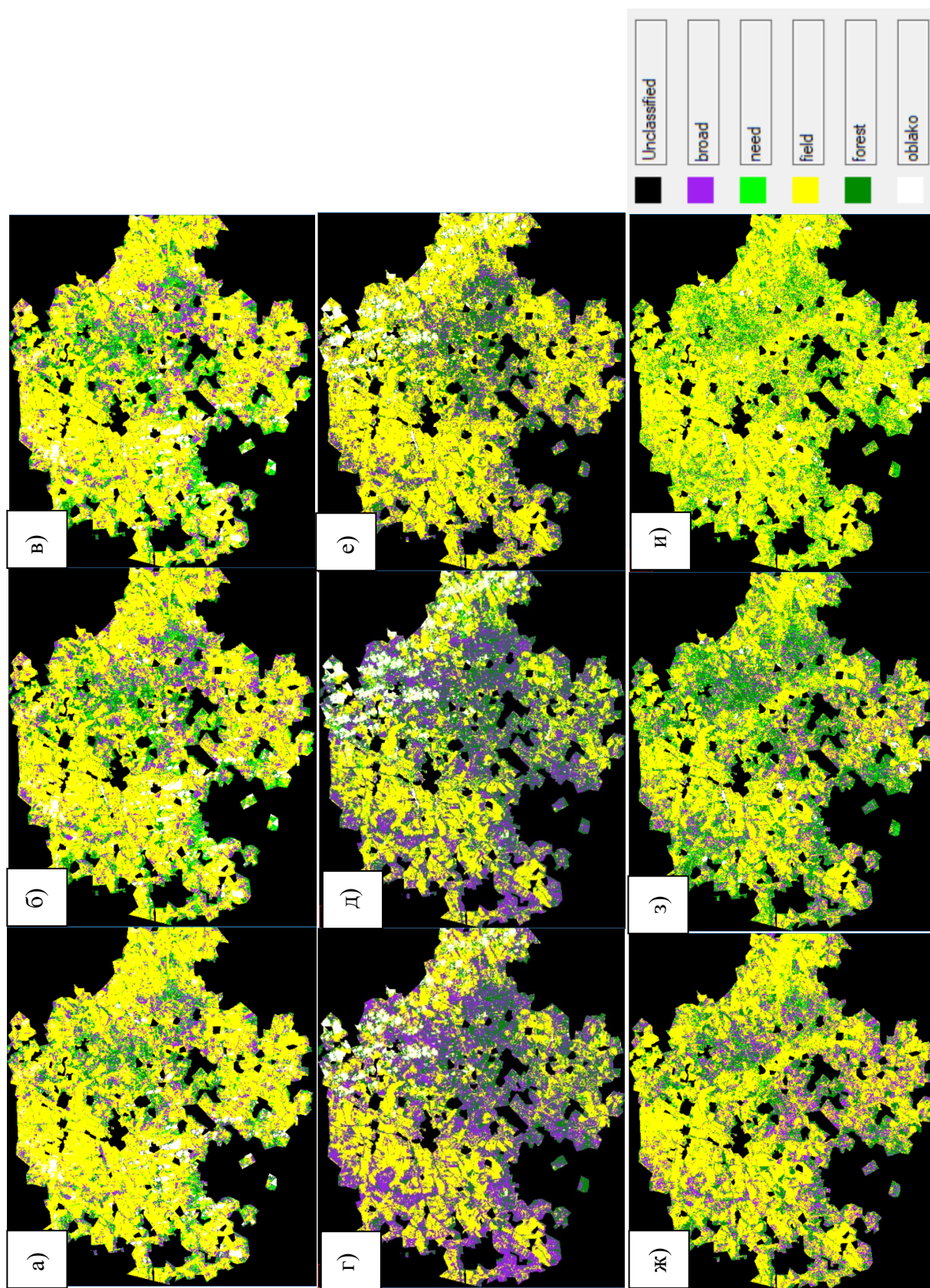


Рис. 3. Итоговый набор тематических карт: а) Spring_432, б) Spring_842, в) Spring_843, г) Summer_432, д) Summer_842, е) Summer_843, ж) Autumn_432, з) Autumn_842, и) Autumn_843

Таблица 2

Распределение площадей по тематическим классам

№	Класс карты	Количество пикселей, шт	Площадь класса, га	% от общей площади
Spring_432				
1	Лиственные молодняки (broad)	2411800	24118	12,54
2	Хвойные молодняки (need)	1550394	15503,94	8,06
3	Обрабатываемые земли (field)	12758866	127588,7	66,32
4	Лес (forest)	1301746	13017,46	6,77
5	Облака (Oblako)	1215197	12151,97	6,32
Итого:		19238003	192380	100,00
Spring_842				
1	Лиственные молодняки (broad)	2707189	27071,89	14,07
2	Хвойные молодняки (need)	1839095	18390,95	9,56
3	Обрабатываемые земли (field)	11781356	117813,6	61,24
4	Лес (forest)	1786453	17864,53	9,29
5	Облака (Oblako)	1123910	11239,1	5,84
Итого:		19238003	192380	100,00
Spring_843				
1	Лиственные молодняки(broad)	2372234	23722,34	12,33
2	Хвойные молодняки (need)	1970523	19705,23	10,24
3	Обрабатываемые земли (field)	12194836	121948,4	63,39
4	Лес (forest)	1503384	15033,84	7,81
5	Облака (Oblako)	1197026	11970,26	6,22
Итого:		19238003	192380	100,00
Summer_432				
1	Лиственные молодняки (broad)	6457054	64570,54	33,56
2	Хвойные молодняки (need)	631212	6312,12	3,28
3	Обрабатываемые земли (field)	7279557	72795,57	37,84
4	Лес (forest)	3908257	39082,57	20,32
5	Облака (Oblako)	961933	9619,33	5,00
Итого:		19238013	192380,1	100
Summer_842				
1	Лиственные молодняки (broad)	5272278	52722,78	27,41
2	Хвойные молодняки (need)	1132122	11321,22	5,88
3	Обрабатываемые земли (field)	6835474	68354,74	35,53
4	Лес (forest)	4565157	45651,57	23,73
5	Облака (Oblako)	1432982	14329,82	7,45
Итого:		19238013	192380,1	100,00
Summer_843				
1	Лиственные молодняки (broad)	2942140	29421,4	15,29
2	Хвойные молодняки (need)	126373	1263,73	0,66
3	Обрабатываемые земли (field)	11105271	111052,7	57,73
4	Лес (forest)	4021329	40213,29	20,90
5	Облака (Oblako)	1042900	10429	5,42
Итого:		19238013	192380,1	100,00

Autumm_432				
1	Лиственные молодняки (broad)	3848276	38482,76	20,00
2	Хвойные молодняки (need)	1360792	13607,92	7,07
3	Обрабатываемые земли (field)	11369839	113698,4	59,10
4	Лес (forest)	2659106	26591,06	13,82
5	Облака (Oblako)	0	0	0
Итого:		19238013	192380,1	100,00
Autumm_842				
1	Лиственные молодняки (broad)	3144539	31445,39	16,35
2	Хвойные молодняки (need)	2175072	21750,72	11,31
3	Обрабатываемые земли (field)	9397237	93972,37	48,85
4	Лес (forest)	4060229	40602,29	21,11
5	Облака (Oblako)	460936	4609,36	2,40
Итого:		19238013	192380,1	100
Autumm_843				
1	Лиственные молодняки (broad)	922521	9225,21	4,80
2	Хвойные молодняки (need)	2090383	20903,83	10,87
3	Обрабатываемые земли (field)	13373111	133731,1	69,51
4	Лес (forest)	2381236	23812,36	12,38
5	Облака (Oblako)	470762	4707,62	2,45
Итого:		19238013	192380,1	100

Как видно из таблицы 2, разброс площадей классов замечен даже внутри одного временного периода для разных сочетаний тематических классов. Это объяснимо тем, что разные спектральные каналы по-разному отображают спектральные характеристики растительности. В некоторых случаях наблюдается значительное перемешивание молодняков с густой травянистой растительностью. В целом для весеннего периода площадь обрабатываемых земель колеблется от 61 до 66 % от общей площади сцены. Доля лесных насаждений занимает от 6 до 9 %. Доля лиственных молодняков меняется от 12 до 14 %, а хвойных – от 8 до 10 %.

Для летнего периода также характерно преобладание обрабатываемых земель, доля которых колеблется от 37 до 57 %. Леса занимают соответственно от 20 до 23 %. Доля лиственных молодняков варьирует от 15 до 27 %, тогда как доля хвойных молодняков – от 0,66 до 3 %.

Данные таблицы 2 показывают также, что на летних снимках идёт значительное перемешивание тематических классов, в особенности лиственных молодняков и сельскохозяйственных земель. Это объясняется тем, что во время активной вегетации спектральные сигналы травянистой растительности и лиственных молодняков достаточно близки по значениям.

Для осеннего периода доля обрабатываемых земель варьирует от 48 до 69 %, доля лесных насаждений – от 12 до 21 %, доля лиственных молодняков – от 4 до 20 %, а доля хвойных молодняков – от 7 до 11 %.

Для **оценки точности** полученных тематических карт было использовано 177 тестовых участков. Для определения точности соответствующего класса количество классифицированных пикселей было отнесено на общее количество пикселей согласно тестовым данным.

Полученные значения показывают, насколько вероятно, что данный класс совпадает с результатами классификации (табл. 3).

Таблица 3

Точность полученных тематических карт

Тематическая карта	Общая точность	Коэффициент Каппа	Достоверность карты
Spring_432	0,63	0,41	Умеренная
Spring_842	0,65	0,46	Умеренная
Spring_843	0,62	0,38	Слабая
Summer_432	0,65	0,47	Умеренная
Summer_842	0,77	0,69	Значительная
Summer_843	0,74	0,64	Значительная
Autumm_432	0,67	0,58	Умеренная
Autumm_842	0,76	0,67	Значительная
Autumm_843	0,70	0,61	Значительная

Как видно из таблицы 4, наилучшую точность показала летняя карта в сочетании спектральных каналов 8-4-2 (рис. 4).

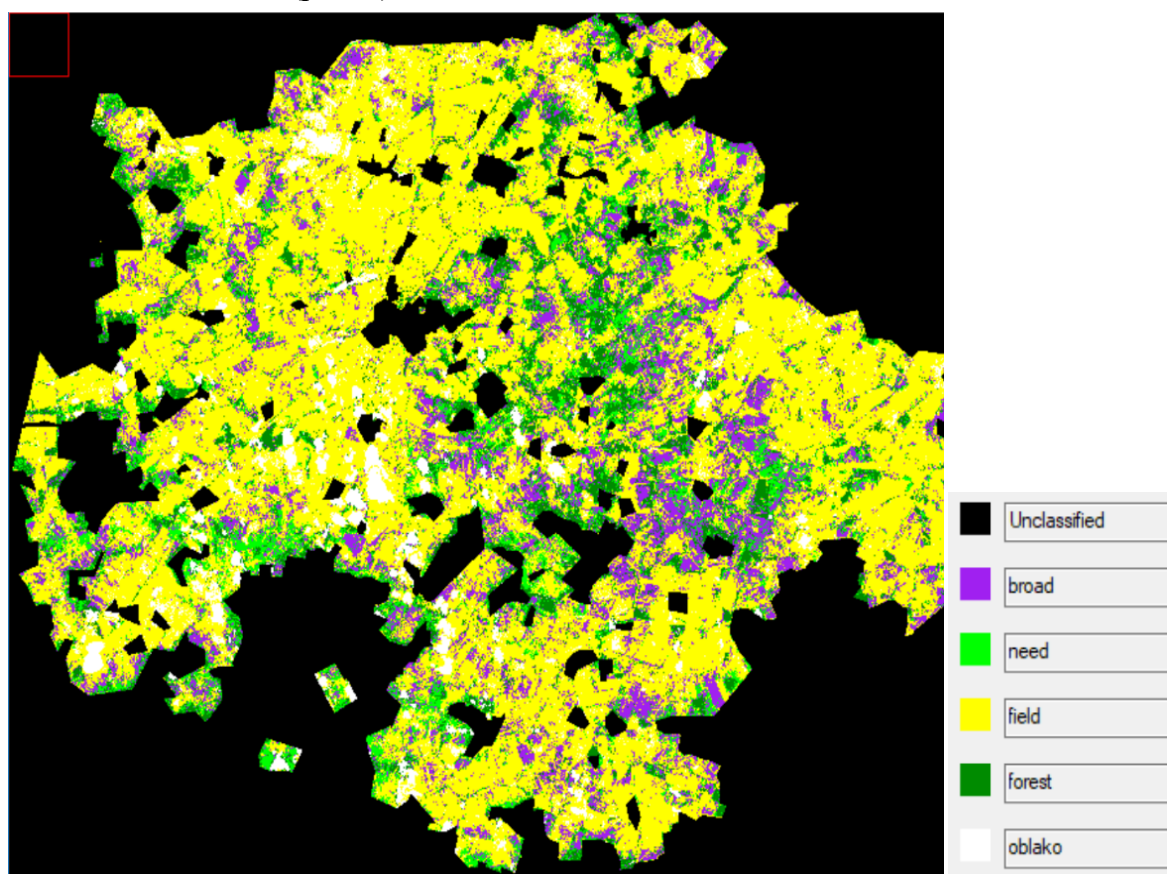


Рис. 4. Тематическая карта Summer_842

Общая точность этой карты составила 77 %, что является довольно высоким результатом, коэффициент Каппа (0,69) также показал значительную согласованность карты с натурными данными. Такие показатели точности объясняются тем, что сканер спутника Sentinel-2 снимает местность в довольно узком диапазоне видимого и ближнего инфракрасного спектра, в которых спектральные сигнатуры лиственных молодняков и густой травянистой растительности имеют близкие значения, что приводит к высокому перемешиванию

этих классов. В то же время тематические классы «Лес» и «Хвойные молодняки» хорошо выделяются из окружающих объектов наземного покрова.

Вместе с тем, если не проводить дифференциацию тематических классов по древесным породам, то общая точность тематической карты составит 85 %, а коэффициент Каппа – 0,78, что повышает точность оценки.

Выводы. Тематическое картографирование молодняков древесных пород на заброшенных сельскохозяйственных землях Яранского района Кировской области позволило определить значительные площади их зарастания древесно-кустарниковой растительностью в 2019 году. Общая площадь сельскохозяйственных земель Яранского района составила 192380,1 га, значительная часть которых (около 33 %) зарастает древесной растительностью.

Проверка тематической карты лесовозобновления показала её высокую точность, которая составила 77 %.

Созданная тематическая карта лесовозобновления на залежах Яранского района Кировской области за 2019 год может быть использована для дальнейшего мониторинга процесса зарастания. Её применение будет способствовать оперативному мониторингу земель залежей. Атрибутивные данные классов тематической карты предоставляют возможность для комплексного анализа процессов зарастания в сочетании с экологическими, социальными или экономическими факторами, что должно способствовать более точному прогнозированию ситуации в сельском хозяйстве Кировской области.

The European Commission support for the production of this publication does not constitute an endorsement of the contents which reflects the views only of the authors, and the Commission cannot be held responsible for any use which may be made of the information contained therein.

Библиографический список

1. Балашкевич Ю.А. Зарастание бывших сельскохозяйственных земель древесной растительностью // Актуальные проблемы лесного комплекса. 2006. №13. С 4-6.
2. Беляев В. В., Кононов, О. Д., Карабан, А. А., Старицын, В. В. Состояние древесной растительности на землях, выбывших из хозяйственного оборота в Архангельской области // Вестник Северного (Арктического) федерального университета. 2013. Вып. 2. С. 5-11.
3. Буланов К.А., Денисов П.В., Косогор С.Н., Вандышева Н.М., Бабак В.А., Трошко К.А., Мартыанов А.С., Середа И.И., Лупян Е.А., Толпин В.А., Бурцев М.А. Модуль работы с данными дистанционного зондирования Земли в Единой федеральной информационной системе о землях сельскохозяйственного назначения (ЕФИС ЗСН) // 16-я Всерос. открытая конф. «Современные проблемы дистанционного зондирования Земли из космоса» (Москва, 12–16 нояб. 2018): сб. тез. Москва: ИКИ РАН, 2018. С. 3
4. Гульбе А.Я. Динамика фитомассы и годичной продукции молодняка березы на залежи в южнотаежной подзоне (Ярославская область) // Вестник Оренбургского гос. ун-та. Приложение «Биоразнообразие и биоресурсы». 2006. № 4. С. 34-37.
5. Козубенко И.С., Бегляров Р.Р., Вандышева Н.М., Бабак В.А., Денисов П.В., Трошко К.А. Использование материалов дистанционного зондирования Земли в Единой федеральной информационной системе о землях сельскохозяйственного назначения (ЕФИС ЗСН) // Применение средств дистанционного зондирования Земли в сельском хозяйстве: материалы 2-й Всерос. науч. конф. с международным участием. Санкт-Петербург, 26–28 сент. 2018. Санкт-Петербург: ФГБНУ АФИ, 2018. С. 19–25.
6. Курбанов Э.А., Воробьев О.Н., Губаев А.В., Лежнин С.А., Незамаев С.А., Александрова Т.А. Оценка зарастания земель запаса Республики Марий Эл лесной растительностью по спутниковым снимкам // Вестник МарГТУ. – Йошкар-Ола: Марийский государственный технический университет. 2010. № 2(9). 2010. С. 14-20.
7. Курбанов Э.А., Воробьев О.Н., Мошкина Л.С., Губаев А.В., Лежнин С.А., Незамаев С.А. Оценка фитомассы березняков на бывших сельскохозяйственных землях Марийского Заволжья: пространственное распределение и динамика накопления // Международное сотрудничество в лесном секторе: баланс образования, науки и производства: материалы международной конференции. Йошкар-Ола: Марийский государственный технический университет. 2009. С. 93-97.
8. Лежнин С.А., Музурова Р.Л. Оценка вторичной сукцессии на залежах Республики Марий Эл // Лесные экосистемы в условиях изменения климата: биологическая продуктивность и дистанционный мониторинг: материалы международной конференции. Йошкар-Ола: ПГТУ. 2019. С. 126-135.

9. Лупян Е.А., Савин И.Ю., Барталев С.А., Толпин В.А., Балашов И.В., Плотников Д.Е. Спутниковый сервис мониторинга состояния растительности («ВЕГА») // Современные проблемы дистанционного зондирования Земли из космоса. 2011. Т. 8, № 1. С. 190–198.
10. Москаленко С.В., Бобровский М.В. Возобновление деревьев на бывших пахотных землях в заповеднике «Калужские засеки» // Бюллетень Брянского отделения РБО. 2014. № 1(3). С. 48–54.
11. О состоянии окружающей среды Кировской области в 2019 году [Электронный ресурс]. Режим доступа: <https://www.kirovreg.ru/econom/ecology/%D0%A0%D0%B5%D0%B3%D0%B4%D0%BE%D0%BA%D0%BB%D0%B0%D0%B4%202019.pdf> – 13.11.2020.
12. Спутниковый мониторинг посевов озимых под урожай 2019 г. в Единой федеральной информационной системе о землях сельскохозяйственного назначения (ЕФИС ЗСН). – URL: <https://mcx.gov.ru/ministry/departments/dit/industry-information/sputnikovyy-monitoring-posevov-ozimyykh-pod-urozhay-2019-g-v-edinoy-federalnoy-informatsionnoy-sisteme-o-zemlyakh-selskokh/>. – 28.11.2020
13. Стыщенко Е. А. Возможности распознавания сельскохозяйственных угодий с использованием методики совместной автоматизированной обработки разносезонных многозональных космических изображений // Современные проблемы дистанционного зондирования Земли из космоса. 2017. Т. 14, № 5. С. 172–183.
14. Alcantara C., Kuemmerle T., Prishchepov A. V., Radeloff V. C. Mapping abandoned agriculture with multi-temporal MODIS satellite data // Remote Sensing of Environment. 2012. Vol. 124. P. 334–347.
15. Grădinaru S. R., Kienast F., Psomas A. Using multi-seasonal Landsat imagery for rapid identification of abandoned land in areas affected by urban sprawl // Ecological Indicators. 2019. Vol. 96. Pt. 2. P. 79–86.
16. Yin H., Prishchepov A.V., Kuemmerle T., Bleyhl B. et al. Mapping agricultural land abandonment from spatial and temporal segmentation of Landsat time series // Remote Sensing of Environment. 2018. Vol. 210. P. 12–24.
17. Prishchepov A. V., Radeloff V. C., Dubinin M., Alcantara C. The effect of Landsat ETM/ETM + image acquisition dates on the detection of agricultural land abandonment in Eastern Europe // Remote Sensing of Environment. 2012. Vol. 126. P. 195–209.
18. Kolečka N., Kozak J., Kaim D., Dobosz M. et al. Mapping secondary forest succession on abandoned agricultural land in the Polish Carpathians // Remote Sensing and Spatial Information Sciences. 2016. Vol. XLI-B8. P. 931–935.
19. Levers C., Schneider M., Prishchepov A. V., Estel S. Spatial variation in determinants of agricultural land abandonment in Europe // Science of The Total Environment. 2018. Vol. 644. P. 95–111.
20. Milenov P., Vassilev V., Vassileva A., Radkov R. et al. Monitoring of the risk of farmland abandonment as an efficient tool to assess the environmental and socio-economic impact of the Common Agriculture Policy // International Journal of Applied Earth Observation and Geoinformation. 2014. Vol.32. P. 218–227.
21. Romo-Leon J. R., van Leeuwen W. J. D., Castellanos-Villegas A. Using remote sensing tools to assess land use transitions in unsustainable arid agro-ecosystems // Journal of Arid Environments. 2014. Vol. 106. P. 27–35.
22. Stefanski J., Chaskovskyy O., Waske B. Mapping and monitoring of land use changes in post-Soviet western Ukraine using remote sensing data // Applied Geography. 2014. Vol.55. P. 155–164.
23. Song W. Mapping Cropland Abandonment in Mountainous Areas Using an Annual Land-Use Trajectory Approach // Sustainability. 2019. Vol. 11. P. 1–24.
24. Wittke S., Xiaowei Y., Karjalainen M., Hyypä J., Puttonen E. Comparison of two-dimensional multitemporal Sentinel-2 data with three-dimensional remote sensing data sources for forest inventory parameter estimation over a boreal forest // International Journal of Applied Earth Observation and Geoinformation. 2019. Vol. 76. P. 167–178.

References

1. Balashkevich Yu.A. Zarastanie byvshikh sel'skokhozyaystvennykh zemel' drevesnoi rastitel'nost'yu [Overgrowth of former agricultural lands with woody vegetation]. *Aktual'nye problemy lesnogo kompleksa*. 2006. №13. P. 4–6.
2. Belyaev V. V., Kononov, O. D., Karaban, A. A., Staritsyn, V. V. Sostoyanie drevesnoi rastitel'nosti na zemlyakh, vybyvshikh iz khozyaystvennogo oborota v Arkhangel'skoi oblasti [The state of woody vegetation on lands abandoned from economic circulation in the Arkhangelsk region]. *Vestnik Severnogo (Arkticheskogo) federal'nogo universiteta*. 2013. Vyp. 2. P. 5–11.
3. Bulanov K.A., Denisov P.V., Kosogor S.N., Vandysheva N.M., Babak V.A., Troshko K.A., Mart'yanov A.S., Sereda I.I., Lupyan E.A., Tolpin V.A., Burtsev M.A. Modul' raboty s dannymi distantsionnogo zondirovaniya Zemli v Edinoi federal'noi informatsionnoi sisteme o zemlyakh sel'skokhozyaystvennogo naznacheniya (EFIS ZSN) [Module for working with Earth remote sensing data in the Unified Federal Information System on Agricultural Lands (EFIS ZSN)]. *16-ya Vseros. otkrytaya konf. «Sovremennye problemy distantsionnogo zondirovaniya Zemli iz kosmosa» (Moskva, 12–16 noyab. 2018)*. Moscow: IKI RAN, 2018. P. 3
4. Gul'be A.Ya. Dinamika fitomassy i godichnoi produktssii molodnyaka berezy na zalezhi v yuzhnataezhnoi podzone (Yaroslavskaya oblast') [Dynamics of phytomass and annual production of young birch on fallows in the southern taiga subzone (Yaroslavl region)]. *Vestnik Orenburgskogo gos. un-ta. Prilozhenie «Bioraznoobrazie i bioresursy»*. 2006. № 4. P. 34–37.
5. Kozubenko I.S., Beglyarov R.R., Vandysheva N.M., Babak V.A., Denisov P.V., Troshko K.A. Ispolzovanie materialov distantsionnogo zondirovaniya Zemli v Edinoi federal'noi informatsionnoi sisteme o zemlyakh sel'skokhozyaystvennogo naznacheniya (EFIS ZSN) [Use of Earth Remote Sensing Materials in the Unified Federal Information System on Agricultural Lands (EFIS ZSN)]. *Primenenie sredstv distantsionnogo zondirovaniya Zemli v sel'skom khozyaystve*. Sankt-Peterburg: FGBNU AFI, 2018. P. 19–25.

6. Kurbanov E.A., Vorob'ev O.N., Gubaev A.V., Lezhnin S.A., Nezamaev S.A., Aleksandrova T.A. Otsenka zarastaniya zemel' zapasa Respubliki Marii El lesnoi rastitel'nost'yu po sputnikovym snimkam [Assessment of overgrowth of the reserve lands of the Republic of Mari El with forest vegetation based on satellite images]. *Vestnik MarGTU. – Ioshkar-Ola: Mariiskii gosudarstvennyi tekhnicheskii universitet*. **2010**. № 2(9). 2010. P. 14-20.
7. Kurbanov E.A., Vorob'ev O.N., Moshkina L.S., Gubaev A.V., Lezhnin S.A., Nezamaev S.A. Otsenka fitomassy bereznyakov na byvshikh sel'skokhozyaistvennykh zemlyakh Mariiskogo Zavolzh'ya: prostranstvennoe raspredelenie i dinamika nakopleniya [Assessment of the phytomass of birch forests on the former agricultural lands of the Mari Trans-Volga region: spatial distribution and dynamics of accumulation]. *Mezhdunarodnoe sotrudnichestvo v lesnom sektore: balans obrazovaniya, nauki i proizvodstva*. Ioshkar-Ola: Mariiskii gosudarstvennyi tekhnicheskii universitet. **2009**. P. 93-97.
8. Lezhnin S.A., Muzurova R.L. Otsenka vtorichnoi suksessii na zalezakh Respubliki Marii El [Estimation of the secondary succession in the deposits of the Republic of Mari El]. *Lesnye ekosistemy v usloviyakh izmeneniya klimata: biologicheskaya produktivnost' i distantsionnyi monitoring*. Ioshkar-Ola: PGTU. **2019**. P. 126-135.
9. Lupyan E.A., Savin I.Yu., Bartalev S.A., Tolpin V.A., Balashov I.V., Plotnikov D.E. Sputnikovyi servis monitoringa sostoyaniya rastitel'nosti («VEGA») [Satellite service for monitoring the state of vegetation ("VEGA")]. *Sovremennye problemy distantsionnogo zondirovaniya Zemli iz kosmosa*. **2011**. T. 8, № 1. P. 190-198.
10. Moskalenko S.V., Bobrovskii M.V. Vozobnovlenie derev'ev na byvshikh pakhotnykh zemlyakh v zapovednike «Kaluzhskie zaseki» [Renewal of trees on the former arable land in the Kaluzhskie Zaseki Nature Reserve]. *Byulleten' Bryanskogo otdeleniya RBO*. **2014**. № 1(3). P. 48-54.
11. O sostoyanii okruzhayushchei sredy Kirovskoi oblasti v 2019 godu [On the state of the environment of the Kirov region in 2019]. URL: <https://www.kirovreg.ru/econom/ecology/%D0%A0%D0%B5%D0%B3%D0%B4%D0%BE%D0%BA%D0%BB%D0%B0%D0%B4%202019.pdf> – 13.11.2020.
12. Sputnikovyi monitoring posevov ozimyykh pod urozhai 2019 g. v Edinoi federal'noi informatsionnoi sisteme o zemlyakh sel'skokhozyaistvennogo naznacheniya (EFIS ZSN) [Satellite monitoring of winter crops for the 2019 harvest in the Unified Federal Information System on Agricultural Lands (EFIS ZSN)]. URL: <https://mcx.gov.ru/ministry/departments/dit/industry-information/sputnikovyy-monitoring-posevov-ozimyykh-pod-urozhay-2019-g-v-edinoy-federal'noy-informatsionnoy-sisteme-o-zemlyakh-selskokh/>. – 28.11.2020
13. Stytsenko E. A. Vozmozhnosti raspoznavaniya sel'skokhozyaistvennykh ugodii s ispol'zovaniem metodiki sovmestnoi avtomatizirovannoi obrabotki raznosezonnykh mnogoazonal'nykh kosmicheskikh izobrazhenii [Possibilities of recognition of agricultural land using the method of joint automated processing of multi-season multi-zone satellite images]. *Sovremennye problemy distantsionnogo zondirovaniya Zemli iz kosmosa*. **2017**. T. 14, № 5. P. 172-183.
14. Alcantara C., Kuemmerle T., Prishchepov A. V., Radeloff V. C. Mapping abandoned agriculture with multi-temporal MODIS satellite data. *Remote Sensing of Environment*. **2012**. Vol. 124. P. 334-347.
15. Grădinaru S. R., Kienast F., Psomas A. Using multi-seasonal Landsat imagery for rapid identification of abandoned land in areas affected by urban sprawl. *Ecological Indicators*. **2019**. Vol. 96. Pt. 2. P. 79-86.
16. Yin H., Prishchepov A.V., Kuemmerle T., Bleyhl B. et al. Mapping agricultural land abandonment from spatial and temporal segmentation of Landsat time series. *Remote Sensing of Environment*. **2018**. Vol. 210. P. 12-24.
17. Prishchepov A. V., Radeloff V. C., Dubinin M., Alcantara C. The effect of Landsat ETM/ETM + image acquisition dates on the detection of agricultural land abandonment in Eastern Europe. *Remote Sensing of Environment*. **2012**. Vol. 126. P. 195-209.
18. Kolecka N., Kozak J., Kaim D., Dobosz M. et al. Mapping secondary forest succession on abandoned agricultural land in the Polish Carpathians. *Remote Sensing and Spatial Information Sciences*. **2016**. Vol. XLI-B8. P. 931-935.
19. Levers C., Schneider M., Prishchepov A. V., Estel S. Spatial variation in determinants of agricultural land abandonment in Europe. *Science of The Total Environment*. **2018**. Vol. 644. P. 95-111.
20. Milenov P., Vassilev V., Vassileva A., Radkov R. et al. Monitoring of the risk of farmland abandonment as an efficient tool to assess the environmental and socio-economic impact of the Common Agriculture Policy. *International Journal of Applied Earth Observation and Geoinformation*. **2014**. Vol.32. P. 218-227.
21. Romo-Leon J. R., van Leeuwen W. J. D., Castellanos-Villegas A. Using remote sensing tools to assess land use transitions in unsustainable arid agro-ecosystems. *Journal of Arid Environments*. **2014**. Vol. 106. P. 27-35.
22. Stefanski J., Chaskovskyy O., Waske B. Mapping and monitoring of land use changes in post-Soviet western Ukraine using remote sensing data. *Applied Geography*. **2014**. Vol.55. P. 155-164.
23. Song W. Mapping Cropland Abandonment in Mountainous Areas Using an Annual Land-Use Trajectory Approach. *Sustainability*. **2019**. Vol. 11. P. 1-24.
24. Wittke S., Xiaowei Y., Karjalainen M., Hyypä J., Puttonen E. Comparison of two-dimensional multitemporal Sentinel-2 data with three-dimensional remote sensing data sources for forest inventory parameter estimation over a boreal forest. *International Journal of Applied Earth Observation and Geoinformation*. **2019**. Vol. 76. P. 167-178.

СОДЕРЖАНИЕ

Thomas A. Mapping of land use / land cover of Klerksdorp–Orkney–Stilfontein–Hartebeestfontein (KOSH) region for the years 2020 and 2019 using Sentinel-2 data.....	6
Zhang J., Liu G., Wang J. Extraction and modeling of individual sikang pine stem based on point cloud data.....	29
Papaiordanidis S., Minakou C., Gitas I.Z. On-the-fly land cover mapping using machine learning with multispectral satellite imagery on Google Earth engine.....	37
Dudumashe N., Thomas A. Assessment of land surface temperature and drought indices for the Klerksdorp-Orkney-Stilfontein-Hartebeesfontein (KOSH) region.....	46
Fang J., Sha J., Guo X., Sun G., Li Q. Comprehensive evaluation of ecological environment in Dazhangxi basin based on multi-source remote sensing data.....	69
Курбанов Э.А., Лежнин С.А., Воробьёв О.Н., Меньшиков С.А., Дергунов Д.М., Ван И., Тарасова Л.В., Смирнова Л.Н. Аналитический обзор публикаций в области применения ДЗЗ и ГИС для оценки динамики растительного покрова.....	91
Shao Q., Huang C., Huang J.F. Forest phenological trends in the middle and high latitude of the northern hemisphere.....	112
Терехин Э.А. Оценка изменений в лесах юга Среднерусской возвышенности по спутниковым данным.....	119
Мартынова М.В., Султанова Р.Р., Габделхаков А.К., Рахматуллин З.З., Одинцов Г.Е. Оценка зарастания сельскохозяйственных земель древесными породами по спутниковым данным Landsat на примере участка Бакалинского района Республики Башкортостан.....	128
Wang Y. Estimation of urban environment in Taipei living circle based on remote sensing ecological index.....	135
Ma J. Monitoring of forest ecosystems disturbances in Mari El Republic.....	147
Лежнин С.А. Оценка зарастания залежей Яранского района Кировской области по спутниковым данным.....	160

CONTENTS

Thomas A. Mapping of land use / land cover of Klerksdorp–Orkney–Stilfontein–Hartebeestfontein (KOSH) region for the years 2020 and 2019 using Sentinel-2 data.....	6
Zhang J., Liu G., Wang J. Extraction and modeling of individual sikang pine stem based on point cloud data.....	29
Papaiordanidis S., Minakou C., Gitas I.Z. On-the-fly land cover mapping using machine learning with multispectral satellite imagery on Google Earth engine.....	37
Dudumashe N., Thomas A. Assessment of land surface temperature and drought indices for the Klerksdorp-Orkney-Stilfontein-Hartebeesfontein (KOSH) region.....	46
Fang J., Sha J., Guo X., Sun G., Li Q. Comprehensive evaluation of ecological environment in Dazhangxi basin based on multi-source remote sensing data.....	69
Kurbanov E.A., Lezhnin S.A., Vorobev O.N., Menshikov S.A., Dergunov D.M., Wang Y., Tarasova L.V., Smirnova L.N. Applications of remote sensing and GIS for estimation of land use / cover change: a review.....	91
Shao Q., Huang C., Huang J.F. Forest phenological trends in the middle and high latitude of the northern hemisphere.....	112
Terekhin E.A. Assessment of changes in the forest of Central Russian Upland using remote sensing data.....	119
Martynova M.V., Sultanova R.R., Gabdelkhakov A.K., Rakhmatullin Z.Z., Odintsov G.E. Assessment of reforestation on abandoned agricultural lands using Landsat data on the example of a site in the Bakalinsky region of the Republic Bashkortostan.....	128
Wang Y. Estimation of urban environment in Taipei living circle based on remote sensing ecological index.....	135
Ma J. Monitoring of forest ecosystems disturbances in Mari El Republic.....	147
Lezhnin S.A. The use of satellite data in the assessment of reforestation on the abandoned agricultural lands in Yaransk district of the Kirov region.....	160

Научное издание

**ЛЕСНЫЕ ЭКОСИСТЕМЫ
В УСЛОВИЯХ ИЗМЕНЕНИЯ КЛИМАТА:
БИОЛОГИЧЕСКАЯ ПРОДУКТИВНОСТЬ И ДИСТАНЦИОННЫЙ МОНИТОРИНГ**

Международный сборник научных статей

Редактор *Л. С. Емельянова*
Компьютерная верстка *С. А. Лежнин*
Переводчик *М. Н. Курдюмова*

Подписано к использованию *02.12.2020*

Поволжский государственный технологический университет
424000 Йошкар-Ола, пл. Ленина, 3

Редакционно-издательский отдел ПГТУ
424006 Йошкар-Ола, ул. Панфилова, 17

Центр устойчивого управления и дистанционного мониторинга лесов
424000 Йошкар-Ола, пл. Ленина, 3